DEVELOPMENT OF APPROACH TO ESTIMATE VOLUME FRACTION OF MULTIPHASE MATERIAL USING DIELECTRICS

A Dissertation

by

SANG ICK LEE

Submitted to the Office of Graduate Studies of
Texas A&M University
in partial fulfillment of the requirements for the degree of

DOCTOR OF PHILOSOPHY

May 2010

Major Subject: Civil Engineering

DEVELOPMENT OF APPROACH TO ESTIMATE VOLUME FRACTION OF MULTIPHASE MATERIAL USING DIELECTRICS

A Dissertation

by

SANG ICK LEE

Submitted to the Office of Graduate Studies of
Texas A&M University
in partial fulfillment of the requirements for the degree of

DOCTOR OF PHILOSOPHY

Approved by:

Chair of Committee,	Dan G. Zollinger
Committee Members,	Robert L. Lytton
	Dallas N. Little
	Mohammed E. Haque
Head of Department,	John Niedzwecki

May 2010

Major Subject: Civil Engineering

ABSTRACT

Development of Approach to Estimate Volume Fraction of Multiphase Material Using Dielectrics. (May 2010)

Sang Ick Lee, B.S., Chung-Ang University, Korea;

M.S., Chung-Ang University, Korea

Chair of Advisory Committee: Dr. Dan G. Zollinger

Most engineering as well as pavement materials are composites composed of two or more components to obtain a variety of solid properties to support internal and external loading. The composite materials rely on physical or chemical properties and volume fraction of each component. While the properties can be identified easily, the volume fraction is hard to be estimated due to the volumetric variation during the performance in the field. Various test procedures have been developed to measure the volume fractions; however, they depend on subjective determination and judgment. As an alternative, electromagnetic technique using dielectric constant was developed to estimate the volume fraction. Empirical and mechanistic approaches were used to relate the dielectric constant and volume fraction. While the empirical models are not very accurate in all cases, the mechanistic models require assumptions of constituent dielectric constants. For those reasons, the existing approaches might produce less accurate estimate of volume fraction. In this study, a mechanistic-based approach using the self consistent scheme was developed to be applied to multiphase materials. The new approach was based on calibrated dielectric constant of components to improve results without any assumptions. Also, the system identification was used iteratively to solve for dielectric parameters and volume fraction at each step. As the validation performed to verify the viability of the new approach using soil mixture and portland cement concrete, it was found that the approach has produced a significant improvement in the accuracy of the estimated volume fraction.

DEDICATION

To my mother and father for their deepest love and unconditional support, and

to my wife, Su Jin Park, for her endless love and help

ACKNOWLEDGEMENTS

My sincere appreciation and thanks go to my committee chair, Dr. Dan G. Zollinger for his great advice and constant support throughout my Ph.D. program. And, I must express my sincere appreciation to Dr. Robert L. Lytton for his noble academic advice and support throughout the course of this research. I also would like to thank Dr. Dallas N. Little and Dr. Mohammed E. Haque for serving on my committee and providing me with comments on my dissertation.

I want to extend my gratitude to all TDR project participants who share their good knowledge with me and to Mr. Praveen Rai for helping me develop the computational program. I will never forget precious and pleasant memories with my friends and colleagues at Texas A&M University.

Last, but definitely not the least, I would like to express my deepest gratitude to my mother and father for their continuous support and love and to my wife for her true love.

TABLE OF CONTENTS

Page

CHAPTER Page

CHAPTER Page

Page

LIST OF FIGURES

Page

Page

Page

LIST OF TABLES

Page

Page

CHAPTER I

INTRODUCTION

BACKGROUND

Almost all engineering and pavement materials are composites, often referred as multiphase materials, such as soil mixture, portland cement concrete, and hot mix asphalt concrete. Each composite material is composed of two or more components for a unique combination of properties. The properties of a composite engineering material obviously depend on physical or chemical properties and volume fraction of an individual component. These properties of each component in composite materials are relatively easy to be identified since a general knowledge on the properties of various constituent materials is available. However, the volume fraction is of a highly irregular nature due to the volumetric content variation of each component during the performance of a composite material. A typical component of interest, for instance, is water.

Water is a critical component contributing to the performance of engineering materials consisting of a soil mixture such as unbound pavement sublayers. Excessive water content in pavement sublayers can weaken the materials and finally reduce pavement service life. The first step for preventing the moisture induced distress is to estimate and monitor the water content in each sublayer. To provide a means for identifying the effect of water in pavement sublayers, the Long Term Pavement Performance (LTPP) Seasonal Monitoring Program (SMP) has monitored water content in unbound base and subgrade materials. In the portland cement concrete, the component of free water also has an important role for the hardening process. During hydration, the free water continually reacts with the compounds of cement and forms chemical bonds from which the concrete gains hardness. In addition, the amount of reacted cement is used as a typical factor to define the degree of hydration. As a result,

---

This dissertation follows the style of the *Journal of Materials in Civil Engineering*.

the quantitative estimate of the volumetric free water or hydrated cement paste content in hydrating concrete may be helpful to understand behavior and properties of early-age concrete.

From the two examples above, it can be noted that the estimate of volume fraction of components can support understanding the behaviors of components in composite materials as well as their bulk properties. To measure the volume fraction, especially of water, different test procedures have been developed based mainly on thermogravimetric and nuclear methods, listed as:

- ASTM D 2216 or AASHTO T 265 Test Methods for Laboratory Determination of Water Content of Soil by Mass
- ASTM D 4643 Standard Test Method for Determination of Water (Moisture) Content of Soil by Microwave Oven Heating
- ASTM D 4959 Standard Test Method for Determination of Water (Moisture) Content of Soil By Direct Heating
- ASTM D 6938 Standard Test Method for In-Place Density and Water Content of Soil and Soil-Aggregate by Nuclear Methods

Although the test methods are widely used to measure laboratory or in-situ water content, they depend on subjective determination and judgment and are time consuming. For those reasons, a more logical approach has been required to measure volume fraction of any types of composite pavement materials. Technology using electromagnetic techniques is one of attractive alternative approaches to determine water content as well as volume fraction. The approach utilizes measured composite dielectric constant in terms of the combination of volume fraction and dielectric constants of constituent materials. While each constituent material has its own intrinsic dielectric constant such as 80 for water, 3-8 for solids, and 1 for air, the composite dielectric constant of their mixture should depend on the volumetric content of each constituent material. Dielectric

constant can be determined from several techniques, typically time domain reflectometry (TDR). In fact, TDR data can be analyzed to determine dielectric constant and other related characteristics. However, it was noted that most existing methods currently used to determine dielectric constant are burdened with systematic errors due to disregarding influences of conductivity and reflectivity that affect the inferred dielectric constant from a TDR trace or electromagnetic data (Lee et al. 2008).

There are two different approaches are used to relate the dielectric constant to volume fraction: one that is empirically based and another that is mechanistically or rationally based. In the empirical approach, formless regression functions are used to relate the composite dielectric constant to the volume fraction of a component usually water content. An early empirical model for a soil mixture was a third degree polynomial developed in 1980 by Topp to determine the volumetric water content based on composite dielectric constant (Topp et al. 1980). Since then many research studies have been conducted to develop empirical models focused on different types of soil. One in particular has been used for the LTPP SMP study to calculate water content in pavement sublayers. However, since the empirical approach is typically valid for only a specific set of circumstances, a consequence is subject to estimated accuracy and applicability.

The other is the mechanistic approach, which relates the composite dielectric constant to the dielectric constants and volume fractions of constituent materials. Various dielectric mixing models based on the mechanistic approach have been developed since a classical binary mixture model for multiphase materials (Maxwell-Garnett 1904). This approach is more reasonable to determine volume fraction because the mixing model can account for the influence of an individual component or composite behavior. However, few mechanistic concepts have developed sufficiently to be used for the analysis of pavement materials. These concepts involve parameters that require definition or calibration relative to the constituent materials. Thus, these mechanistic

concepts require development in order to determine volume fractions of components in multiphase pavement materials.

OBJECTIVE AND SCOPE OF RESEARCH

The use of dielectric properties can provide a reliable nondestructive approach to estimate constituent volume fractions of a multiphase material. Because the composite dielectric constant measured does not provide volumetric contents of components directly, it can be analyzed to determine the final results based on an appropriate methodology. For that reason, various approaches and models have been developed and used to estimate volume fractions of different composite material types; however, several inadequacies and limitations were found concerning the application to pavement materials. Therefore, the main objective of this research is to develop an approach suitable for different multiphase pavement materials. To achieve this objective, the following must be performed:

- A critical review of the standard test methods approaches currently used to determine volume fraction using dielectric constant.
- Develop a mechanistic-based approach which can be applied to multiphase pavement materials.
- Apply the new approach to different pavement materials.
- Compare the results from the new approach to ground truth data or measured laboratory data for the validation of new approach.
- Develop a computational program for automatic implementation of new approach.

In order to address the items described above, a program of work consisting of four parts: 1) literature reviews, 2) approach development, 3) application and validation of new approach, and 4) computational program development. The results of this effort

are presented in the following chapters in terms of the development and results of the research.

In order to provide the sufficient background, Chapter II presents theoretical and technical information through various literature reviews. This chapter provides a basic overview of common and pavement composite materials, a definition of dielectric constant which is a primary focus in the study, and several mathematical dielectric models currently used to analyze multiphase materials. Also, critical and comprehensive reviews of standard test methods and existing approaches were conducted, as a means to facilitate understanding of the need for a new approach to estimate volume fraction of composite materials using component dielectrics.

Chapter III presents a new approach consisting of three steps to estimate volume fractions of components for composite pavement materials. This chapter describes mainly how the new approach was developed, including the self consistent scheme which is a fundamental to the new approach, bounding conditions associated with the self consistent scheme, and the system identification used as a solution methodology to determine model parameters.

The application of the developed approach to verify its viability is presented in the Chapter IV. The verification was performed using two composite materials: one being a soil mixture and the other portland cement concrete mixture. Each component volumetric relationship was incorporated into self consistent modeling frame work where their volume fractions were calculated using the raw data collected from other studies. In addition, the effectiveness of the approach was validated by comparing the results from the new method to those from the laboratory.

Chapter V presents a computer program developed to be used to estimate soil water content based on the new approach. Since the approach executes a loop in the

system identification process, a computer program was required to expedite the calculation process. Thus, this chapter features the program in terms of an algorithm used for calculation step and input and output data tables as well as process of quality check.

Finally, Chapter VI describes the findings and conclusions obtained from the study and suggests recommendations of future research necessary to advance this area of study.

CHAPTER II

LITERATURE REVIEW

COMPOSITE MATERIALS

A composite material is a mixture of two or more constituent materials which have different properties (Hashin 1969a; Mazumdar 2002; Nicholls 1976). The composites include all engineered materials which consist of several constituents having different physical or chemical properties. Most civil engineering materials consist of the composite materials because they require a variety of solid properties to support internal or external loading. Table 2-1 lists the classes of composite materials used in construction.

Table 2-1 Classes of Composite Materials in Construction (Nicholls 1976)

Composite Class	Example
Aggregate-Binder Composite (Bulky Discrete Phases)	- Portland cement concrete - Autoclaved calcium-silicate concrete - Bituminous mixes - Synthetic polymer-aggregate mixes - Rigid foams - Sintered products - Stabilized soils
Fiber-Reinforced Composite (Elongate Discrete Phases)	- Asbestos cement product - Inorganic cement (Portland cement and autoclaved calcium silicates) reinforced with other fibrous materials - Bitumen-aggregate mixes containing fiber reinforcement - Plastic reinforced with glass, asbestos, hemp, or other fiber
Laminate Composite	- Laminated timber and plywoods - Laminated plastic and fiber-reinforced plastics - Structural sandwich panels

A composite material can be defined as a medium which is a mixture of several different media with well-defined interfaces (Hashin 1969a). The composites consist of phases which are regions that are filled by materials of the same physical properties. If a composite is formed, for instance, by reinforcing fibers in a matrix resin, it is a 2-phase material since each of two materials has its own properties. The term "phase" can be described as element, constituent, or component, and "composites" can thus be multiphase materials. Several examples of 2-phase materials are illustrated in Figure 2-1. The type of composites used in this study as pavement materials will be Figure 2-1 (b) 2-phase suspension. In the type of material, one phase is a "matrix" while the other is in the form of "inclusions" which are embedded in the matrix.

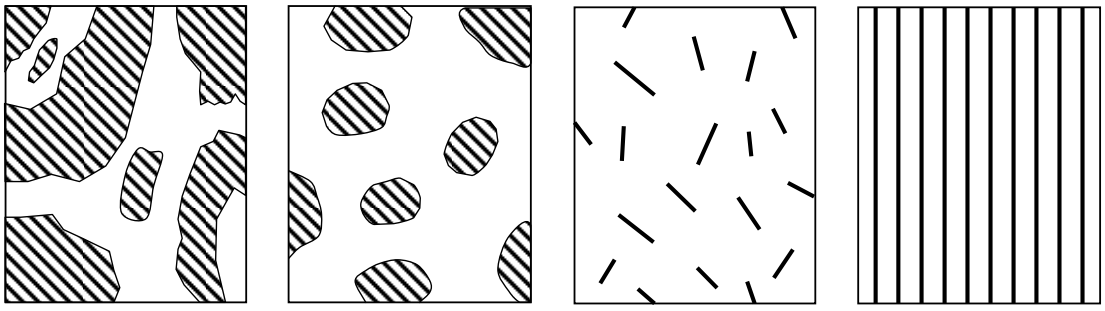

(a) General 2-phase (b) 2-phase suspension (c) short fiber composite (d) Continuous fiber composite

Figure 2-1 Typical types of 2-phase material

Theoretically, the constituents in a composite material maintain their identities or inherent properties (Nicholls 1976). They do not dissolve in another material but are integrated all together in their effect on behavior. However, there is an exception for civil engineering materials, which include portland cement concrete (PCC). PCC is a composite material that consists of cement, water, aggregates, and air. The constituents are mixed together and reacted to produce a hard material through a chemical reaction referred to as hydration (Mindess et al. 2003; Somayaji 2001). Since hydration between hydraulic cement and water forms new compounds having strength-producing properties,

the cement and water constituents in the composite do not maintain their identities before hydration. Therefore, PCC shows different properties of a constituent, portland cement, before and after hydration.

Fundamental Assumptions for Composite Materials

Although the physical properties of each component can be easily identified, it is difficult to identify the component properties in a composite since generally the phase geometry has variable formations (Hashin 1969a; Nielsen 2005). Therefore, in order to analyze composite materials for classifying their properties, two fundamental assumptions are required: homogeneity and isotropy.

The first assumption is homogeneity which refers to the independence of physical properties with respect to position with a given matrix. In the theory of composite material, this assumption can be further elaborated by stating that the contribution of any one part to the behavior of a multiphase material is a function of the statistics of the phase geometry. In short, geometrical bias of one phase does not dominate the behavior of other phases.

Isotropy means that the properties of a composite material are not affected by the orientation of the coordinate system. While the assumption of homogeneity is always used for all composite cases, isotropy can be inappropriate assumption in some cases such as continuous fiber reinforced materials shown in Figure 2-1 (d) (Hashin 1969a). Nevertheless, in this study, both concepts would be used as the fundamental assumptions requiring to measure volume fraction of pavement materials such as soil mixture and PCC.

Composite Pavement Materials

The materials used for pavement layers are composites since roadways should stand against traffic loads and environmental effects leading to internal or external stress: soil mixture, PCC, and hot mix asphalt concrete.

Soil mixture

Soil mixture is defined as all the materials above the bedrock and consists of mineral particles, air, and water (Jackson and Dhir 1983; Somayaji 2001). The material is generally used as a sublayer material in pavement system. As an aggregate composite, the soil mixture is a 3-phase system consisting of solids, water, and air. In fact, the soil mixture was not a manufactured product for use in portland cement or hot mix asphalt concrete. However, it can be defined as a composite material since the constituent materials work together but remain in their original form and maintain their original properties.

In order to develop a theory on the use of the dielectric properties of soil mixtures, soil is assumed to be a dilute suspension of spherical particles. As mentioned above, there are elements playing a role of matrix and spherical particles in composite materials. The soil system may be described by a matrix in which spherical particles having different diameters are imbedded. The air and solid elements play the role of a matrix and spherical particles, respectively. On the other hand, the element of water acts as matrix or particles, which is depend on the degree of saturation. While water element plays a role of matrix in fully saturated soil mixture, air is the matrix in unsaturated soil. Figure 2-2 shows the diagrams comparing multiphase systems of soil mixture relative to the degree of saturation.

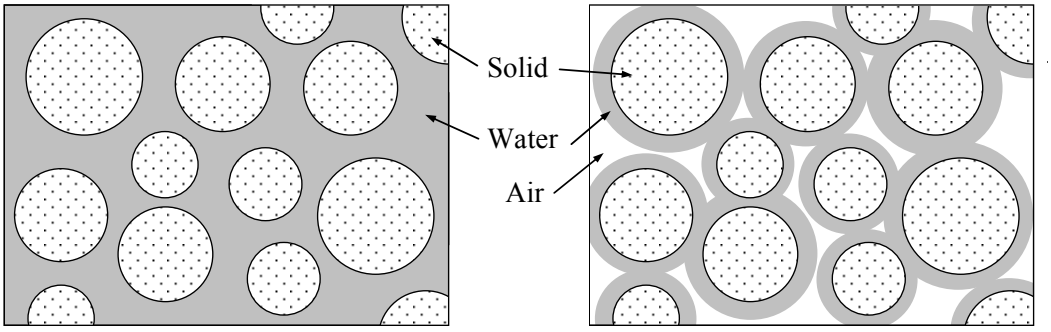

(a) Fully Saturated (a) Unsaturated

Figure 2-2 Multiphase system of soil mixture by saturation

Portland cement concrete

PCC which is an aggregate-binder composite type is a common composite construction material. The term "concrete" refers to a solid mass by binding together aggregate particles using cementitious material. This composite material consists of solid materials embedded in a hard matrix of cement binder that fills the space between the particles and glues them together (Mindess et al. 2003). The binding medium is the product of hydration. Although PCC is a mixture of different raw materials (cement, water, and aggregate), some constituents change due to hydration which is chemical reaction taking place between cement and water. During hydration process, water reacts with the compound of cements and forms a variety of hydrated products over time. Thus, hydration results in the reduction of water content and consequently produces the hydrated products.

While other composites have fixed number of phases in resulting materials, PCC shows a variety of phases (Mehta and Monteiro 2006). Also, the constituent materials, especially portland cement and water, do not remain in their original form. Mixing ingredients together forms a 4-phase system consisting of cement, water, aggregate, and air prior to hydration which is of course involves a chemical reaction between cement and water. However, the number of phases in a PCC mixture during hardening process increases since a certain amount of the single element of portland cement develops into a

hydrated cement product. Therefore, fresh concrete can be generally defined as 5-phase system even though the number of phases depends on several structure models. After hydration, the hardened concrete transforms into 4-phase material where the element of PCC has a totally different chemical and physical makeup compared to fresh concrete. Figure 2-3 shows the schematic diagram for volume change of the constituents in PCC due to hydration process. A detailed structural model for measuring volume fraction of fresh concrete will be further described in Chapter IV.

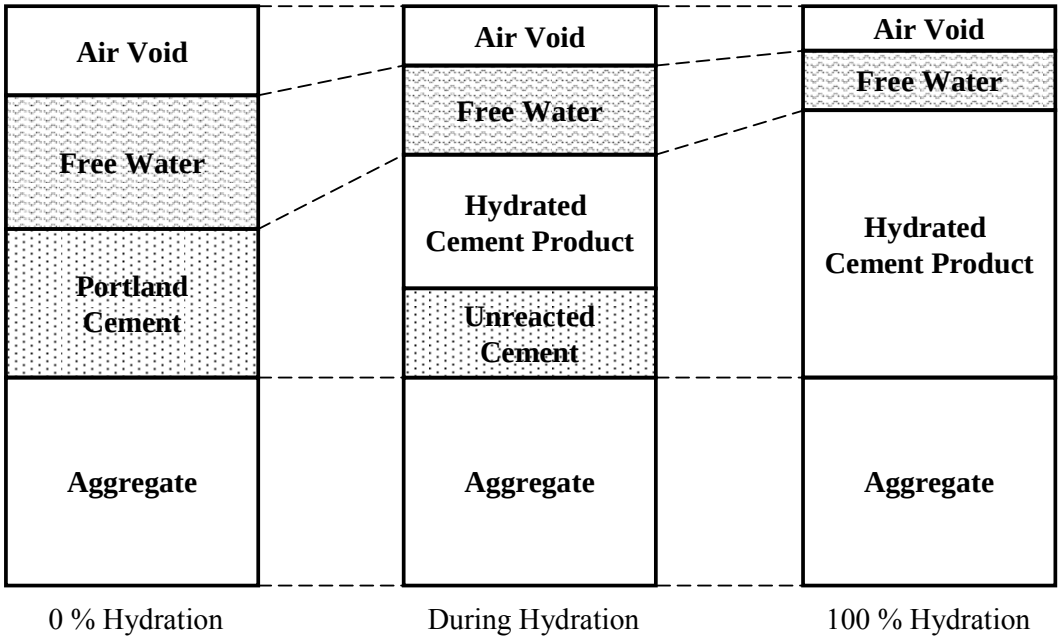

Figure 2-3 Changes of constituents in portland cement concrete by hydration

Hot mix asphalt concrete

Hot Mix Asphalt (HMA) concrete is another aggregate-binder composite material primarily used for flexible pavement system. Similar to PCC, HMA concrete includes asphalt cement to bind together aggregate particles in the composite. The asphalt cement obtained from crude petroleum by distillation is a sticky, semisolid, and highly viscous material in ambient temperature condition. It can be liquefied by heating to allow mixing with aggregates. Being very sticky, the cement adheres to the aggregates

and binds them to form a cemented matrix. After the mixture of cement concrete and aggregate is compacted to increase its strength, HMA concrete turns into strong material which can sustain heavy traffic loads on highway or airport (Roberts et al. 1996).

The main constituent materials of HMA concrete are asphalt binder and aggregate particles. Since the aggregate is heated prior to mixing with the asphalt binder to remove moisture, an HMA concrete mixture can be defined as 3-phase material consisting of asphalt cement, aggregate, and air. In the field in a flexible pavement, the material becomes a 4-phase material with the addition of a water element which might be penetrated into pavement by external effects such as precipitation. Figure 2-4 illustrates the structure of HMA concrete mixture. Typical multiphase systems of all composite pavement materials such as PCC, HMA concrete, and soil mixture are illustrated in Figure 2-5.

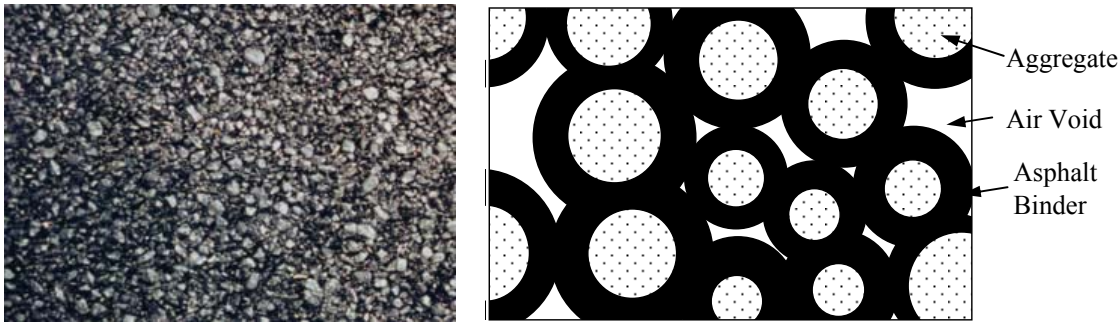

(a) HMA Surface (b) HMA Structure

Figure 2-4 HMA concrete

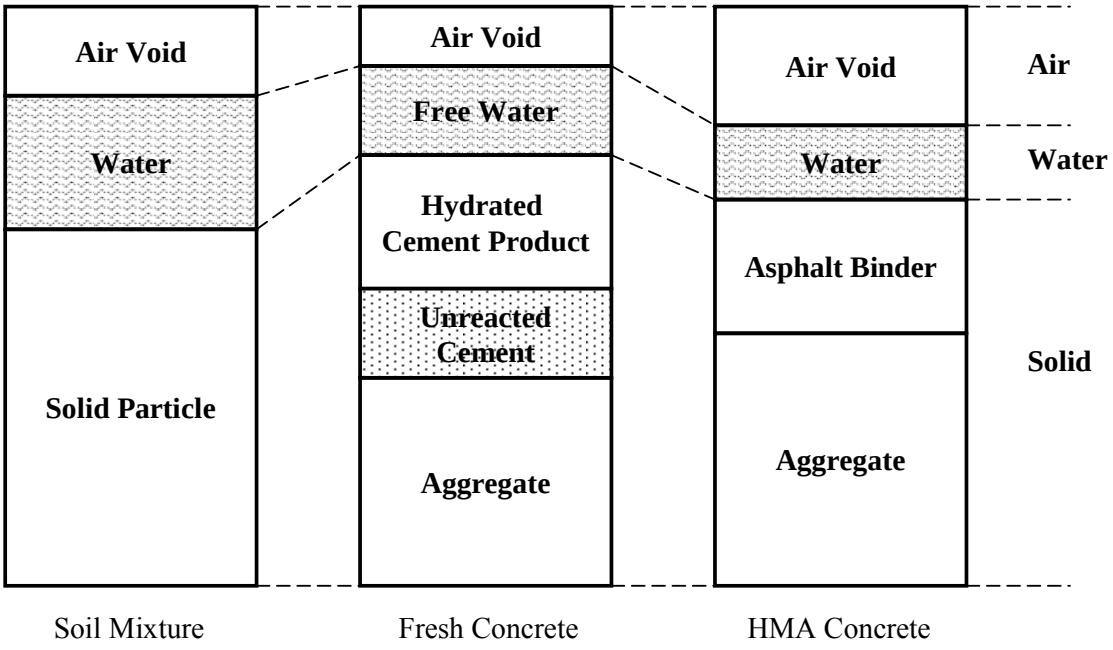

Figure 2-5 Multiphase system of each pavement material

TEST METHODS TO MEASURE VOLUME FRACTION

Composite pavement materials such as aggregate or cement concrete, consist of several components of water, air, and other solids. Among the constituent materials, the water content is a main factor to express different constituent relationships in a given multiphase material and to identify the relationship between behavior and properties of a material. For instance, an increase of moisture in an unbound base course can lower strength, affect pavement response to traffic loading and then reduce service life of pavement. Therefore, several standard test methods have been developed and used to measure moisture content or density of pavement materials. The test methods can be divided mainly into two types: the thermogravimetric and nuclear.

Thermogravimetric Methods

A typical standard test method using heat is designated in the American Society for Testing and Materials (ASTM) D 2216 "Standard Test Methods for Laboratory Determination of Water (Moisture) Content of Soil and Rock by Mass" which is

identical to American Association of State Highway and Transportation Officials (AASHTO) Standard T 265 “Laboratory Determination of Moisture Content of Soils”. For the test method, the water content is defined as the weight of water removed by drying a test specimen in a heating oven (110 ± 5 °C) for a specific time and calculated as (AASHTO 2000; ASTM 2008d):

$$\text{Gravimetric water content (\%)} = \frac{\text{weight of water}}{\text{weight of oven-dry soil}} \times 100 \qquad (2\text{-}1)$$

The weight of soil sample remaining after oven drying is considered as the weight of the solid particles. This method provides relatively accurate results compared with any other thermogravimetric methods but is time-consuming and destructive to the sampled soil. Therefore, it is hard to use this method for repetitive measurements which might be required in the field to monitor the variation of water over time at a given location. This type of test method is currently used as a standard method for measuring water content in soil mixture or aggregate.

The other standard test methods using the thermogravimetric method include ASTM D 4643 “Standard Test Method for Determination of Water (Moisture) Content of Soil by Microwave Oven Heating” and ASTM D 4959 “Standard Test Method for Determination of Water (Moisture) Content of Soil By Direct Heating”. The ASTM D4643 and D4959 are similar to ASTM D2216 but are conducted by incrementally drying of soil sample by a microwave oven or direct heating (hot plate, gas stove, blowtorch, etc), respectively. That is, a moist soil sample is placed in a microwave oven or direct heating apparatus and dried at a set interval until the weight of sample becomes constant within a specified limit of 0.1 percent or less of last two measurements of sample weight. The ASTM D4643 and D4959 test methods can be used instead of ASTM D2216 to produce more rapid results and to minimize the possibility of yielding a higher water content by ASTM D 2216 due to overheating the soil. However, they can

not be used when highly accurate results are required as minor moisture variation will affect the results. In addition, both methods may not be appropriate for repetitive measurements at exactly the same location since they are destructive test methods.

The gravimetric water content determined from the tests should be converted into volumetric content to calculate volume fractions of constituent materials. In order to determine volumetric water content, density or specific gravity of the soil or aggregate mixture is required. The volumetric water content can be expressed in terms of the unit weights (density) of water and solid and the gravimetric water content as:

$$w = \frac{S \cdot e}{G_s} = \theta \frac{\gamma_w}{\gamma_d} \tag{2-2}$$

Thus, Equation (2-4) can be expressed as:

$$\theta = w \frac{\gamma_d}{\gamma_w} \tag{2-3}$$

where

w = gravimetric water content (%)
S = degree of saturation
e = void ratio
G_s = specific gravity
γ_w = unit weight of water (g/cm^3)
γ_d = dry unit weight (density) of soil (g/cm^3)
θ = volumetric water content (%)

Detailed weight-volume relationships of soil mixture consisting of three components will be discussed in Chapter IV. The determinations of density and specific gravity can be conducted through the test methods of ASTM C 127 or AASHTO T 85

for coarse aggregate and ASTM C 128 or AASHTO T 84 for fine aggregate. The Test Method Tex-201-F "Bulk Specific Gravity and Water Absorption of Aggregate" which is a testing procedure published by Texas Department of Transportation (TxDOT) is also used to determine the bulk specific gravity of aggregate. The test methods require the measurement of the weight of the test sample in a saturated surface-dry (SSD) condition since the density and specific gravity of aggregate should be calculated by:

$$\text{Specific gravity} = \frac{A}{B - C} \tag{2-4}$$

$$\text{Dry density } (\text{g/cm}^3) = 0.9975 \times \frac{A}{B - C} \tag{2-5}$$

where

A = weight of oven-dry sample (g)

B = weight of SSD sample (g)

C = weight of saturated sample in water (g)

The SSD condition is defined where the permeable pores of a particle are filled with water but its surface is dry. Care is taken to prepare the sample where only surface water on sample is removed after submerging in water for a period of 24 ± 4 hours. However, the test procedures to determine the SSD condition of an aggregate sample are based on subjective determination (Krugler et al. 1992). ASTM C 127 and AASHTO T 85 depend on technician judgment and visual identification to determine the SSD point as defined in the test procedure:

"Remove the test sample from the water and roll the sample in a large absorbent cloth until all visible films of water are removed(AASHTO 2004b; ASTM 2008b)."

ASTM C 128 and AASHTO T 84 employ the slump test of a tamped cone to determine the SSD condition of fine aggregate. However, the procedure is vague as to where the SSD point is and also dependent upon the technician judgment as follows:

"If the surface moisture is still present, the fine aggregate will retain the molded shape. Slight slumping of the molded fine aggregate indicates that it has reached a surface-dry condition (AASHTO 2004a; ASTM 2008c)"

In addition, Test Method Tex-201-F for determining the SSD point of aggregate relies on the visual judgment by color defined in the test procedure as:

"
- **Compare the color of the two samples, while continuing the drying process.**
- **The surface dry condition is met when the test sample has the same color as the dry comparison sample.**
- **It is sometimes necessary to stand back several meters (feet) when comparing the samples to see slight differences in color. (TxDOT 2005)"**

These subjective measures for identifying the SSD condition can produce less accurate estimate of water content which is the most significant factor to estimate volume fraction of components in a multiphase material.

Nuclear Methods

Another widely used technique for repetitive in-situ measurement of water content and density is the nuclear method. This test method described in ASTM D 6938 "Standard Test Method for In-Place Density and Water Content of Soil and Soil-Aggregate by Nuclear Methods" can be used for nondestructive measurement of in-situ density and water content in a soil mixture. Nuclear device employs the interaction of gamma radiation to measure density of soil or soil-aggregate. The density of material is measured by counting the number of photons emitted from a source at a detector in the

equipment, based on two methods: direct transmission and backscatter methods (ASTM 2008a). In the direct transmission method, the source rod is placed at a depth up to 12 in. in material being tested and the detector is on the surface. The detector counts the number of gamma photons from the source rod, travelling through the material and colliding with electrons in the material, as seen in Figure 2-6 (a). Since the collisions reduce the number of photons that reach the detector, the density of material can be calculated. In the backscatter method, where the source and detector are on the surface of material, photons emitted from the source penetrate the material and the detector measures the number of scattered photons as shown in Figure 2-6 (b). The fewer the photons reaching the detector, the higher the density of the material (Troxler 2006).

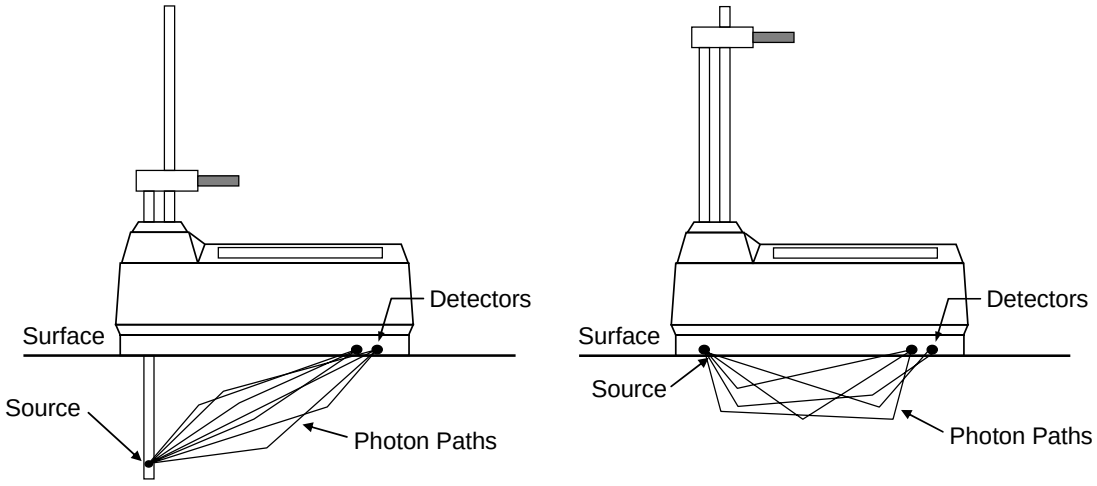

(a) Direct transmission method (b) Backscatter method

Figure 2-6 Principles of nuclear device (Troxler 2006)

Moisture content is determined in the same way of the backscatter method in density measurement. The nuclear device uses a neutron source to measure hydrogen (water) content of a material instead. Fast neutrons emitted from the source penetrate the material and are thermalized. The thermalization occurs when the fast neutrons from the source are slowed to velocities where additional collisions with hydrogen will not further slow the neutrons (Troxler 2006). Since the detector is sensitive to thermalized

or slow neutrons, the counts obtained is used for determining the hydrogen (moisture) content of the material. That is, as the moisture content increases, the neutrons are thermalized at a higher rate and so the moisture count at the detector increases. Figure 2-7 shows a nuclear device for water content and density measurement in the field.

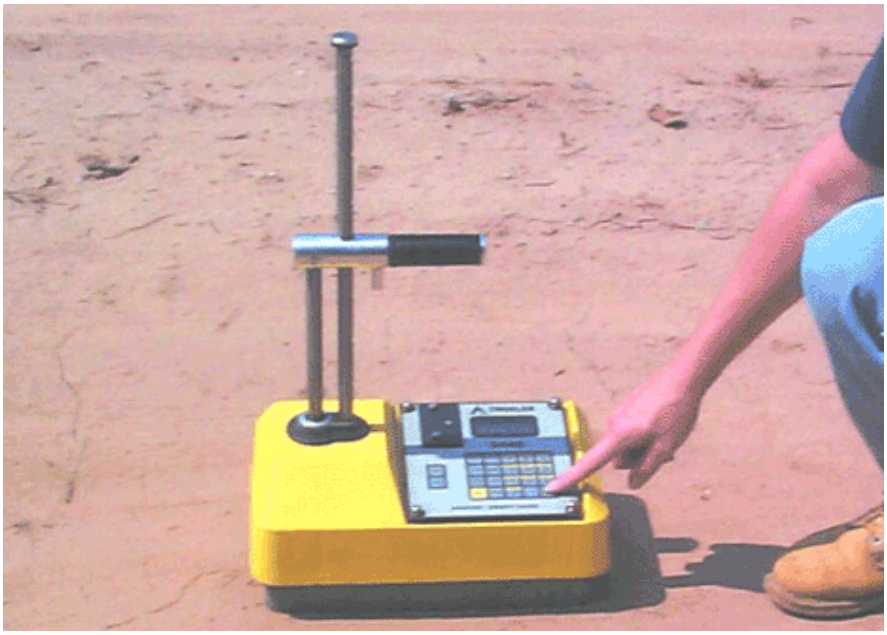

Figure 2-7 Nuclear device in the field (Barry et al. 2006)

As compared with the thermogravimetric methods, it provides relatively fast results without any additional tests such as the determinations of sample weights in different conditions. In addition, the use of the nuclear method makes it possible to measure water content repetitively at the same location. However, the method requires highly trained operators and extensive safety precautions due to a radiation hazard. Most of all, the major disadvantage of the technique is site-specific calibration is usually required since the signal is relatively sensitive to factors other than water content in soil (Roth et al. 1990).

OVERVIEW OF DIELECTRIC CONSTANT

In the approach of electrics, material can be divided into conductor and dielectric material. Whereas a conductor is a material capable of transmitting electric current, such as copper or aluminum, dielectric material is a non-conducting material or insulator that does not conduct electric current but can sustain an electric field. Dielectric materials can be solids, liquids, or even gases. Almost all construction materials are included in solid dielectrics such as soil, cement, glass, or plastic.

Complex Permittivity

The parameters of interest for dielectric materials can be described with respect to electromagnetic fields. The electromagnetic field defined as a physical field produced by electrically charged objects is concerned with four vector quantities as;

(1) Electric flux density, D (coulombs/square meter, C/m^2)
(2) Electric field strength, E (volts/meter, V/m)
(3) Magnetic flux density, B (webers/square meter, W/m^2)
(4) Magnetic field strength, H (amperes/meter, A/m)

Two electromagnetic properties show the interaction of a material with electric and magnetic fields: complex permittivity and complex magnetic permeability. Along with the four quantities (E, D, B, and H), the two properties can be characterized by the constitutive relations as (Shen and Kong 1995):

$$D = \varepsilon E \text{ (definition of permittivity)} \quad (2\text{-}6)$$

$$B = \mu H \text{ (definition of permeability)} \quad (2\text{-}7)$$

where

μ = permeability (henry/meter, H/m)
ε = complex permittivity (farad/meter, F/m)

For most dielectric materials such as soils and concrete, the effect of magnetic permeability is negligible since they are nonmagnetic as the magnetic permeability is the same as the permeability of free space:

$$\mu = \mu_0 = 4\pi \times 10^{-7} \text{ H/m} \tag{2-8}$$

where

μ_0 = permeability of free space

Therefore, the dielectric materials can be described only by the complex permittivity of materials since consideration of magnetic permeability is not feasible. In dielectric materials, there is a physical separation between positively and negatively charged entities on an atomic level (metallic/covalent bond). Because the charges are bound by atomic forces, they can not travel. However, when an electric field is applied, the bound positive and negative entities can shift their positions. This shift of their positions allows a dielectric material to store energy as potential energy. This ability to store energy when an electric field is applied is called polarization (Diefenderfer 2002). Thus, the constitutive relation, Equation (2-6), describing the electromagnetic response of a dielectric material can be expressed as:

$$D = \varepsilon_0 E + P \tag{2-9}$$

where

ε_0 = permittivity of free space (8.854×10^{-12} F/m)

E = applied electric field strength (V/m)

P = induced polarization

When the electric field is applied to homogeneous and isotropic material, the induced polarization is proportional to the applied field as (Lin 1999; TransTech System 2003):

$$P = \chi_e \varepsilon_0 E \tag{2-10}$$

where

χ_e = dimensionless electric susceptibility

The electric susceptibility of dielectric materials describes how easily it polarizes in response to an electric field. The susceptibility of a material is related to its permittivity relative to the permittivity of free spaces as:

$$\chi_e = \frac{\varepsilon}{\varepsilon_0} - 1 = \varepsilon_r - 1 \tag{2-11}$$

where

ε = complex permittivity of material

ε_r = relative complex permittivity or dielectric constant

It is noted that the electric susceptibility (χ_e) is zero for free space or vacuum because the polarization does not occur due to non-bound charges in free space. Thus, relative complex permittivity of air is approximately equal to 1.0. From Equation (2-9) and (2-11), the electric flux density is obtained as follows:

$$D = \varepsilon_0 \left(1 + \chi_e\right) E = \varepsilon_0 \varepsilon_r E \tag{2-12}$$

Relative Complex Permittivity (Dielectric Constant)

In order to quantify the ability of a material to polarize relative to free space, a relative permittivity is used usually (Lin 1999). The dielectric characteristics of a material can be expressed by a complex permittivity having real and imaginary components as follows:

$$\varepsilon = \varepsilon' - j\varepsilon'' \tag{2-13}$$

where

ε' = real part of complex permittivity

ε'' = imaginary part of complex permittivity

j = $\sqrt{-1}$

The real part of the complex permittivity indicates how much electric energy is stored in a material when an external electric field (voltage) is applied to it; that is, a given material with high permittivity can store more charge than a material with lower permittivity. The imaginary part indicates how much electric energy is lost when an external electric field is applied, which represents attenuation and dispersion. By dividing each side of Equation (2-13) by the permittivity of free space, ε_0, the dimensionless quantities are obtained as:

$$\frac{\varepsilon}{\varepsilon_0} = \frac{\varepsilon'}{\varepsilon_0} - j\frac{\varepsilon''}{\varepsilon_0} \tag{2-14}$$

or

$$\varepsilon_r = \varepsilon_r' - j\varepsilon_r'' \tag{2-15}$$

where

ε_r' = real part of relative complex permittivity

ε_r'' = imaginary part of relative complex permittivity

The relative complex permittivity or dielectric constant in Equation (2-15) can be expressed adding the conductivity of a dielectric material to the loss of external electric fields as follows:

$$\varepsilon = \varepsilon_r' - j\left(\varepsilon'' + \frac{\sigma}{\omega\varepsilon_0}\right) \tag{2-16}$$

where

σ = dielectric conductivity (Siemens/meter, S/m)

ω = angular frequency (rad/sec)

The term $\sigma/\omega\varepsilon_0$ indicates a characteristic of a material containing free electrons and represents the loss of electric field due to conductivity which describes the ability of a material to transmit electrical current (Ledieu et al. 1986). If the conductivity of a material is low (< 0.1 S/m), the loss term can be negligible. Thus, sometimes, the real part of the relative complex permittivity is simply referred to as the dielectric constant. However, as will be discussed in Chapter IV, the consideration of conductivity results in more accurate dielectric constant (relative complex permittivity) of a material. In this study, the term "dielectric constant" will be used instead of the term "relative complex permittivity", and the term "relative" is dropped from the definition as in engineering practice (Avelar Lezama 2005). Table 2-2 lists the dielectric constant values of some materials found in pavement layers.

Table 2-2 Typical Dielectric Constant of Materials (Daniels 1996; Davis and Annan 1989)

Material	Dielectric Constant	Material	Dielectric Constant
Water	79 – 81	Silt	4 – 8
Granite	4 – 6	Clay	2 – 6
Limestone	4 – 8	Air	1
Sand	3 – 6	Ice	3 – 4

The devices for quantifying dielectric constants of materials, such as TDR, GPR or Percometer, employ a technique that measures behavior of electromagnetic wave applied in materials. The propagation velocity of electromagnetic waves in a composite material is a function of the composite dielectric constant of the material in which the wave is propagating. Due to high dielectric constant value of water in comparison to other constituent materials, the response of electromagnetic wave applied to multiphase materials is a function of volumetric water content. Therefore, the dielectric constant can be a key parameter to estimate water content as well as volume fractions of other components in a multiphase material.

MEASUREMENT OF DIELECTRIC CONSTANT

As described previously, the dielectric constant is a key parameter to estimate water content in a multiphase material due to the magnitude of dielectric constant value of water in comparison to any other constituent material. Therefore, the measurement of dielectric constant of a composite material may be the first step to estimate water content in the composite. Although a number of devices have been applied to measure dielectric constants of pavement materials, three kinds of devices are mainly used in the field: time domain reflectometry, percometer, and ground penetrating radar.

Time Domain Reflectometry

Time Domain Reflectometry (TDR) equipment was originally developed for measuring electromagnetic wave travel times to detect breaks or shorts in electrical conductors. Subsequently, it was adapted to collect sufficient data to allow for the water content to be estimated. The use of TDR technique to measure in-situ water content was introduced in 1975 (Davis and Chudobiak 1975; Diefenderfer et al. 2000). The TDR system records an electromagnetic waveform that can be analyzed as it is transmitted and reflected to characterize the nature of objects which reflect the waves. The waveform pulse is transmitted along a coaxial metallic cable which acts as a waveguide at a velocity that is influenced by the dielectric constant of material surrounding the conductors. Changes in dielectric constant of the surrounding material occur as its moisture content or conductivity (the reciprocal of resistance) changes. Signal reflectivity also varies (from 1 to -1) as a function of the degree of open to short circuitry, respectively, and exists in the wave reflections as evidenced by slope changes in the return wave pulse recorded by the TDR readout unit (Rada et al. 1995).

TDR measurement in LTPP SMP

Although there are several TDR systems in accordance with the number of rods in the probe, TDR with three-rod probe is mainly used to estimate in-situ water content and especially, to monitor subsurface water conditions in pavement structure by Long Term Pavement Performance (LTPP) program's Seasonal Monitoring Program (SMP). The LTPP SMP was initiated to understand the environmental factors and effects on pavement performance in 1992, including 64 LTPP sections. As a part of the program, TDR have been used to monitor water content in pavement sublayers. Figure 2-8 presents the TDR probe developed and fabricated by FHWA for use in the SMP. The center conductor in coaxial cable is connected to the center of the three stainless steel rods which are inserted horizontally into the sublayer at the point of monitoring. The outer shield of coaxial cable is connected to the two outer rods. The recorded TDR signal rises to a peak (initial inflection point) as the electromagnetic wave enters the

probe rods, followed by a fall in the return signal to a fianl inflection point as the wave hits the end of the probes as illustrated in Figure 2-9. Figure 2-10 present a typical TDR trace obtained from a soil mixture. The distance between the initial inflection point (Point D_l) and final inflection point (Point D_2) is known as the "apparent" length of the probe, L_a (Rada et al. 1995; Zollinger et al. 2008).

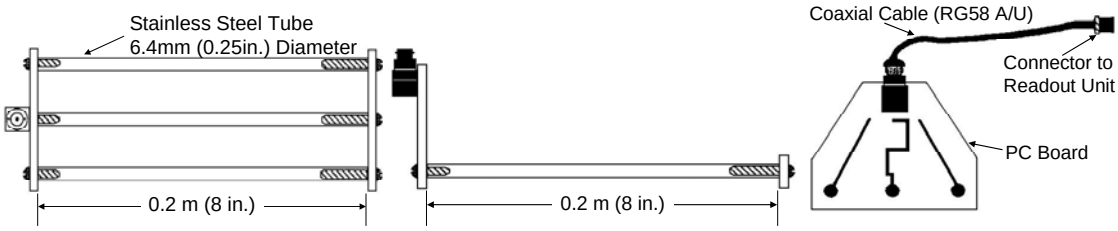

(a) Top View (b) Side View (c) End View

Figure 2-8 TDR probe of FHWA (Lee et al. 2008)

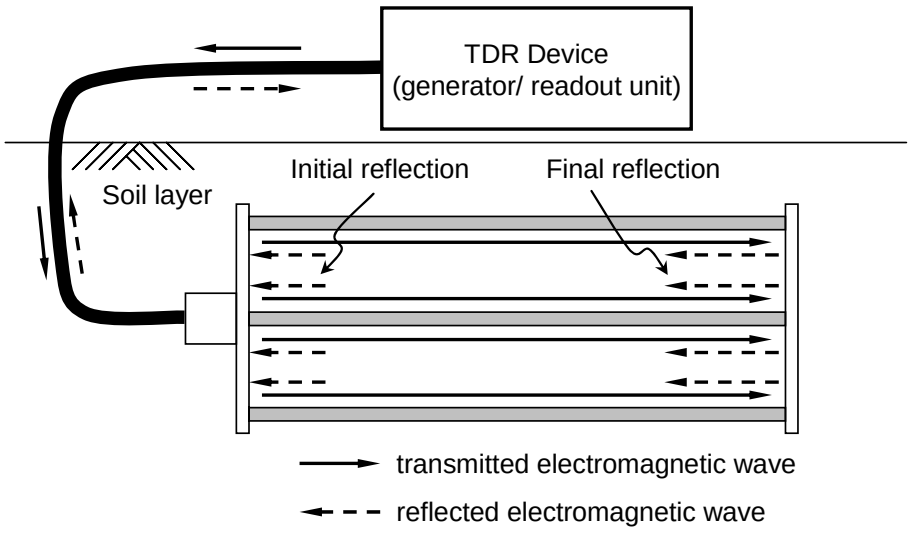

Figure 2-9 TDR system in soil layer

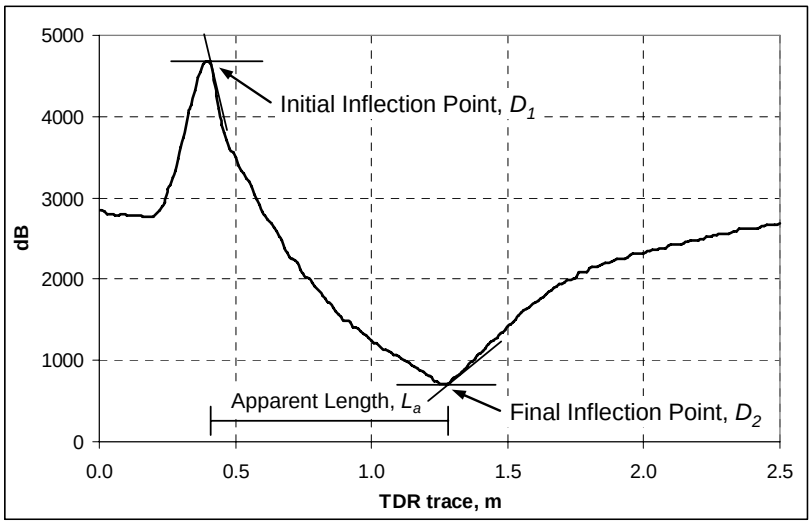

Figure 2-10 Typical TDR trace (Lee et al. 2008)

Ten TDR probes have been used to measure in-situ dielectrics of different pavement sublayers at SMP test sections, which were placed in one hole located in the outer wheel path. At most sites, the TDR installation hole was located at approximately 0.76 m (2.5 ft) from the outside edge of the white stripe and at least 1.2 m (4 ft) away from joints and/or cracks to avoid unrepresentative surface moisture infiltration (Rada et al. 1995). Figure 2-11 provides a schematic of the TDR instrumentation.

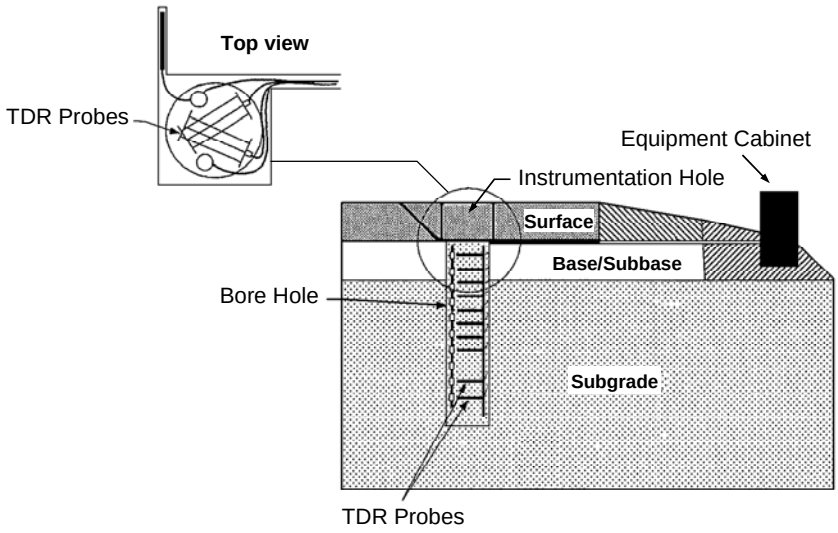

Figure 2-11 Illustration of instrumental installation (Rada et al. 1995)

The TDR probes were placed at specified depths according to the type of sublayer and its thickness. If the top granular base (or subbase) layer was greater than 305 mm (12 in), the first TDR probe was placed 152 mm (6 in) below the surface layer and/or bottom of the lowest stabilized layer; otherwise, the probe was placed at mid depth of the top granular base (or subbase) layer. The next seven TDR probes were placed at 152 mm (6 in) intervals and the last two probes were placed at 305 mm (12 in) intervals (Rada et al. 1995).

Interpretation of TDR Trace

The waveform obtained from the TDR sensor must be analyzed to determine the in-situ dielectric constant. Existing procedures for the interpretation of TDR data have included determining the apparent length so as to compute the dielectric constant of the material surrounding the TDR probe. The initial inflection point is located where the signal enters the probe rods while the final inflection point occurs at the end of the probes. Both are displayed in the TDR readout device. The distance between the inflection points is the apparent length value used to determine the dielectric constant of surrounding material. The apparent length value can be determined using a variety of methods.

Klemunes studied ways to find the most accurate methodology to determine the apparent length of the TDR signal response (Klemunes 1995). The study investigated and compared five methods: (1) Method of Tangents, (2) Method of Peaks, (3) Method of Diverging Lines, (4) Alternate Method of Tangents, and the (5) Campbell Scientific Method. Differences among the methods are centered on the procedure of locating the initial and final inflection points of the TDR trace. From the study, the method of tangents was found to be the most accurate while the least accurate methods are the alternate method of tangents and the method of diverging lines. The method of tangents employs the tangent lines at the local values of the TDR traces to isolate the inflection

points. The initial inflection point is located at the intersection of the horizontal and negatively sloped tangents (i.e. local maximum) of the TDR trace and the final inflection point is at the intersection of the horizontal and positively sloped tangents (i.e. local minimum) as shown in Figure 2-12 (a). However, the method can not be applied to very dry or partially frozen soils, so that the method of peaks is used for those soil type situations (Klemunes 1998). In the method of peaks, the initial inflection point is determined by locating the intersection of the tangents drawn on both sides of the maximum point and the final inflection point is at the intersection of the tangents drawn of both sides of the minimum point as shown in Figure 2-12 (b).

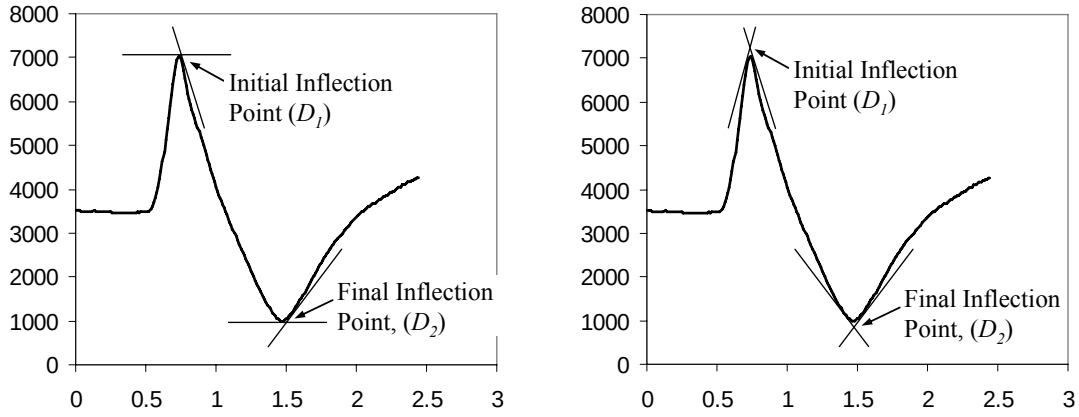

(a) Method of tangents (b) Method of peaks

Figure 2-12 Trace interpretation methods (Lee et al. 2006)

Computation of Dielectric Constant

To measure dielectric constant using TDR device, an electromagnetic signal is transmitted along the TDR probes in a given material. When the signal reaches the end of the probe, it is reflected back to the data acquisition unit and the reflected signal is recorded. The velocity of the reflected electromagnetic wave in the probe can be expressed with the travel time and the length of probe as:

$$c = \frac{2L}{\Delta t} \tag{2-17}$$

where

c = velocity of electromagnetic wave

L = actual length of TDR probe

Δt = the travel time of the TDR signal

As well, the electromagnetic wave velocity in the probe depends on the dielectric constant and magnetic permeability of the surrounding material (relative to the speed of light in a vacuum) and can be expressed as (Dalton et al. 1984; Roth et al. 1990):

$$c = \frac{1}{\sqrt{\varepsilon\mu}} c_0 \tag{2-18}$$

where

ε = dielectric constant of material

μ = relative magnetic permeability of material

c_0 = speed of light in vacuum

Assuming the effects of ferromagnetic components in soils are not significant, the magnetic permeability of soil can be set to unity ($\mu = 1$) (Topp et al. 1980). Thus, the relative dielectric constant can be defined from Equation (2-17) and (2-18) as:

$$\varepsilon = \left(\frac{\Delta t \cdot c_0}{2L} \right)^2 \tag{2-19}$$

The travel time of the signal is also dependent on the dielectric constant which includes signal propagation in material surrounding TDR probe; hence, the apparent

probe length can be determined by the travel time of the signal if it were propagating at the speed of light:

$$L_a = \frac{\Delta t \cdot c_0}{2} \tag{2-20}$$

where

L_a = apparent length of probe (m)

Consequently, the dielectric constant of material can be expressed as the ratio of apparent length to actual length of TDR probe from Equation (2-19) and (2-20):

$$\varepsilon = \left(\frac{L_a}{L} \right)^2 \tag{2-21}$$

In the application of TDR method for LTPP SMP sites, the dielectric constant can be computed with the phase velocity considering the propagation as follows (Klemunes 1995):

$$\varepsilon = \left(\frac{L_a}{L \cdot V_p} \right)^2 = \left(\frac{D_2 - D_1}{L \cdot V_p} \right)^2 \tag{2-22}$$

where

L = actual length of TDR probe (m, e.g. 0.203 m for FHWA probe)

V_p = phase velocity setting on TDR cable tester (usually 0.99); this is the ratio of the actual propagation velocity to the speed of light.

In short, the dielectric constant is derived from the relationship between the speed of light and the velocity of wave delayed due to the wave propagation caused by dielectric properties of the material surrounding the TDR probe.

Percometer

Adek™ Percomenter is one of several instruments to measure immediately dielectric properties of materials as shown in Figure 2-13 (a). The measurement with Percometer makes it possible to obtain quick dielectric constant and conductivity of dielectric materials. It is noted that Percometer is used to measures dielectric constant based on evaluating the change in the electrical capacity of the probe (electrode) attributable to the influence of surrounding materials on 40~50 MHz. The dielectric constant measured by Percometer is the real part of the complex relative dielectric permittivity (Schmidtgen 2009).

As shown in Figure 2-13 (b), the Percometer has two basic probe types: the surface probe and the tube probe. The surface probe, with sensor diameter 60 mm, was designed to measure the dielectric constant and conductivity on the surface of materials such as aggregate or concrete samples. The effective penetration depth of surface probe is 2~3 cm, which depends on the medium. The tube probe was designed to be inserted into soft material samples such as soil or subgrade materials. As suggested by the manufacturer, the tube probe should be inserted at least 10 cm depth to obtain relatively accurate measurements (Adek 2009). Table 2-3 presents the specification and description of Percometer by the types of probe.

(a) Percometer with surface probe (b) Surface and tube probes

Figure 2-13 Percometer and probes (Adek 2009)

Table 2-3 Specification of Percometer by Probe Types (Adek 2009)

Probe Type	Sensor Size	Measurement Range		Accuracy	Recommended Application
		Dielectrics Constant	Productivity (μS/m)		
Surface Probe	D = 6 cm	1 ~ 32	0 ~ 2000	±0.10+1 %	Laboratory use, Tube suction test
Tube Probe	L = 18 cm	1 ~ 81	0 ~ 1000	±0.25+2 %	Laboratory test
	L = 100cm	1 ~ 15	0 ~ 1000	±0.05+1 %	Field test of low D.C. material

Ground Penetrating Radar

Ground Penetrating Radar (GPR) can be defined as a geophysical technique based on the electromagnetic waves transmitted into the material instead of acoustic wave which is used in the seismic reflection technique. By analyzing the transmitted and reflected electromagnetic signal waves at each layer-layer interface, the GPR system can determine thickness as well as dielectric properties of each pavement layer (Davis and Annan 1989; Maser 2000; Weiler et al. 1998).

The GPR system, as shown in Figure 2-14, mainly consists of four parts: a transmitter to generate electromagnetic signal, an antenna to propagate and receive the signal, a receiver to capture and amplify a reflected signal, and a processor to process the reflected signal. The transmitter in a GPR system generates a short pulse of a high frequency (10-1000 MHz) electromagnetic signal. The pulse leaving the antenna becomes a transmitted signal and travels through the pavement surface. As the transmitted signal (A_0) continues to propagate into the pavement layers, the process of signal transmission and reflection is repeated at each layer-layer interface due to the difference of layer's electromagnetic properties such as dielectric constant. As illustrated in Figure 2-14, the reflected signals (A_1, A_2, A_3) are the pulses reflected from

the surface and the top of base and subgrade, respectively (Lytton 1995). The amplitudes returned to the receiver and the time delays (Δt_i) between reflections are used to calculate the thickness (d_i) and dielectric constant (ε_i) of each pavement layer. A layer with higher water content will cause an increase in the wave amplitude reflected from the top of the layer since the composite dielectric constant of the layer increases. On the other hand, if the amounts of air void increase then the wave reflected will decrease due to lower dielectric constant of the layer (Liu and Scullion 2009).

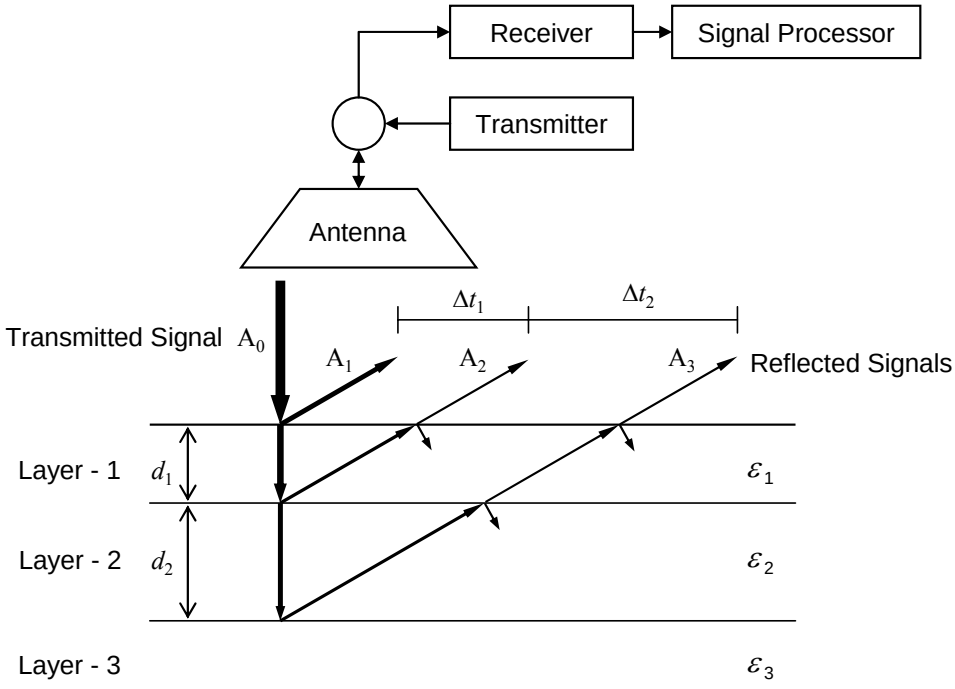

Figure 2-14 Principle of ground penetrating radar (Lytton 1995)

Conventional GPR has been used as a tool to detect buried objects under ground or to digitize images of a reflected radar signal from each layer in a pavement system. However, by an inverse analysis technique, the use of GPR makes it possible to determine the composition of each pavement layer as well as to measure air voids, asphalt content, water content, and thickness in pavement layers (Lytton 2000). Also, the GPR unit developed lately in Texas Transportation Institute (TTI) can not only

collect data at highway speeds (60 mph) but also find surface distress by video image and obtain test location by Global Positioning System (GPS) (Liu and Scullion 2009). The TTI's GPR vehicle is shown in Figure 2-15.

Figure 2-15 TTI's GPR vehicle with digital camera and GPS (Liu and Scullion 2009)

MATHEMATICAL DIELECTRIC CONSTANT MODELS

A number of mathematical models have been developed to account for the relationship between composite dielectric constant and physical properties such as volume fraction of elements in a multiphase material. The relationship can be described either by an empirical approach deriving a regression model from experimental results or by a mechanistic approach taking dielectrics constant and volume fractions of constituent materials into account.

Empirical Approach

A relatively simple approach to establish the relationship between dielectric constant and volumetric water content would be empirical modeling. The empirical models can be developed by regression analysis using dielectric constant and water content data

produced by experiment or observation. Several types of models have been developed based on the empirical approach depending on form or parameters of each model.

Polynomial and square root models

Empirical models were developed for estimating water content in a soil mixture through dielectric constants obtained from TDR (Dalton et al. 1984; Dasberg and Hopmans 1992; Nadler et al. 1991; Topp et al. 1982a; Topp et al. 1982b; Topp et al. 1980). The first empirical model developed for the relationship was Topp's equation. The model employs third-order polynomial model regression function to relate the dielectric constant to the volumetric water content in a soil (Topp et al. 1980):

$$\theta = -5.30 + 2.92\varepsilon - 0.055\varepsilon^2 + 0.00043\varepsilon^3 \quad (2\text{-}23)$$

where

θ = volumetric water content (%)

ε = dielectric constant of soil mixture

Topp's empirical function is valid for four soils ranging from a sandy loam to heavy clays and fits a range of soils which have an average bulk density ranging from 1.3 to 1.4 g/cm^3 and water content ranging from 10 to 50 percent. The model is widely used for calculating water contents of soils, but the accuracy is not always good for soils out of those ranges (Dirksen and Dasberg 1993; Jacobsen and Schjønning 1995; Weitz et al. 1997).

Nadler developed another empirical third-order polynomial model with different types of soil (Nadler et al. 1991):

$$\theta = -7.25 + 3.67\varepsilon - 0.123\varepsilon^2 + 0.0015\varepsilon^3 \quad (2\text{-}24)$$

This is an empirically derived model which fits silty loam that has water content ranging from 7 to 28 percent. Also, the soils used for laboratory test were wetted with either distilled water or NaCl or $CaCl_2$ to figure out the influence of soil salt concentration (Nadler et al. 1991).

Baran suggested that Topp's equation was valid for the compacted crushed gravel and the clay subgrade materials that their dry densities are 1.5 g/cm^3 and 1.85 g/cm^3, respectively. However, since he found that the Topp's equation can not be used for crushed stone materials having high densities, the following equation was suggested for dense paving materials (Baran 1994);

$$\theta = -6.216 + 2.383\varepsilon - 0.0598\varepsilon^2 + 0.0006\varepsilon^3 \quad (2\text{-}25)$$

Another type of empirical model is a calibration functions with a linear dependency between water content and square root of dielectric constant ($\sqrt{\varepsilon}$). This square root function of empirical model was first suggested by Ledieu et al. in 1986 (Ledieu et al. 1986). The model was developed using soils (loam) which have water contents between 10.5 percent and 36.5 percent and bulk densities between 1.38 and 1.78 g/cm^3;

$$\theta = 11.38\sqrt{\varepsilon} - 17.58 \quad (2\text{-}26)$$

If the bulk density is considered, Equation (2-26) is expressed as follows;

$$\theta = 11.38\sqrt{\varepsilon} - 3.38\rho_b - 15.29 \quad (2\text{-}27)$$

where

ρ_b = bulk density of soil (g/cm^3)

Besides those models described above, many other calibrations using third-order polynomial and square root functions have been established for specific soils or groups of soil types. Table 2-4 lists the two types of empirical equation developed based on different types of soils.

Table 2-4 Empirical Third-Order Polynomial Models

Type	Source	Formula for Water Content (%)	Soil Types
Third-order polynomial equation	Topp et al. (1980)	$\theta = -5.30 + 2.92\varepsilon - 0.055\varepsilon^2 + 0.00043\varepsilon^3$	mineral soils
	Nadler et al. (1991)	$\theta = -7.25 + 3.67\varepsilon - 0.123\varepsilon^2 + 0.00150\varepsilon^3$	silty loam
	Roth et al. (1992)	$\theta = -7.28 + 4.48\varepsilon - 0.195\varepsilon^2 + 0.00361\ \varepsilon^3$	mineral soils
		$\theta = -2.33 + 2.85\varepsilon - 0.043\varepsilon^2 + 0.00030\varepsilon^3$	organic soils
	Dasberg et al. (1992)	$\theta = -7.51 + 4.24\varepsilon - 0.185\varepsilon^2 + 0.00380\varepsilon^3$	sandy loam
		$\theta = -10.96 + 5.81\varepsilon - 0.227\varepsilon^2 + 0.00320\varepsilon^3$	clay loam
	Jacobsen et al. (1993)	$\theta = -7.01 + 3.47\varepsilon - 0.116\varepsilon^2 + 0.00180\varepsilon^3$	mineral soils
	Baran (1994)	$\theta = -6.22 + 2.38\varepsilon - 0.0598\varepsilon^2 + 0.00060\varepsilon^3$	mineral soils
Square root equation	Ledieu et al. (1986)	$\theta = 11.38\sqrt{\varepsilon} - 17.58$ $\theta = 11.38\sqrt{\varepsilon} - 3.38\rho_b - 15.29$	mineral soils
	Malicki et al. (Malicki et al. 1996)	$\theta = \frac{\sqrt{\varepsilon} - 0.819 - 0.168\rho_b - 0.159\rho_b^2}{7.17 + 1.18\rho_b}$	mineral soils
	Herkelrath et al.(Herkelrath et al. 1991) (Jacobsen and Schjønning 1995)	$\theta = 12.73\sqrt{\varepsilon} - 5.1$	organic soil

Klemunes model

Klemunes developed an improved empirical model using soil samples obtained from 28 LTPP sites. Water content in this model should be calculated based on apparent length which can be determined from trace of TDR signal instead of dielectric constant. The

TDR traces were obtained from the soil samples prepared at various combinations of water content and compaction levels. The water content and dry density of each combination was determined by laboratory testing after the TDR trace was obtained. A total of 415 data points were obtained; however, outliers and TDR traces that were impossible to interpret were removed from the dataset. Consequently, 397 data points were available and used to develop Klemunes' models which employ a hierarchal methodology (i.e. level 1 to level 4) relative to the level of information available and the desired accuracy (Klemunes 1995; Klemunes 1998).

At level 1, the water content would be determined without any information about the properties of the soil, such as coarse/fine-grained or AASHTO system of soil classification. Therefore, level 1 has the lowest explained variance and the highest standard error. At level 2, water content is determined on the basis of the soil being identified as either coarse or fine-grained. The accuracy of this level is better than that of level 1. At level 3, the volumetric water content is based on the AASHTO classification, accounting for the soil's gradation and the characteristics of fraction passing sieve No.40.

The most accurate level of Klemunes' model is level 4 since this involves testing the soil at various water and density levels in the laboratory and correlating the results with the TDR recordings. Accordingly, a calibration curve is developed for a range of volumetric water contents expected in the field. The following equation is used to predict the volumetric water content for each of the four levels. Table 2-5 provides the specific regression coefficients for each level.

$$\theta(\%) = \frac{(5L_a - 1) - B_0 \dfrac{\gamma_d}{G_s \gamma_w}}{B_1} \qquad (2\text{-}28)$$

where

L_a = apparent length

γ_d , γ_w = unit weight of the soil and water

G_s = specific gravity of the soil

B_0, B_1 = regression coefficients

Table 2-5 Coefficient for Klemunes Model

LEVEL	Soil Type	B_0	B_1
Level 1	All-type	1.41	7.98
Level 2	Coarse	1.06	9.30
	Fine	1.50	7.56
Level 3	A-1-b	1.43	7.69
	A-2-4	1.00	9.57
	A-3	1.11	9.02
	A-4	1.77	6.25
	A-6	-1.56	12.26
	A-7-5	1.04	8.49
	A-7-6	1.02	10.31
Level 4	Determined based on a site-specific calibration		

Empirical model used in LTPP SMP

In LTPP SMP, TDR information has been collected to monitor subsurface moisture conditions in pavement structures. Dielectric constant obtained from TDR traces should be used in "the third-order polynomial dielectric constant (K_a)–soil gradation approach" to determine water contents of subsurface. As part of the third-order polynomial K_a–soil gradation approach, four models were developed for the volumetric water content computation. While the first three models take the third-order polynomial K_a model based on soil types, the fourth model applies to only fine-gradation soils and incorporates the contribution of the gradation into the model (Jiang and Tayabji 1999). The procedure of the model selection scheme is illustrated in Figure 2-16.

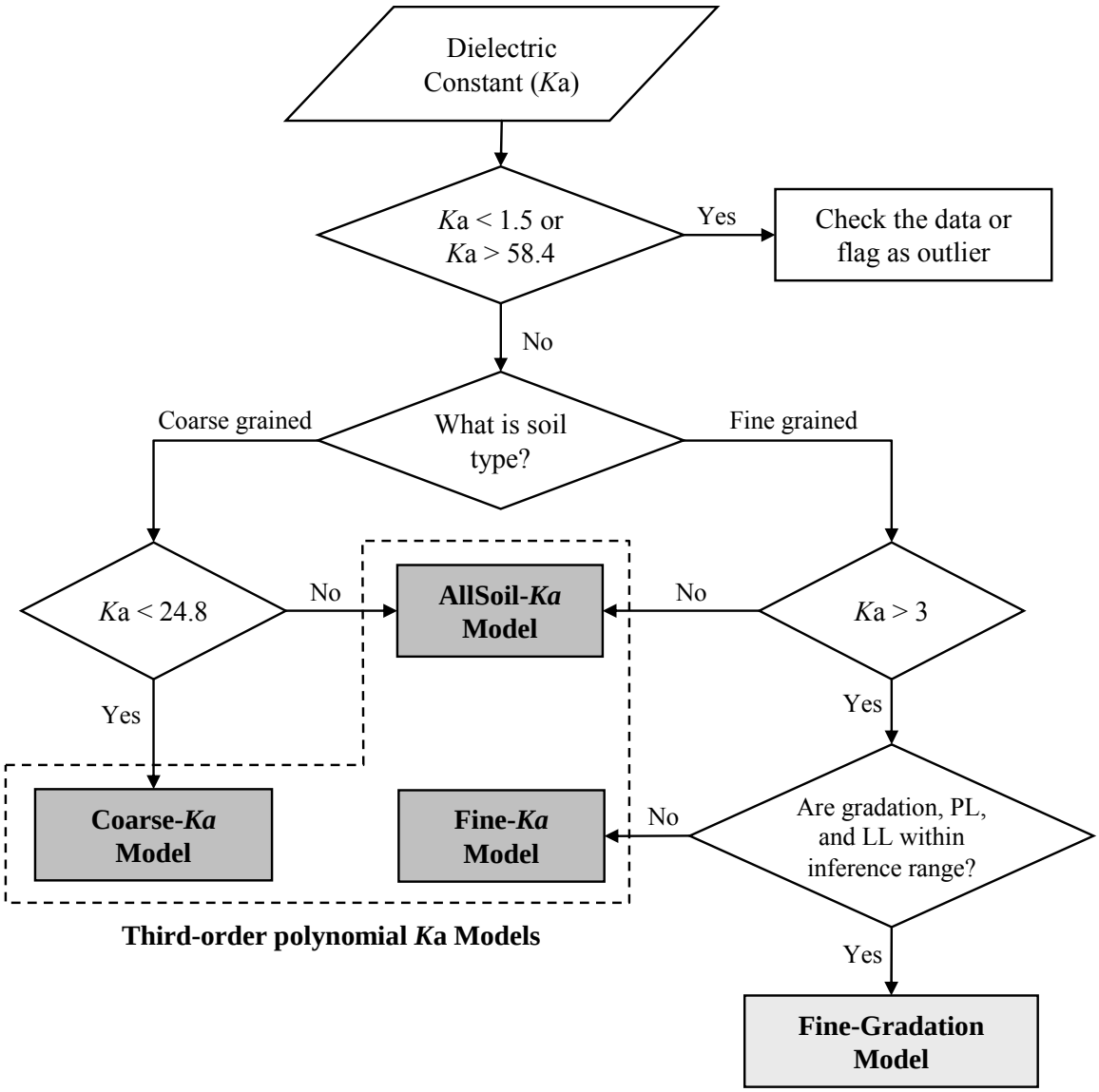

Figure 2-16 Volumetric moisture model selection process

The third-order polynomial K_a models were developed based on the regression of dielectric constants and volumetric water contents from the dataset obtained in Klemunes' study. Although both coarse and fine grained soil groups show similar third-order polynomial functional forms, the coarse-grained soil has a different trend compared with fine-grained soil. Hence, in order to provide a more accurate model, data

for coarse-grained soil and fine-grained soil were modeled separately. The models are valid only within the dielectric constant range or the inference space that was used to develop the model. The three empirical regression equations developed using the dielectric constant as the sole independent variable are given below with the regression coefficients shown in Table 2-6:

$$\theta(\%) = a_0 + a_1 K_a + a_2 K_a^2 + a_3 K_a^3 \tag{2-29}$$

where

Ka = dielectric constant

a_0, a_1, a_2, a_3 = Regression coefficients

Table 2-6 Coefficients for Volumetric Moisture Models (Jiang and Tayabji 1999)

Model Type	a_0	a_1	a_2	a_3
Coarse-K_a model	-5.7875	3.41763	-0.13117	0.00231
Fine-K_a model	0.4756	2.75634	-0.061667	0.000476
All Soil-K_a model	-0.8120	2.38682	-0.04427	0.000292

To refine the regression model and to increase the accuracy of moisture estimation for fine-grained soil, another model was developed using gradation, plastic limit, and liquid limit as independent variables. The following equation provides the volumetric moisture content model for fine-grained soil with variables:

$$\begin{aligned}\theta(\%) = {} & a_0 + a_1 K_a + a_2 K_a^2 + a_3 K_a^3 + a_4 G11\_2 + a_5 G1\_2 + a_6 No4 \\ & + a_7 No10 + a_8 No200 + a_9 PL + a_{10} LL\end{aligned} \tag{2-30}$$

where

$a_0, a_1, \ldots, a_{10}$ = Regression coefficients

This model was used for computing the volumetric water content for the fine-grained soils where gradation and other parameters were available and within the inference region of the model. Table 2-7 shows the descriptions, values, and inference ranges of these variables. The four models are selected based on the dielectric constant and properties of soil to calculate water content.

Table 2-7 Coefficient and Other Parameters for Fine-Grained Model (Jiang and Tayabji 1999)

Variable	Description	Coef.	Value	Inference Range
Intercept		a_0	1761.78	
K_a	Dielectric constant	a_1	2.9145	3 - 58.4
K_a^2		a_2	-0.07674	
K_a^3		a_3	0.000722	
G11_2	%passing 1½-sieve	a_4	-19.6649	99 - 100
G1_2	%passing ½-sieve	a_5	4.3667	97 - 100
No4	%passing No.4 sieve	a_6	-5.1516	90 - 100
No10	%passing No.10 sieve	a_7	2.7737	84 - 100
No200	%passing No.200 sieve	a_8	0.06057	12.6 - 94.6
PL	Plastic limit	a_9	-0.2057	0 - 45
LL	Liquid limit	a_{10}	0.10231	0 - 69

Mechanistic Approach

Since there is no one empirical model to be applied to all types of materials, various dielectric constant models have been developed based on a mechanistic approach. It is known that the mechanistic approach takes into account physical properties of each component in a composite material. Therefore, mechanistic models, also referred as a dielectric mixing model, relate the composite dielectric constant of a multiphase material

to the dielectric constant and volume fractions of its components. The relationship between dielectric constant and volume fraction in a dielectric mixing model can be expressed as an explicit or implicit equation:

$$\varepsilon = f\left(\varepsilon_i, v_i\right) \text{ or } f\left(\varepsilon, \varepsilon_i, v_i\right) = 0 \tag{2-31}$$

where

ε = composite dielectric constant of multiphase material

i = number of components in multiphase material

ε_i = dielectric constant of i^{th} component

v_i = volume fraction of i^{th} component ($\sum v_i = 1.0$)

In this approach, composite dielectric constant should be influenced by the dielectric constant as well as the volume fraction of each component. For example, the dielectric constant of a soil mixture is assumed to be the result of a volumetric mixing of dielectric constants of solid, water, and air components. Figure 2-17 illustrates the relationship of components of a soil mixture in a mechanistic approach.

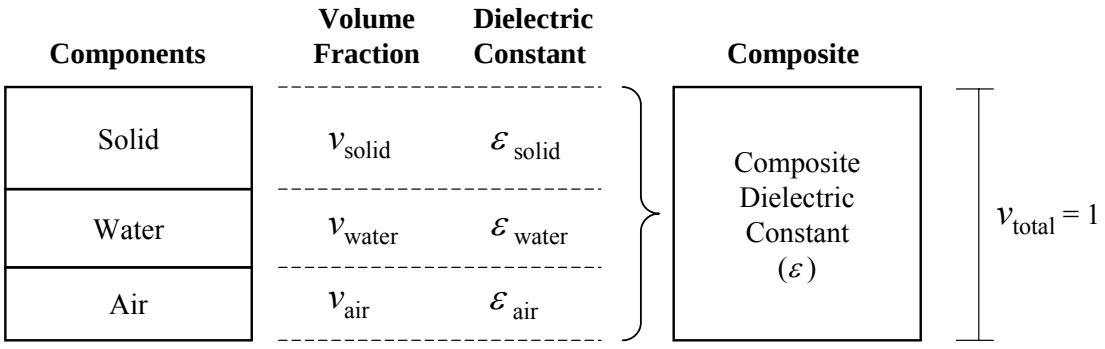

Figure 2-17 Relationship of components in soil mixture

Classical binary mixture models

Binary mixing models have been established to identify the relationship between the composite dielectric constant and the dielectric constants and volume fractions of constituents in 2-phase materials. Each binary model basically involves the relationship based on the shape of inclusions enclosed in a matrix of a heterogeneous system. A Rayleigh model which is a binary mixing model that is referred to as the Maxwell-Garnett model considers a distribution of spheres with a dielectric constant (ε_2) in a matrix with a different dielectric constant (ε_1) as shown in Figure 2-18 (Gallone et al. 2007; Maxwell-Garnett 1904; Rayleigh 1892). With volume of the spheres (v_2) embedded in a volume of matrix (v_1), the model is:

$$\frac{\varepsilon - 1}{\varepsilon + 2} = v_1 \frac{\varepsilon_1 - 1}{\varepsilon_1 + 2} + v_2 \frac{\varepsilon_2 - 1}{\varepsilon_2 + 2} \tag{2-32}$$

where

ε_1 = dielectric constant of matrix

ε_2 = dielectric constant of spheres

v_1 = volume fraction of matrix

v_2 = volume fraction of spheres ($v_1 + v_2 = 1$)

However, Rayleigh model is theoretically valid only for small volume of spheres ($v_2 < 0.2$) and for much higher electrical resistivity of the spheres than that of the matrix (Gallone et al. 2007).

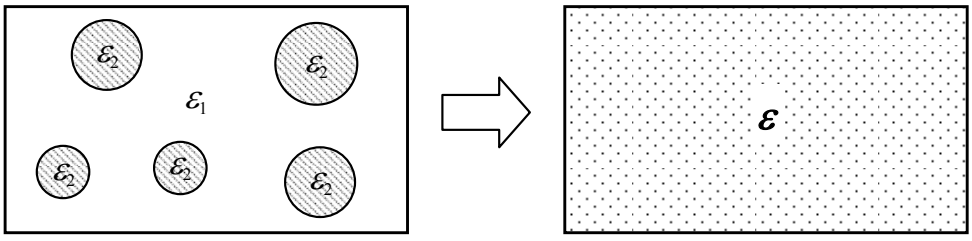

Figure 2-18 Geometry of composite for Rayleigh model

Since the Rayleigh's mixing model, several binary mixing models have been developed to represent the composite dielectric constant of a 2-phase material in terms of the volume fractions and dielectric constants of the individual constituents. Table 2-8 presents the list of the binary mixing models for spheres embedded in a matrix applicable to a soil mixture and the volumetric limitation of each model. The formulas in Table 2-8 are mainly found in van Beek's work (Brown 1956; Mandel 1961; Tinga et al. 1973; van Beek 1967; Wang and Schmugge 1980).

Table 2-8 Mixing Models for 2-Phase Materials with Sphere Particles

Reference	Formula*	Limitation
Rayleigh (1892)	$\frac{\varepsilon-1}{\varepsilon+2}=v_1\frac{\varepsilon_1-1}{\varepsilon_1+2}+v_2\frac{\varepsilon_2-1}{\varepsilon_2+2}$	$v_2<0.20$
Brown (1956)	$\varepsilon=v_1\varepsilon_1+v_2\varepsilon_2$	
Bruggeman (1935)	$\frac{\varepsilon_2-\varepsilon}{\varepsilon_2-\varepsilon_1}\left(\frac{\varepsilon_1}{\varepsilon}\right)^{1/3}=1-v_2$	
Wagner (1914)	$\frac{\varepsilon-\varepsilon_1}{3\varepsilon_1}=v_2\frac{\varepsilon_2-\varepsilon_1}{\varepsilon_2+2\varepsilon_1}$	$v_2<0.05$
Poisson (1821) Lorentz (1880)	$\varepsilon=\frac{1+2v_2}{1-v_2}$	$\varepsilon_1=1.0$ (vacuum)
Mandel (1961)	$\frac{\varepsilon-\varepsilon_1}{4\varepsilon-\varepsilon_1}=v_2\frac{\varepsilon_2-\varepsilon_1}{2\varepsilon+\varepsilon_2}$	$v_2<0.2$

* $v_1+v_2=1.0$

Complex refractive index model

The second type of mechanistic model is a dielectric mixing model for multiphase materials based on assumption or estimation of geometric arrangement of the constituents. The Complex Refractive Index model (CRIM) is a typical model type using the assumption for multiphase material. Actually, CRIM is a specific instance of

the Lichtenecker-Rother equation (Lichtenecker and Rother 1931; Martinez and Byrnes 2001):

$$\varepsilon^{\alpha} = \sum_{i=1}^{n} v_i \varepsilon_i^{\alpha} \tag{2-33}$$

where

α = geometric arrangement factor (-1.0 to 1.0)

It is known that the geometric arrangement factor (α) presents the relationship between the direction of effective layering of the components to the direction of the applied electric field. If electric field is parallel to the composite layer, the geometric arrangement factor is 1.0, and if the field is perpendicular to the layer, the factor is -1.0. Theoretically, the case of an isotropic multiphase material, the factor was found to be 0.5 (Birchak et al. 1974; Roth et al. 1992). Figure 2-19 illustrates the scheme of the geometric arrangement factor of materials on the direction of electric field.

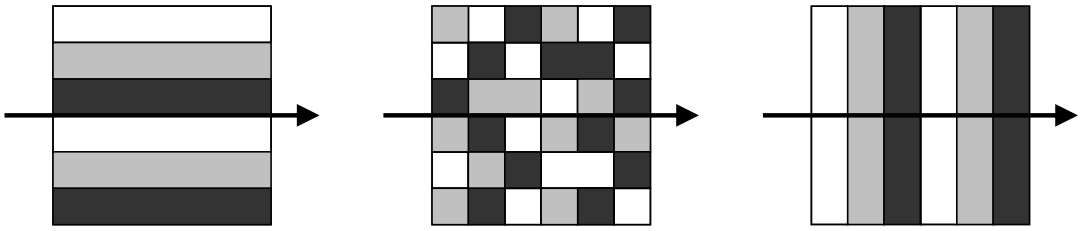

(a) $\alpha = 1.0$ (b) $\alpha = 0.5$ (c) $\alpha = -1.0$

Figure 2-19 Geometric arrangement factors by direction of electric field

When the geometry arrangement factor is 0.5, Equation (2-33) brings about the CRIM equation as:

$$\sqrt{\varepsilon} = \sum_{i=1}^{n} v_i \sqrt{\varepsilon_i} \tag{2-34}$$

That is, the CRIM is a special case of the Lichtenecker and Rother model with a fixed arrangement factor of 0.5, which is for homogeneous materials. The CRIM provides a simple approach to estimate dielectric properties or volume fraction of multiphase materials. Although the model is theoretically valid only for one dimensional layered composites, it is often used effectively to model the properties of more complex composites in practice (Ajo-Franklin et al. 2004). However, the model has a limitation that it is valid only for low conductivity material whose value is less than 10 mS/m (Martinez and Byrnes 2001).

Several studies were performed to determine the α factor for different materials. It was found that the CRIM fits 2-phase soil mixture consisting of water and dry solid by Birchak et al (Birchak et al. 1974). Whalley proved the α factor having a value of 0.5 by considering 3-phase soil mixture divided into solids, water, and air (Whalley 1993). However, Roth et al. found the α value to be 0.46 for a TDR calibration data set based on 3-phase soil system (Roth et al. 1990). Dodson et al. and Dirksen found different α values for several mineral soils with 4-pahse soil mixture (Dirksen and Dasberg 1993; Dobson et al. 1985). Accordingly, other models using 3 or 4-phase soil system should be discussed to investigate different approaches based on the Lichtenecker-Rother equation but not the CRIM formula.

Three-Phase Mixture

In 3-phase system, a wet soil mixture was divided into solid particle, water, and air for applying dielectric mixing models. The mixing model given by Equation (2-33) can be extended to a 3-phase system to describe a soil mixture by;

$$\varepsilon^{\alpha} = v_w \varepsilon_w^{\alpha} + v_s \varepsilon_s^{\alpha} + v_a \varepsilon_a^{\alpha} \tag{2-35}$$

where

ε_s, ε_w, ε_a = dielectric constant of solid, water, and air

v_s, v_w, v_a = volume fraction of solid, water, and air

$v_s + v_w + v_a$ = 1.0

Based on the extended Lichtenecker-Rother model in Equation (2-33), many studies have been performed to determine the α value or to evaluate the 3-phase model using different soil types and experimental conditions.

Roth et al. has found an α value in a 3-phase soil system based on the measured water content and composite dielectric constant and the assumed dielectric constant of each component (Roth et al. 1990). The composite dielectric constant was obtained using a TDR probe consisting of two parallel rods. Equation (2-35) was modified to calculate each volume fraction using a single variable of porosity, and to obtain a single calibration curve as:

$$\varepsilon^{\alpha} = \theta\varepsilon_w^{\alpha} + (1-\eta)\varepsilon_s^{\alpha} + (\eta-\theta)\varepsilon_a^{\alpha} \tag{2-36}$$

where

θ = volumetric fraction of water

η = soil porosity

11 mineral and 2 organic soils were used as samples to determine the α value by a weighted nonlinear regression. The assumed dielectric constants of elements are 80.36 for water, 3.9 for solid of mineral soils, 5.0 for solid of organic soils, and 1.0 for air. After minimizing the sum of weighted least squares error between the measured and calculated volumetric water contents, the optimum value for α was founded to be 0.46 (Roth et al. 1990).

Another calibration for 3-phase soil system was achieved by Jacobsen et al. (Jacobsen and Schjønning 1993; Jacobsen and Schjønning 1995). They fitted the α

value to the data from 10 mineral soils ranging from a coarse sandy soil to a sandy clay loam. The values of 3.5, 81.0, and 1.0 were used for the assumption of the dielectric constant for solid, water, and air, respectively. Based on the sample test results and the assumption, the optimum α value was found to be 0.66. Bohl et al. investigated the accuracy and applicability of the 3-phase mixing model based on a data set obtained from 40 mineral and organic soils (Bohl and Roth 1994). Table 2-9 compares the α values and each source and assumed dielectric constants of components for the studies described above.

Table 2-9 Comparison of Calibrated 3-Phase Models

Model	α Value	Soil Sample	Assumed Dielectric Constants		
			Solid	Water	Air
Roth et al (1990)	0.46	11 mineral	3.9	80.36	1.0
		2 organic	5.0		
Bohl et al. (1994)	0.50	21 mineral	3.9	80.36	1.0
		19 organic	5.0		
Jacobson et al. (1995)	0.66	10 mineral	3.5	81.0	1.0

Four-Phase Mixture

In 4-phase mixing models, the single water component in 3-phase system is separated into bound water and free water under the assumption that solid particles are covered by a thin water layer (thickness $\delta = 3 \times 10^{-8}$ cm) of chemically bound water, which has a much lower dielectric number ($\varepsilon_{bw} \cong 3.2$) than free water ($\varepsilon_{fw} \cong 81$) (Dobson et al. 1985; Weitz et al. 1997). The 4-phase system of a wet soil can be expressed by extending Equation (2-33) as:

$$\varepsilon^{\alpha} = v_{bw}\varepsilon_{bw}^{\alpha} + v_{fw}\varepsilon_{fw}^{\alpha} + v_s\varepsilon_s^{\alpha} + v_a\varepsilon_a^{\alpha} \tag{2-37}$$

where

ε_{bw}, ε_{fw} = dielectric constant of bound water and free water

v_{bw}, v_{fw} = volume fraction of bound water and free water

$v_{bw} + v_{fw} + v_s + v_a$ = 1.0

Dobson et al. calibrated the 4-phase mixing model using five soil samples ranging from sandy loam to silty clay and a wide range of soil water contents (Dobson et al. 1985). The equation of the Lichtenecker-Rother model was rewritten for a 4-phase system as follows;

$$\varepsilon^{\alpha} = \theta_{bw}\varepsilon_{bw}^{\alpha} + \theta_{fw}\varepsilon_{fw}^{\alpha} + (1-\eta)\varepsilon_{s}^{\alpha} + (\eta-\theta)\varepsilon_{a}^{\alpha} \tag{2-38}$$

where

θ_{bw}, θ_{fw} = volumetric bound and free water content

In Dobson's study, it was found that when the α value is 0.65, the 4-phase model is matched best with their sample data sets, using dielectric constant of components: 4.7 for solid, 1.0 for air, and dielectric values calculated by Debye equation for bound and free water (Debye and Hückel 1923; Dobson et al. 1985; Lane and Saxton 1952). The modified Debye equation to calculate the dielectric constants of bound and free water at given frequency and temperature is as follows (Debye and Hückel 1923; Dobson et al. 1985; Lane and Saxton 1952):

$$\varepsilon_{fw} = \varepsilon_{w\infty} + \frac{\varepsilon_{w0} - \varepsilon_{w\infty}}{1 + j2\pi f \tau_w} - j\frac{\sigma_{eff}}{2\pi f \varepsilon_0}\frac{\rho_s - \rho_b}{\rho_s m_v} \tag{2-39}$$

where

$\varepsilon_{w\infty}$ = high frequency limit of ε_w ($\approx$ 4.9)

ε_{w0} = static dielectric constant of water

f = frequency (Hz)

τ_w = relaxation time of water

σ_{eff} = effective conductivity empirically derived with the function of soil texture (= -1 .645 + 1.939ρ_b – 0.02013S + 0.10594C)

S and C = percentage of san and clay, respectively

ρ_b = bulk density of soil

ρ_s = specific density of soil

m_v = ρ_b W_w/W_s

W_w/W_s = mass ratio of water to dry soil solids

Actually, since the dielectric constant of bound water (ε_{bw}) is not well known and its volume fraction (θ_{bw}) is available only after complicated calculations, they were estimated approximately by (Dobson et al. 1985):

$$m_v^{\beta}\varepsilon_{fw}^{\alpha} = \theta_{bw}\varepsilon_{bw}^{\alpha} + \theta_{fw}\varepsilon_{fw}^{\alpha} \tag{2-40}$$

where

β = empirical constant depending on textural composition of soil

In addition to Dobson's study, several calibrations were performed to find the α value in the dielectric 4-phase mixing model. Dirksen et al. calibrated the model based on the data set obtained from eight mineral soil samples. The TDR measurements were carried out to obtain the composite dielectric constants of soil mixtures, and the dielectric constants of components were assumed as listed in Table 2-10. The volume fraction of bound water covering particle surfaces was estimated by (Dirksen and Dasberg 1993; Weitz et al. 1997):

$$\theta_{bw} = l\delta\rho_b S \tag{2-41}$$

where

l = number of molecular water layers of bound water

δ = thickness of one molecular water layer (3×10^{-8} cm)

ρ_b = bulk density of soil

S = specific surface of soil matrix

Although the volume fraction of bound water should be calculated with Equation (2-40), the Dirksen's study has assumed, due to the lack of adequate information, the bound water as a monomolecular water layer (l = 1.0) with the dielectric behavior similar to ice whose dielectric constant is 3.2 (Dirksen and Dasberg 1993). They found eight α values varied between 0.39 and 0.81 for eight soil samples.

Jacobson et al. found α value to be 0.70 for the 4-phase system based on the same soil sample used for their calibration of 3-phase model (Jacobsen and Schjønning 1993; Jacobsen and Schjønning 1995). The dielectric value of bound water was also assumed to be 3.2 as used in Dirksen's study. Table 2-10 presents calibrated α values and corresponding types of soil samples and the assumed dielectric constants of four components.

Table 2-10 Comparison of Calibrated 4-phase Models

Model	α value	Soil Sample	Assumed Dielectric Constants			
			Solid	Free Water	Bound Water	Air
Dobson et al. (1985)	0.65	5 minerals	4.7	Equation (2-39)	Equation (2-40)	1.0
Dirksen et al. (1993)	0.39 ~ 0.81	8 minerals	5	81	3.2	1.0
Jacobsen et al (1993)	0.70	10 minreals	5	81	3.2	1.0

Maxwell-DeLoor mixing model

In contrast with 3- and 4-phase α mixing models above, the Maxwell-De Loor mixing model does not contain empirical parameter such as α but uses only physical parameters such as soil porosity and dielectric constants of elements. In fact, this dielectric mixing model assumes a specific geometry instead. According to an approach found by de Loor, the soil particles are considered as a host medium containing distributed and oriented inclusions (air, bound water, and free water). Based on the Maxwell equation, the dielectric equation of de Loor's approach can be written for a 4-phase soil system with plate-shaped soil particles as the host medium as (De Loor 1956; De Loor 1968; Dirksen and Dasberg 1993; Dobson et al. 1985):

$$\varepsilon = \frac{3\varepsilon_s + 2\theta_{fw}\left(\varepsilon_{fw} - \varepsilon_s\right) + 2\theta_{bw}\left(\varepsilon_{bw} - \varepsilon_s\right) + 2\left(\eta - \theta\right)\left(\varepsilon_a - \varepsilon_s\right)}{3 + \theta_{fw}\left(\frac{\varepsilon_s}{\varepsilon_{fw}} - 1\right) + \theta_{bw}\left(\frac{\varepsilon_s}{\varepsilon_{bw}} - 1\right) + \left(\eta - \theta\right)\theta_{fw}\left(\frac{\varepsilon_s}{\varepsilon_a} - 1\right)} \qquad (2\text{-}42)$$

where

θ = volumetric fraction of all water components (= θ_{bw} + θ_{fw})

Although the empirical and mechanistic models described can be applied to various composite pavement materials, several inadequacies and limitations were found concerning the application to pavement composite materials. For the empirical models, it is relatively easy to estimate volume fraction since they do not need to determine any additional parameters. However, physical or rational scientific justification of the relationship is void of the model forms and they yield accurate results only for a specific material type used to calibrate empirical coefficients. On the other hand, since the mechanistic mixing models can take account of the influence of individual components in a composite material, they may be theoretical and more universally applicable to describe the relationship between the dielectric constant and the volume fraction. Nevertheless, the geometric arrangement factor of a given material should be assumed or

determined by the regression analysis with sufficient laboratory test data. In addition, the binary mixing models have volumetric limitation on constituent materials. The use of a mixing model either with the regression or with the assumption may result in systematic errors causing less accurate estimate results. Thus, it was suggested that a new approach should be developed to improve the accuracy for estimating the volume fraction of components in a given pavement material.

CHAPTER III

DEVELOPMENT OF NEW APPROACH

SELF CONSISTENT APPROACH AND BOUNDS OF DIELECTRIC CONSTANT

As described previously, since the existing approaches should be implemented based on regression or assumption, the use of the approaches may result in systematic errors which cause less accurate final determination of volume fraction of components. In order to remove or minimize the error resulting from the use of the existing approach, a new approach was developed based on self consistent scheme using the system identification as a solution methodology.

Self Consistent Approach

A simple method for estimating volume fraction of a composite material might fit a mathematical equation to laboratory test data using the composite material. However, the mathematical equation produced would hardly fit other test data obtained from different composite materials. Therefore, a more fundamental and mechanistic approach, not requiring experimental data, should be proposed. In this regard, self consistent approach can be readily applicable to dielectric problems of composite materials. The approach does not need empirical parameters or volumetric limitations founded in any mechanistic models. The approach requires only assumptions of macroscopic homogeneity and isotropy of multiphase materials, which were defined as the fundamental assumptions of multiphase materials; that is, in a multiphase system, a particle is assumed to be of spherical shape and to be imbedded directly in a homogeneous matrix. Based on these assumptions, Böttcher developed a theory of dielectric properties of heterogeneous materials, such as self consistent approach (Böttcher and Bordewijk 1978; Böttcher 1938; Landauer 1952):

$$v_1 \frac{\varepsilon_1 - \varepsilon}{\varepsilon_1 + 2\varepsilon} + v_2 \frac{\varepsilon_2 - \varepsilon}{\varepsilon_2 + 2\varepsilon} = 0 \tag{3-1}$$

where

ε = composite dielectric constant

$\varepsilon_1, \varepsilon_2$ = dielectric constants of phase 1 and 2

v_1, v_2 = volume fractions of phase 1 and 2 ($v_1 + v_2 = 1.0$)

Bounds of Dielectric Constant

In order to justify the self consistent scheme, the composite dielectric constant should always fall between reasonable bounds for homogenous and isotropic multiphase materials. The bounds in terms of phase dielectric constant and phase volume fraction were first developed for isotropic composite materials by Wiener (Hashin 1969b; Wiener 1912):

$$\frac{1}{\frac{v_1}{\varepsilon_1} + \frac{v_2}{\varepsilon_2}} < \varepsilon < \varepsilon_1 v_1 + \varepsilon_2 v_2 \tag{3-2}$$

Hashin et al. derived improved lower and upper bounds for the composite dielectric constant of a homogeneous and isotropic composite material. (Hashin 1969b; Hashin and Shtrikman 1962):

$$\text{Lower Boundary } \varepsilon_- = \varepsilon_1 + \frac{v_2}{\frac{1}{\varepsilon_2 - \varepsilon_1} + \frac{v_1}{3\varepsilon_1}} \tag{3-3}$$

$$\text{Upper Boundary } \varepsilon_+ = \varepsilon_2 + \frac{v_1}{\frac{1}{\varepsilon_1 - \varepsilon_2} + \frac{v_2}{3\varepsilon_2}} \tag{3-4}$$

Appendix A presents the derivation of lower and upper bounds of Equation (3-3) and (3-4). It is noted that the composite dielectric constants computed from Equation (3-1) always fall between the lower and upper bounds of Equation (3-3) and (3-4). Figure 3-1 presents an example for the bounding method application with a soil mixture. The dielectric constants of solid (ε_1) and water (ε_2) are assumed to be 4.0 and 81.0, respectively, and the composite dielectric constant was computed using Equation (3-1). As seen in the figure, the composite dielectric constants are consistent with component values of the dielectric constant and their volume fractions.

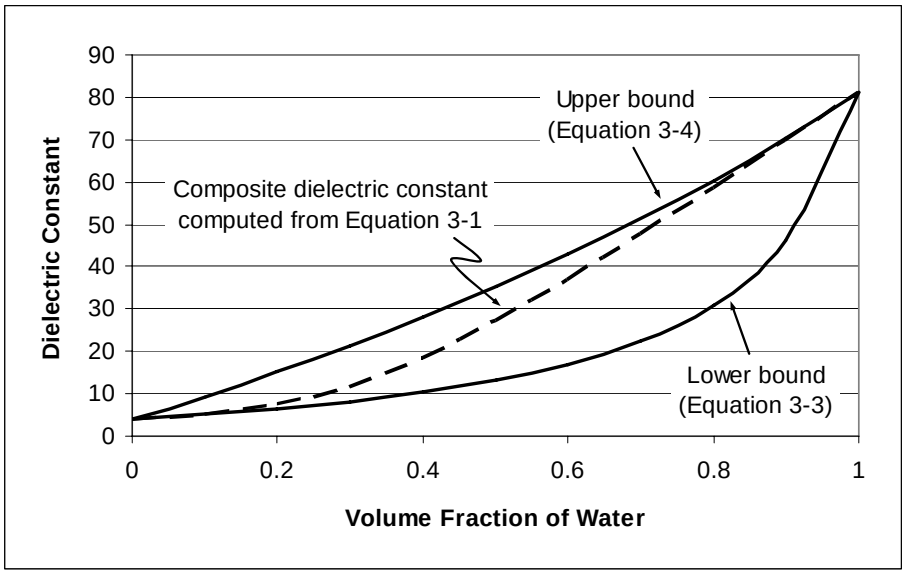

Figure 3-1 Bounding of dielectric constant as a function of volume fraction of water

Application of Self Consistent Model for Multiphase Material

The Böttcher's self consistent model can accounts for the dielectric properties and volumetric proportioning of an individual component in a composite material. Although the Böttcher's model was derived for 2-phase materials, the model can be extended for multiphase materials consisting of more than 2 components as:

$$\sum_{i=1}^{n} v_i \left(\frac{\varepsilon_i - \varepsilon}{\varepsilon_i + 2\varepsilon} \right) = 0 \tag{3-5}$$

where

n = number of components

v_i = volume fraction of i^{th} component ($\sum v_i = 1.0$)

ε_i = dielectric constant of i^{th} component

In fact, Boersma proposed that the extended model can be used for a multi-component system, but any verifications were not performed to prove the applicability of the model (Boersma and van Turnhout 1999). The use of this formula requires that a single or multiple particles are evenly dispersed in a homogeneous matrix. Appendix B presents the derivation of the proposed self consistent model of Equation (3-5). The extended self consistent model can be used for soil mixtures since soil is defined as an uncemented aggregate of solid particles with water and air to fill the empty spaces in the matrix between the solid particles (Das 2002). Applying the Equation (3-5) to a soil mixture which is composed of solid, water, and air, the model can be expressed as:

$$v_s \left(\frac{\varepsilon_s - \varepsilon}{\varepsilon_s + 2\varepsilon} \right) + v_w \left(\frac{\varepsilon_w - \varepsilon}{\varepsilon_w + 2\varepsilon} \right) + v_a \left(\frac{\varepsilon_a - \varepsilon}{\varepsilon_a + 2\varepsilon} \right) = 0 \tag{3-6}$$

where

ε = composite dielectric constant of soil mixture

v_s = volume fraction of solid

v_w = volume fraction of water

v_a = volume fraction of air

ε_s = dielectric constant of solid

ε_w = dielectric constant of water

ε_a = dielectric constant of air (= 1.0)

The model can be applicable to PCC as well since concrete is a composite consisting of granular material (aggregate) dispersed in a hard matrix of cement material (Mindess et al. 2003). If PCC is assumed to be composed of five components (aggregate, unreacted cement, hydrated cement product, free water, and air voids) during hydration then the new self consistent model is configured as follows:

$$v_{agg}\left(\frac{\varepsilon_{agg}-\varepsilon}{\varepsilon_{agg}+2\varepsilon}\right)+v_{uc}\left(\frac{\varepsilon_{uc}-\varepsilon}{\varepsilon_{uc}+2\varepsilon}\right)+v_{hcp}\left(\frac{\varepsilon_{hcp}-\varepsilon}{\varepsilon_{hcp}+2\varepsilon}\right)+v_{w}\left(\frac{\varepsilon_{w}-\varepsilon}{\varepsilon_{w}+2\varepsilon}\right)+v_{a}\left(\frac{\varepsilon_{a}-\varepsilon}{\varepsilon_{a}+2\varepsilon}\right)=0 \quad (3\text{-}7)$$

where

ε = composite dielectric constant of portland cement concrete

v_{agg} = volume fraction of aggregate solid

v_{uc} = volume fraction of unreacted cement

v_{hcp} = volume fraction of hydrated cement product

ε_{agg} = dielectric constant of aggregate solid

ε_{uc} = dielectric constant of unreacted cement

ε_{hcp} = dielectric constant of unhydrated cement product

PROCEDURE OF NEW APPROACH

The new approach for the calculation of the volume fraction of a composite pavement material consists of three steps:

Step 1. Determine composite dielectric constant of a given composite material.

Step 2. Given the measured volume fraction data along with the composite dielectric constant calculated at Step 1, backcalculate the dielectric constant of each component in the composite material and calibrate the self consistent model based on known composite material properties.

Step 3. Using the component dielectric constants calibrated in Step 2, forward calculate the volume fraction of the composite material based on composite dielectric constant determined for other times.

Actually, Step 2 and Step 3 are not a sequence process. Step 2 is the calibration step performed only once to obtain the component dielectric constants which are required for Step 3 to forward calculate volume fraction of the composite material at other times. The system identification method of analysis was used to obtain solution at each step.

Determination of Composite Dielectric Constant (Step 1)

The essential input parameter to estimate volume fraction of a composite material is the composite dielectric constant. The parameter represents the combined effect of the volume fractions and the dielectric constants of components in the individual materials. For pavement materials such as soil or PCC, since water has higher dielectric constant value compared with any other components, the composite dielectric constant is mainly influenced by the volumetric water content in the composite material. While the percometer can immediately measure the dielectric constant, the waveform obtained from the TDR device requires interpretation to determine the dielectric constant, as noted in Chapter II. In this study, a new methodology for interpreting TDR trace will be proposed to minimize the systematic error arising from existing methods to calculate the composite dielectric constant of a soil material.

Calibration of Component Properties (Step 2)

In many studies regarding the estimate of volume fraction with mechanistic mixing models, the dielectric constants of constituent materials were assumed even though each has its inherent dielectric constant value. The use of assumed constituent dielectric constants may result in systematic error which can yield less accurate results for estimating volume fraction of composite materials. For soil materials, a variety of

dielectric constants was used for water or solid particles, such as 79~81 for water or 3~5 for particles, along with the assumptions used in related studies. Table 3-1 lists the assumed particle and water dielectric constants used in different studies.

Table 3-1 Assumed Dielectric Values Used for Soil Mixture Studies

Source Study	Assumed Dielectric Constant	
	Solid Particle	Water
Roth et al. (1990) Bohl and Roth (1994)	3.9 for mineral soils 5.0 for organic soils	80.36
Dasberg and Hopmans (1992)	3.9	80.4
Dirksen and Dasberg (1993)	5.0	81.0
Jacobsen and Schjønning (1995)	3.5	81.0
Weitz et al. (1997)	4.0	81.0
Ajo-Franklin et al. (2004)	4.27 ~ 6.3 by solid type	80.0

In order to minimize the systematic error resulting from these assumptions, the new approach employs the calibration process to determine the dielectric constant of each constituent component. To initiate a new approach to calculate the volume fraction of a given composite material, the dielectric constant of each component in the material should be identified. The composite dielectric constant of a multiphase material varies by combination of the dielectric constant and the volume fraction of constituent materials as seen in Figure 3-2. Given the dielectric constant of each component, it is possible to estimate more accurately the volume fraction in a composite material since this approach can account for the effect of individual constituent dielectric properties on the volume fractions.

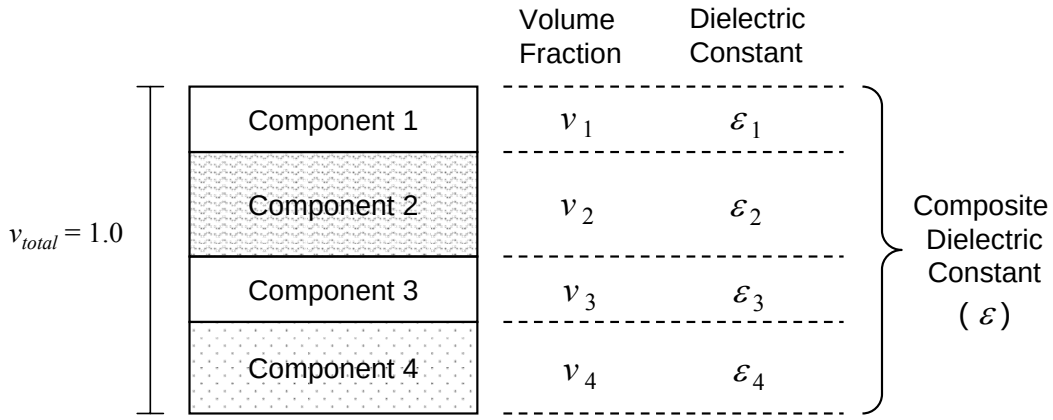

Figure 3-2 Relationship of volume fraction and dielectric constant of a composite material

The constituent dielectric constant can be determined through backcalculation using measured data of volume fraction and corresponding composite dielectric constant, along with the self consistent model listed in Equation (3-5) as:

$$f\left(\varepsilon_1, \varepsilon_2, \cdots, \varepsilon_i\right) = v_1\left(\frac{\varepsilon_1 - \varepsilon}{\varepsilon_1 + 2\varepsilon}\right) + v_2\left(\frac{\varepsilon_2 - \varepsilon}{\varepsilon_2 + 2\varepsilon}\right) + \cdots + v_i\left(\frac{\varepsilon_i - \varepsilon}{\varepsilon_i + 2\varepsilon}\right) = 0 \qquad (3\text{-}8)$$

where

ε_i = constituent dielectric constants to be calibrated

v_i = measured volume fraction of each component

ε = measured composite dielectric constant

The backcalculation to calibrate each constituent dielectric constant was performed using the system identification method which will be described next subchapter. Once the individual constituent dielectric values were calibrated for a given composite material, the calibrated values can be used further to estimate volume fractions based on composite dielectric constant measured at any other times.

Forward Calculation of Volume Fraction (Step 3)

In the forward calculation of volume fraction of a phase in a composite material, the self-consistent model in Equation (3-5) is used together with the parameters calibrated in Step 2 to determine the new values of the phase volume fractions using the composite dielectric constants derived from previous data collection as:

$$f\left(v_1, v_2, \cdots, v_i\right) = v_1\left(\frac{\varepsilon_1 - \varepsilon}{\varepsilon_1 + 2\varepsilon}\right) + v_2\left(\frac{\varepsilon_2 - \varepsilon}{\varepsilon_2 + 2\varepsilon}\right) + \cdots + v_i\left(\frac{\varepsilon_i - \varepsilon}{\varepsilon_i + 2\varepsilon}\right) = 0 \qquad (3\text{-}9)$$

where

v_i = volume fraction of each component to be calculated

ε_i = calibrated constituent dielectric constants

ε = measured composite dielectric constant

The composite dielectric constants are determined by measurement at different times or throughout a given monitoring period of the composite material. Thus, once a particular material characteristics such as the constituent dielectric constants are 'identified' by Step 2, all future calculation of volume fractions can be determined by use of the system identification process in Step 3 using a new composite dielectric constant measured in Step 1. Figure 3-3 illustrates the application procedure of the new approach to determine volume fraction of a given material.

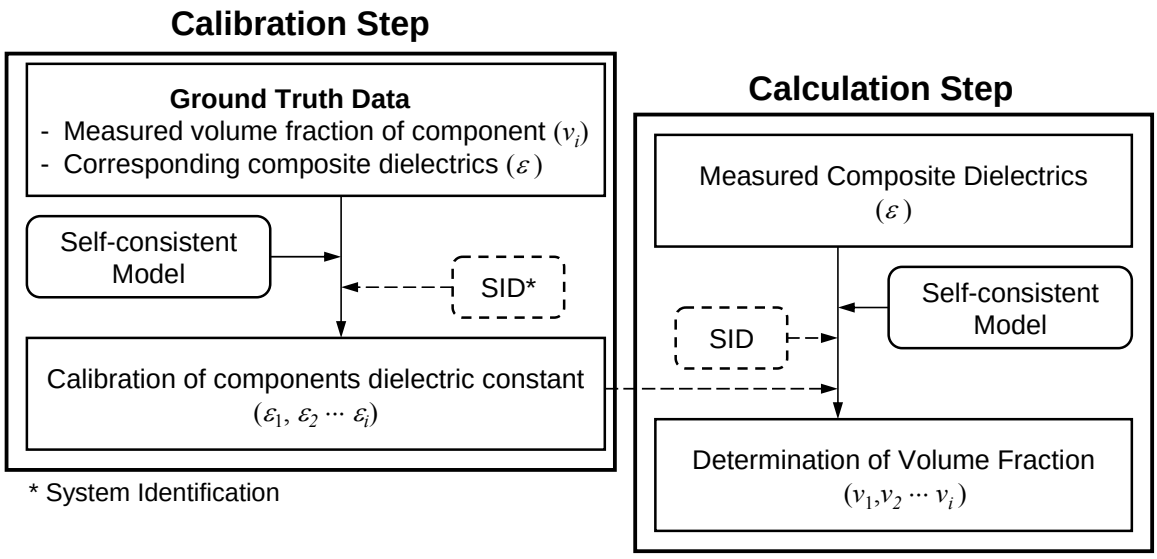

Figure 3-3 Procedure of new approach

SYSTEM IDENTIFICATION AS SOLUTION METHODOLOGY

In order to estimate volume fraction of a given composite, the calibration and the forward calculation should be performed in Step 2 and 3, respectively. The method of solving for the dielectric constants or the volume fractions in each step was by use of the system identification process.

Overview of System Identification

The purpose of system identification (SID) process is to determine parameters in a mathematical model which describes the behavior of a real physical system in a rationally satisfying method. It is noted that the real physical system and the mathematical model are identical when output of the model is the same as that of the system; otherwise, the model should be adjusted until the error between both outputs is reduced sufficiently (Natke 1982). In this study, the real physical system is measured values such as composite dielectric constant of a composite material, and the mathematical model is the proposed self consistent model.

There are three different error minimization models in the SID process depending on the choice of errors combined with the model: forward model, inverse model, and generalized model shown in Figure 3-4. The forward model approach employs the output errors between the model and the system to minimize them based on the same input. In the inverse model approach, the input error is used to be minimized based on same output. If one part of the model is invertible, the generalized error between the output from forward model and that from inverse model can be defined as seen in Figure 3-4 (c) (Natke 1982).

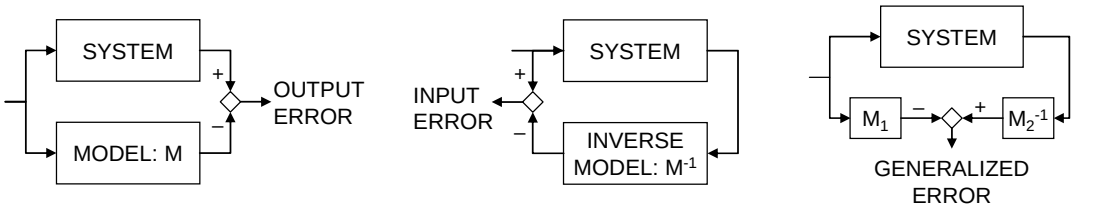

(a) Forward Model (b) Inverse Model (c) Generalized Model

Figure 3-4 Methods for system identification process (Natke 1982)

The forward approach is not as complicated as the inverse or generalized model approach in which the mathematical model is required to be inverted. Also, in the proposed approach for estimating volume fraction, while a single mathematical model is used, the different input data are required for each step: the measured composite dielectric constant and volume fraction for Step 2 and the measured composite and constituent dielectric constants for Step 3. Therefore, the SID process based on the forward model was used in this study.

When the output error between the system and the model is small enough to meet an established error criterion, it is considered as that an optimal model describing the system is obtained. However, if the error does not meet the criterion, the parameters in the mathematical model should be adjusted by a parameter adjustment process which will be described in next subchapter. Figure 3-5 depicts the iteration scheme of an SID

process based on the forward model and a parameter adjustment algorithm for the calculation process in the new approach.

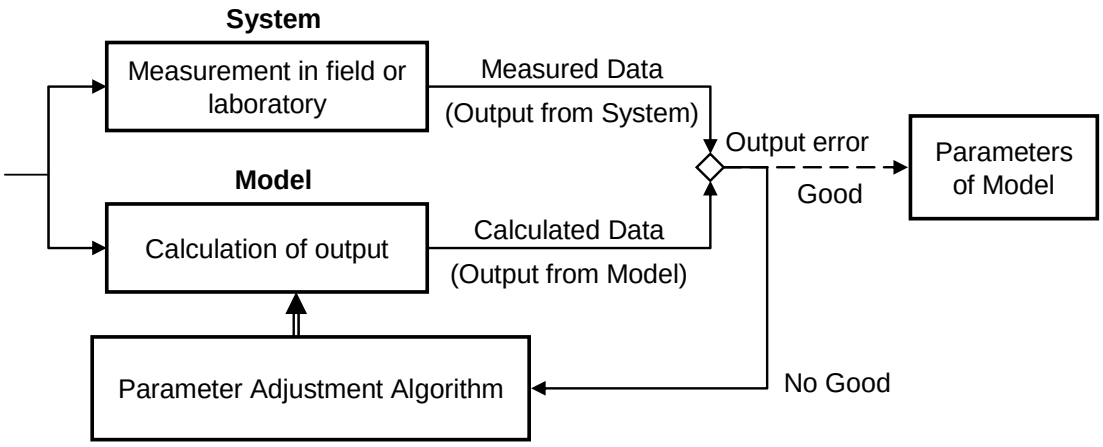

Figure 3-5 Scheme of system identification process

Parameter Adjustment Algorithm

A process is required to adjust parameters in a mathematical model in which to meet an error criterion in SID process. The adjustment process is performed iteratively until the error becomes small enough. A parameter adjustment algorithm was developed based on the Taylor series expansion as follows (Wang and Lytton 1993)

$$[F_{ki}][\beta_i] = [r_k] \tag{3-10}$$

where

F_{ki} = sensitivity matrix = $\sum_{k=1}^{m}\sum_{i=1}^{n}\frac{\partial f_k}{\partial p_i}\frac{p_i}{f_k}$ ($m \times n$ matrix)

m = number of measured data points

n = number of model parameters to be determined

f_k = mathematical model

p_i = model parameters to be determined

β_i = change vector (relative change of parameters) = $[\beta_1\ \beta_2 \ldots \beta_n]^T$

r_k = residual vector (error between system and model outputs) = $[r_1\ \ r_2 \ldots\ r_m]^T$

While the number of parameters (n) determines the numbers of rows in the change vector [β_i] and columns in the sensitivity matrix [F_{ki}], the number of rows in [F_{ki}] and [r_k] depends on the number of measured data points (m). The minimization of error contained within the residual vector [r_k] is analogous to the reduction of error employed in least squared error analysis as elaborated in Appendix C. The squared error between the actual and predicted output is allocated based on the magnitude of the weighting parameters in the sensitivity matrix [F_{ki}]. The model parameters (p_i) should be adjusted to diminish the remaining squared error; however, because of the presence of random error, the residual matrix [r_k] should not be forced to zero (Zollinger et al. 2008). Since the elements in the residual vector [r_k] are determined based on model parameters (p_i) assumed at each iteration process, they are known values. The sensitivity matrix [F_{ki}] which reflects the sensitivity of the output from mathematical model (f_k) to the assumed parameters (p_i) is also a known value. Therefore, the unknown change vector [β_i] presents the relative changes of the model parameters and is the target matrix to be minimized in the process. Equation (3-10) can be rewritten as:

$$\left[\beta_i\right] = \left[F_{ki}^T F_{ki}\right]^{-1}\left[F_{ki}\right]^T\left[r_k\right] \tag{3-11}$$

As the change vector [β_i] is obtained initially based on assumptions, it is updated for the next iteration as:

$$p_i^{j+1} = p_i^j\left(1+\beta_i\right) \tag{3-12}$$

where

j = iteration count

By minimizing the change vector [β_i], solutions for the model parameters are found. In order to achieve the solution, the iteration process using Equation (3-12) is continued until the remaining squared error is minimized within the desired convergence limits. The convergence criterion in this study was set to 5.0 percent; that is, the iteration was repeated until the elements in change vector [β_i] are less than 0.05.

CHAPTER IV

APPLICATIONS OF NEW APPROACH

The new approach proposed in this study is unique in that the need for regression in the traditional sense is eliminated. The mechanistic model which accounts for the influence of the individual constituents of composite material was applied in the new approach for estimating volume fraction of constituent materials based on the dielectric properties. Therefore, the approach is appropriate for composite pavement materials to monitor in-situ water content or measure the variation of volume fraction of each component by time. In this chapter, to verify the applicability of the new approach, it was applied to two pavement materials, a soil mixture and PCC, and validated through the comparisons with laboratory data.

SOIL MIXTURE

It is well known that the water content in a pavement sublayer has a significant effect on the structural stiffness and performance of the pavement system. An increase in water content in a sublayer composed of a soil mixture (unbound base material) will affect the layer and likely result in reducing pavement service life. Therefore, to monitor water content in a sublayer, it is useful to understand the environmental effects (moisture related) on pavement performance.

Volumetric Relationship of Soil Mixture Components

In nature, soils can be describe with 3-phase system consisting of solid, water, and air, as shown in Figure 4-1. The total volume of a soil mixture can be considered as 1.0 and be expressed as:

$$V = V_s + V_w + V_a = 1.0 \qquad (4\text{-}1)$$

where

V = total volume of soil mixture

V_s = volume of soil solid

V_w = volume of water

V_a = volume of air

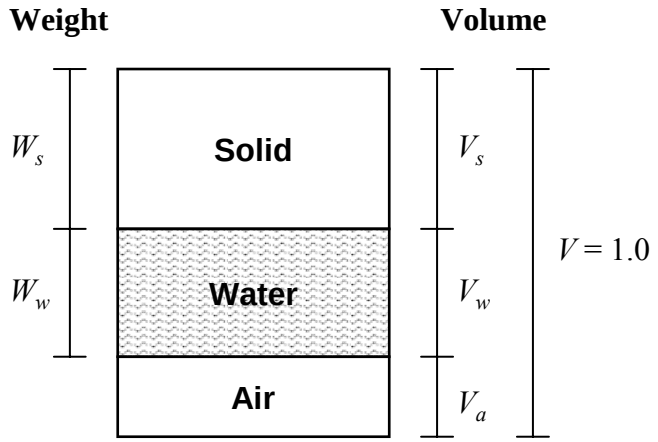

Figure 4-1 3-Phase of soil mixture

Therefore, the volume relationship used for 3-phase soil mixture can be expressed with respect to the unit weight and the specific gravity of the components. The specific gravity of solid can be given as:

$$G_s = \frac{1}{\gamma_w}\frac{W_s}{V_s} \tag{4-2}$$

or

$$W_s = G_s \gamma_w V_s \tag{4-3}$$

where

G_s = specific gravity of soil solid

γ_w = unit weight of water (g/cm^3)

W_s = weight of soil solid (g)

The dry unit weight defined as the weight per unit volume of soil excluding water can be expressed as:

$$\gamma_d = \frac{W_s}{V} \tag{4-4}$$

where

γ_d = unit weight (dry density) of soil (g/cm^3)

Thus, the volume occupied by solid in a soil mixture is:

$$V_s = \frac{\gamma_d}{G_s \gamma_w} \tag{4-5}$$

Because the total volume of soil mixture equals 1.0, it is convenient to express the volumes of the water, air and solids in terms of volumetric contents as:

$$V_{total} = V_s + V_w + V_a = \frac{\gamma_d}{G_s \gamma_w} + \theta + \left(1 - \frac{\gamma_d}{G_s \gamma_w} - \theta\right) = 1.0 \tag{4-6}$$

where

θ = volume fraction of water

Using the volumetric relationship determined in Equation (4-6) and the dielectric constant of each component as shown in Figure 4-2, the proposed self consistent model for soil mixture can be written based on Equation (3-6) (Lee et al. 2008):

$$\frac{\gamma_d}{G_s\gamma_w}\frac{\varepsilon_1-\varepsilon}{\varepsilon_1+2\varepsilon}+\theta\frac{\varepsilon_2-\varepsilon}{\varepsilon_2+2\varepsilon}+\left(1-\frac{\gamma_d}{G_s\gamma_w}-\theta\right)\frac{\varepsilon_3-\varepsilon}{\varepsilon_3+2\varepsilon}=0 \qquad (4\text{-}7)$$

where

ε = composite dielectric constant of soil mixture

ε_1 = dielectric constant of solids

ε_2 = dielectric constant of water

ε_3 = dielectric constant of air (= 1.0)

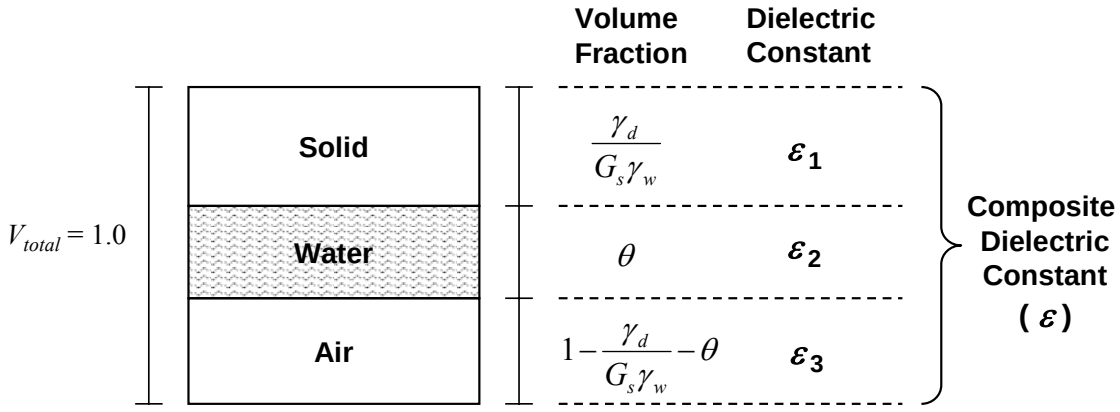

Figure 4-2 Relationship of volume fraction and dielectric constant of soil mixture

Data Collection

In order to apply the new approach for a soil mixture, the LTPP SMP database was used to access TDR trace data as well as the information on the pavement sections. As described in Chapter II, in the LTPP SMP, TDR was used to characterize the dielectric nature of pavement sublayers in 64 LTPP sections. Ten TDR probes were installed for each LTPP SMP section at specified depths in the unbound base and subgrade layers below the outer wheel path (Jiang and Tayabji 1999). The LTPP SMP database provides the user with the automated TDR traces, the installed depth and TDR probe information, and the material properties necessary for computing water contents (LTPP 2009). The

LTPP database has stored approximately 274,000 automated TDR traces for 64 LTPP test sections since 1993.

In this study, all TDR traces in the database were interpreted for estimating water content of pavement sublayer using the new approach. Also, for each LTPP SMP section, the dielectric constants of components in the soil mixtures were calibrated using ground truth data which are the measured in-situ water content and dry density values and corresponding manual TDR traces obtained during the installation of each TDR site. Table 4-1 lists the input table name and description obtained from LTPP SMP database for the process of the new approach to estimate the volume fractions in each soil.

Table 4-1 Description of Input Data Obtained from LTPP SMP Database

Input Table	Description
SMP_TDR_AUTO	Automated TDR trace : Sampled 245 intervals defining TDR wave form
SMP_TDR_DEPTHS_LENGTH	- Installed TDR depth from the pavement surface - TDR probe information
SMP_TDR_MOISTURE_SUPPORT	Material properties at each TDR site
TDR Installation Data	- Ground truth data · Water content (θ) · Dry density (γ_d) - Corresponding manual TDR traces

Determination Process for Water Content in Soil Mixture

Using the collected LTPP TDR trace data, soil water content and dry density of the associated pavement sublayers were determined based on the new approach consisting of the following three steps.

Determination of the composite dielectric constant (Step 1)

The existing methodology used in the analysis of LTPP SMP TDR traces to determine the dielectric constant is shown in Equation (2-22). The dielectric constant for the soil mixture has been determined by comparing the 'apparent' electrical length (L_a) of the probe from the TDR signal to its actual length. Clearly, this method of determination of the dielectric constant is independent of the conducting medium's other electrical properties besides the dielectric constant that could influence the resultant value since the soil magnetic permeability is, for instance, assumed to be unity. Saline or alkaline soils can create an effective electrical short with the shielding rods due to the ions in the water, which can increase the effect of conductivity on the value of the dielectric constant. Consequently, trace interpretation difficulties and erroneous determinations result because of the soil's high electrical conductivity, suggesting that an improved method of determining the dielectric constant would involve the consideration of the effect of the soil conductivity.

The dielectric constant of a soil is in reality a complex number, composed of a real part related to the expansion of the electric field and an imaginary part related to the contraction of the electric field, as shown in Equation (2-16). It is assumed in the apparent length method of analyzing TDR data that the imaginary part is negligible. As previously noted, the imaginary part is a measure of the ratio of the electrical conductivity of the soil to the dielectric property that is currently computed from TDR data. Ignoring the conductivity and the reflectivity causes a systematic error which results from imposing an incorrect model on the measured data. This error can be corrected or minimized by changing the model to one that more accurately reflects the actual physics of wave transmission through a dielectric medium. That is, the conductivity and reflectivity are required to be determined with the dielectric constant of a composite material.

Transmission Line Equation

It is noticed that voltage traveled through a composite dielectric material is a function of not only the dielectric constant but also of the conductivity and the reflectivity. Both of these parameters affect the inferred dielectric constant, or, in other words, they influence the value as it would be deducted from the characteristics of the trace. The systematic error caused by ignoring conductivity and reflectivity can be minimized by the use of the transmission line equation, accounting more completely for the actual physics of wave transmission through a dielectric medium in the model.

The voltage on the transmission line can be written as (Shen and Kong 1995; Zollinger et al. 2008):

$$V(z) = V_{+}e^{-jkz} + V_{-}e^{+jkz} \tag{4-8}$$

where

V = applied voltage

z = distance along the transmission line (TDR probe, m) = $\frac{c}{\sqrt{\varepsilon}}t$

c = velocity of electromagnetic wave = $\frac{1}{\sqrt{\mu_0 \varepsilon_0}}$

μ_0 = permeability of free space = 4π x 10^{-7} H/m

ε_0 = permittivity of free space = $\frac{1}{36\pi} x 10^{-9}$ F/m

t = travel time of wave

V_+ = voltage amplitude in the positive z direction

V_- = voltage amplitude in the negative z direction

k = dispersion coefficient = $k_R - jk_I$

k_R = real component

k_I = imaginary component

ε = dielectric constant of soil mixture

ω = angular frequency (rad/sec)

σ = soil conductivity (S/m)

The reflection coefficient and the relative voltage are defined respectively, as follows:

$$\Gamma_L = \frac{V_-}{V_+} \tag{4-9}$$

and

$$v(z) = \frac{V(z)}{V_+} \tag{4-10}$$

where

Γ_L = reflection coefficient (or reflectivity)

$v(z)$ = relative voltage as a function of the distance (z)

So, the Equation (4-8) can be developed further:

$$V(z) = V_+(e^{-jkz} + \Gamma_L e^{+jkz}) \tag{4-11}$$

and then

$$\begin{aligned} v(z) &= e^{-jkz} + \Gamma_L e^{+jkz} = e^{-j(k_R - jk_I)z} + \Gamma_L e^{+j(k_R - jk_I)z} \\ &= e^{-jk_R z - k_I z} + \Gamma_L e^{+jk_R + k_I z} \end{aligned} \tag{4-12}$$

In Equation (4-12), the dispersion coefficient (k) can be expressed for a slightly conducting or dielectric medium as (Shen and Kong 1995):

$$k = \omega\sqrt{\mu_0 \varepsilon}\left[1 - j\left(\frac{\sigma}{2\omega\varepsilon}\right)\right] \tag{4-13}$$

Thus, the real and imaginary components can be obtained as follows:

$$k_R = \omega\sqrt{\mu_0\varepsilon} \tag{4-14}$$

and

$$k_I = \frac{\sigma}{2}\sqrt{\frac{\mu_0}{\varepsilon}} \tag{4-15}$$

By being replaced with the distance (z) of TDR probe and the dispersion coefficient (k) of dielectric medium, the relative voltage can be expressed in terms of the time of travel as follows:

$$\begin{aligned} v(t) &= e^{-j\omega c\sqrt{\mu_0}t-\frac{\sigma c\sqrt{\mu_0}}{2\varepsilon}t} + \Gamma_L e^{+j\omega c\sqrt{\mu_0}t+\frac{\sigma c\sqrt{\mu_0}}{2\varepsilon}t} \\ &= Re\left[e^{-j\omega\frac{t}{\sqrt{\varepsilon_0}}-\frac{\sigma t}{2\varepsilon\sqrt{\varepsilon_0}}} + \Gamma_L e^{+j\omega\frac{t}{\sqrt{\varepsilon_0}}+\frac{\sigma t}{2\varepsilon\sqrt{\varepsilon_0}}} \right] \\ &= e^{-\frac{\sigma t}{2\varepsilon\sqrt{\varepsilon_0}}}\cos\left(\omega\frac{t}{\sqrt{\varepsilon_0}}\right) + \Gamma_L e^{+\frac{\sigma t}{2\varepsilon\sqrt{\varepsilon_0}}}\cos\left(\omega\frac{t}{\sqrt{\varepsilon_0}}\right) \\ &= \left(e^{-\frac{\sigma t}{2\varepsilon\sqrt{\varepsilon_0}}} + \Gamma_L e^{+\frac{\sigma t}{2\varepsilon\sqrt{\varepsilon_0}}} \right)\cos\left(\omega\frac{t}{\sqrt{\varepsilon_0}}\right) \end{aligned} \tag{4-16}$$

The use of the transmission line equation to analyze the TDR data corrects for the systematic error introduced by assuming that conductivity and reflectivity have no influence on the shape of the transmitted voltage with distance down the length of the TDR probe. The dielectric constants produced after correcting for the effects of conductivity and reflectivity will more correctly and precisely reflect the actual moisture state of the soil mixture (Zollinger et al. 2008). The concept of the transmission line equation and electromagnetics involved in the new approach is addressed in Appendix D.

Use of SID for Dielectric Constant Determination

The SID was used as the method of solving for the dielectric constant, conductivity, and reflectivity parameters. In order to fit the voltages from Equation (4-16) to those from the TDR trace, the three parameters (ε, σ, and Γ) were iterated until the output error between the equation and the TDR trace is less than 5.0 percent by satisfying the following which is based on the parameter adjustment algorithm (Equation (3-10)) and Equation (4-16) for each point selected from the trace:

$$[F] \qquad [\beta] \qquad = \qquad [r]$$

$$\begin{bmatrix} \frac{\partial v(t_1)_c}{\partial \varepsilon}\frac{\varepsilon}{v(t_1)_c} & \frac{\partial v(t_1)_c}{\partial \sigma}\frac{\sigma}{v(t_1)_c} & \frac{\partial v(t_1)_c}{\partial \Gamma}\frac{\Gamma}{v(t_1)_c} \\ \frac{\partial v(t_2)_c}{\partial \varepsilon}\frac{\varepsilon}{v(t_2)_c} & \frac{\partial v(t_2)_c}{\partial \sigma}\frac{\sigma}{v(t_2)_c} & \frac{\partial v(t_2)_c}{\partial \Gamma}\frac{\Gamma}{v(t_2)_c} \\ \vdots & \vdots & \vdots \\ \frac{\partial v(t_m)_c}{\partial \varepsilon}\frac{\varepsilon}{v(t_m)_c} & \frac{\partial v(t_m)_c}{\partial \sigma}\frac{\sigma}{v(t_m)_c} & \frac{\partial v(t_m)_c}{\partial \Gamma}\frac{\Gamma}{v(t_m)_c} \end{bmatrix}_{m\times 3} \times \begin{bmatrix} \frac{\varepsilon^{j+1}-\varepsilon^j}{\varepsilon^j} \\ \frac{\sigma^{j+1}-\sigma^j}{\sigma^j} \\ \frac{\Gamma^{j+1}-\Gamma^j}{\Gamma^j} \end{bmatrix}_{3\times 1} = \begin{bmatrix} \frac{v(t_1)_{meas}-v(t_1)_c}{v(t_1)_c} \\ \frac{v(t_2)_{meas}-v(t_2)_c}{v(t_2)_c} \\ \vdots \\ \frac{v(t_m)_{meas}-v(t_m)_c}{v(t_m)_c} \end{bmatrix}_{m\times 1} \tag{4-17}$$

where

$v(t_m)_c$ = calculated voltage based on the current values of ε, σ, and Γ

$v(t_m)_{\text{meas}}$ = measured voltage from TDR trace

m = number of selected data points between initial and final deflection points

j = iteration count

The number of recorded voltage points from the TDR trace determines the number of rows in [F] and [r] while the numbers of rows in [β] and column in [F] depend on the parameters. Solving for [β]:

$$[\beta] = \left[F^T F\right]^{-1}\left[F^T\right][r] \tag{4-18}$$

The SID calculates the voltages ($v(t_n)_c$) along with unknown values (ε, σ, and Γ) to be determined for each iteration and then compares them with the measured voltage ($v(t_n)_{meas}$) measured from TDR. When each element in the [β] matrix is less than 0.05 through iteration, solutions for parameters (ε, σ, and Γ) are found.

The size of the random error (i.e. measurement error in the TDR device) should be determined by statistical evaluation of repeated TDR measurements that are not presently available. Inherent in this analysis are the minimum number of points (N) from the TDR trace that should be used to provide a reasonably accurate estimate of the dielectric constant. Accordingly, this analysis suggests that using twice as many data points as the number of coefficients to be determined, which would be six in this case, might be sufficient in estimated dielectric constant, conductivity, and reflectivity assuming a measurement error of 3 percent in the TDR voltage trace. In this regard, the six points would be selected between the first and second inflection points, where the first and second inflection points are points 1 and 6, respectively, and the other four points were equally distributed between the inflection points. Figure 4-3 shows an example of manual TDR trace and selected six data points between the inflection points.

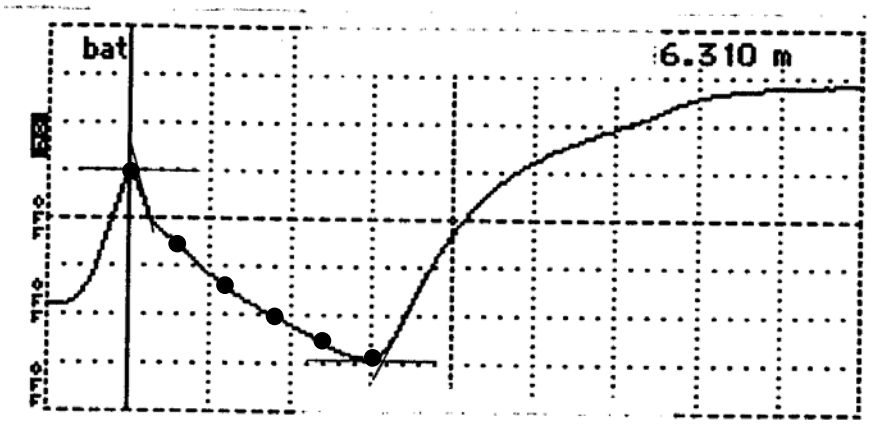

Figure 4-3 Manual TDR trace and selected points (LTPP section 308129, TDR No. 8)

In fact, six data points were selected in TDR trace for the purpose of calibration in which to characterize the manual TDR traces obtained during TDR installation. For the calibration process, the ground truth data (in-situ water content and dry density) were also required with the TDR trace data. In the computational program developed for the new approach, all data points between the inflection points were used to determine the three dielectric properties since the data are available in the automated TDR trace obtained at different times throughout the monitoring period. The program will be discussed later.

Calibration of soil component dielectrics (Step 2)

In order to calculate the water content and dry density, the new approach requires the following calibrated values for each LTPP SMP site and layer at which TDR probes were placed:

- Dielectric constant of solids (ε_1)
- Dielectric constant of water (ε_2)
- Dielectric constant of air (ε_3)
- Specific gravity (G_s)

These values are calibrated using the ground truth data and corresponding TDR trace previously described. During installation, tests for water content and dry density measurements were performed on the material placed around TDR probes with additional material samples retained for laboratory analyses (Rada et al. 1995). The ground truth data consisted of measured water content dry density values and manual TDR traces. The data can be also obtained from the reports of LTPP SMP Site Installation and Initial Data Collections for the selected test sections.

With a composite dielectric constant from step 1, the values for the noted dielectric constants and specific gravity are adjusted based on the ground truth data.

Since the dielectric constant of air is 1.0 (i.e. ε_3 = 1.0), only three values of dielectric constants of water and soil solid and specific gravity are backcalculated based on Equation (4-7):

$$f\left(\varepsilon_1,\varepsilon_2,G_s\right)=\frac{\gamma_d}{G_s\gamma_w}\frac{\varepsilon_1-\varepsilon_c}{\varepsilon_1+2\varepsilon_c}+\theta\frac{\varepsilon_2-\varepsilon_c}{\varepsilon_2+2\varepsilon_c}+\left(1-\frac{\gamma_d}{G_s\gamma_w}-\theta\right)\frac{\varepsilon_3-\varepsilon_c}{\varepsilon_3+2\varepsilon_c}=0 \tag{4-19}$$

where

ε_c = calculated composite dielectric constant of soil

These unknown values (ε_1, ε_2, and G_s) can be solved using partial derivatives of Equation (4-19) and SID analysis previously outlined step as follows:

$$[F] \qquad [\beta] \quad = \quad [r]$$

$$\left[\frac{\partial\varepsilon_c}{\partial\varepsilon_1}\frac{\varepsilon_1}{\varepsilon_c} \quad \frac{\partial\varepsilon_c}{\partial\varepsilon_2}\frac{\varepsilon_2}{\varepsilon_c} \quad \frac{\partial\varepsilon_c}{\partial G_s}\frac{G_s}{\varepsilon_c}\right]_{1\times3}\times\begin{bmatrix}\dfrac{\varepsilon_1^{j+1}-\varepsilon_1^j}{\varepsilon_1^j}\\ \dfrac{\varepsilon_2^{j+1}-\varepsilon_2^j}{\varepsilon_2^j}\\ \dfrac{G_s^{j+1}-G_s^j}{G_s^j}\end{bmatrix}_{3\times1}=\left[\frac{\varepsilon_{meas}-\varepsilon_c}{\varepsilon_c}\right]_{1\times1} \tag{4-20}$$

where

ε_c = calculated soil dielectric constant based on current values of ε_1, ε_2, and G_s along with ground truth data

ε_{meas} = measured soil dielectric constant determined from step 1

Solving for each element in sensitivity matrix [F]:

$$\frac{\partial \varepsilon_c}{\partial \varepsilon_i} = \frac{\partial f(\varepsilon_1, \varepsilon_2, G_s) \Big/ \partial \varepsilon_i}{\partial f(\varepsilon_1, \varepsilon_2, G_s) \Big/ \partial \varepsilon_c} \tag{4-21}$$

and

$$\frac{\partial \varepsilon_c}{\partial G_s} = \frac{\partial f(\varepsilon_1, \varepsilon_2, G_s) \Big/ \partial G_s}{\partial f(\varepsilon_1, \varepsilon_2, G_s) \Big/ \partial \varepsilon_c} \tag{4-22}$$

where

ε_i = ε_1 and ε_2

Since the ground truth data were measured only once at each section, [F] and [r] have a single row. The numbers of rows in [β] and column in [F] are three due to the self consistent model including three parameters for the calibration step. Solving for [β]:

$$[\beta] = \left[F^T F\right]^{-1} \left[F^T\right][r] \tag{4-23}$$

Typical values of ε_1 range between 3 and 8 while typical values of G_s range between 2.6 and 2.9 (Daniels 1996; Das 2002). The SID method calculates the dielectric constant (ε_c) along with assumed parameters and the ground truth density and water content data for each iteration and then compares it with the measured dielectric constant (ε_{meas}) determined from Step 1. When the elements in change vector [β] are less than 0.05, the loop terminates and parameters (ε_1, ε_2, and G_s) at that iteration is reported as the final result. The calibrated values are further used to calculate volumetric water content and dry density associated with each TDR measurements at other times.

The analysis results of selected TDR traces, as examples, are shown in Table 4-2. The four LTPP sections in Table 4-2 were selected to represent a range of soil types which were gravel, sand, silt, and clay. For each section, TDR trace and corresponding ground truth water content and dry density measured at TDR installation were used to calibrate the dielectric constant of solid and water and specific gravity.

Table 4-2 Calibrated Values for Representative Sections

Section/ TDR No.	Soil Type	Measured Values		Calibrated Values		
		VWC* (%)	Dry Density (g/cm^3)	Dielectric Constant		Specific Gravity (G_s)
				Solid (ε_1)	Water (ε_2)	
364018/ 9	Gravel	26.12	2.24	3.70	79.7	2.70
091803/ 4	Sand	33.28	2.26	3.65	80.4	2.74
131031/ 8	Silt	40.75	1.80	3.47	79.9	2.77
421606/ 6	Clay	19.01	1.94	3.38	80.0	2.78

* Volumetric Water Content

Forward computation of water content and dry density (Step 3)

In the forward calculation of volumetric water content and dry density that is performed in step 3, the self consistent model in Equation (4-7) is used together with the calibration constants ε_1, ε_2, and G_s to determine values of water content and dry density from the dielectric constant of soil mixture derived from subsequent TDR data collection records.

Another systematic error resulting from the empirical method used previously to estimate water content from TDR application in the LTPP study was due to assuming that the dry density of soil was unvarying with moisture content. Although the dry density value of soil mixture in the unbound base or subgrade layer may be changed as a result of the variation of water or air content in the material, the existing method is based on a constant dry density measured at TDR installation. This error can be removed by

considering the dielectric effect of the air in soil mixture and calculating the dry density of soil every time the water content is estimated (Lee et al. 2008). With a composite dielectric constant determined from step 1, the two unknown values can be found using the self consistent model of Equation (4-7) as:

$$f\left(\gamma_d,\theta\right)=\frac{\gamma_d}{G_s\gamma_w}\frac{\varepsilon_1-\varepsilon_c}{\varepsilon_1+2\varepsilon_c}+\theta\frac{\varepsilon_2-\varepsilon_c}{\varepsilon_2+2\varepsilon_c}+\left(1-\frac{\gamma_d}{G_s\gamma_w}-\theta\right)\frac{\varepsilon_3-\varepsilon_c}{\varepsilon_3+2\varepsilon_c}=0 \tag{4-24}$$

The new composite dielectric constants are determined by analysis of the TDR traces obtained at different times throughout the monitoring period. Thus, once particular soil characteristics (ε_1, ε_2, and G_s) are "identified" by step 2, all future calculations of volumetric water content and dry density can be determined from a new soil mixture dielectric constant measured in step 1 using the SID as follows:

$$\begin{matrix}[F] & & [\beta] & = & [r]\end{matrix}$$

$$\left[\frac{\partial\varepsilon_c}{\partial\gamma_d}\frac{\gamma_d}{\varepsilon_c}\quad\frac{\partial\varepsilon_c}{\partial\theta}\frac{\theta}{\varepsilon_c}\right]_{1\times2}\times\left[\begin{matrix}\dfrac{\gamma_d^{j+1}-\gamma_d^{j}}{\gamma_d^{j}}\\[2ex]\dfrac{\theta^{j+1}-\theta^{j}}{\theta^{j}}\end{matrix}\right]_{2\times1}=\left[\frac{\varepsilon_{meas}-\varepsilon_c}{\varepsilon_c}\right]_{1\times1} \tag{4-25}$$

where

ε_c = calculated soil dielectric constant based on current values of θ and γ_d along with calculation values

Solving for each element in sensitivity matrix [F]:

$$\frac{\partial\varepsilon_c}{\partial\gamma_d}=\frac{\partial f(\theta,\gamma_d)\big/\partial\gamma_d}{\partial f(\theta,\gamma_d)\big/\partial\varepsilon_c} \tag{4-26}$$

and

$$\frac{\partial \varepsilon_c}{\partial \theta} = \frac{\partial f(\theta, \gamma_d) \big/ \partial \theta}{\partial f(\theta, \gamma_d) \big/ \partial \varepsilon_c} \tag{4-27}$$

The matrix [*F*] and [*r*] have one row because the calculation is performed using a composite dielectric constant obtained from a single TDR measurement. The number of rows in [β] and column in [*F*] are two due to two unknown parameters (θ and γ_d) in the self consistent model. Solving for [β]:

$$[\beta] = \left[F^T F\right]^{-1} \left[F^T\right][r] \tag{4-28}$$

This calculation process is continued within a loop that terminates when each element of the change vector [β] is less than 0.05. Figure 4-4 illustrates the whole procedure of new approach used to estimate the volume fraction of a soil mixture of the unbound base or subgrade layers using TDR trace data.

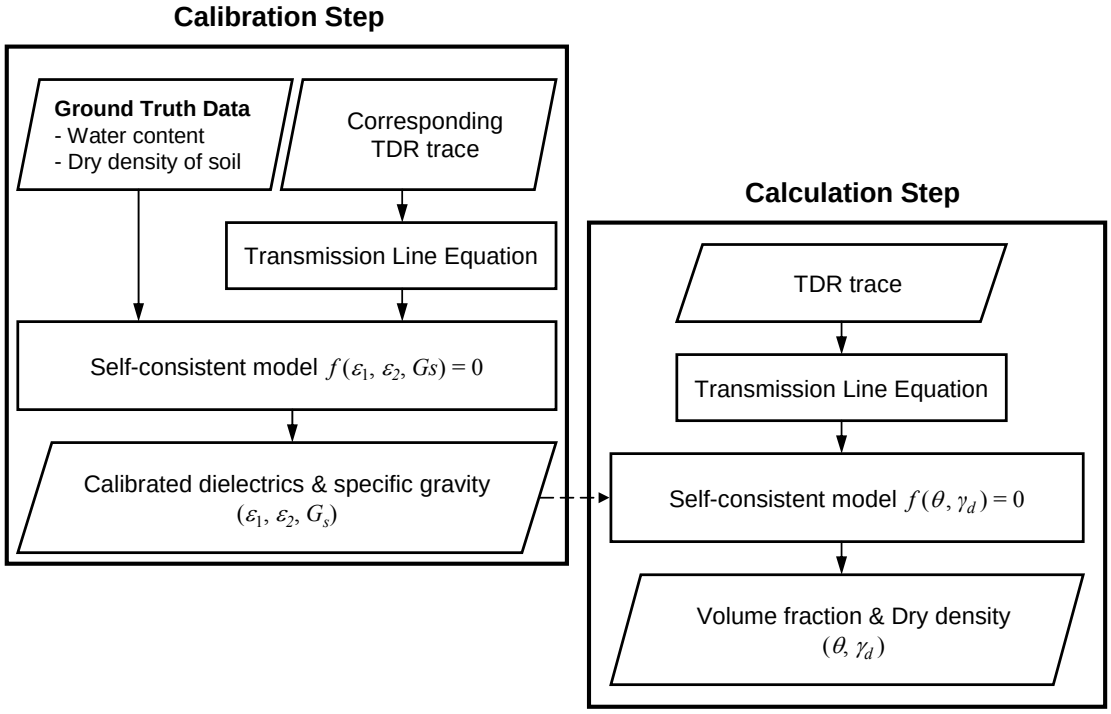

Figure 4-4 Procedure of new approach for soil mixture

Validation of New Approach for Soil Mixture

The effectiveness of the new procedures was manifest by comparing the water contents computed both from the existing empirical method and from the new method to the laboratory water content tests from representative LTPP SMP sites. While the new procedures consist of the transmission line equation method for determining soil dielectric constant and the self consistent method for calculating water content, the existing methods are based on the apparent length method and the third-order polynomial dielectric constant (K_a)–soil gradation model which were described in Chapter II. Ground truth data that is linked to specific TDR traces for LTPP SMP soils were identified from two sources.

1. Laboratory Validation – Data obtained from Klemunes' study of collecting TDR data in a laboratory where soil water content and density are known, using samples obtained from LTPP sites (Klemunes 1995).

2. Field Validation – Available information from LTPP sites in which forensic evaluations were performed. TDR traces were taken in the field just prior to removal of the equipment and soil sampling.

These sources provide important reference water contents to evaluate the capabilities of the new approach. The sources provided the only data available to perform validation specific to the LTPP study.

Laboratory validation

The first validation effort consisted of computing the water content and dry density for the test data noted in Klemunes' thesis work (Klemunes 1995). Data from four of the 28 LTPP SMP sections used in this study were selected to provide a range of soil types (i.e., gravel, sand, silt, and clay). For each section, TDR trace and corresponding ground truth water content and dry density measured at TDR installation were used to calibrate the dielectric constants of solid and water and specific gravity. Table 4-3 presents the ground truth data and the calibrated values for each section.

Table 4-3 Calibration of Dielectric Constant and Specific Gravity

Section	Soil Type	Measured Values		Calibrated Values		
		VWC (%)	Dry Density (g/cm^3)	Dielectric Constant		Specific Gravity (G_s)
				Solid (ε_1)	Water (ε_2)	
271028	Gravel	7.06	2.017	3.79	80.6	2.724
231026	Sand	19.35	1.960	3.79	80.0	2.782
091803	Silt	20.38	2.264	3.89	81.0	2.864
081053	Clay	21.57	1.634	3.79	80.0	2.890

Using the calibrated information and the TDR traces obtained at different water contents, the volumetric water content and dry densities were computed as shown in Table 4-4 along with estimates from the empirical model and the laboratory test results. Figure 4-5 indicates the associated water content difference of each method for each trial on the laboratory test result. As can be seen, the new method provides significantly accurate estimates of actual water contents with the majority of estimates falling within 5 percent of the laboratory derived data. Given the circumstances surrounding the collection of the different types of water data involved in this analysis, the degree of comparability is remarkable.

The validation of estimated dry densities was also performed by comparison to measured values obtained from the laboratory test. Figure 4-6 shows the high capability and accuracy of the new approach in estimating dry density with a maximum resulting difference of less than 6 percent. This verification was considered to be laboratory based because the soil mixtures and TDR traces were obtained in a laboratory setting where the sampling and data collection were more controlled.

Table 4-4 Comparison of Results

Test Section		Soil Type	Dry Density (g/cm^3)		Volumetric Water Contents (%)			
			Lab. Result	New Method	Lab Result	Existing Method		New Method
271028	C	Gravel	1.730	1.810	7.09	9.36	Coarse-K_a	7.79
	F		1.712	1.700	12.50	13.92	Coarse-K_a	12.17
	K		1.766	1.869	18.98	20.06	Coarse-K_a	19.78
231026	B	Sand	1.574	1.558	14.88	15.40	Coarse-K_a	14.25
	F		1.635	1.610	22.98	21.78	Coarse-K_a	21.95
	M		1.605	1.569	7.54	8.34	Coarse-K_a	7.18
091803	C	Silt	0.976	0.989	38.45	29.63	Fine-K_a	38.05
	I		0.965	0.924	27.12	21.01	Fine-K_a	28.07
	P		0.965	0.927	29.65	20.48	Fine-K_a	28.94
	W		0.973	0.923	39.30	32.35	Fine-K_a	38.16
081053	G	Clay	1.406	1.350	44.07	51.80	Fine-Gradation	44.81
	K		1.400	1.321	48.83	51.80	Fine-Gradation	48.03
	U		1.377	1.440	30.72	29.67	Fine-Gradation	31.29

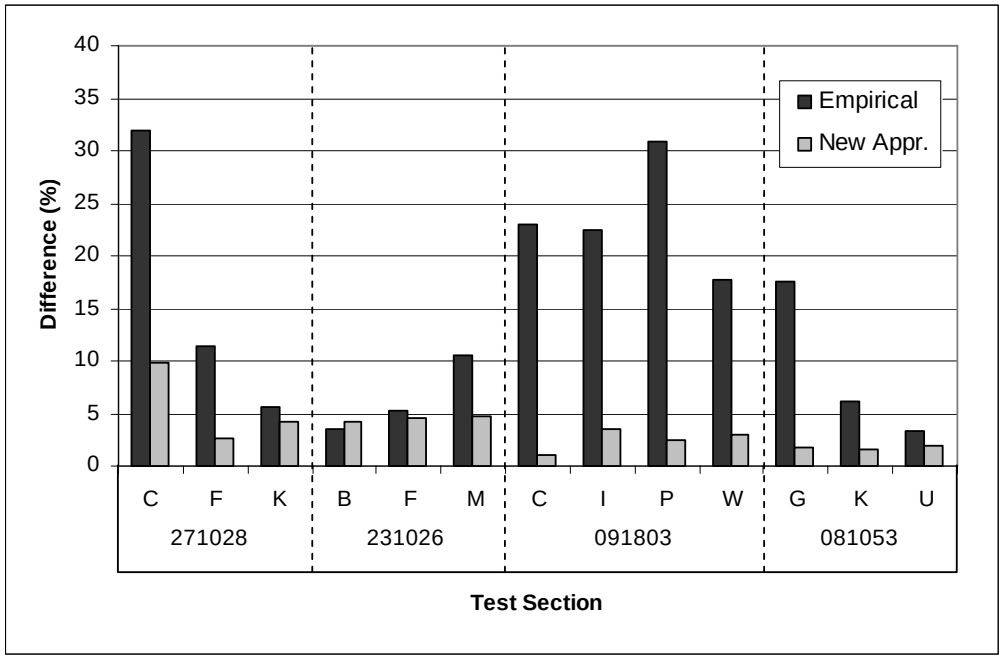

Figure 4-5 Errors of volumetric water content on ground truth data

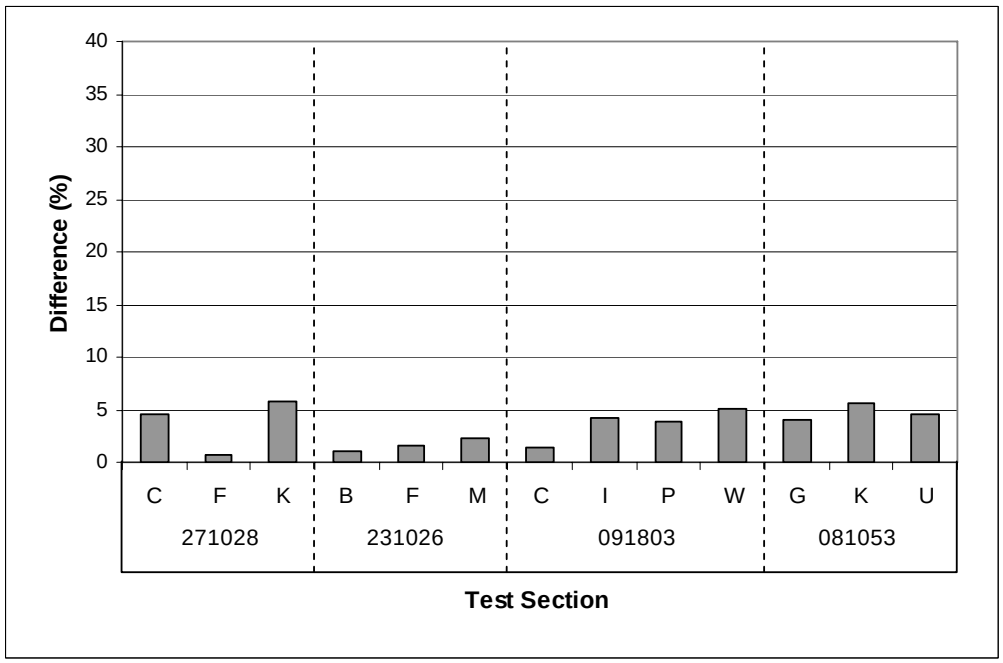

Figure 4-6 Errors of estimated dry density on ground truth data

Field validation

Another evaluation was performed using the data developed for a forensic report on LTPP SMP section 091803 located in southern Connecticut. In this case, the calibration process was conducted using the ground truth water content obtained during the equipment installation as shown in Table 4-5. The calibration values were used to estimate water content based on the other TDR traces obtained during the forensic investigation. These resulting water estimates were compared to the laboratory test results for samples taken just after the TDR traces were obtained during the forensic activities.

Table 4-5 Calibration Values for LTPP Section 091803

Layer Type	Soil Type	Measured Values		Calibrated Values		
		VWC (%)	Dry Density (g/cm^3)	Dielectric Constant		Specific Gravity (G_s)
				Solid (ε_1)	Water (ε_2)	
Base	Gravel	25.71	2.255	3.69	79.8	2.44
Subbase	Silty Gravel	32.92	2.260	3.65	80.4	2.74

Those test comparisons can be seen in Table 4-6 with the resulting difference quantities in Figure 4-7. In general, the amount of difference is significantly less for the new method as compared to the existing method. This was not the case for TDR number 3 and 7, but the difference for both methods was less than 5 percent. The values of dry density estimated by the new approach were evaluated by comparing them to measured values. As shown in Figure 4-8, the resulting differences on measured values were slightly higher than for the laboratory verification but still highly accurate at less than 7 percent.

Table 4-6 Comparison of Results for LTPP Section 091803

Layer Type	Soil Type	TDR No.	Depth (mm)	Dry Density (g/cm^3)		Volumetric Water Content (%)			
				Lab Result	New Method	Lab Result	Existing Method		New Method
Base	Medium brown gravel	1	330	2.229	2.297	17.39	20.69	Coarse-K_a	16.25
		2	437	2.255	N/A*	15.81	N/A*	-	N/A*
Subbase	Grayish brown silty gravel with large rock	3	584	2.163	2.243	27.94	26.96	Coarse-K_a	26.75
		4	737	2.163	2.293	26.00	22.54	Coarse-K_a	26.34
		5	889	2.166	2.021	19.82	22.54	Coarse-K_a	19.19
		6	1041	2.192	2.343	16.80	20.69	Coarse-K_a	17.11
		7	1194	2.192	2.196	20.75	21.25	Coarse-K_a	21.67
		8	1346	2.091	1.988	25.76	25.94	Coarse-K_a	25.57

* Impossible to interpret TDR trace

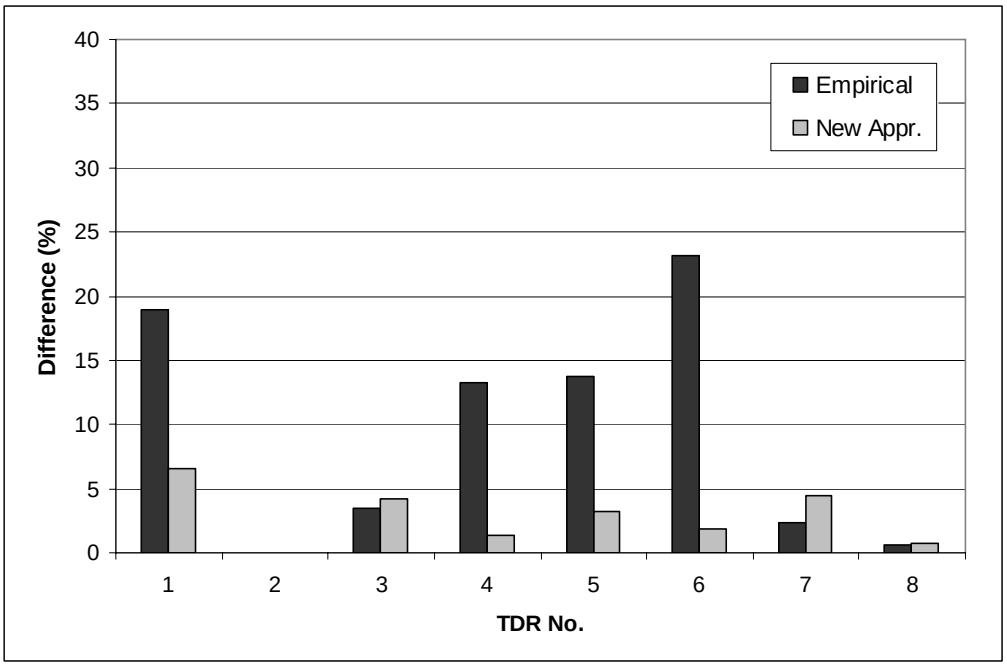

Figure 4-7 Errors of volumetric water content on ground truth data for LTPP Section 091803

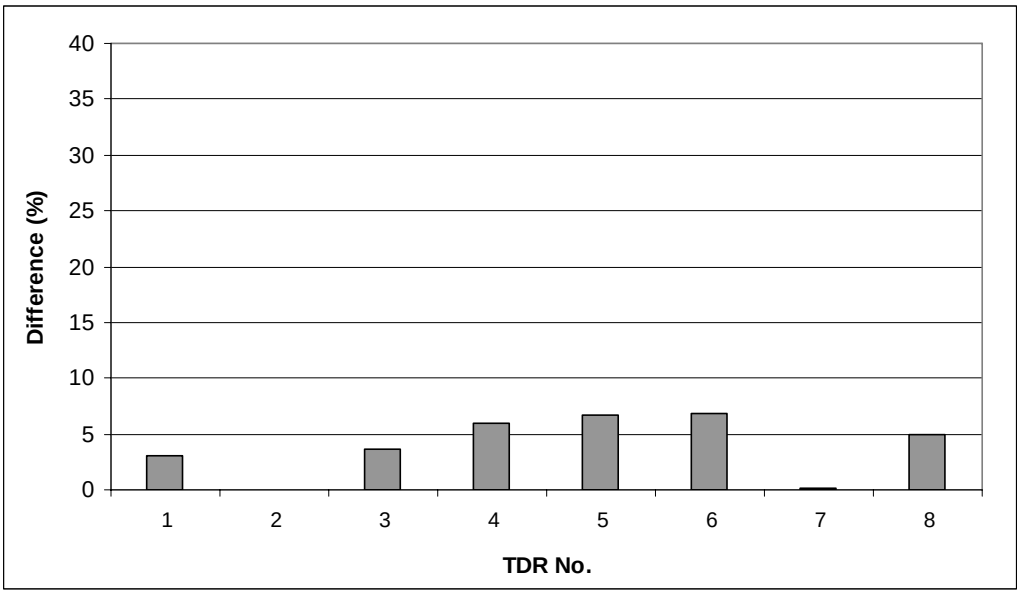

Figure 4-8 Errors of estimated dry density on ground truth data for LTPP Section 091803

From both validations, the new method resulted in more accurate and robust water content estimates when compared to the laboratory test results than did the existing method. The resulting differences for both methods were less then 5 percent even where the new method did not show less difference. Also, the dry density values estimated from the new approach were close to the values measured in the laboratory with differences mainly below 5 percents.

PORTLAND CEMENT CONCRETE

During the hydration process of portland cement concrete (PCC) which is a composite material used in pavements, the free water continually reacts with the compounds of cement and forms chemical bonds. The development of the process results in the reduction of free movement of water molecules, and consequently the concrete gains hardness. Thus, the measurement of the amount of free water in fresh cement concrete is a very important part for understanding cement hydration. In order to estimate water content in cement concrete, many techniques have been used while the concrete was

going through the hydration process such as X-ray diffraction, electron microscopy, or thermal analysis. However, these methods are not suitable for continuous testing and are not appropriate for in-situ measurement (Zhang et al. 1996).

For decades, there has been increased interest in test methods using dielectric properties of PCC for estimating water content (Camp and Bilotta 1989; Gu and Beaudoin 1996; Hager III and Domszy 2004; van Beek et al. 1997; van Beek et al. 1999; Zhang et al. 1996). They have shown that the dielectric constant of PCC is sensitive to the water content and the degree of hydration; that is, as the dielectric constant of a PCC sample is higher, the sample contains higher water content and needs more time to complete hydration. The dielectric constant is a beneficial parameter to estimate the water content since it can provide a continuous non-destructive measurement technique used even during hydration. Based on the dielectric constant, estimating the volume fraction of free water and any other components is useful to understand the hydration of PCC.

Volumetric Relationship of PCC Components

In order to estimate the volume fraction of each component in PCC mixture, volumetric relationships are required, which can be ascertained using the self consistent model. While the soil mixture can be clearly defined as a 3-phase material consisting of solid, water, and air void, PCC mixture is far more complex due to the several phases in hydrated cement paste (HCP). Different models for hydrated cement concrete were proposed to describe the structure and the weight-volume relationship of its components: Powers-Brownyard HCP model, Feldman-Sereda model, and Breugel model (Powers 1947; Taylor 1997).

Structural models for hydrated cement concrete

From the volumetric standpoint, the Powers-Brownyard HCP model assumes that hardened portland cement paste consists of three components: unreacted cement,

hydration product, and capillary pores. On the other hand, during hydration for which the water is present in the paste, the model categorizes water into two types: evaporable and non-evaporable water. The evaporable water includes the waters both in capillary pores and in gel pores. The water in gel pores is included within the hydration products. The non-evaporable water whose content is proportional to the amount of hydration that has taken place contains all chemically combined water. As the hydration of cement takes place, the volume fraction of capillary water (w_{cap}), as part of the initially water filled space, decreases and the pores increase. The hydration product includes reacted cement, gel water (w_g), and non-evaporable water (w_n). Figure 4-9 illustrated the diagrams of the Powers-Brownyard model for the phases of cement paste during hydration (Taylor 1997).

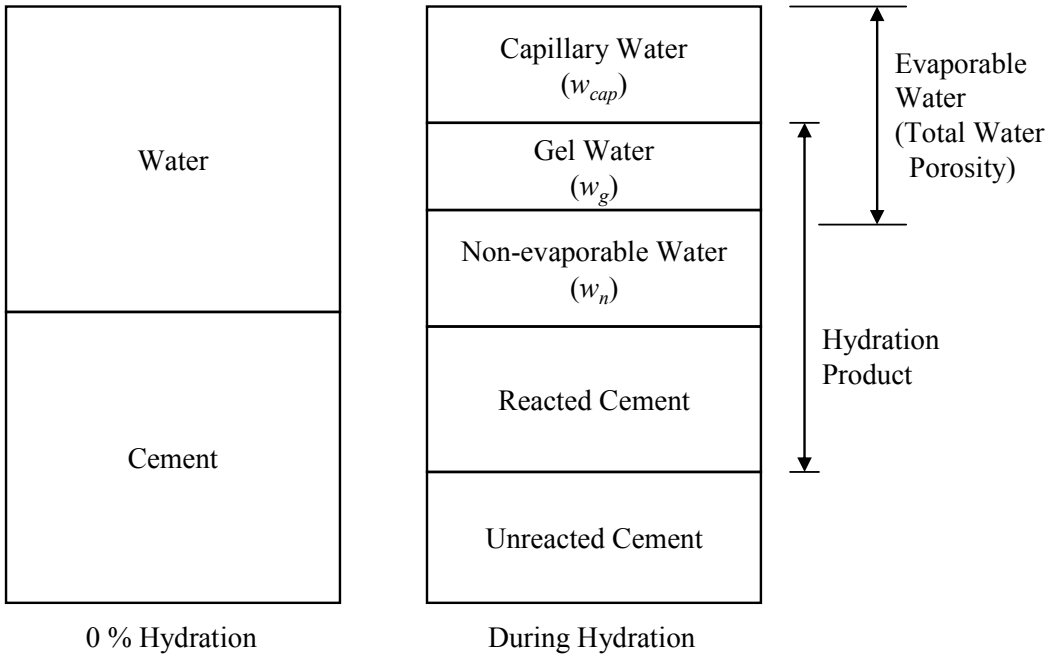

Figure 4-9 Diagram of volumetric proportions of cement paste by hydration process based on the Powers-Brownyared model (Taylor 1997)

Feldman and Sereda developed a structural model that the gel consists of C-S-H layers as a three dimensional structure which surrounds capillary pores as shown in

Figure 4-10 (Feldman and Sereda 1970; Taylor 1997). In this model, the interlayer water held chemically between the surfaces of C-S-H layers is regarded as the gel water in Powers-Brownyard's model. The water held by the surface energy of the gel particles is the adsorbed water which is non-evaporable water. On the other hand, the free water, also called capillary water, is held in capillaries but not held by any surface forces of the gel particles. Figure 4-10 (a) shows a schematic formation of cement paste microstructure in hydration process and Figure 4-10 (b) illustrates the Feldman-Sereda model for C-S-H structure in a part boxed of Figure 4-10 (a).

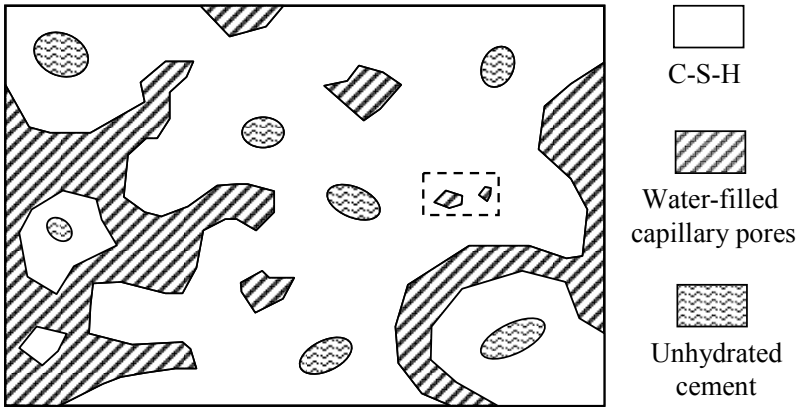

(a) Microstructural formation of cement paste in hydration (Mindess et al. 2003)

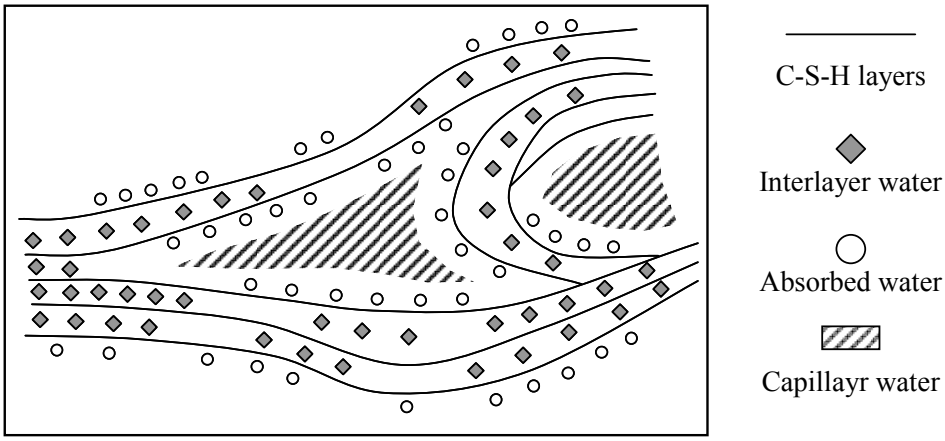

(b) Feldman-Serada model for C-S-H structure (Taylor 1997)

Figure 4-10 Schematic diagram of hydrated cement paste by Feldman-Serada model

Breugel proposed a way to classify a hydrating water into three different forms: chemically bound water, physically bound water, and free (capillary) water (Breugel 1991). The water which is tightly bonded on the surface of hydration product is the chemically bound water. This water is regarded to be an inherent part of the solid matter making up the hydration product. The physically bound water whose amount actually depends on the relative humidity on the pore system is adsorbed on the gel particles and regarded as a part of the gel which is not available for future hydration. As the classification of Powers-Brownyared Model, the chemically and physically bound waters can be defined as the non-evaporable waters (w_n). In the Breugel's water system, if water can be removed by oven drying (105°C) of cement paste, it can be classified as free or evaporable water. The free water is available for hydration of cement paste. The schematic water system of Breugel's classification is illustrated in Figure 4-11.

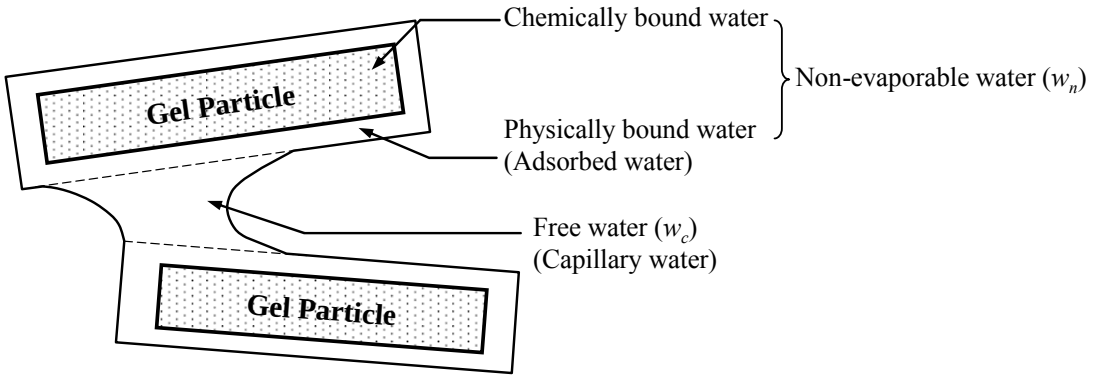

Figure 4-11 Schematic formation of water system (Breugel 1991)

Development of a volumetric model for quantification of each component

Although the existing models are used widely to describe the structure relationship of hydrated PCC, another model was required, in this study, to describe the volumetric relationship for estimating the volume fraction of each component. The volumetric model is necessary for the quantification of individual volume components as a fraction of the fresh concrete volume. In order to meet the purpose, the Breugel model was

modified for PCC with reference to Powers-Brownyard and Feldman-Sereda models (Avelar Lezama 2005).

Since the quantitative analysis of the hydrating PCC needs definition of basic weight-volume relationships, the modified Breugel model was developed based on the commonly accepted components and arrangement. Concrete can be defined as the mixture of five components:

(a) Free water
(b) Hydrated cement paste product (including physically and chemically bound waters)
(c) Unreacted cement
(d) Aggregate (including gravel and sand)
(e) Air

Because the physically bound water is considered as an inherent part of the solid hydration product and the chemically bound water as a part of the gel, they are included in the component of hydrated cement product. The relative humidity is an indicator of the amount of water in portland cement. Since capillary pores have comparatively large size (1.3μm), they are considered to be empty when the ambient relative humidity is less than 45 percent; thus, the free (capillary) water would be evaporated at low relative humidity (Breugel 1991). However, the chemically bound water cannot move into the capillary pores and remains adsorbed in the gel pores even at low ambient humidity (Verbeck 1956). Figure 4-12 shows the relationship between relative humidity and all types of water in cement concrete.

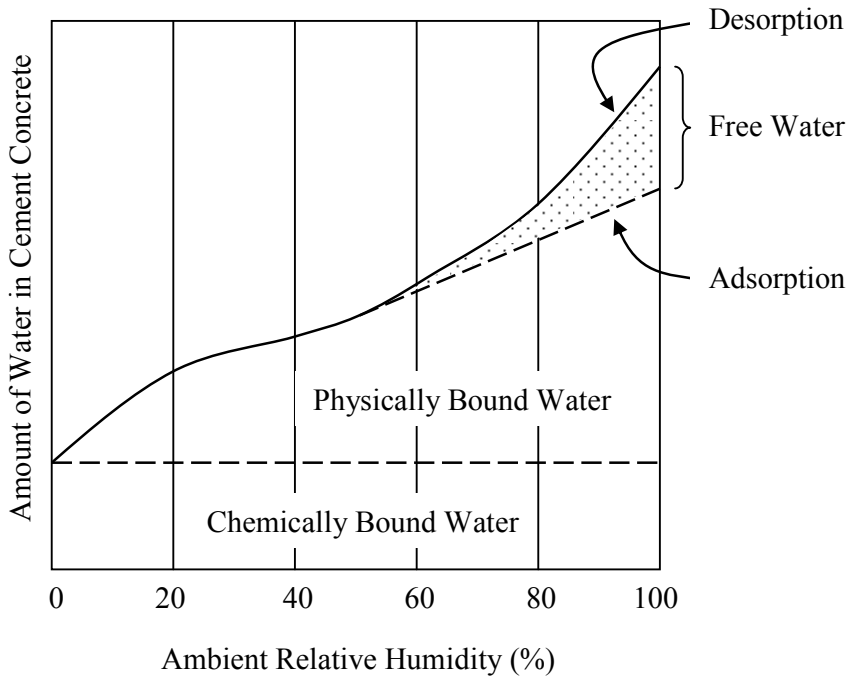

Figure 4-12 Relationship between water and relative humidity (Breugel 1991)

In this study, the modified Breugel model is used as a volumetric model to estimate the volumetric contents of components in fresh PCC based on dielectric properties. Figure 4-13 illustrates the weight and volume relationships of the modified Breugel model.

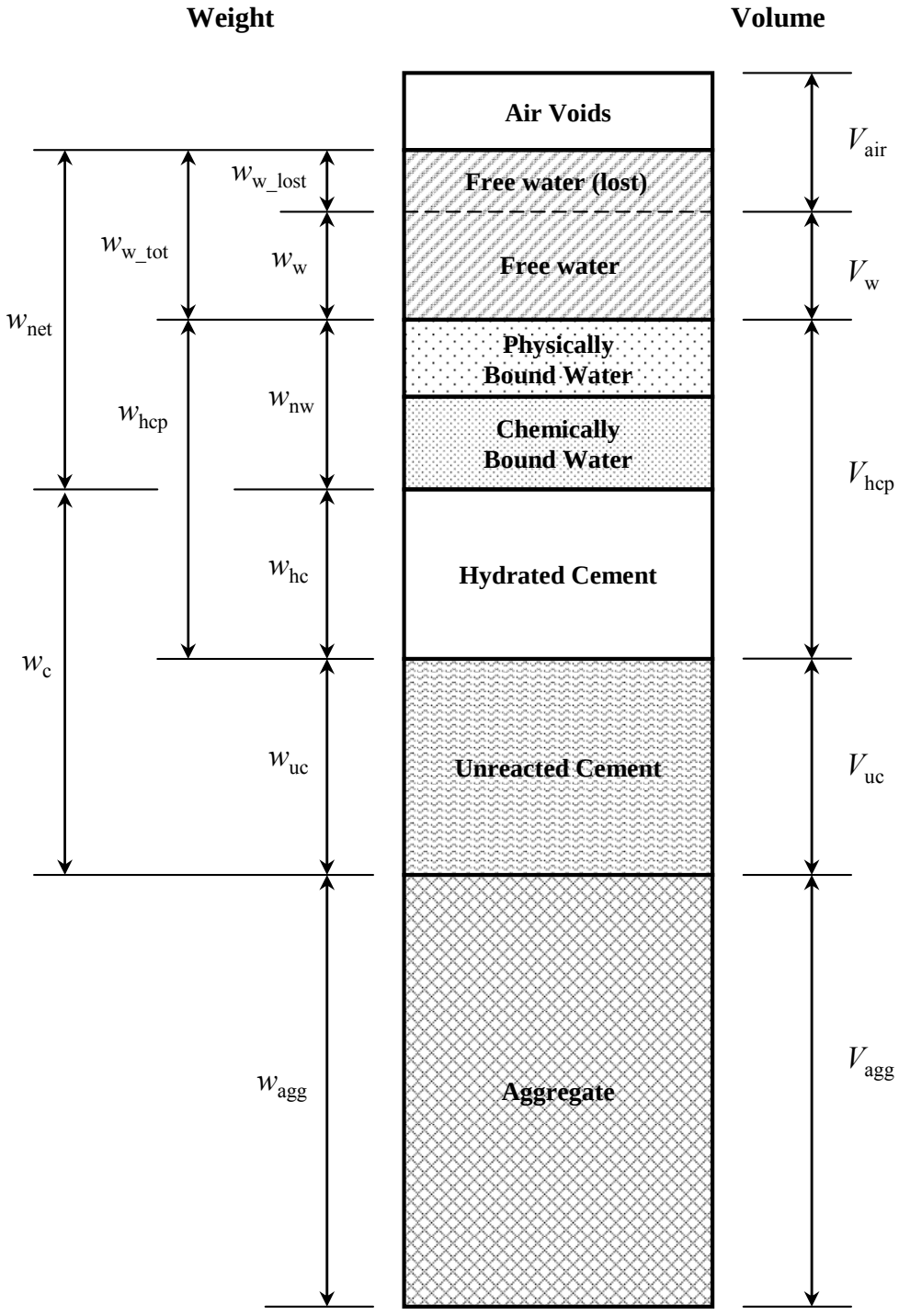

Figure 4-13 Modified Breugel weight-volumetric model for portland cement concrete (Avelar Lezama 2005; Breugel 1991)

Volumetric relationship of components

In order to develop the weight-volume relationships, a cement concrete mixture should be separated into five phases whose dielectric constants can be determined individually, as shown in Figure 4-13. The total volume of a PCC in hydration process can be expressed as:

$$V_{\text{total}} = \sum V_i = V_w + V_{hcp} + V_{uc} + V_{agg} + V_{air} \quad (4\text{-}29)$$

where

V_{total} = total volume of cement concrete
V_i = volume of component *i*
V_w = volume of free water
V_{hcp} = volume of hydrated cement concrete
V_{uc} = volume of unreacted cement
V_{agg} = volume of aggregate
V_{air} = volume of porosity (air voids)

Assuming that the weight of porosity is negligible, the total weight of cement concrete is:

$$w = \sum w_i = w_w + w_{nw} + w_{hc} + w_{uc} + w_{agg} = w_w + w_{hcp} + w_{uc} + w_{agg} \quad (4\text{-}30)$$

where

w = total volume of cement concrete
w_i = weight of component *i*
w_{w} = weight of free water
w_{nw} = weight of non-evaporable water
w_{hc} = weight of hydrated cement
w_{uc} = weight of unreacted cement

w_{agg} = weight of aggregate

w_{hcp} = weight of hydrated cement product

Development of a weight-volume relationship requires satisfying the conservation of mass principle during hydration. In the view of the PCC system, the principle can be defined in terms of the net mass transfer to or from a fresh concrete mixture during a hydration as equal to the net change in the total mass of PCC (Moran and Shapiro 1988). The component which transfers to or from fresh PCC is assumed to only be water molecules, i.e. free water. The other components such as cement or aggregate do not transfer during hydration (Avelar Lezama 2005). Therefore, during hydration, the change of free water content is equivalent to any change in weight of PCC. In an equation form, the conservation of mass principle for concrete cement is:

$$\Delta m_{pcc} = m_{pcc@final} - m_{pcc@initial} = \Delta w_{w\_lost} \tag{4-31}$$

where

Δm_{pcc} = net change in mass within cement concrete

$m_{pcc@final}$ = total mass of concrete after hydration

$m_{pcc@initial}$ = total mass of concrete before hydration

Δw_{w_lost} = weight change of free water for hydration

From the principle and Equation (4-31), the basic water weight relationship can be derived as follows;

$$w_{net} = w_{nw} + w_{w\_tot} = w_{nw} + w_w + w_{w\_lost} \tag{4-32}$$

where

w_{net} = weight of net water from mix design

w_{nw} = weight of non-evaporable water

w_{w_tot} = total weight of free water

w_w = weight of free water left in capillary voids

w_{w_lost} = weight of free water lost to the atmosphere

It is noted that the weight of all water types described in Equation (4-32), except for weight of net water (w_{net}), are time-dependent. The volume changes of each component can be determined based on both of the volumetric model and the mass conservation principle. The volumetric content of each component can be simply expressed based on the individual volume components as a fraction of the total concrete volume as:

$$\theta_i = \frac{V_i}{V_{total}} \tag{4-33}$$

where

θ_i = volumetric content of component i

Therefore, the cement concrete has a total volumetric content equal to one:

$$\sum \theta_i = \theta_w + \theta_{hcp} + \theta_{uc} + \theta_{agg} + \theta_{air} = 1 \tag{4-34}$$

where

θ_w = volumetric content of free water

θ_{hcp} = volumetric content of hydrated cement paste

θ_{uc} = volumetric content of unreacted cement

θ_{agg} = volumetric content of aggregate

θ_{air} = volumetric content of air void (porosity)

Among the components of PCC, only aggregate does not have any change on volume or weight during hydration process; that is, the volume of aggregate in fresh

concrete is equal to that in harden concrete. Thus, the volumetric aggregate content can be simply determined as:

$$\theta_{agg} = \frac{V_{agg}}{V_{total}} \tag{4-35}$$

During cement hydration, a series of chemical reactions occurs, and hence the cement with mixed water forms the new solids referred to as hydration products. Thus, to what extent hydration has proceeded is very important to understand the volume change of PCC. The degree of hydration can be defined as the ratio of the amount of reacted cement to the original amount of cementitious material present in the mixture as (Parrot et al. 1990; Robbins 2007):

$$\alpha(t) = \frac{\text{amount of cement reacted at time } t}{\text{amount of original cement at } t = 0} \tag{4-36}$$

where

$\alpha(t)$ = degree of hydration at a given time t

The change of volumetric contents of other components depends upon the degree of hydration; that is, the volumetric change of each component, except of aggregate, is dependent upon the degree of hydration and time as the degree of hydration varies with time. So, the degree of hydration defined in Equation (4-36) can be expressed as the ratio between the amount of hydrated cement and that of cement from mix design as follows:

$$\alpha(t) = \frac{w_{hc}(t)}{w_c} \tag{4-37}$$

where

$w_{hc}(t)$ = time dependent weight of hydrated cement

w_c = weight of cement from mix design

Since the amount of dry bulk cement decreases while that of hydrated cement increases during hydration, the volume of unreacted cement is also time-dependent and varies with hydration where its weight can be expressed simply as:

$$w_{uc}(t) = w_c - w_{hc}(t) \tag{4-38}$$

where

$w_{uc}(t)$ = time dependent weight of unreacted cement

The amount of unreacted cement can be presented combining Equation (4-37) and (4-38) as follows:

$$w_{uc}(t) = w_c\,[1 - \alpha\,(t)] \tag{4-39}$$

Because the volumetric term is appropriate to quantify each component in a composite material using dielectric properties, the Equation (4-39) should be converted volumetrically based on the following definition:

$$V_{uc} = \frac{w_{uc}}{G_s \gamma_w} \tag{4-40}$$

where

G_s = specific gravity of portland cement

The specific gravity of unreacted cement is well known as about 3.15 (Mindess et al. 2003; Neville 1995). Thus, the volume of unreacted cement can be expressed as;

$$V_{uc} = V_c\left[1 - \alpha\left(t\right)\right] \tag{4-41}$$

where

V_c = volume of portland cement from mix design

Being replaced with Equation (4-33), the volumetric content of unreacted cement is defined as the following:

$$\theta_{uc} = \theta_c \left[1 - \alpha(t) \right] \tag{4-42}$$

where

θ_c = volumetric content of portland cement from mix design

The hydration products require the space occupied by dry bulk cement and additional space which is around 1.4 times of the volume of cement (Powers 1947). The available additional space would be water filled space which is required in fresh concrete to provide the space required by the hydration products. The volumes of the unreacted cement and the hydrated cement product can be approximated along with the volumetric factor for additional space and the degree of hydration as (Avelar Lezama 2005; Powers 1947; Powers and Brownyard 1946):

$$\theta_{uc+hcp} = \theta_c + f_v \, \theta_c \, \alpha(t) \tag{4-43}$$

where

θ_{uc+hcp} = volumetric content of both unreacted cement and hydrated product

f_v = volumetric factor (≈ 1.4)

In Avelar Lezema's study whose experimental data was used for his approach, the volumetric factor was assumed as 1.10 (Avelar Lezama 2005). As seen in Figure 4-13, the volumetric content of hydrated cement product (θ_{hcp}) contains physically and

chemically bound water as well as hydrated cement. By subtracting Equation (4-42) from Equation (4-43), the volumetric content of hydrated cement product can be obtained as:

$$\theta_{hcp} = \theta_{uc+hcp} - \theta_{uc} = \left(1 + f_v\right)\theta_c \alpha\left(t\right) \tag{4-44}$$

Next component for quantification is free water which is a main element to be estimated. The volume of free water can be approximated indirectly by calculating a weight fraction between the free water (w_w) which is time-dependent and the initial net water (w_{net}) based on the initial mix design (Avelar Lezama 2005). The weight-volume relationship of net water and free water can be assumed to be identical because the specific gravity values of both waters are 1.0 (Mamlouk and Zaniewski 2005):

$$\frac{V_w}{V_{net}} = \frac{w_w \Big/ G_s\gamma_w}{w_{net} \Big/ G_s\gamma_w} = \frac{w_w}{w_{net}} \tag{4-45}$$

where

V_w = time dependent volume of free water

V_{net} = volume of initial net water used on the mix design

Therefore, the volume of free water can be expressed as follows:

$$V_w = \left(\frac{w_w}{w_{net}}\right) V_{net} \tag{4-46}$$

From Equation (4-33) and (4-46), the volumetric content of free water is defined as the following:

$$\theta_w = \left(\frac{w_w}{w_{net}} \right) \theta_{net} \tag{4-47}$$

where

θ_{net} = volumetric content of initial net water used on the mix design

The last component to be quantified is air voids which is the porosity consisting of air-filled, empty space in hydrated PCC. The volumetric air void content can be calculated based on Equation (4-34) and the other components determined as follows:

$$\theta_{air} = 1 - \left(\theta_w + \theta_{hcp} + \theta_{uc} + \theta_{agg} \right) \tag{4-48}$$

The volume fractions (θ_i) of all components except for aggregate are time dependent by hydration. Table 4-7 presents the quantification form of the volumetric content and dielectric constant for each component.

Table 4-7 Description of Each Component

Component	Volume Relationship	Dielectric Constant	Remark
Free Water	$\theta_w = \left(\frac{w_w}{w_{net}} \right) \theta_{net}$	ε_1	Time-dependent
Hydrated Cement Product	$\theta_{hcp} = \left(1 + f_v\right) \theta_c \alpha(t)$	ε_2	Time-dependent
Unreacted Cement	$\theta_{uc} = \theta_c \left[1 - \alpha(t)\right]$	ε_3	Time-dependent
Aggregate	θ_{agg} (from mix design)	ε_4	
Air Void	$\theta_{air} = 1 - \left(\theta_w + \theta_{hcp} + \theta_{uc} + \theta_{agg} \right)$	ε_5	Time-dependent
Total (composite)	$\sum \theta_i = 1$	ε_c	

Based on the fundamental assumption that the PCC is composed through statistical homogeneity and isotropy mentioned previously, the proposed self consistent model for PCC can be obtained as follows:

$$\theta_w \frac{\varepsilon_1 - \varepsilon}{\varepsilon_1 + 2\varepsilon} + \theta_{hcp} \frac{\varepsilon_2 - \varepsilon}{\varepsilon_2 + 2\varepsilon} + \theta_{uc} \frac{\varepsilon_3 - \varepsilon}{\varepsilon_3 + 2\varepsilon} + \theta_{Agg} \frac{\varepsilon_4 - \varepsilon}{\varepsilon_4 + 2\varepsilon} + \theta_{Air} \frac{\varepsilon_5 - \varepsilon}{\varepsilon_5 + 2\varepsilon} = 0 \qquad (4\text{-}49)$$

where

ε = composite dielectric constant of cement concrete mixture

ε_1 = dielectric constant of free water

ε_2 = dielectric constant of hydrated cement product

ε_3 = dielectric constant of unreacted cement

ε_4 = dielectric constant of aggregate

ε_5 = dielectric constant of air (= 1.0)

Equation (4-49) can be expressed including the volume relationship of each component as:

$$\begin{aligned} &\theta_{net}\left(\frac{w_w}{w_{net}}\right)\frac{\varepsilon_1 - \varepsilon}{\varepsilon_1 + 2\varepsilon} + \theta_c\left(1 + f_v\right)\alpha(t)\frac{\varepsilon_2 - \varepsilon}{\varepsilon_2 + 2\varepsilon} + \theta_c\left[1 - \alpha(t)\right]\frac{\varepsilon_3 - \varepsilon}{\varepsilon_3 + 2\varepsilon} + \theta_{Agg}\frac{\varepsilon_4 - \varepsilon}{\varepsilon_4 + 2\varepsilon} \\ &+ \left\{1 - \theta_{net}\left(\frac{w_w}{w_{net}}\right) - \theta_c\left(1 + f_v\right)\alpha(t) - \theta_c\left[1 - \alpha(t)\right] - \theta_{agg}\right\}\frac{\varepsilon_5 - \varepsilon}{\varepsilon_5 + 2\varepsilon} = 0 \end{aligned} \qquad (4\text{-}50)$$

The first and fifth terms in Equation (4-50) can be simplified as follows:

$$\begin{aligned} &\theta_w \frac{\varepsilon_1 - \varepsilon}{\varepsilon_1 + 2\varepsilon} + \theta_c\left(1 + f_v\right)\alpha(t)\frac{\varepsilon_2 - \varepsilon}{\varepsilon_2 + 2\varepsilon} + \theta_c\left[1 - \alpha(t)\right]\frac{\varepsilon_3 - \varepsilon}{\varepsilon_3 + 2\varepsilon} + \theta_{Agg}\frac{\varepsilon_4 - \varepsilon}{\varepsilon_4 + 2\varepsilon} \\ &+ \left\{1 - \theta_w - \left[1 + f_v\alpha(t)\right]\theta_c - \theta_{agg}\right\}\frac{\varepsilon_5 - \varepsilon}{\varepsilon_5 + 2\varepsilon} = 0 \end{aligned} \qquad (4\text{-}51)$$

Using the adopted volumetric relationship of each component, the modified Breugel model of Figure 4-13 can be illustrated as Figure 4-14.

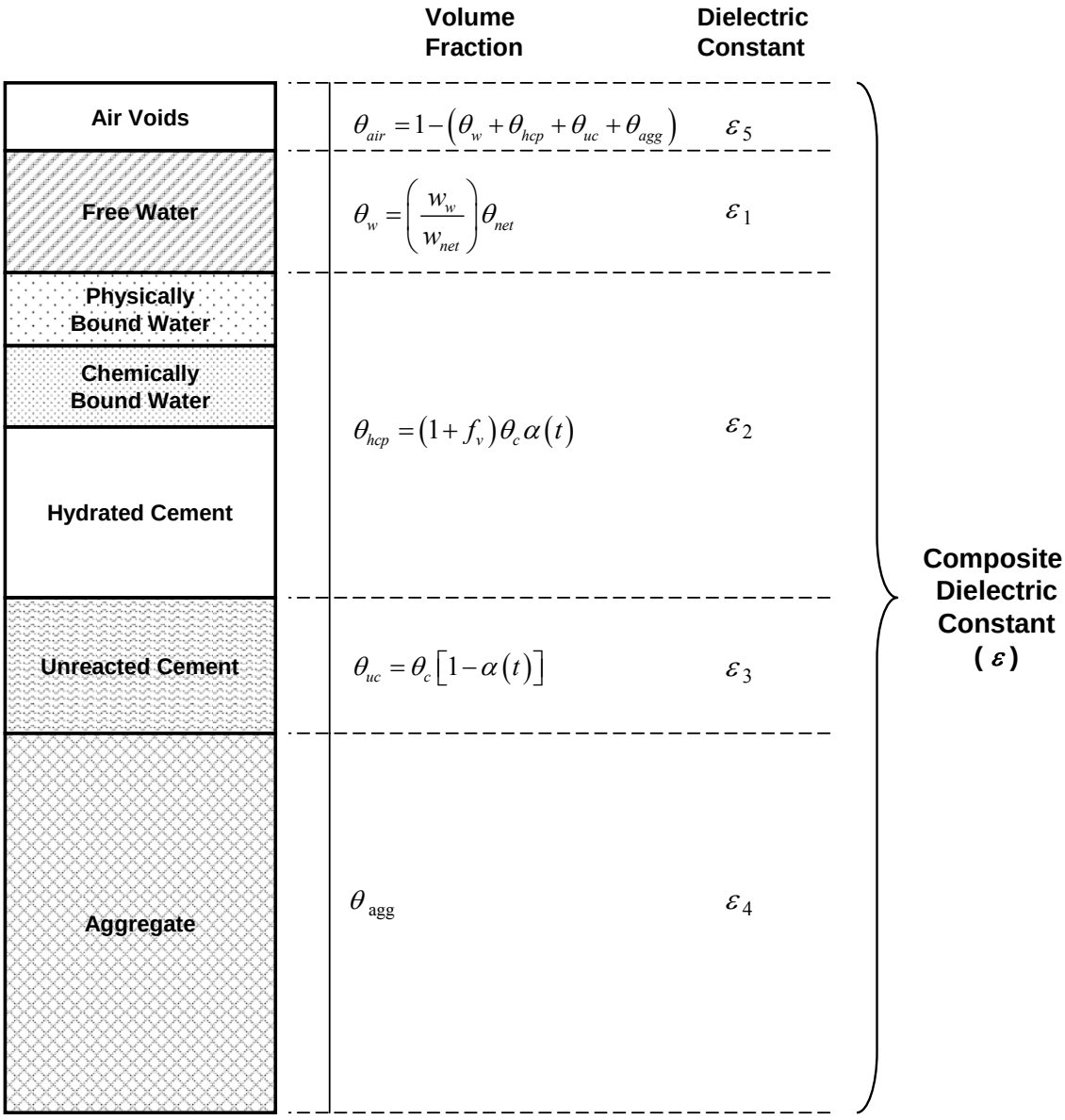

Figure 4-14 Portland cement concrete with volumetric contents and dielectric constant

Data Collection

The new approach for characterizing moisture loss in a hydrating PCC mixture was developed using experimental data collected from Avelar Lezama's study (Avelar Lezama 2005). In his study, he tried to identify key time-dependent changes in water availability and its effect on cement hydration and early-age concrete properties. Also, the study performed the evaluation of the potential that dielectric properties have on the approximation of concrete properties of moisture content, curing quality, or hydration. Accordingly, he collected moisture, hydration, strength, relative humidity, and dielectric constant data from PCC samples. Table 4-8 presents the experimental design for the test and observation. The samples did not use any mineral or admixtures to prevent unintended influence on moisture content or hydration process.

Table 4-8 Experimental Design (Avelar Lezama 2005)

Factor	Description
Environment	- 40°C (104°F), 40% relative humidity - No wind or solar exposure
Cementitious Material	- ASTM C150 Type I Portland cement - Cement Factor: 332 kg/m^3 (6 bags/yd^3)
Aggregate	- ASTM C33 Gradation; Max. Size = 38 mm (1.5 in) - Coarse Aggregate Factor = 0.7, about 1,116 kg/m^3 (1,900 lbs/yd^3) - Siliceous gravel and sand
Admixtures	- No admixtures were used

Preparation of specimen

Since moisture loss would depend on the exposed area of specimen and was sensitive to shallow depth, the moisture loss specimens were shallow and wide to minimize variability in the prepared specimens. In addition, the specimen had a round shape so that it can minimize water concentration of concrete-mold interface and facilitate moisture loss from the concrete mixture as shown in Figure 4-15.

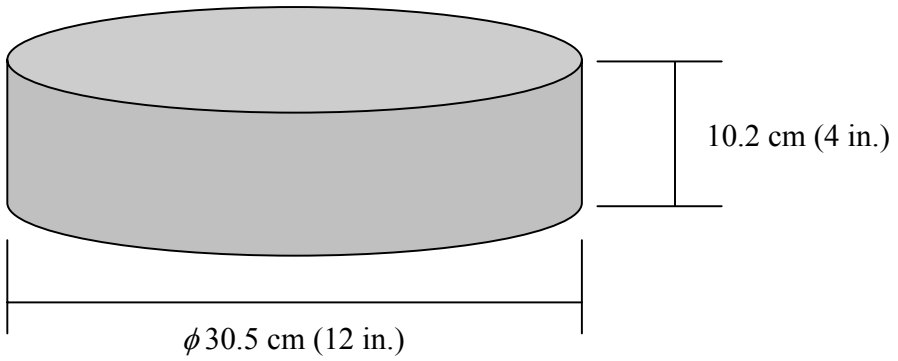

Figure 4-15 Specimen for test program

The test was performed with the factorial design of four different water/cement (w/c) ratios (0.32, 0.36, 0.40, and 0.44) and two curing conditions (exposed and covered). Since covered specimens tend to retain higher amount of moisture on the surface for longer time, the dielectric constants of these specimens produce much higher dielectric constant than exposed specimen even in same moisture content of each w/c ratio. Therefore, in this study, only results obtained from exposed specimens were used for estimating volume fraction of cement concrete mixture. During hydration of the specimens, the following measurements were performed:

- Compressive strength by ASTM C39 "Standard Test Method for Compressive Strength of Cylindrical Concrete Specimens"
- Total water mass remaining or loss by ASTM C232 "Standard Test Methods for Bleeding of Concrete"
- Surface dielectric constant using Adek™ Percometer.

Measurement of degree of hydration by compressive strength test

The measurement of compressive strength was carried out for the actual degree of hydration through the use of the strength hydration model:

$$\alpha(t) = \frac{f(t)}{f_{ult}} \tag{4-52}$$

where

$f(t)$ = time-dependent compressive strength of concrete (MPa)

f_{ult} = ultimate compressive strength (MPa)

The degree of hydration is a significant factor since it can be used to estimate the time dependent volumetric contents such as unreacted cement and hydrated cement product. The test was performed through ASTM C39 at the age of 1, 3, 7, 28, 56, and 90 days for each concrete sample, and the ultimate concrete strength was estimated using a linear regression analysis of the test results. Figure 4-16 shows the degree of hydration of each w/c ratio as the specimens harden.

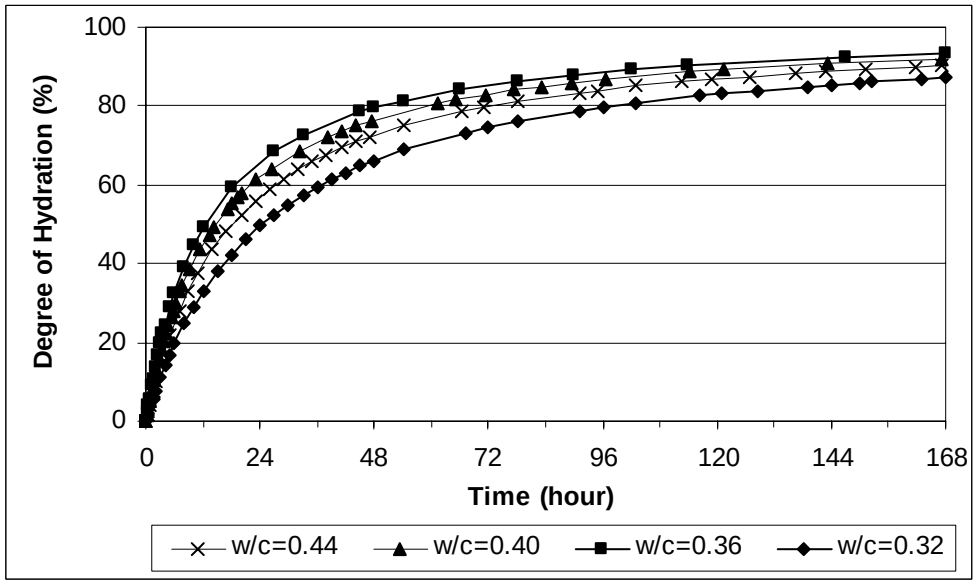

Figure 4-16 Degree of hydration by compressive strength test (Avelar Lezama 2005)

Measurement of moisture loss and availability

Since the water is only component to transfer to or from cement concrete during hydration process, the weight change of free water content is equivalent to any weight change of the sample. The total amount of moisture loss was indirectly determined through the measurement of the actual total water weight remaining in the concrete samples as it hardened. The measurement was completed in two stages, bleeding and post-bleeding.

For the measurement during the bleeding stage, disposable paper towel were used because of their high suction allowed for the bled water to be trapped without removing cement particles. The towels were laid on the surface of specimen with a lid on the rim to prevent the absorbed bled water from evaporating. The amount of bled water was measured using the difference between dry towels mass and towel mass after absorption. The measurements were repeated until the difference was lower than 1.0 grams with 15 or 30 minute intervals. At the post bleeding stage, the entire specimen was measured using weight scale, which was progressively increasing in intervals, because the loss rates would decrease as concrete hardens.

The trend of moisture loss showed that the rate is very high at the beginning of hydration process, and then slowed down as concrete hardened. Figure 4-17 (a) presents the accumulated sample moisture loss with time, based on gravimetric measurements for each w/c ratio. Figure 4-17 (b) shows moisture loss in terms of the fraction of free water weight loss to net water weight (w_{w_lost} / w_{net}).

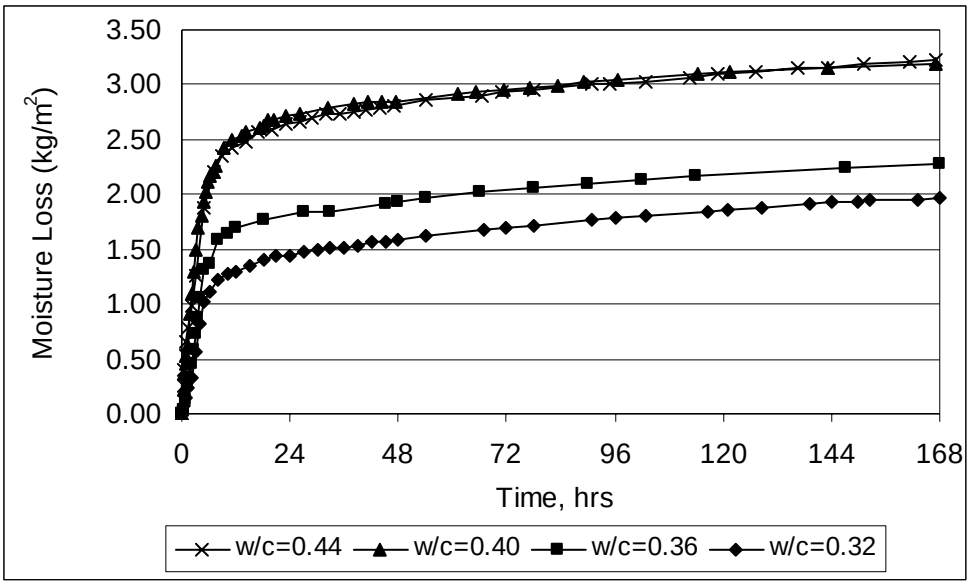

(a) Moisture loss on area

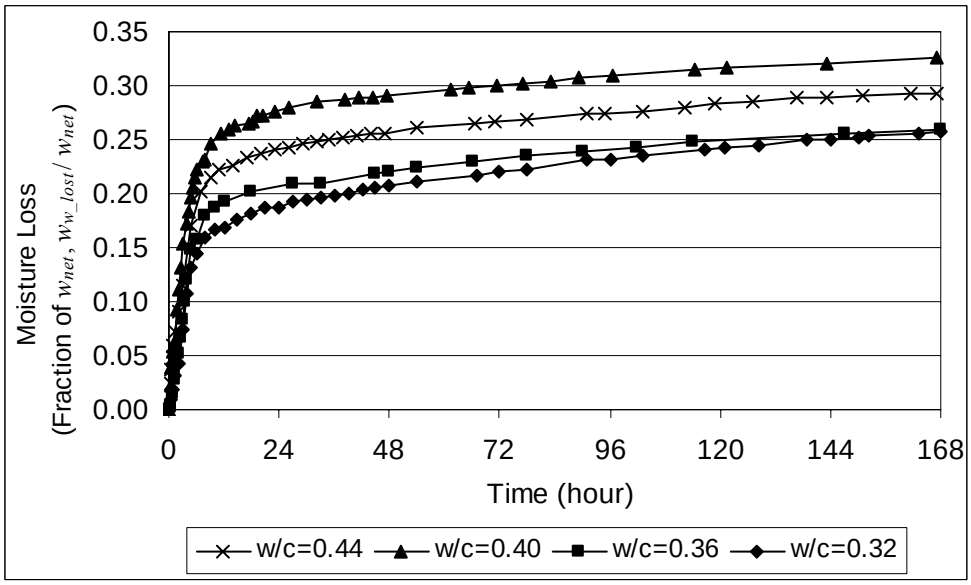

(b) Moisture loss on unit weight of net water

Figure 4-17 Moisture loss of cement concrete by time

Since the amount of water loss should be determined through the measurement of the weight of remaining water in the samples, the remaining portion of initial net water should be approximated first to quantify the free water loss (w_{w_lost}) from the sample. The remaining water consists of free water (w_w) and non-evaporable water (w_{nw}) as shown in Figure 4-13, and their relationship can be presented using Equation (4-32) as follows:

$$w_w = w_{net} - w_{nw} - w_{w\_lost} \tag{4-53}$$

To determine the weight variation of non-evaporable water, it is necessary to assume that the amount of that water is proportional to the degree of hydration. The non-evaporable water is taken as a specific fraction on the amount of cement. That is, a given proportion of non-evaporable water is combined with original cement as concrete is hydrated and it can be defined as (Copeland and Hayes 1953; Neville 1995);

$$w_{nw} = f_n \, w_c \, \alpha(t) \tag{4-54}$$

where

f_n = non-evaporable water factor (0.2 ~ 0.3)

w_c = weight of original cement from mix design

Figure 4-18 presents the water weight variation with hydration of a concrete sample whose w/c ratio was 0.36, based on non-evaporable water factor (f_n) of 0.26 obtained from Avelar Lezama's laboratory test (Avelar Lezama 2005). Since each type of water in Figure 4-18 is proportional to the weight of net water (w_{net}), they follow another form of Equation (4-53) as follows:

$$W_{w\_lost} = 1.0 - W_{nw} + W_w \tag{4-55}$$

where

W_{w_lost} = weight proportion of net water (= w_{w_lost} / w_{net})

W_{nw} = weight proportion of non-evaporable water (= w_{nw} / w_{net})

W_w = weight proportion of free water (= w_w / w_{net})

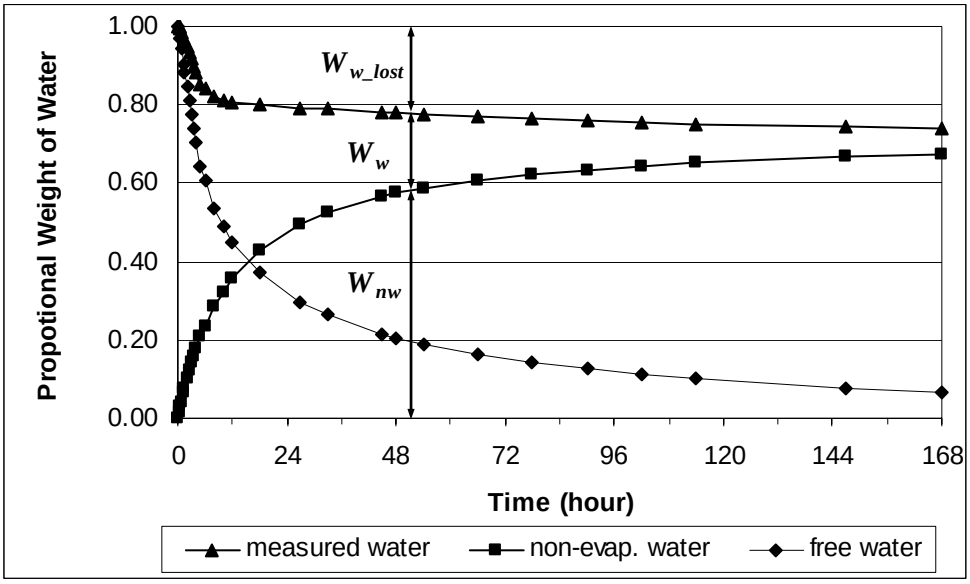

Figure 4-18 Fractional weight variation of water (0.36 w/c)

Measurement of dielectric constant

The Adek™ Percometer was used as an instrument for the surface measurement of the composite dielectric constant of the PCC samples as shown in Figure 4-19. The device is a reliable and easy-to-use instrument for measurements of dielectric constant. The instrument used in the study consists of a surface probe with sensor diameter 60 mm for measurements on the face of material samples and the central unit for control and memory of measurement data. Table 4-9 presents the description of the Percometer used to measure the dielectric constant of concrete samples. In order to reduce the systematic error, the measurement of dielectric constant was carried out at the same time with the moisture loss measurement. In addition, the dielectric constant is measured at five random locations and they are averaged to determine the dielectric value to minimize the random error.

Figure 4-19 Measurement of composite dielectric constant of concrete sample (Avelar Lezama 2005)

Table 4-9 Description of Adek™ Percometer (Adek 2009; Avelar Lezama 2005)

Parameter	Value
Sensor Diameter	60 mm (2.36 in.)
Measurement Range	Dielectric constant: 1.0 ~ 32.0 Electric conductivity: 0 ~ 2,000 µS/cm
Operational Temperature	– 40 ~ 80 °C (– 40 ~ 176 °F)
Accuracy of Measurement (Dielectric constant)	± 0.1 ~ 1.0 %

The dielectric constant before setting time were not considered since concrete prior to final setting point tends to have a lot of moisture on surface and thus it could

cause excessive dielectric values out of measuring range. Figure 4-20 illustrates the measurement of dielectric constants with time as concrete hardened and moisture loss.

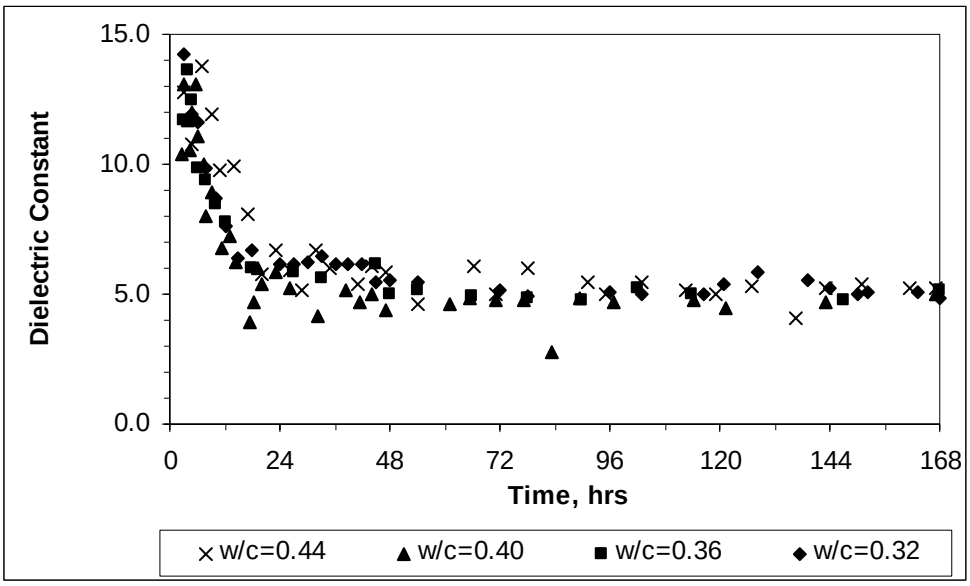

Figure 4-20 History of dielectric constant by time

Volume fraction from test results

Using the volumetric relationship of the adopted model, the proportions of each concrete component was calculated based on the determined water loss and availability, non-evaporable water, and the degree of hydration. The volumetric factor (f_v) was assumed as 1.10 to calculate the content of hydrated cement product (Avelar Lezama 2005). As seen in Figure 4-21, each component shows rapid volumetric change, except for air void, as time and hydration advance. Figure 4-22 shows the dielectric constant measured by time and the corresponding changes in volume fractions of components with 0.36 w/c. Since the volume fraction of aggregate has always the same value, 78 percent in this specimen, the component is not included in that figure.

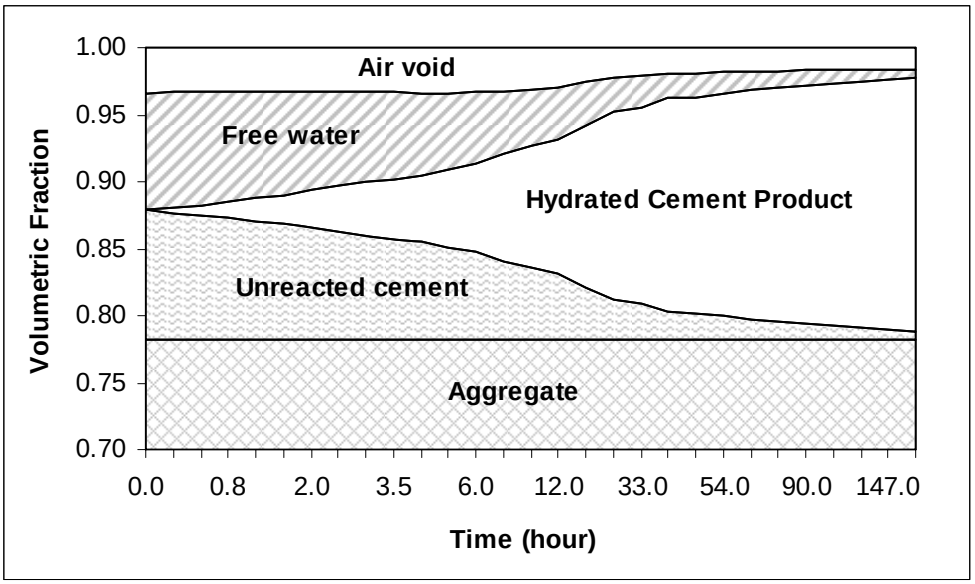

Figure 4-21 Volumetric variation of components (0.36 w/c)

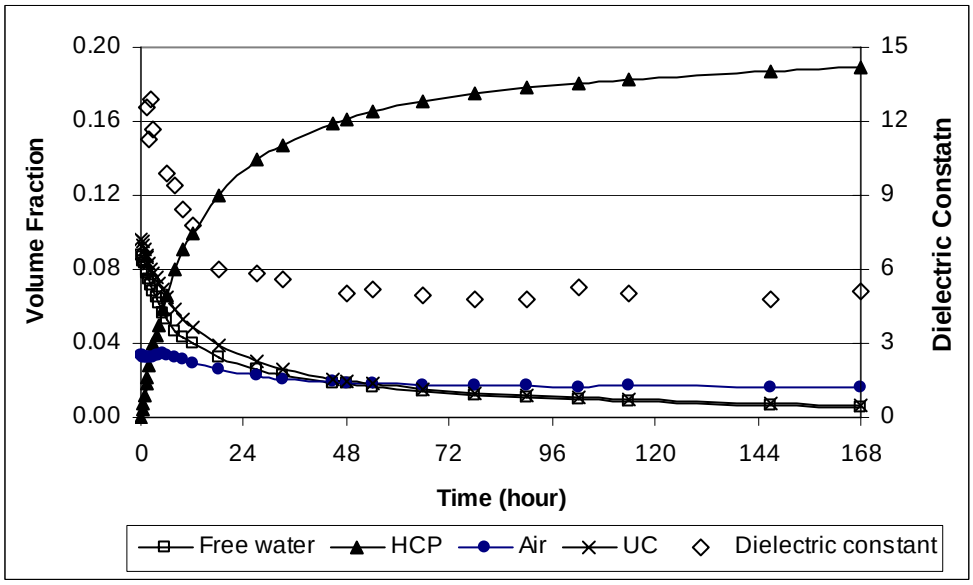

Figure 4-22 Volumetric variation of components by dielectric constant (0.36 w/c)

Determination Process for PCC

In order to estimate component volume fraction of PCC during hydration, the new approach was used along with measured composite dielectric constants over time.

Determination of composite dielectric constant (Step 1)

The composite dielectric constants of the PCC samples were measured immediately using the Percometer without any calculation. To minimize the random error, the dielectric constant averaged from five point measurements at random locations to represent the dielectric constant of each sample for each age.

Calibration of cement concrete component dielectrics (Step 2)

This approach would be more fundamental, which regards PCC as a composite mixture, because it can account for the effect of individual constituent dielectric properties on the volume fraction. In this regard, the proposed self consistent model of a PCC mixture was developed for a five-phase composite system (free water, unreacted cement, hydrated cement product, aggregate, and air void). In order to determine the volume fraction of each component, the new approach requires the calibrated dielectric constant of five components as follows:

- Dielectric constant of free water (ε_1)
- Dielectric constant of hydrated cement product (ε_2)
- Dielectric constant of unreacted cement (ε_3)
- Dielectric constant of aggregate (ε_4)
- Dielectric constant of air (ε_5)

With a composite dielectric constant from step 1, the constituent dielectric constants of the self consistent model are calibrated based on the measured data. Since the dielectric constant of air can be set to unity (ε_5 = 1.0), only four values of dielectric constants are found based on the self consistent scheme as follows:

$$f(\varepsilon_1,\varepsilon_2,\varepsilon_3,\varepsilon_4) = \theta_w \frac{\varepsilon_1-\varepsilon}{\varepsilon_1+2\varepsilon} + \theta_{uc} \frac{\varepsilon_2-\varepsilon}{\varepsilon_2+2\varepsilon} + \theta_{hcp} \frac{\varepsilon_3-\varepsilon}{\varepsilon_3+2\varepsilon} + \theta_{agg} \frac{\varepsilon_4-\varepsilon}{\varepsilon_4+2\varepsilon} + \theta_{air} \frac{\varepsilon_5-\varepsilon}{\varepsilon_5+2\varepsilon} = 0 \quad (4\text{-}56)$$

The data required for calibration is the measured volume fraction of each component and the corresponding composite dielectric constant. Table 4-10 describes the list of parameters used in the calibration step. In this study, the measured data were obtained from Avelar Lezama's test results for the mixture with a 0.36 w/c.

Table 4-10 List of Parameters for Calibration Step

Value	Parameters	Abbr.	Source
Known Values	Volumetric content of free water	θ_w	Laboratory Test Results
	Volumetric content of HCP	θ_{hcp}	
	Volumetric content of unreacted cement	θ_{uc}	
	Volumetric content of aggregate	θ_{agg}	
	Measured composite dielectric constant	ε	
	Dielectric constant of Air	ε_5	1.0
Parameters to be Calibrated	Dielectric constant of free water	ε_1	
	Dielectric constant of HCP	ε_2	
	Dielectric constant of unreacted cement	ε_3	
	Dielectric constant of aggregate	ε_4	

The dielectric constant of each component can be found by applying the SID approach to Equation (4-56). Similarly as the calibration of a soil mixture, a matrix analysis can be used to solve the resulting equations for each unknown value to be calibrated, as follows:

$$[F] \qquad [\beta] \quad = \quad [r]$$

$$\left[\frac{\partial \varepsilon_c}{\partial \varepsilon_1}\frac{\varepsilon_1}{\varepsilon_c} \quad \frac{\partial \varepsilon_c}{\partial \varepsilon_2}\frac{\varepsilon_2}{\varepsilon_c} \quad \frac{\partial \varepsilon_c}{\partial \varepsilon_3}\frac{\varepsilon_3}{\varepsilon_c} \quad \frac{\partial \varepsilon_c}{\partial \varepsilon_4}\frac{\varepsilon_4}{\varepsilon_c}\right]_{1\times 4}\begin{bmatrix}\frac{\varepsilon_1^{j+1}-\varepsilon_1^j}{\varepsilon_1^j}\\ \frac{\varepsilon_2^{j+1}-\varepsilon_2^j}{\varepsilon_2^j}\\ \frac{\varepsilon_3^{j+1}-\varepsilon_3^j}{\varepsilon_3^j}\\ \frac{\varepsilon_4^{j+1}-\varepsilon_4^j}{\varepsilon_4^j}\end{bmatrix}_{4\times 1} = \left[\frac{\varepsilon_{meas}-\varepsilon_c}{\varepsilon_c}\right]_{1\times 1} \tag{4-57}$$

where

ε_c = calculated composite dielectric constant based on the current values of ε_1, ε_2, ε_3, and ε_4 along with measured data

ε_{meas} = measured composite dielectric constant from step 1

Solving for each element in sensitivity matrix [F]:

$$\frac{\partial \varepsilon_c}{\partial \varepsilon_i} = \frac{\partial f(\varepsilon_1,\varepsilon_2,\varepsilon_3,\varepsilon_4)\Big/\partial \varepsilon_i}{\partial f(\varepsilon_1,\varepsilon_2,\varepsilon_3,\varepsilon_4)\Big/\partial \varepsilon_c} \tag{4-58}$$

where

ε_i = ε_1, ε_2, ε_3, and ε_4

The matrix Equation (4-57) can be solved as follows:

$$[\beta] = \left[F^T F\right]^{-1}\left[F^T\right][r] \tag{4-59}$$

The SID method calculates the dielectric constant (ε_c) along with unknown values (ε_1, ε_2, ε_3, and ε_4) to be calibrated and the measured data for each iteration, and then compares it with the measured dielectric constant (ε_{meas}) obtained with the Percometer. When the elements in the change vector [β] are less than 0.05 by iteration, each dielectric value is reported as the final result. The calibrated dielectric constant is used to further calculate the volumetric contents based on Percometer measurement at other times.

To determine the dielectric constant of each component, the calibration was derived from the known volume fraction data produced from laboratory testing for a given concrete mixture (0.36 w/c). In the dielectric constant measurements, there were inconsistent variation trends that the measured dielectric values decrease over time. Thus, these inappropriate data points were removed to calibrate reasonable component dielectric values. Figure 4-23 illustrates the selected time-dielectric constants and volume fraction of elements from a concrete sample with 0.36 w/c which were used for the calibration.

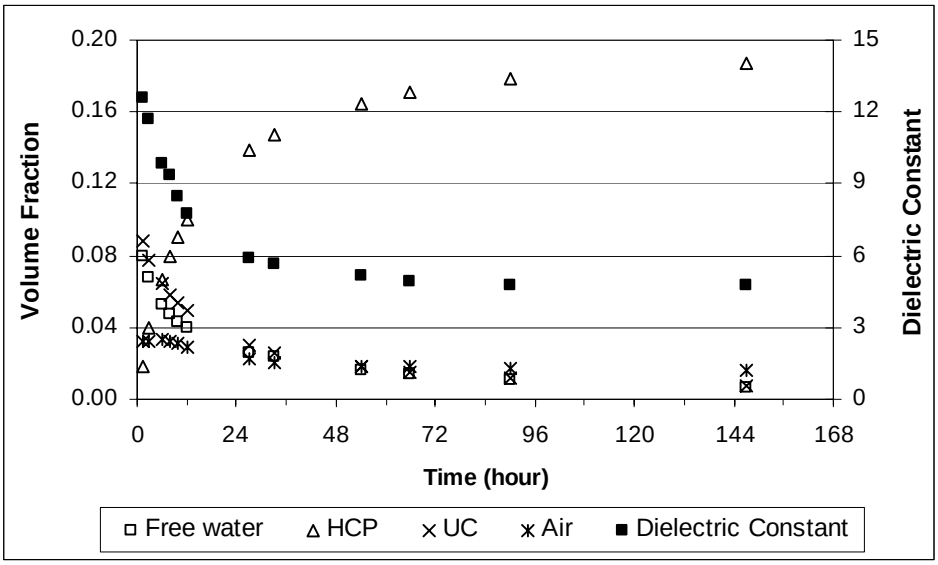

Figure 4-23 Time-dielectric constant used for calibration (0.36 w/c)

With the proposed self consistent model and the SID, the calibration was carried out using selected dielectric constant values. Table 4-11 shows the calibration results for each hour and corresponding dielectric constant. In the results, the calibrated dielectric constants of aggregate shows significant variation during first 27 hours although typical dielectric value of aggregate is 3.0 ~ 6.0 (Davis and Annan 1989; Instruments 2002). These higher values at early stages were due to the presence of moisture absorbed in aggregate pores. Therefore, the dielectric constants of aggregate were adjusted for those early stages.

Table 4-11 Calibrated Values for Each Hour for 0.36 w/c Ratio

Hour	Measured Dielectric Constant	Calibrated Dielectric Constant			
		Water (ε_1)	HCP (ε_2)	UC (ε_3)	Agg. (ε_4)
1.25	12.572	80.058	4.178	3.429	12.419
3	11.690	80.043	4.319	3.486	11.857
6	9.864	80.020	4.442	3.393	10.246
8	9.368	80.017	4.486	3.210	9.858
10	8.434	80.009	4.422	3.388	8.813
12	7.764	80.006	4.359	3.406	8.083
27	5.860	80.000	4.367	3.368	5.990
33	5.614	80.002	4.308	3.356	5.733
54	5.172	80.010	4.299	3.342	5.280
66	4.956	80.000	4.243	3.337	5.054
90	4.756	80.004	4.321	3.332	4.826
147	4.784	80.006	4.345	3.334	4.913

Adjustment of Aggregate Dielectric Constant at Early Age

The calibrated dielectric values of aggregate during the first 27 hours were higher than the typical dielectric values of mineral aggregates, as shown in Figure 4-24. Since the

aggregate occupies about 78 percent of the volume of concrete sample, the effect of this change in dielectric constant must be accounted for in the calibration and the forward calculation process.

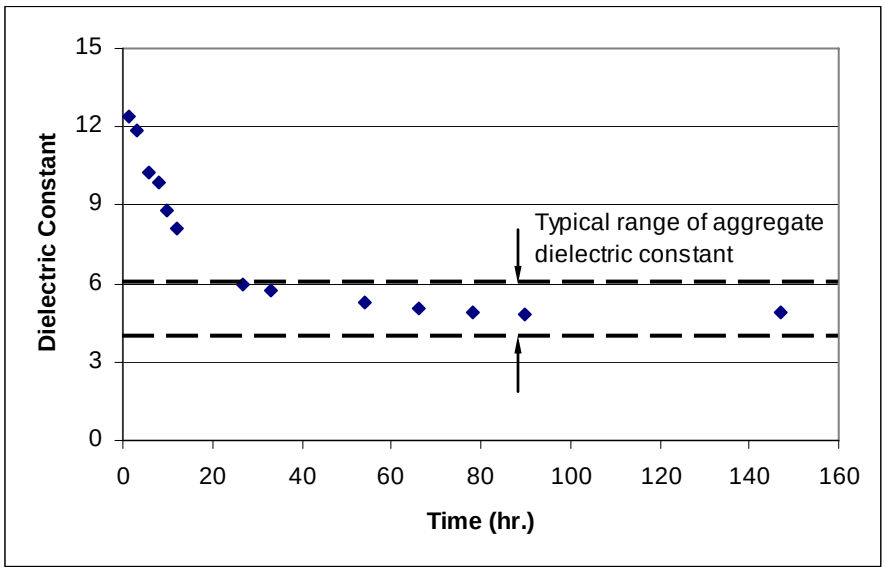

Figure 4-24 Calibrated dielectric constant of aggregate

The varying dielectric values of aggregate at early ages mostly likely is due to moisture content absorbed in aggregate pores and held around aggregate. Initially, the aggregates are in a wet condition which tends to decrease with time. This variation of dielectric constants shows that the absorbed water comes out from the aggregate pores as hydration process (or the curing process), causing the dielectric value to decrease due to the reduction of water within and around the aggregate. In order to account for the change in aggregate dielectric values during hydration, a prediction model as described in Figure 4-25 and Table 4-12 was developed to relate the calibrated aggregate dielectric constants with time or equivalent time as:

$$y = 13.215\, e^{-0.040t} \tag{4-60}$$

where

y = dielectric constant of aggregate

t = equivalent time (hr., $0 < t < 24$)

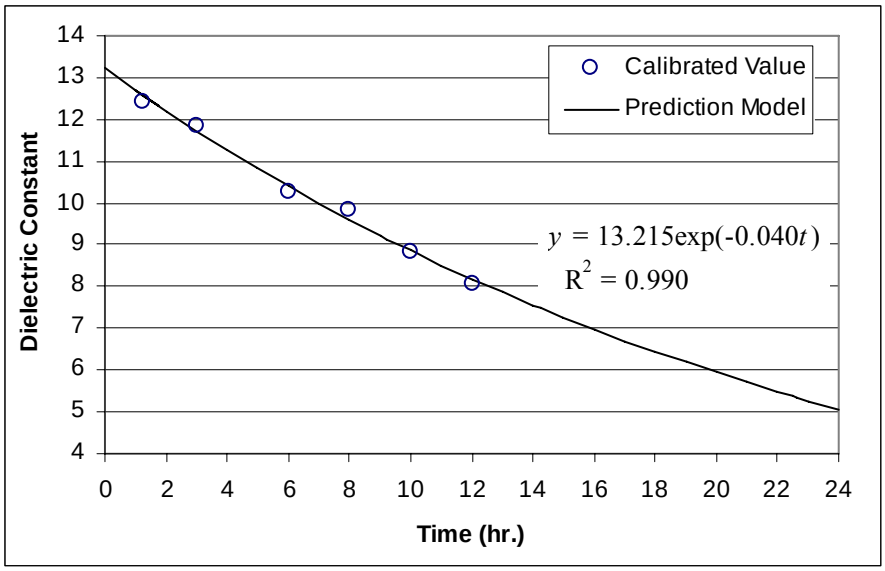

Figure 4-25 Prediction model for calibrated dielectric constant of aggregate

Table 4-12 Model Parameter Estimates and Standard Errors

Description		Value
R^2		0.9900
Standard Error of Estimate		0.0185
Observations		6
Standard Error of Coefficient	13.215	0.0155
	-0.040	0.0020

It is important to recognize that this correlation pertains only the early age time period until the dielectric values reach a stable dielectric constant similar to that of dry aggregate (which is around 5.0). Although shown in Figure 4-25 as elapsed time, the correlation is better served using equivalent age. That is, the correlation is only relevant

during the first 24 hours when the absorbed moisture is assumed to decrease over time due to hydration.

Determination of Final Calibration Values

The final calibrated dielectric constants of free water, HCP, and unreacted cement were determined by averaging all calibrated values. For the aggregate component, the prediction model in Equation (4-60) was used for the first 24 hours while the averaged value from 27 to 147 hours was used for the calculation after 24 hour. Table 4-13 presents the final calibrated value of each component that were used to forward calculate volume fraction of other concrete samples made of same materials.

Table 4-13 Final Calibrated Dielectric Constant for Each Component

Component	Calibrated Dielectric Constant
Water (ε_1)	80.015
HCP (ε_2)	4.341
UC (ε_3)	3.365
Aggregate (ε_4)	• $13.215e^{-0.040t}$ for $0< t <24$ • 5.299 for $t > 24$

Forward computation of volume fraction (Step 3)

In the forward calculation of volume fractions of components in PCC, the self consistent model was used together with the calibrated values (ε_1, ε_2, ε_3, and ε_4) to determine the volume fractions from values of composite dielectric constants. These composite dielectric values were obtained from different concrete samples which were made from the same constituent materials but with different mix designs. Therefore, once a particular material characteristics ε_1, ε_2, ε_3, and ε_4 are identified at a previous step, future calculations of volume fractions can be determined from the SID using new

composite dielectric constant measurements. In the calculation step, the target values to be determined are the four volume fractions of elements (θ_w, θ_{uc}, θ_{hcp}, θ_{agg}, and θ_{air}) and the degree of hydration, (α (t)); however, the number of unknown values can be reduced using the volume relationship in Table 4-7.

In Equation (4-50), the unknown values are only two as the weight of free water (w_w) and the degree of hydration (α (t)) while the other values can be obtained from mix design and the calibration process. Thus, the self consistent model for the calculation step can be expressed as the function of two variables: weight of free water (w_w) and degree of hydration (α (t)), as follow:

$$f\left(w_w,\alpha(t)\right)=\theta_{net}\left(\frac{w_w}{w_{net}}\right)\frac{\varepsilon_1-\varepsilon_c}{\varepsilon_1+2\varepsilon_c}+\theta_c\left(1+f_v\right)\alpha(t)\frac{\varepsilon_2-\varepsilon_c}{\varepsilon_2+2\varepsilon_c}+\theta_c\left[1-\alpha(t)\right]\frac{\varepsilon_3-\varepsilon_c}{\varepsilon_3+2\varepsilon_c}$$
$$+\theta_{Agg}\frac{\varepsilon_4-\varepsilon_c}{\varepsilon_4+2\varepsilon_c}+\left\{1-\theta_{net}\left(\frac{w_w}{w_{net}}\right)-\theta_c\left(1+f_v\right)\alpha(t)-\theta_c\left[1-\alpha(t)\right]-\theta_{agg}\right\}\frac{\varepsilon_5-\varepsilon_c}{\varepsilon_5+2\varepsilon_c}=0 \quad (4\text{-}61)$$

Equation (4-61) can be simplified as follows:

$$f\left(\theta_w,\alpha(t)\right)=\theta_w\frac{\varepsilon_1-\varepsilon_c}{\varepsilon_1+2\varepsilon_c}+\theta_c\left(1+f_v\right)\alpha(t)\frac{\varepsilon_2-\varepsilon_c}{\varepsilon_2+2\varepsilon_c}+\theta_c\left[1-\alpha(t)\right]\frac{\varepsilon_3-\varepsilon_c}{\varepsilon_3+2\varepsilon_c}$$
$$+\theta_{Agg}\frac{\varepsilon_4-\varepsilon_c}{\varepsilon_4+2\varepsilon_c}+\left\{1-\theta_w-\left[1+f_v\alpha(t)\right]\theta_c-\theta_{agg}\right\}\frac{\varepsilon_5-\varepsilon_c}{\varepsilon_5+2\varepsilon_c}=0 \quad (4\text{-}62)$$

Consequently, the target values to compute the volume fraction of PCC are the volumetric content of free water (θ_w) and the degree of hydration ($\alpha(t)$). Table 4-14 lists the parameters used in this calculation step.

Table 4-14 List of Parameters for Calculation Step

Value	Parameters	Abbr.	Source
Unknown Parameters	Volumetric content of free water	θ_w	
	Degree of hydration	$\alpha(t)$	
Known values	Composite dielectric constant	ε_c	Percometer
	Volumetric content of aggregate	θ_{agg}	Mix eesign
	Volumetric content of portland cement	θ_c	
	Dielectric constant of free water	ε_1	Calibration values
	Dielectric constant of HCP	ε_2	
	Dielectric constant of unreacted cement	ε_3	
	Dielectric constant of aggregate	ε_4	
	Dielectric constant of air	ε_5	1.0

Using a similar use of SID method, the volumetric free water content and the degree of hydration can be determined as follows:

$$[F] \qquad [\beta] \qquad = \qquad [r] \tag{4-63}$$

$$\left[\frac{\partial \varepsilon_c}{\partial \theta_w}\frac{\theta_w}{\varepsilon_c} \quad \frac{\partial \varepsilon_c}{\partial \alpha(t)}\frac{\alpha(t)}{\varepsilon_c}\right]_{1\times 3}\left[\begin{array}{c}\dfrac{\theta_w^{j+1}-\theta_w^j}{\theta_w^j}\\ \dfrac{\alpha(t)^{j+1}-\alpha(t)^j}{\alpha(t)^j}\end{array}\right]_{1\times 2}=\left[\frac{\varepsilon_{meas}-\varepsilon_c}{\varepsilon_c}\right]_{1\times 1}$$

where

ε_c = calculated composite dielectric constant based on the current values of θ_w and $\alpha(t)$ along with calibration data

As stated at the calibration step, the Equation (4-63) can be also solved as follows:

$$[\beta] = \left[F^T F\right]^{-1} \left[F^T\right][r] \tag{4-64}$$

Solving for each element in sensitivity matrix [F]:

$$\frac{\partial \varepsilon_c}{\partial \theta_w} = \frac{\partial f(\theta_w, \alpha(t)) \big/ \partial \theta_w}{\partial f(\theta_w, \alpha(t)) \big/ \partial \varepsilon_c} \tag{4-65}$$

and

$$\frac{\partial \varepsilon_c}{\partial \alpha(t)} = \frac{\partial f(\theta_w, \alpha(t)) \big/ \partial \alpha(t)}{\partial f(\theta_w, \alpha(t)) \big/ \partial \varepsilon_c} \tag{4-66}$$

The SID method is used to iteratively calculate the dielectric constant (ε_c) on the basis of two unknown parameters comparing it to the dielectric constant (ε_{meas}) obtained from Percometer measurements. In this process, the solution for free water content and degree of hydration are found by minimizing the change vector [β]. The calculation step is continued within a loop that terminates when each element of the change vector [β] is less than 0.05. Figure 4-26 illustrates the procedure of new approach used to estimate volume fraction of fresh concrete mixtures.

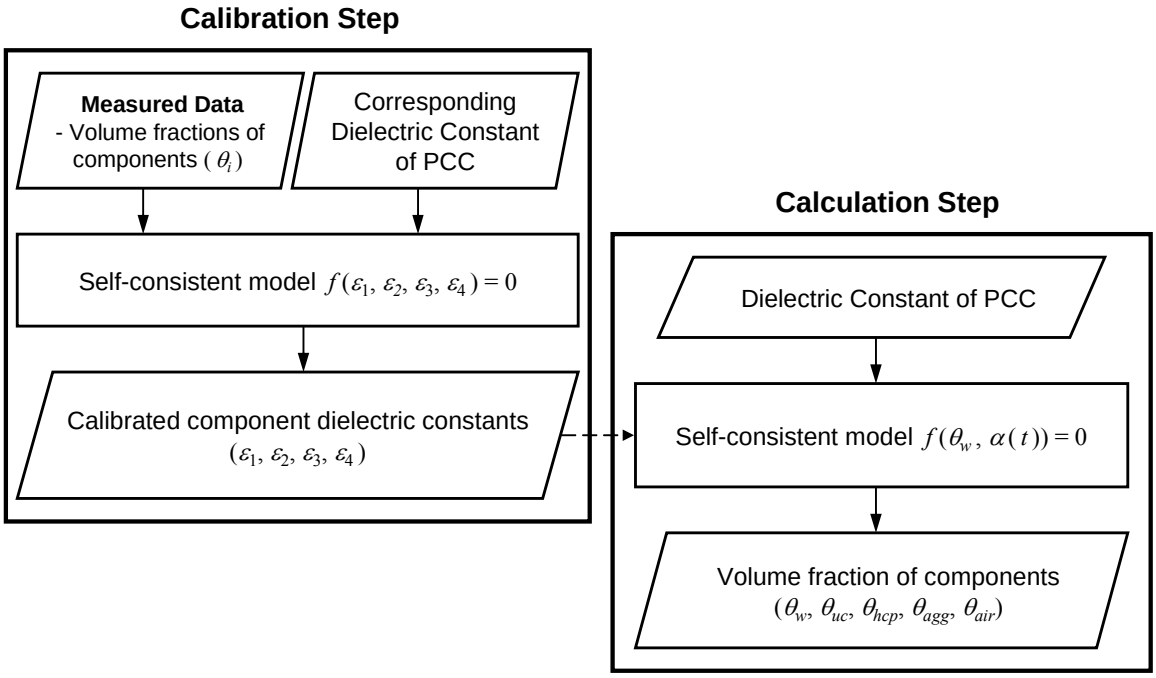

Figure 4-26 Procedure of new approach for portland cement concrete

Validation of New Approach for PCC

In order to discuss the result of estimating volume fraction for PCC, the new approach was analyzed by comparing the volume fraction computed from the proposed self consistent model to laboratory results. The laboratory test data were based on PCC samples, which were made with 0.32, 0.40, and 0.44 w/c, obtained from Avelar Lezama's study. The three w/c samples were made of the same materials as the sample (0.36 w/c) which was used for calibrating component dielectric constants. Using the calibrated information and the dielectric constant measured over time, the volume fractions of each sample were computed and the compared to the results from laboratory tests. Figure 4-27 to Figure 4-29 show the data of component volume fractions obtained from the laboratory test and corresponding dielectric constant measured using Percometer for 0.32, 0.40, and 0.44 w/c samples.

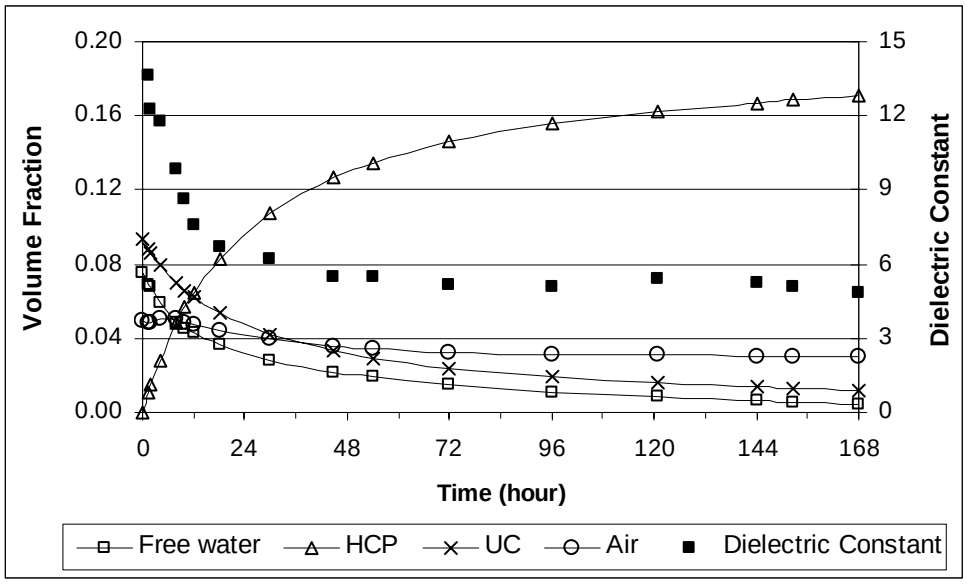

Figure 4-27 Measured volume fraction and dielectric constant (0.32 w/c)

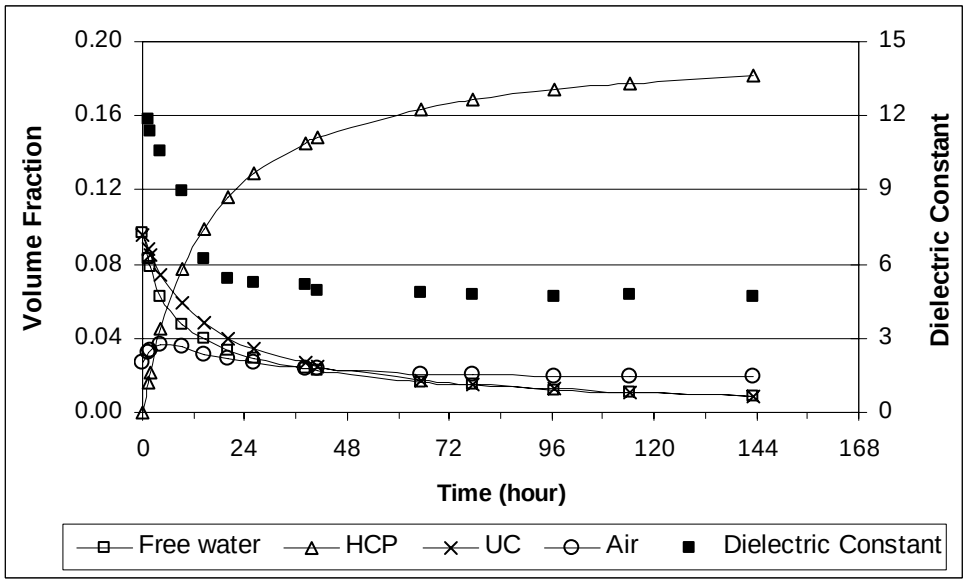

Figure 4-28 Measured volume fraction and dielectric constant (0.40 w/c)

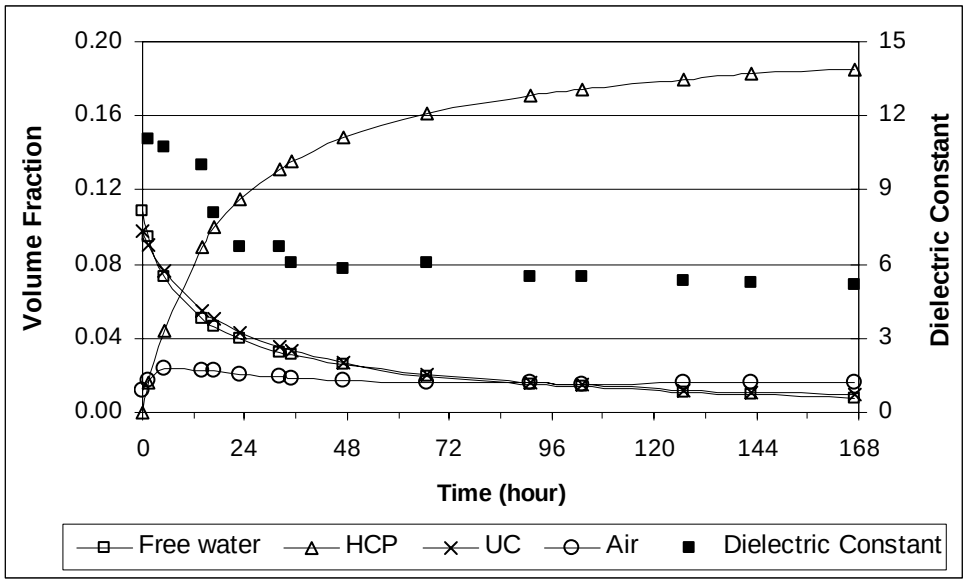

Figure 4-29 Measured volume fraction and dielectric constant (0.44 w/c)

In estimating volume fraction of 0.32 w/c sample, the prediction model in Equation (4-60) was used to determine aggregate dielectric constants for the first 18 hours while the single averaged value (5.299) was used from 30 to 168 hours. For the samples with higher w/c of 0.40 and 0.44, the prediction model was used for the first 20.25 and 23 hours, respectively. The calibrated dielectric constants of other components (water, HCP, and unreacted cement) had the use of the values in Table 4-14. Table 4-15, Table 4-16, and Table 4-17 present the volume fraction of each element and the degree of hydration obtained from the laboratory test and the new approach for 0.32, 0.40, and 0.44 w/c, respectively.

Table 4-15 Volume Fraction and Degree of Hydration (0.32 w/c)

Time (hr.)	Free Water		HCP		Unreacted Cement		Aggregate		Air		Degree of Hydration	
	Lab.*	Cal.**	Lab.	Cal.	Lab.	Cal.	Lab.	Cal.	Lab.	Cal.	Lab.	Cal.
1.5	0.069	0.074	0.011	0.012	0.088	0.088	0.783	0.783	0.049	0.044	0.058	0.059
2	0.067	0.073	0.015	0.015	0.086	0.086	0.783	0.783	0.049	0.043	0.076	0.078
4	0.059	0.064	0.027	0.028	0.080	0.080	0.783	0.783	0.051	0.045	0.140	0.144
8	0.049	0.054	0.048	0.049	0.070	0.070	0.783	0.783	0.050	0.044	0.246	0.252
10	0.046	0.049	0.057	0.058	0.066	0.065	0.783	0.783	0.049	0.044	0.290	0.298
12	0.043	0.046	0.064	0.066	0.062	0.062	0.783	0.783	0.047	0.043	0.329	0.335
18	0.037	0.040	0.083	0.085	0.054	0.052	0.783	0.783	0.044	0.039	0.424	0.436
30	0.028	0.031	0.108	0.110	0.042	0.041	0.783	0.783	0.039	0.036	0.551	0.564
45	0.022	0.024	0.127	0.129	0.033	0.031	0.783	0.783	0.036	0.032	0.648	0.662
54	0.019	0.021	0.134	0.139	0.029	0.027	0.783	0.783	0.035	0.030	0.688	0.711
72	0.015	0.016	0.146	0.149	0.024	0.022	0.783	0.783	0.033	0.030	0.746	0.763
96	0.011	0.012	0.156	0.159	0.019	0.017	0.783	0.783	0.032	0.029	0.797	0.816
121	0.008	0.009	0.163	0.167	0.016	0.014	0.783	0.783	0.031	0.028	0.832	0.853
144	0.006	0.007	0.167	0.172	0.014	0.011	0.783	0.783	0.030	0.027	0.855	0.879
153	0.006	0.006	0.168	0.173	0.013	0.010	0.783	0.783	0.030	0.027	0.862	0.888
168	0.005	0.005	0.171	0.175	0.012	0.010	0.783	0.783	0.030	0.027	0.873	0.896

* Results from laboratory test

** Results from new approach

Table 4-16 Volume Fraction and Degree of Hydration (0.40 w/c)

Time (hr.)	Free Water		HCP		Unreacted Cement		Aggregate		Air		Degree of Hydration	
	Lab.*	Cal.**	Lab.	Cal.	Lab.	Cal.	Lab.	Cal.	Lab.	Cal.	Lab.	Cal.
1	0.083	0.075	0.016	0.015	0.088	0.088	0.782	0.782	0.032	0.040	0.079	0.076
2	0.078	0.071	0.021	0.021	0.085	0.086	0.782	0.782	0.033	0.041	0.107	0.105
4	0.063	0.058	0.045	0.044	0.074	0.075	0.782	0.782	0.036	0.042	0.225	0.220
9	0.047	0.043	0.078	0.076	0.059	0.060	0.782	0.782	0.035	0.040	0.387	0.377
14	0.039	0.036	0.099	0.096	0.048	0.050	0.782	0.782	0.032	0.036	0.493	0.479
20	0.033	0.031	0.116	0.114	0.040	0.041	0.782	0.782	0.029	0.032	0.580	0.570
26	0.029	0.027	0.129	0.127	0.034	0.035	0.782	0.782	0.026	0.030	0.642	0.632
38	0.023	0.022	0.145	0.142	0.026	0.028	0.782	0.782	0.024	0.027	0.723	0.706
41	0.022	0.021	0.148	0.144	0.025	0.027	0.782	0.782	0.023	0.026	0.738	0.718
65	0.016	0.015	0.164	0.159	0.018	0.020	0.782	0.782	0.021	0.024	0.816	0.792
77	0.015	0.013	0.169	0.164	0.015	0.017	0.782	0.782	0.020	0.023	0.840	0.819
97	0.012	0.011	0.174	0.170	0.013	0.015	0.782	0.782	0.019	0.023	0.868	0.846
114	0.010	0.010	0.178	0.173	0.011	0.013	0.782	0.782	0.019	0.022	0.886	0.864
143	0.009	0.008	0.182	0.179	0.009	0.010	0.782	0.782	0.019	0.021	0.907	0.890

Table 4-17 Volume Fraction and Degree of Hydration (0.44 w/c)

Time (hr.)	Free Water		HCP		Unreacted Cement		Aggregate		Air		Degree of Hydration	
	Lab.*	Cal.**	Lab.	Cal.	Lab.	Cal.	Lab.	Cal.	Lab.	Cal.	Lab.	Cal.
1.5	0.095	0.097	0.016	0.016	0.090	0.090	0.782	0.782	0.017	0.015	0.077	0.078
5	0.073	0.080	0.044	0.045	0.077	0.076	0.782	0.782	0.024	0.016	0.217	0.212
14	0.051	0.056	0.090	0.092	0.055	0.054	0.782	0.782	0.023	0.017	0.436	0.446
17	0.046	0.051	0.099	0.102	0.050	0.049	0.782	0.782	0.022	0.016	0.484	0.495
23	0.040	0.043	0.115	0.117	0.043	0.042	0.782	0.782	0.021	0.016	0.560	0.569
32	0.033	0.036	0.131	0.133	0.035	0.034	0.782	0.782	0.019	0.015	0.639	0.648
35	0.031	0.034	0.135	0.137	0.033	0.032	0.782	0.782	0.019	0.015	0.659	0.668
47	0.026	0.028	0.148	0.150	0.027	0.026	0.782	0.782	0.017	0.013	0.722	0.732
66.5	0.020	0.022	0.161	0.163	0.021	0.020	0.782	0.782	0.016	0.013	0.786	0.796
91	0.015	0.016	0.171	0.174	0.016	0.015	0.782	0.782	0.016	0.013	0.834	0.846
103	0.013	0.015	0.175	0.177	0.015	0.013	0.782	0.782	0.016	0.013	0.851	0.862
127	0.011	0.012	0.180	0.182	0.012	0.011	0.782	0.782	0.016	0.013	0.875	0.886
143	0.009	0.010	0.182	0.184	0.011	0.010	0.782	0.782	0.016	0.014	0.888	0.899
167	0.008	0.008	0.185	0.187	0.010	0.009	0.782	0.782	0.016	0.014	0.902	0.913

The evaluation of estimated free water and HCP contents which are main factors to be estimated in hydrated concrete were performed through a comparison to the measured values obtained from the laboratory test. Figure 4-30 illustrates the associated differences of volume fractions of free water and HCP between the calculated and laboratory test results for the sample with 0.32 w/c. The estimate of volumetric HCP content shows high accuracy with a maximum difference of less than 4 percent, while the differences of free water content estimates are relatively higher than those of HCP content but still less than 10 percent.

Figure 4-31 and Figure 4-32 show the associated difference on the estimate of each volume fraction for the higher treatments (0.40 and 0.44 w/c). The differences of a few estimates on the higher treatments are close to 10 percent, which is slightly higher than the lower treatment (0.32), but still highly accurate at less than 11 percent. As well, the estimates of HCP content produce relatively accurate results for both cases of which the differences are not over 4 percent. In conclusion, the variation between the free water content estimates from the new approach and the measured values were less than 11 percent with vast majority falling under 10 percent.

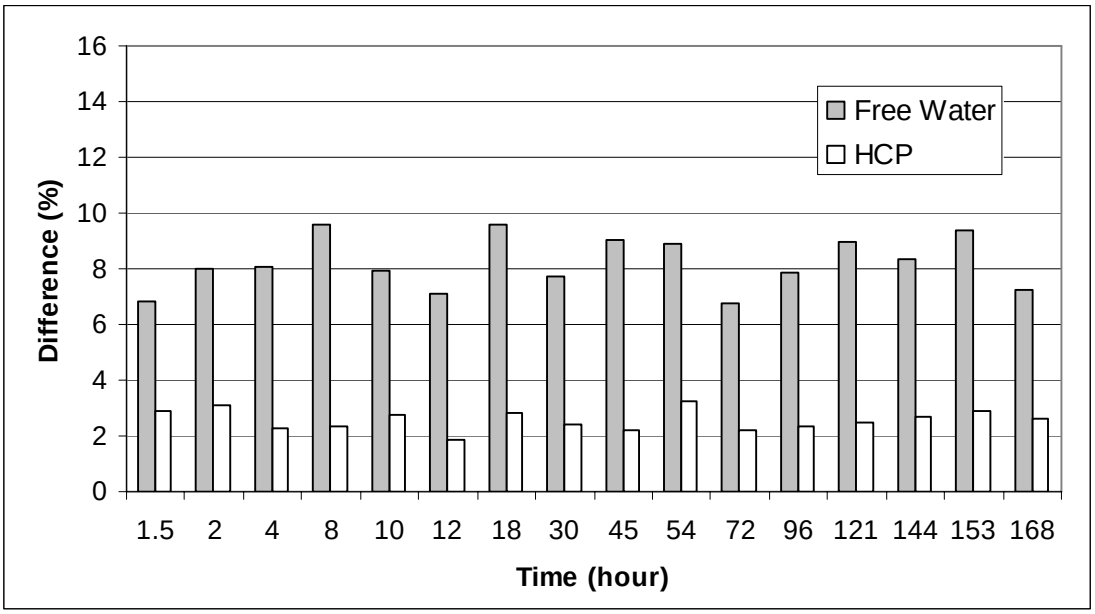

Figure 4-30 Errors of volumetric free water and HCP content on laboratory test results (0.32 w/c)

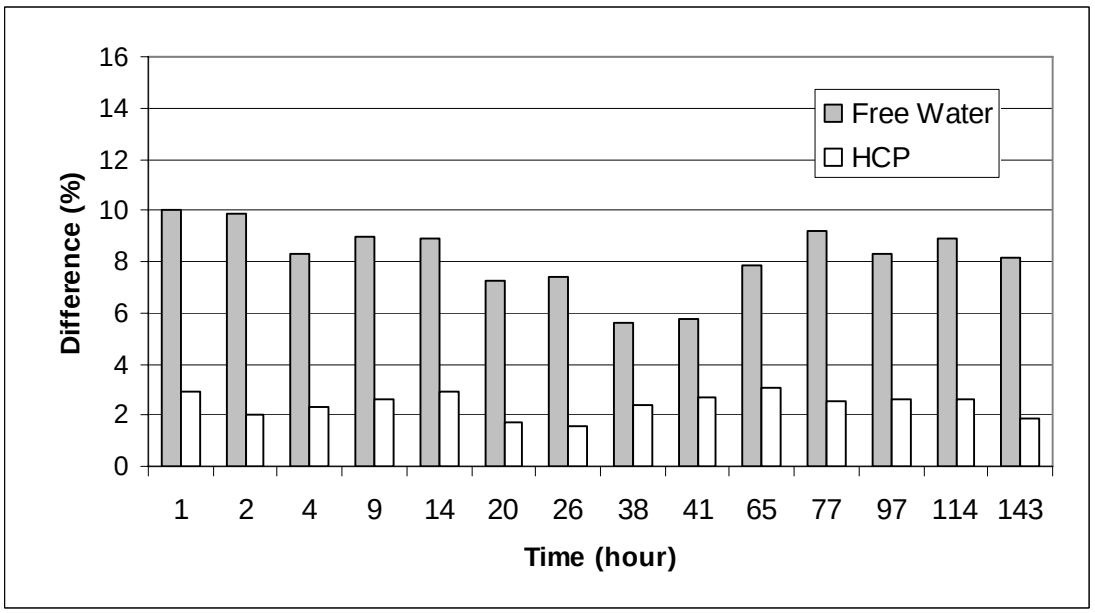

Figure 4-31 Errors of volumetric free water and HCP content on laboratory test results (0.40 w/c)

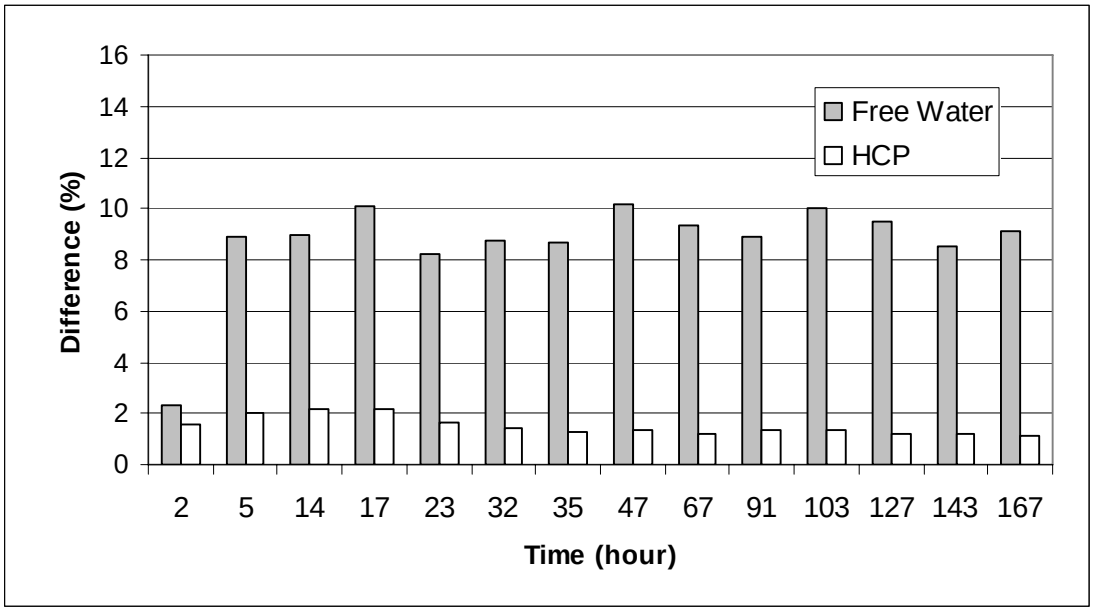

Figure 4-32 Errors of volumetric free water and HCP content on laboratory test results (0.44 w/c)

An additional comparison was performed to evaluate the change of w/c ratio by time. The values of w/c ratio estimated by the new approach were evaluated by comparing them to measured values. The variation of w/c ratio by time can provide information about the behavior of water and cement in hydrating concrete. Figure 4-33 illustrates the variations of measured and estimated w/c ratio for 0.32 w/c sample by time and the associated error between them. The w/c ratios were estimated slightly higher than laboratory test results, but the difference between them shows high accuracy with less than 3 percent. Figure 4-34 and Figure 4-35 show the measured and estimated w/c ratio of each time and the difference on the estimate for the higher treatments (0.40 and 0.44 w/c). While the w/c ratio values for the sample with 0.40 w/c were underestimated on the measured values, those for the sample with 0.44 w/c were slightly overestimated. However, the new approach provides significantly accurate estimates of w/c ratio for both samples with the majority of estimates falling within 4 percent of the laboratory derived data. Through the validation exercises, it was found that the new

approach is capable of estimating relatively accurate volume fractions of components in fresh PCC and helping to understand the behavior and properties of early-age concrete.

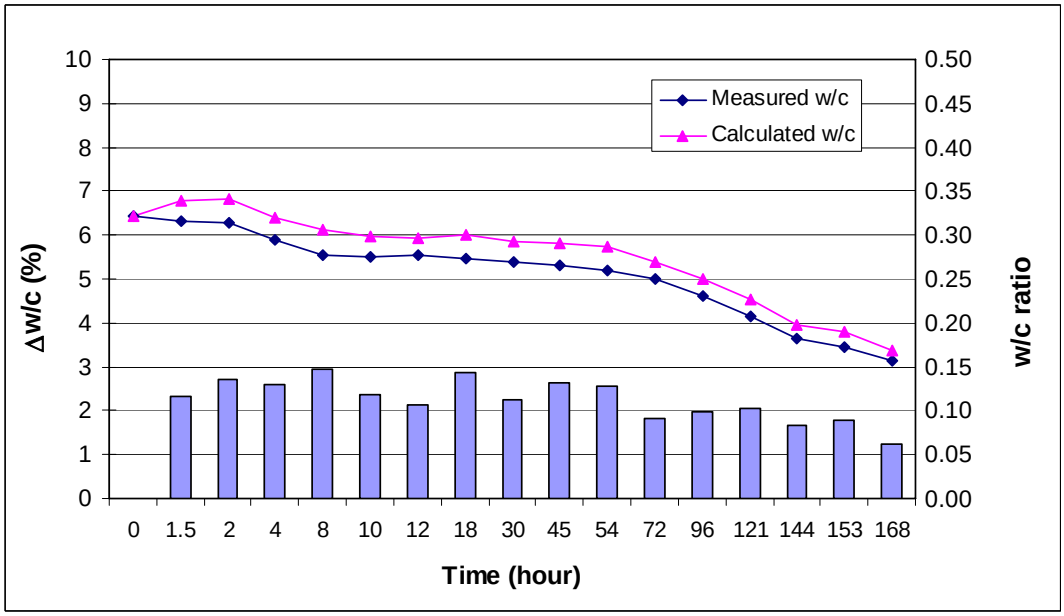

Figure 4-33 Comparison of measured and estimated variation of w/c ratio (0.32 w/c)

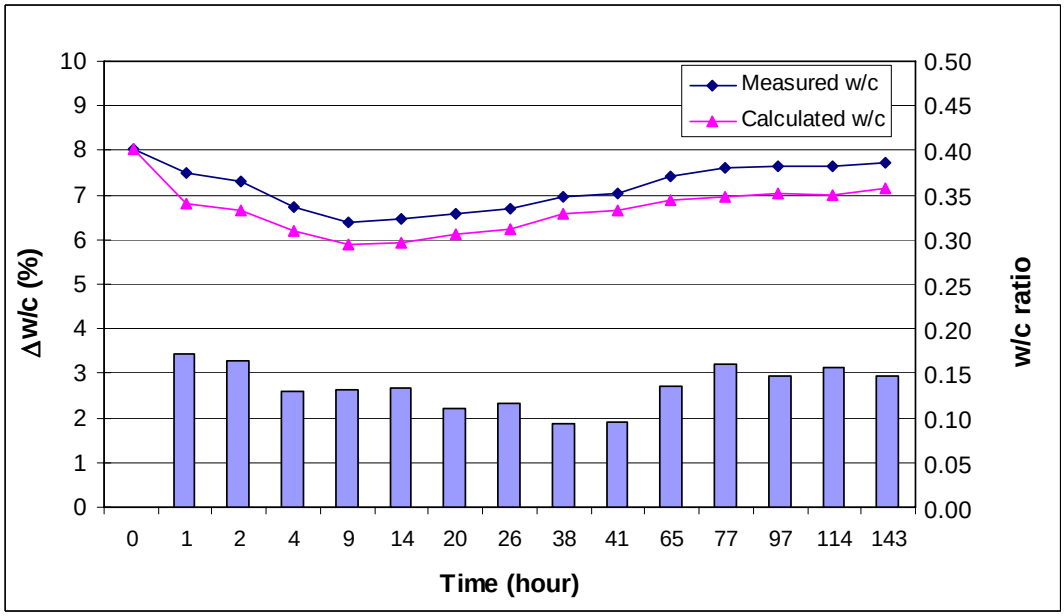

Figure 4-34 Comparison of measured and estimated variation of w/c ratio (0.40 w/c)

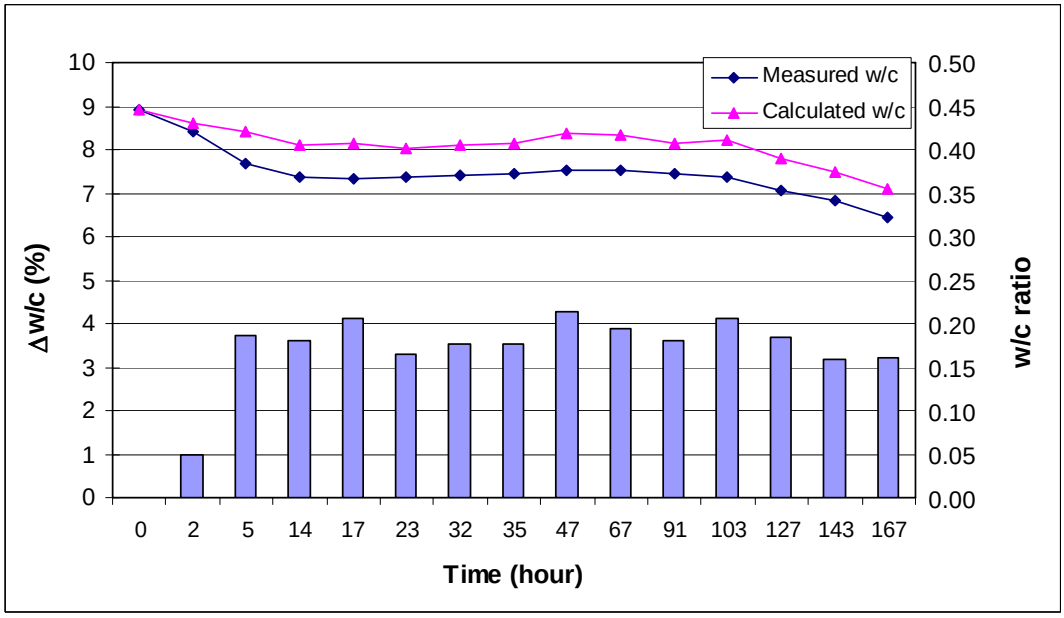

Figure 4-35 Comparison of measured and estimated variation of w/c ratio (0.44 w/c)

CHAPTER V

DEVELOPMENT OF COMPUTER PROGRAM

A computational program was developed, using the Microsoft® Visual Basic®, to interpret TDR traces and estimate soil water content using the new approach. In fact, the program is to calculate water content and dry density using the automated TDR traces collected in LTPP SMP study to monitor subsurface water condition in pavement structures. Since the LTPP database has approximately 274,000 automated TDR traces to be analyzed and the new approach needs to run the loop system in SID process, a computational program should be required to expedite the calculation process. The automated TDR traces acquired from the LTPP Information Management System (IMS) database were used to run the program.

The computational program can be used to automate the interpretation process with consideration given to certain user input data to ensure the highest quality end product (Zollinger et al. 2008). The program generates the output database tables that are consistent with the format used by the LTPP database that also serves as quality control tools for reviewing results. Figure 5-1 shows the main TDR trace viewing and interpretation screen of the program and Table 5-1 summarizes the procedures used in the program. The manual of the program is located in Appendix E.

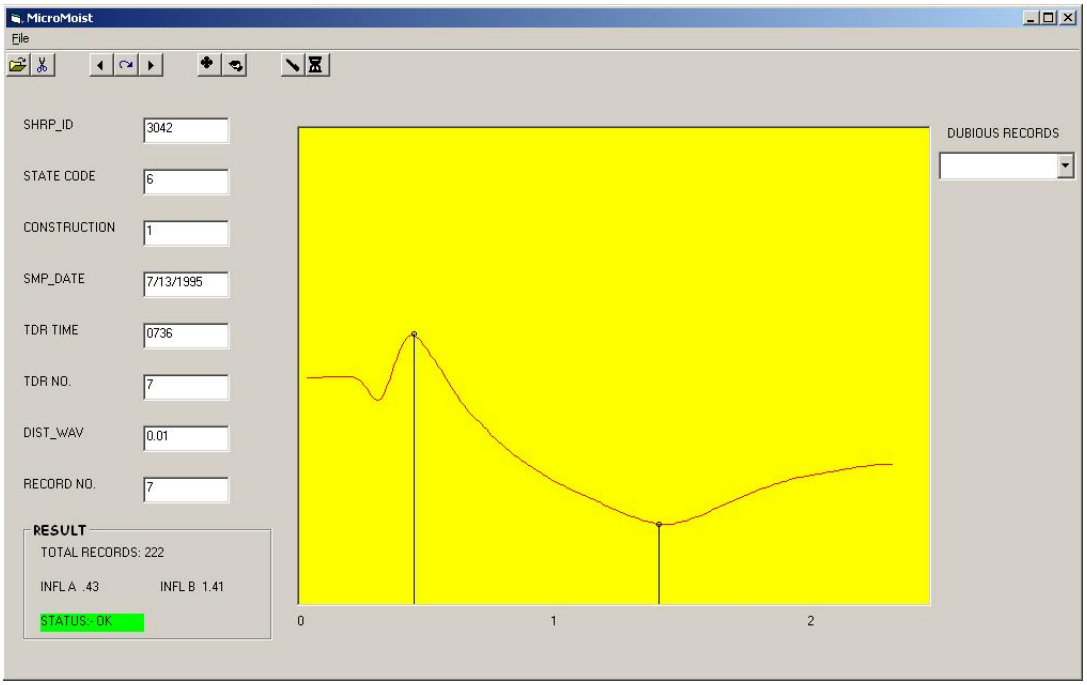

Figure 5-1 Main display of developed program

Table 5-1 Summary of Developed Program (Zollinger et al. 2008)

Procedures	Description
Determination of inflection points	Local beginning and ending points of the range of data to be analyzed
Calculation of dielectric constant	Transmission line equation and SID (function of dielectric constant, conductivity, and reflectivity of the soil composite)
Calculation of water content and dry density	Proposed self consistent model and SID (calibrated to site-specific conditions using ground truth data)
Input table	SMP_TDR_AUTO SMP_TDR_DEPTHS_LENGTH SMP_TDR_CALIBRATE
Output table	SMP_TDR_AUTO_DIELECTRIC SMP_TDR_MOISTURES

PROGRAM ALGORITHM

The program logic flow consists of three parts;

1. Determination of TDR trace inflection points.
2. Calculation of the soil dielectric properties.
3. Computation of the soil water content and dry density.

These three steps are automatically performed by opening the automatic TDR trace data table with logical checks.

Determination of Inflection Points

A local peak point in the TDR trace is created as the electromagnetic wave enters the TDR probe. From this point, the trace falls to a local minimum point and then rebounds upward at a lower rate as the wave hits the end of the probe. Figure 5-2 shows two types of inflection points on TDR traces that the first inflection point is either on the local maximum point and or on the global maximum point. For both TDR traces, the descending zones of the traces represent the waveform at the TDR sensor surrounded by soil composite. While a complete TDR trace consists of 245 data points, only portion between the inflection points is of interest for soil parameter computation because it represents the in-situ soil characteristics. Thus, the range of points which present the voltages used for the transmission line equation (TLE) analysis should be identified by the inflection points.

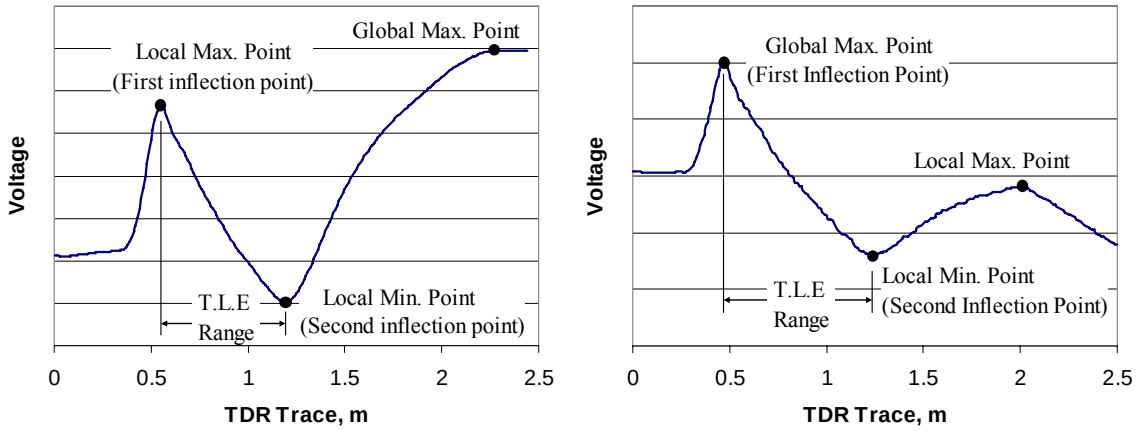

(a) Local maximum (b) Global maximum

Figure 5-2 Inflection points in TDR traces

The inflection points are determined by the program using a step-wise routine. Depending on the distance between wave points, which usually is 0.01 m but sometimes 0.02 m, in either case, the local maxima search routine is limited to the left portion of the trace. For traces with a wave point distance of 0.01 m, the maxima search routine is limited to the first 200 data points. For traces with a wave point spacing of 0.02 m, the maxima search routine only involves the first 100 data points. This generalization reduces the number of iterations and accelerates the process without reducing the utility of the program. The determination of inflection points using step-wise reduction involves the following steps:

1. Identify the global maximum point (P_i) within the generalized range (i.e., first 200 or 100 data points).
2. Find the local maximum point starting from P_i by comparing it with the three points before and after P_i.
    a. If the point is smaller than one of six points, change to the point to the left (p_{i-1}) and compare again. Continue until the condition in b. below is satisfied.

   b. If the point is larger than all six points, identify the point as the first inflection point.
   c. As in the TDR trace in Figure 5-2 (b), when a local maximum point is not found even though the changes and comparisons are carried on up to first data point (p_1), the global maximum point is identified as the first inflection point.
3. Find the local minimum point starting from the next point of the first inflection point (p_{i+1}) by similar routine used in step 2, because the second inflection point is always right side of the first in the TDR trace.
   a. If the point is larger than one of six points, change to the point to the right (p_{i+2}) and compare again.
   b. If the point is smaller than all six points, identify the point as the second inflection point.
4. Flag as error TDR trace if the program cannot find local maximum or minimum point (i.e. uninterpretable trace).

Along with the determination of the inflection points, the above routine helps to locate records with a positive slope which are identified as "Dubious Records" an improperly configured since TDR trace manifests a negative slope between the inflections. Where both points fall at the same location or the magnitude of the second point is higher than that of the first point, the trace is deemed to have a positive slope. Such a case may indicate the potential for frost and is flagged as an error record. The user, if necessary, can review each TDR trace and manually adjust each inflection point location. Figure 5-3 illustrates the flow chart of the inflection point determination.

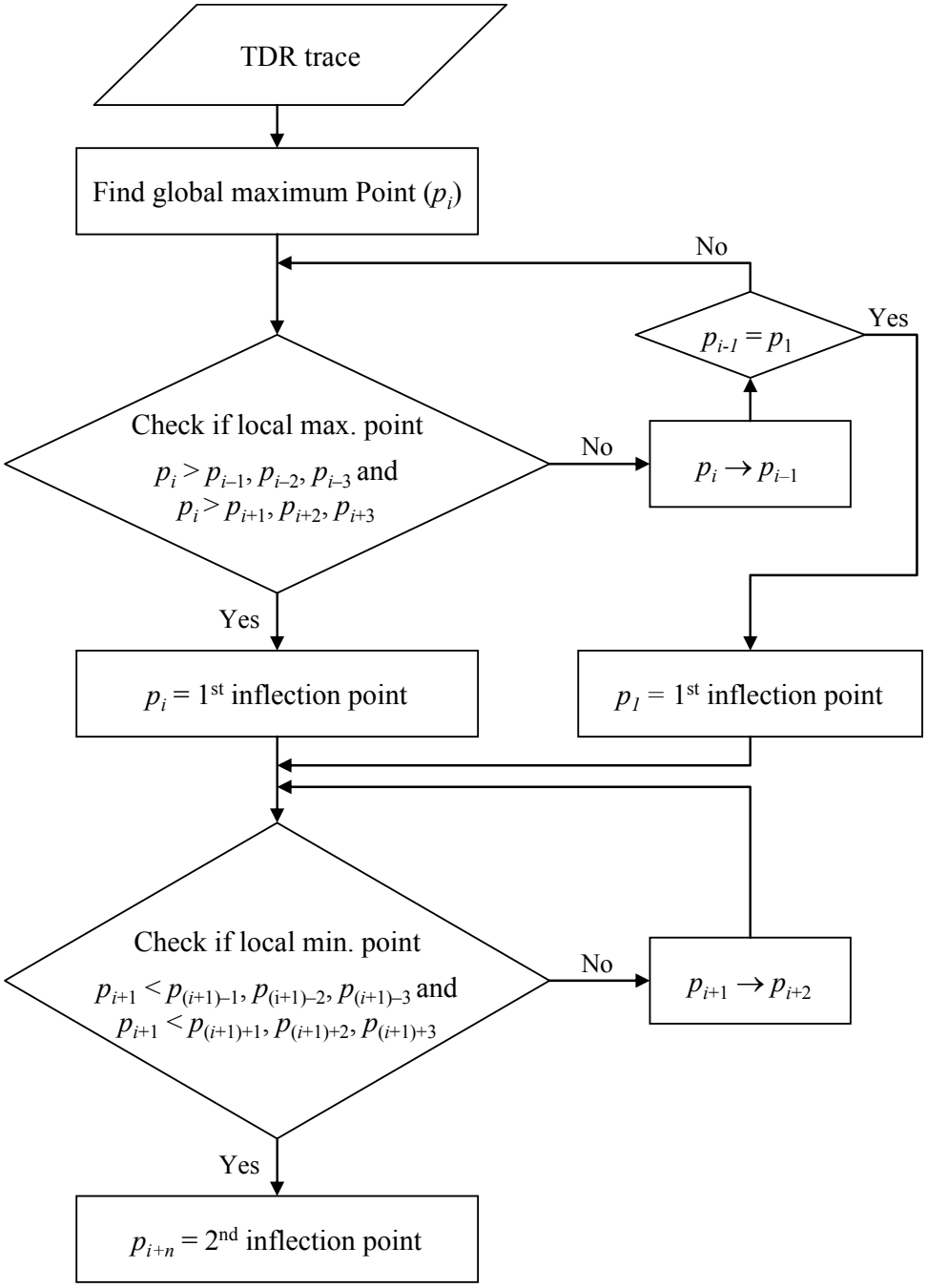

Figure 5-3 Flowchart for determination of inflection points

Calculation of Dielectric Constant, Reflectivity, and Conductivity

Once the inflection points are determined, the program calculates the dielectric constant, conductivity, and reflectivity using the transmission line equation and the SID solution method previously defined. The calculation is conducted based on fitting the measured voltage trace between the inflection points as described Chapter IV. All voltage data points between the inflection points were used in the program to determine the dielectric properties, while six points from the manual TDR traces obtained during TDR installation were used in the calibration process. Therefore, the accuracy of TDR interpretation was improved. The calculation process involves following steps:

1. Provide initial guesses of dielectric constant, reflectivity, and conductivity as well as the range of acceptable variation.
    a. Equation (2-22) is used to determine the initial value of the dielectric constant. It serves as an initial guess and reduces the number of iterations to determine the most likely value. The soil composite dielectric constant ranges between 1 to 85 and is increased or decreased by a constant factor after each iteration as indicated by the change vector $[\beta]$ generated from the SID method.
    b. Reflectivity is assigned 0.1 as an initial value but can vary within range of -1 to 1. Within the SID iteration, the reflectivity also varies by a factor similar to the dielectric constant, depending on the elements in the change vector.
    c. Conductivity is assigned a value of 0.5 initially, but the range is not fixed. The adjustment factor is applied to the conductivity depending on the magnitude of the change vector.
2. Calculate the parameters based on the SID method.
    a. The change vector $[\beta]$ (3×1 matrix) is determined based on the algorithm implemented in the program. The use of SID method calculates the relative voltage based on the inputted parameters and then compares it

with the measured relative voltage obtained from the TDR trace. The change vector is the measure of variation between each parameter.

b. This calculation process is contained within a loop which terminates when all elements of the change vector are less than 0.01.

The steps above are implemented for each trace, and the values of dielectric constant, reflectivity, and conductivity are stored in the SMP_TDR_AUTO_ DIELECTRIC table. The dielectric constant is then used to calculate water content and dry density. Figure 5-4 illustrates this calculation procedure.

The constants used to compute the dielectric constant are the voltage and relative distance, the magnetic permeability of free space, and the electric permittivity of free space. While the voltage and relative distance are obtained from each TDR trace, the magnetic permeability and the electric permittivity are fixed values which are $4\pi \times 10^{-7}$ H/m and $1/36\pi \times 10^{-9}$ F/m, respectively. Therefore, users do not need to change any constants for the computation of the dielectric constant in the program.

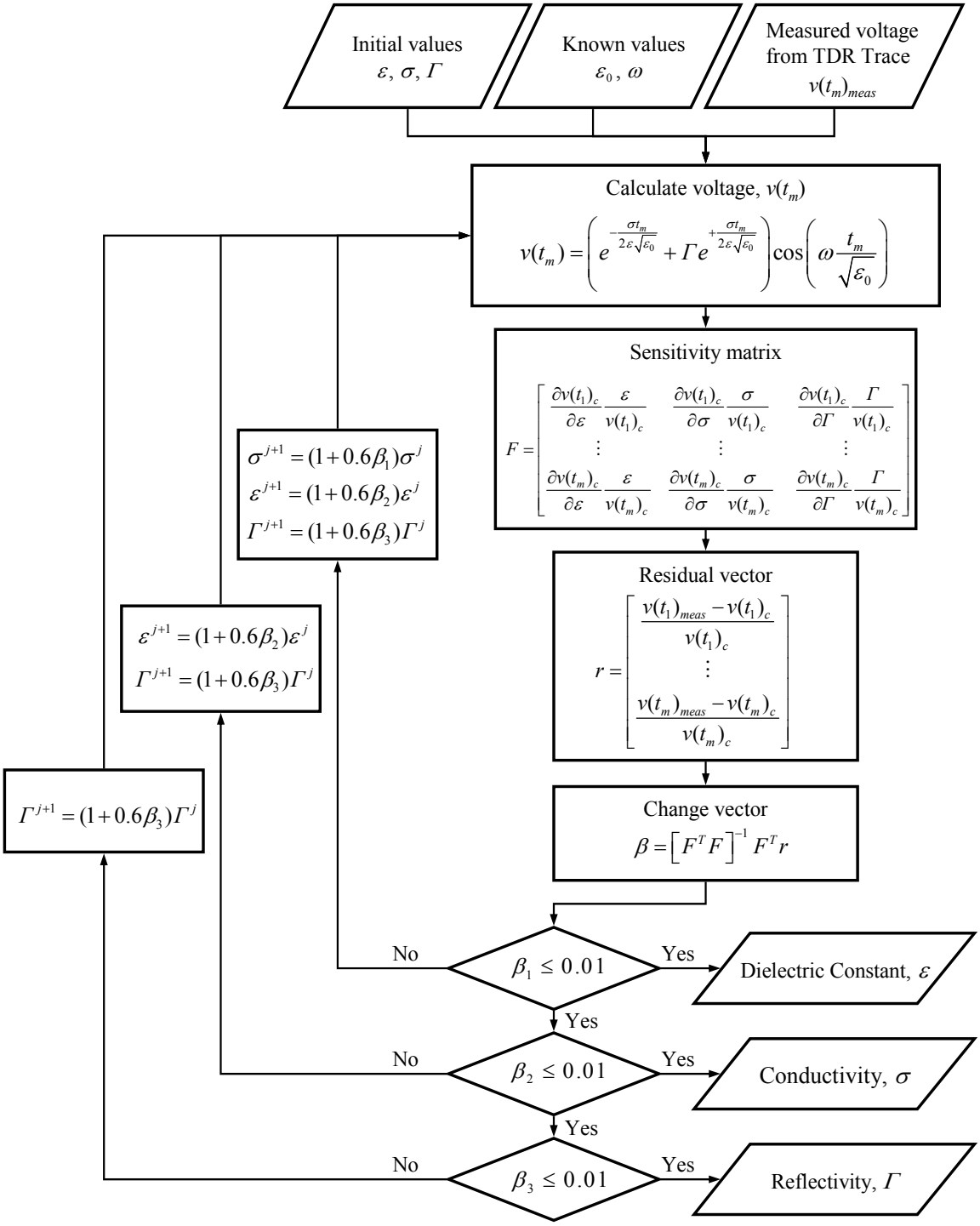

Figure 5-4 Flowchart for calculating dielectric constant, conductivity, and reflectivity

Calculation of Water Content and Dry Density

The water content and dry density are calculated based on the proposed self consistent model and SID. The parameters (ε_1, ε_2, and G_s) for the calculation process were calibrated to site-specific conditions based on the ground truth data and corresponding TDR traces obtained during installation. The composite dielectric constant of soil, determined from the previous process, is also an input into the model. The following procedure was followed for the calculation in the program:

1. Assign initial values to the unknown parameters of volumetric water content and dry density.
    a. Each TDR location has water content and dry density data measured during the installation process, which are stored in the calibration table. These values are used as seed values for the SID method.
    b. The values of dry density and volumetric water content range between 1.0 to 3.0 g/cm^3 and 0 to 1.0, respectively.
2. Calculate the dry density and water content based on the proposed self consistent model and SID method.
    a. The algorithm implemented in the program is a loop system which calculates the composite dielectric constant (ε_c) using the inputted parameters and then comparing it with measure composite dielectric constant (ε_{meas}). Equation (4-24) is used for the calculation process.
    b. The change vector [β] is the measure of variation in water content and dry density calculated from ε_c and the inputted parameters.
    a. Once the variation is less than 1.0 percent, the loop terminates and the values of water content and dry density are reported.

The volumetric water content and dry density calculated from the above procedure are presented in the output table, SMP_TDR_MOISTURE. The density of water and the dielectric constant of air are fixed values as 1.0 g/cm^3 and 1.0, respectively.

In the new approach, the physical properties of the TDR probe, such as length of TDR, are not considered in the computation process. Therefore, the program can be used to interpret other types of TDR probes as long as calibration data are available. Figure 5-5 illustrates the procedure for calculating the dry density and water content values.

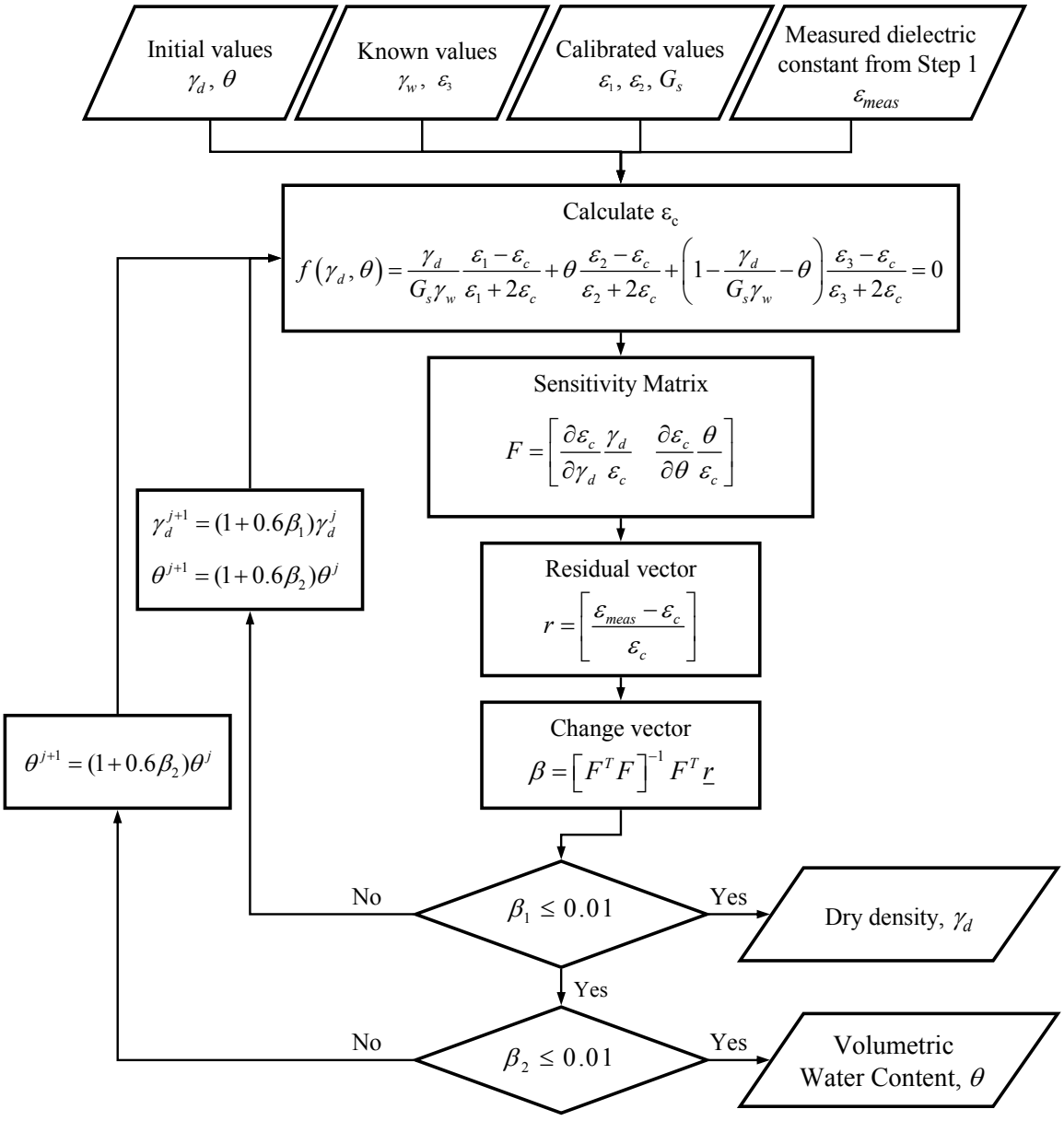

Figure 5-5 Flowchart for calculating water content and dry density

PROGRAM INPUT AND OUTPUT TABLE

As with all computational programs, a specific format of input data is required to process the TDR traces, and a format of output data should be generated to present the results. Since the program was developed to be used in LTPP SMP, the input and output database was designed based on the format of LTPP IMS database. All input and output database are the table format of Microsoft® Access®.

Input Table

The program needs the following three input tables: (1) SMP_TDR_AUTO for TDR trace reading, (2) SMP_TDR_DEPTHS_LENGTH for TDR depth information, and (3) SMP_TDR_CALIBRATE for calibrated soil data. While the first two tables can be obtained from the LTPP IMS database, the other was developed for the new program.

SMP_TDR_AUTO

The program first needs the TDR trace point data obtained from SMP_TDR_AUTO table containing TDR sensor response waveforms. The measured waveform is sampled at 245 intervals and stored in the WAVP_1 through WAVP_245 fields. The distance interval between data points recorded in DIST_WAV_POINTS field is 0.01 or 0.02 m. This raw TDR trace data can be acquired from the LTPP database and should be imported into Microsoft® Access® database format for processing. Table 5-2 shows the field information included in the SMP_TDR_AUTO table. The table structure is required to remain the same as in the LTPP IMS database to be used in the program.

Table 5-2 Field Names and Description of SMP_TDR_AUTO Table

Field Name	Description
SHRP_ID	Test section identification number assigned by LTPP
STATE_CODE	Numerical code for state or province
CONSTRUCTION_NO	Event number used to relate changes in pavement structure with other time dependent data elements
SMP_DATE	Measurement date
TDR_TIME	TDR measurement time (HHMM)
TDR_NO	ID number of TDR probe (1 to 10)
DIST_WAV_POINTS	Distance between waveform points (0.01 or 0.02 m)
WAVP_1 ~ 245	245 data points defining TDR waveform

SMP_TDR_DEPTHS_LENGTH

Each TDR probe has the information on the physical characteristics, such as the installed depth below the pavement surface and probe length for each TDR probe at each site (Elkins et al. 2003). As shown in Table 5-3, the SMP_TDR_DEPTHS_ LENGTH contains these physical characteristics of the TDR probes. The table links to SMP_TDR_AUTO table using SHRP_ID, STATE_CODE, TDR_NO, and CONSTRUCTION_NO to identify the depth of each TDR. The length of the TDR probe has been used to determine dielectric constant in the existing method, but the new program does not need this information anymore. This table can be obtained from the LTPP IMS database into Microsoft® Access® database format.

Table 5-3 Field Names and Description of SMP_TDR_DEPTHS_LENGTH Table

Field Name	Description
SHRP_ID	Test section identification number assigned by LTPP
STATE_CODE	Numerical code for state or province
CONSTRUCTION_NO	Event number used to relate changes in pavement structure with other time dependent data elements
INSTALL_DATE	Instrumentation installation date
TDR_NO	ID number of TDR probe (1 to 10)
TDR_DEPTH	Depth from pavement surface to TDR probe (m)
TDR_PROBE_LENGTH	Actual length of TDR probe (m)

SMP_TDR_CALIBRATE

In order to estimate the soil parameters, the new approach needs the calibration values which do not exist in LTPP IMS database. As shown in Table 5-4, the SMP_TDR_ CALIBRATE table developed to run the new program contains the calibrated dielectric constants and specific gravity as well as the ground truth data. The calibration was accomplished using the proposed self consistent scheme and the SID based on the ground truth data. The calibrated values are used to calculate water content by linking SMP_TDR_CALIBRATE by STATE_CODE, SHRP_ID, and TDR_NO fields. The installation date, TDR depth, and layer and soil types are obtained from the SMP installation report.

Table 5-4 Field Names and Description of SMP_TDR_CALIBRATE Table

Field Name	Description
SHRP_ID	Test section identification number assigned by LTPP
STATE_CODE	Numerical code for state or province
INSTALL_DATE	Instrumentation installation date
CONSTRUCTION_NO	Event number used to relate changes in pavement structure with other time dependent data elements
TDR_NO	ID number of TDR probe (1 to 10)
TDR_DEPTH	Depth from pavement surface to TDR probe at installation (m)
LAYER_TYPE	Type of sublayer at TDR probe installation
SOIL_TYPE	Soil type of layer at TDR probe installation
DRY_DENSITY	Measured dry density of soil at installation (g/cm^3)
VOLUMETRIC_ MOISTURE_CONTENT	Measured volumetric water content of soil at installation
DIELECTRIC_SOILDS	Calibrated dielectric constant value of solid
DIELECTRIC_WATER	Calibrated dielectric constant value of water
DIELECTRIC_AIR	Dielectric constant value of air (= 1.0)
SPECIFIC_GRAVITY	Calibrated specific gravity of soil

Output Table

Two tables are generated after running the program with input data: SMP_TDR_AUTO_ DIELECTRIC and SMP_TDR_ MOISTURE.

SMP_TDR_AUTO_DIELECTRIC

The SMP_TDR_AUTO_DIELECTRIC stores the dielectric constant, conductivity, and reflectivity parameters determined from the analysis of automatic TDR traces based on the transmission line equation, as described in Table 5-5. The dielectric constants in this

table are used to compute water content and dry density of soil as the main factor; hence, the SOIL_DIELECTRIC_CONSTANT field can be an input for the computation as well.

Table 5-5 Field Names and Description of SMP_TDR_AUTO_DIELECTRIC Table

Field Name	Description
SHRP_ID	Test section identification number assigned by LTPP
STATE_CODE	Numerical code for state or province
CONSTRUCTION_NO	Event number used to relate changes in pavement structure with other time dependent data elements
SMP_DATE	Measurement date
TDR_TIME	TDR measurement time (HHMM)
TDR_NO	ID number of TDR probe (1 to 10)
INFLEC_A	First inflection point in TDR trace (m)
INFLEC_B	Second inflection point in TDR trace (m)
SOIL_DIELECTRIC_ CONSTANT	Computed dielectric constant of soil
SOIL_CONDUCTIVITY	Computed conductivity of soil
SOIL_REFLECTIVITY	Computed reflectivity of soil

SMP_TDR_ MOISTURE

The SMP_TDR_ MOISTURE table contains volumetric and gravimetric water content and dry density computed from TDR traces. The dry density is used to convert volumetric to gravimetric water content using Equation (2-3) in Chapter II. Table 5-6 shows the field name and description of SMP_TDR_MOISTURE table. Figure 5-6 depicts the process of the input and output tables in the developed program.

Table 5-6 Field Names and Description of SMP_TDR_AUTO_MOISTURE Table

Field Name	Description
SHRP_ID	Test section identification number assigned by LTPP
STATE_CODE	Numerical code for state or province
CONSTRUCTION_NO	Event number used to relate changes in pavement structure with other time dependent data elements
SMP_DATE	Measurement date
TDR_TIME	TDR measurement time (HHMM)
TDR_NO	ID number of TDR probe (1 to 10)
TDR_DEPTH	Depth from pavement surface to TDR probe at installation (m)
LAYER_TYPE	Type of sublayer at TDR probe installation
SOIL_TYPE	Soil type of layer at TDR probe installation
SOIL_DIELECTRIC_ CONSTANT	Computed dielectric constant of soil
DRY_DENSITY	Computed dry density of soil (g/cm^3)
VOLUMETRIC_ MOISTURE_CONTENT	Computed volumetric water content
GRAVIMETRIC_ MOISTURE_CONTENT	Computed gravimetric water content
ERROR_COMMENT	Assigned error code

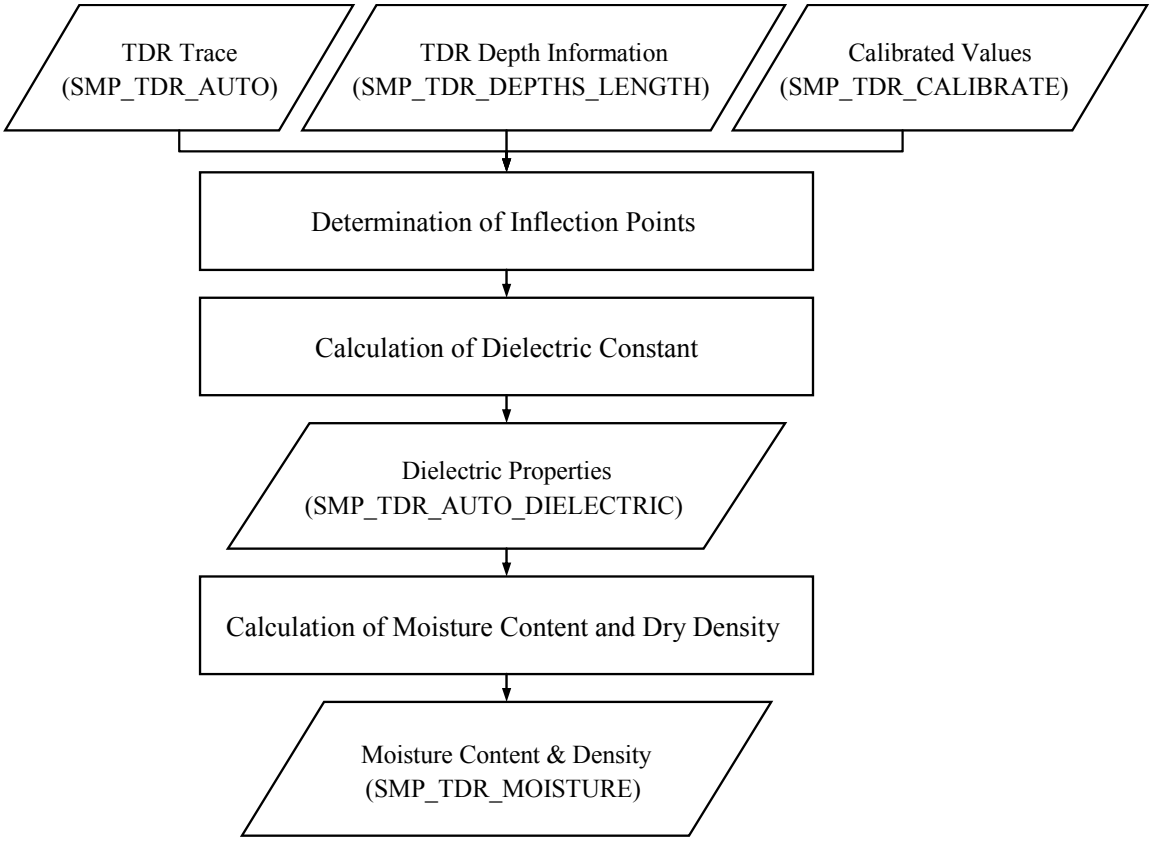

Figure 5-6 Process of input and output data table in developed program

QUALITY CHECKS ON THE PROGRAM COMPUTATIONS

In order to facilitate the process of the new approach, the program was developed to analyze all TDR traces and compute parameters automatically. However, additional consideration needed to be given to unique data requiring user input to ensure the results having higher quality. For instance, TDR traces not exhibiting a negative slope could not be analyzed using the proposed approach. Therefore, various quality control and quality assurance (QC/QA) tools were incorporated in the program. As part of the purpose, flagging function and manual review procedure were developed for the data processing activities.

TDR Trace Error

As previously noted, some TDR traces do not exhibit a negative slope between the inflection points, which are not interpretable as shown in Figure 5-7. The error trace may be caused by the abnormal operation of TDR device or the environmental effects near TDR probes, such as temperature or very high salinity of the soil. The program identifies the error trace while determining the inflection points. If the program cannot capture a negative slope between the inflection points, the trace is flagged as uninterpretable TDR trace in the program. The number of the questionable TDR trace is displayed as "Dubious Trace" in the program display. Also, the error code "TDR_ERR" is assigned to ERROR_COMMENT filed in the SMP_TDR_MOISTURE table.

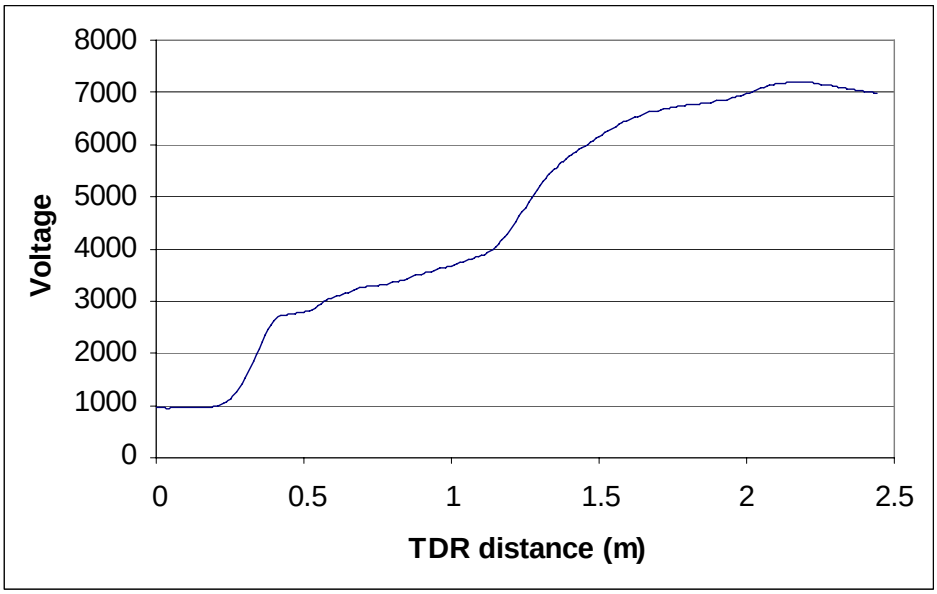

Figure 5-7 TDR Traces which has no a negative slope

Dry Density Error

The measured ground truth values of dry density reported in the LTPP database were in the range of 1.3 to 2.5 g/cm^3. Most of the dry densities calculated from the program were also within this range as well. However, the dry density values of some TDR traces were calculated less than 1.3 g/cm^3, most likely due to unreasonably high moisture

content or frozen soil material. In these instances, the program assigns the error code "DD_ERR" for those TDR traces in the SMP_TDR_MOISTURE table.

Unavailable Calibration Data

As previously noted, the calibrated values of dielectric constants and specific gravity must be provided to estimate the water content in the program. However, some sections could not have ground truth data such as the measured water contents or corresponding TDR traces which to support the calibration of the dielectric constants of the soil components. Without the information, the new approach cannot be calibrated and generate accurate computations. In the cases where the calibration data from installation activities were unavailable, the error code "CALI_ERR" is assigned to ERR_COMMENT field. The error codes used to identify TDR trace inconsistencies are listed in Table 5-7.

Table 5-7 Error Codes used in the Program

Error Code	Description
TDR_ERR	TDR trace does not have a negative slope.
DD_ERR	Calculated dry density is less than 1.3 g/cm^3.
CALI_ERR	Calibration data from installation activities are unavailable.

User Quality Check of Inflection Points

When opening an input table of SMP_TDR_AUTO, the program automatically processes all TDR traces and displays the traces and inflection points on the screen or assigns error codes to uninterpretable traces. However, even with the automatic process, it may be necessary for user to perform QC/QA to make sure the positions of inflection points or the error in the trace. Thus, the program was designed to provide users with a visual feature to allow review of TDR trace. This feature also allows users to identify unique traces not detected by the automated checks, while providing a visual verification

of those traces that were flagged. As part of the viewing function, the user has the capability of modifying the ranges used in the transmission line equation for cases where they were improperly identified by the program.

REVIEW OF RESULTS FROM PROGRAM

As a post-processing QC review, the results generated from the new program were reviewed using pivot table presenting the variation of water content and dry density by time or season. Also, it was carried out to compare the water contents from the program to those from the existing methods. These reviews were performed using automated TDR data of LTPP SMP test sections.

Seasonal Variation of Water Content and Dry Density

In order to review the final results from the developed program, a post-processing QC review was performed using the pivot table. Water content and dry density values determined by the program were plotted to the pivot tables in Microsoft Excel® as shown in Figure 5-8. The pivot table configuration allows large quantities of data to be reviewed relatively quickly, while the graphical nature makes questionable or anomalous data readily identifiable. Problematic or frequently occurring trends in the data can also be easily recognized through the process.

This QC process provides users with the capability of reviewing all estimates from the program considering climate or several environmental factors of each LTPP test section. Outliers or anomalous data identified can be manually flagged as a final QC/QA process. Also, the pivot tables played an important role for the beta testing during the program development. The review provided valuable insight, identified issues with the software, and was an integral part of the debugging process.

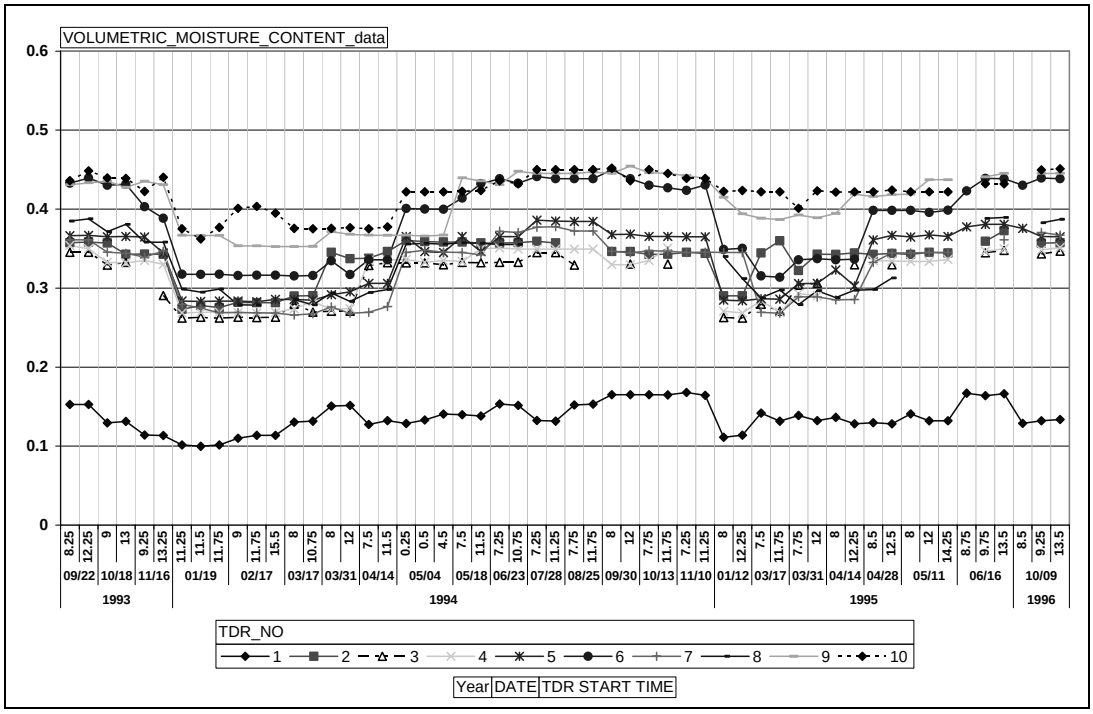

Figure 5-8 Example of water content seasonal trend plot

The post-processing QC review also served as a trial for incorporating the variation or the trends into the analysis of the results. The plots in Figure 5-9 and Figure 5-10 indicate the seasonal variations of volumetric water content and dry density generated from the new program. The upper side of plot presents the values of dry density for 10 TDR probes, and the lower indicates the volumetric water content corresponding to each probe. The first data points indicate the measured values which were used for the calibration at TDR installation.

The LTPP section 404165 in Figure 5-9 is located in northern Oklahoma classified as the LTPP Southern Region and a dry-no freeze zone (Peirce 1995). The plots do not show the wide variation of dry density and water content because the section is located in a no freezing region with a less amount of precipitation.

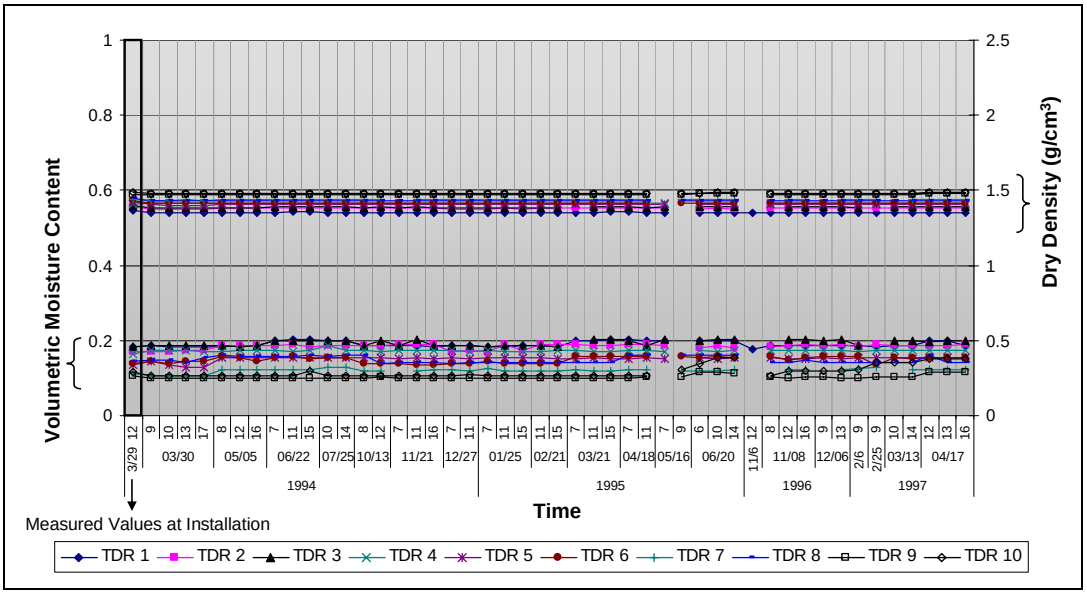

Figure 5-9 Variation of water content and density for section 404165 (dry-no freeze zone)

On the other hand, as seen in Figure 5-10, the variation of LTPP section 274040 located in northern Minnesota demonstrates significant variations on volumetric water content, compared to the section 404165 (van Sambeek and Urbach 1996). The section is classified as the LTPP North Central Region and a wet-freeze zone. The plots of dry density also shows the significant variation by season; in that, the values in thawing and rainy season are slightly lower than those in any other periods since dry density is influenced by the seasonal factors such as temperature, precipitation, and freeze/thaw condition.

The post-processing QC plots can provide the clear graphical presentations of the program results as well as the vertical variations by season or depth for all TDR trace in each LTPP section. The post-processing QC plots indicating the seasonal variations of water content and dry density of all 64 LTPP SMP test sections are available in Appendix F.

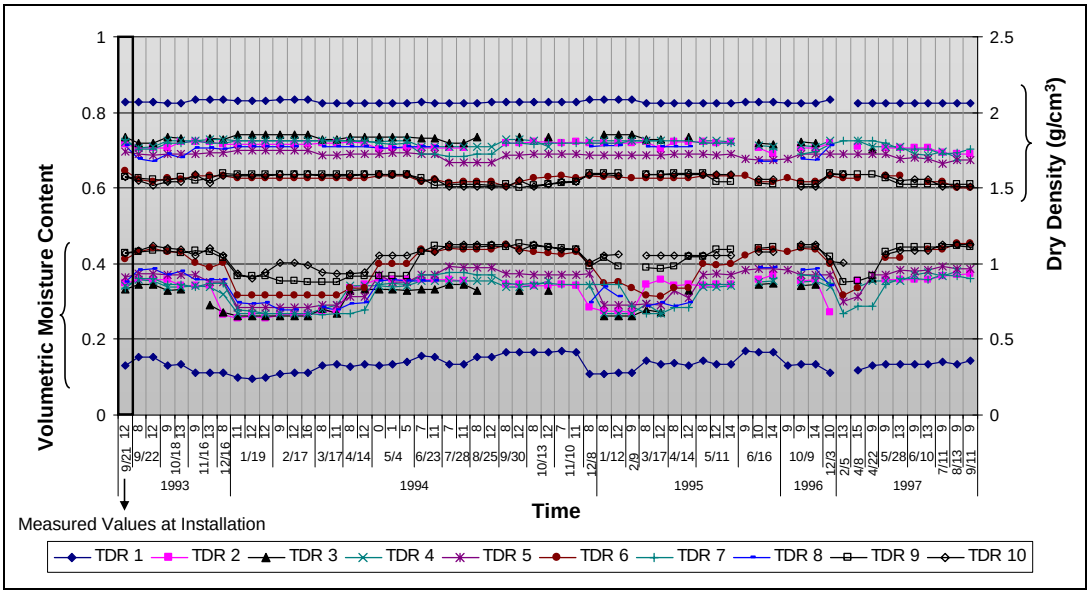

Figure 5-10 Variation of water content and density for section 274040 (wet-freeze zone)

Comparison between New and Existing Data

With the water content and density data manually computed using the self consistent model, a series of comparisons has been performed to validate the new procedure in Chapter IV. However, since limited data was used for the previous validation, additional comparison was made to ensure that the computational program was working properly. In many cases, the similar trends of results show up for both new and existing computational processes. However, significant differences are present in some cases. In these situations, the new approach produces water content estimate that is closer to the in-situ water content measured during TDR installation as compared with the existing empirical method.

As an example, Figure 5-11, for LTPP section 404165 located in northern Oklahoma, presents the range of three years water contents determined by the existing methods and the new approach, respectively. Also, the ground truth water content obtained during TDR installation is included in the figures. While the water contents data in Figure 5-11 (a) were acquired from existing LTPP IMS database, the data in

Figure 5-11 (b) were determined by the developed program using corresponding TDR traces. As seen in Figure 5-11 (a), the volumetric water contents from the empirical method range form 0.1 to 0.3. For some of TDR sensors, the predictions are significantly higher than the measured in-situ water content. On the other hand, the results from the new approach, as shown in Figure 5-11 (b), correlate more closely with the measured water content.

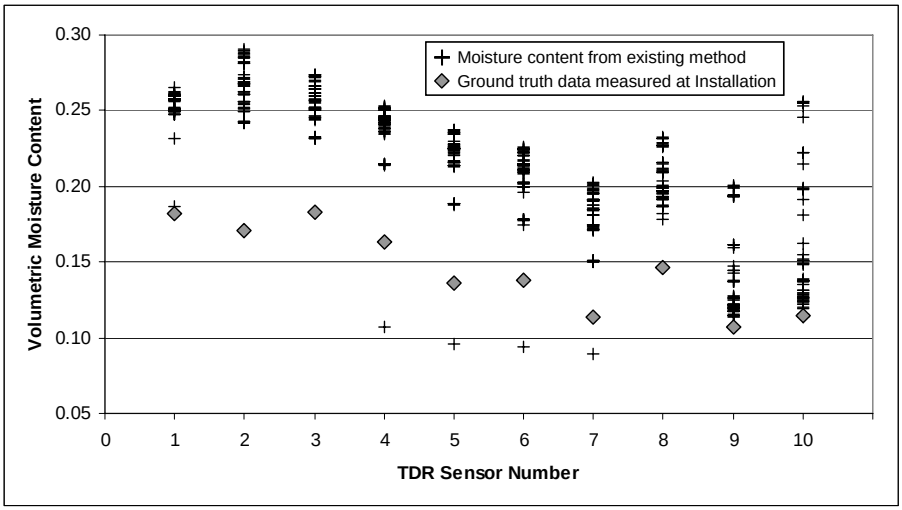

(a) Water contents from existing method

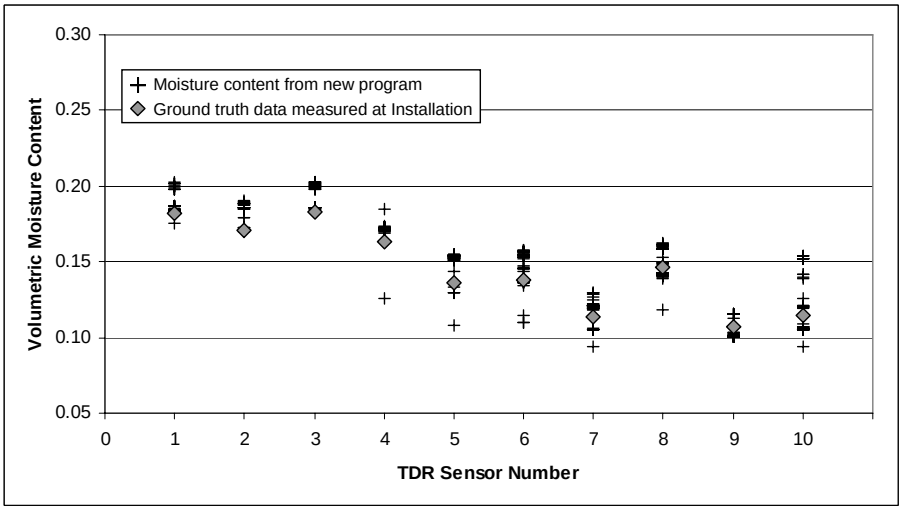

(b) Water contents from new approach (Program)

Figure 5-11 Comparison of water content results for LTPP section 404165

Another example for LTPP section 274040 can be found in Figure 5-12. The LTPP section 274040 is located in northern Minnesota and classified as wet-freeze climatic region. As can be seen Figure 5-12 (a), almost all water contents from the existing method are significantly less than the ground truth data except for TDR sensor No. 1. However, the results from the new program correlate more closely with the ground truth water content.

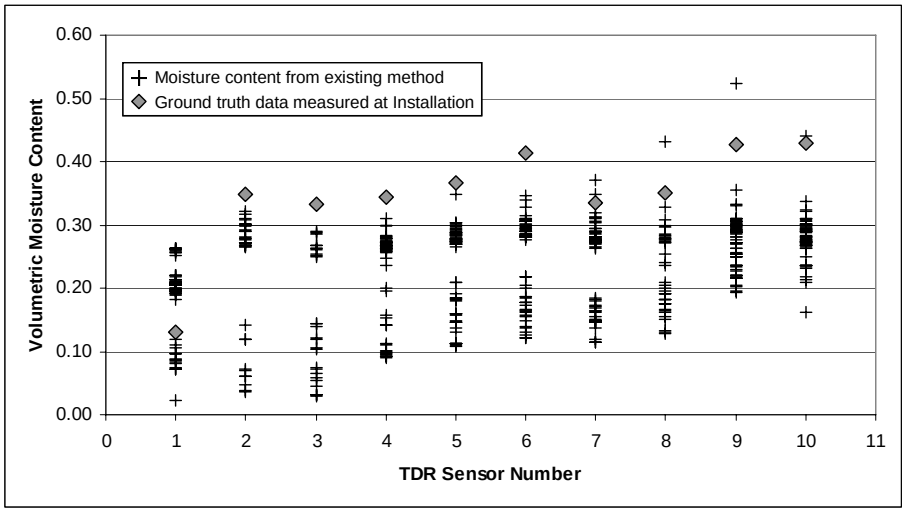

(a) Water contents from existing method

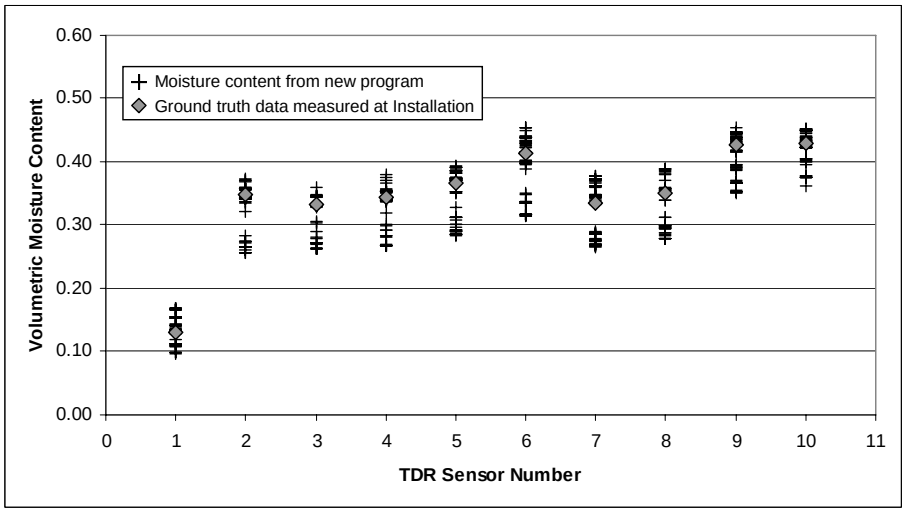

(b) Water contents from new approach (Program)

Figure 5-12 Comparison of water content results for LTPP section 274040

This is expected clearly, since the new approach makes more effective of the ground truth data in developing the calibrated values used in the model, the results are closer to the ground truth data and more appropriately distributed as compared with those from the existing method. Also, from this situation, it is obviously verified that the empirical methods are not valid for the whole range of soil water content and for the all soil types not used for source data.

CHAPTER VI

CONCLUSION AND RECOMMENDATION

SUMMARY AND CONCLUSION

The estimate of volume fraction of each component in a composite material can support to understand the material properties and its performance in the field. In particular, the estimate of water content in unbound sublayer material will provide useful information not only to figure out the performance but also to reduce the moisture-induced damage of pavement system. For PCC, the free water and HCP content estimates can help to understand the hydration and early-age concrete behavior. Therefore, several test methods had been developed and used mainly to measure laboratory or in-situ water content. However, since they rely on the subjective determination or are time consuming, a more logical method has been needed to estimate volume fraction of composite pavement materials. As the result, test methods using dielectric properties of the materials have been used as an alternative, because it is relatively accurate and fast and provides a nondestructive in-situ measurement.

Since the dielectric constant of composite material depends on the volumetric content and dielectric properties of each component, it can be used as a main parameter to estimate constituent volume fractions. The composite dielectric constant can be measured using some devices such as TDR, Percometer, or GPR. In order to relate composite dielectric constant to physical properties such as volume fraction of components in a multiphase material, the empirical and mechanistic approaches were used. The empirical models were established by regression analysis using volume fraction which is usually water content and dielectric constant data produced by experiment or observation. Although the models are relatively simple to use, they are not very accurate for some composite material types not used to calibrate the regression coefficients. In the mechanistic approach, the dielectric mixing models were developed

relating the composite dielectric constant to the dielectric constant and volume fraction of each constituent. Compared with the empirical models, the mechanistic models are theoretically reasonable to describe the relationship since they can account for the influence of the individual constituent materials. However, the mechanistic models currently used require the assumptions for the geometric arrangement factor and constituent dielectric constants. These regression and assumptions of both approaches may result in systematic error causing less accurate estimate results.

In order to remove or minimize the systematic error, the new approach was proposed based on the self consistent scheme which is one of mechanistic models and the SID as a solution methodology. Subsequently, the two pavement materials, soil and PCC mixtures, were used to verify the applicability and perform the validation of the approach. The new approach consisting of three steps can be summarized as:

Step 1. Determine composite dielectric constant of a given composite material.

- For TDR application, the calculation of conductivity and reflectivity using the transmission line equation can provide a more precise estimate of the composite dielectric constant.
- The use of percometer immediately provides surface dielectric constant without any analysis.

Stpe 2. Based on the measured volume fraction data along with the composite dielectric constant, calibrate the dielectric constant of each component in the composite material using the SID.

- For soil mixtures, the three values were calibrated by the use of the following self consistent model as:

$$f\left(\varepsilon_1,\varepsilon_2,G_s\right)=\frac{\gamma_d}{G_s\gamma_w}\frac{\varepsilon_1-\varepsilon_c}{\varepsilon_1+2\varepsilon_c}+\theta\frac{\varepsilon_2-\varepsilon_c}{\varepsilon_2+2\varepsilon_c}+\left(1-\frac{\gamma_d}{G_s\gamma_w}-\theta\right)\frac{\varepsilon_3-\varepsilon_c}{\varepsilon_3+2\varepsilon_c}=0$$

- For PCC, the four values were calibrated through the following as:

$$f(\varepsilon_1,\varepsilon_2,\varepsilon_3,\varepsilon_4)=\theta_w\frac{\varepsilon_1-\varepsilon}{\varepsilon_1+2\varepsilon}+\theta_{uc}\frac{\varepsilon_2-\varepsilon}{\varepsilon_2+2\varepsilon}+\theta_{hcp}\frac{\varepsilon_3-\varepsilon}{\varepsilon_3+2\varepsilon}+\theta_{agg}\frac{\varepsilon_4-\varepsilon}{\varepsilon_4+2\varepsilon}$$
$$+\theta_{air}\frac{\varepsilon_5-\varepsilon}{\varepsilon_5+2\varepsilon}=0$$

Stpe 3. Based on the calibrated component dielectric constants, forward calculate the volume fraction along with composite dielectric constant determined for other times.

- For soil mixtures, the following model was used together with the calibrated constant (ε_1, ε_2, and G_s) to calculate the dry density (γ_d) and volumetric water content (θ) as:

$$f\left(\gamma_d,\theta\right)=\frac{\gamma_d}{G_s\gamma_w}\frac{\varepsilon_1-\varepsilon_c}{\varepsilon_1+2\varepsilon_c}+\theta\frac{\varepsilon_2-\varepsilon_c}{\varepsilon_2+2\varepsilon_c}+\left(1-\frac{\gamma_d}{G_s\gamma_w}-\theta\right)\frac{\varepsilon_3-\varepsilon_c}{\varepsilon_3+2\varepsilon_c}=0$$

- For PCC, the following model was used together with the calibrated constant (ε_1, ε_2, ε_3, and ε_4) to calculate the volumetric content of free water (θ_w) and degree oh hydration ($\alpha(t)$) as:

$$f\left(\theta_w,\alpha(t)\right)=\theta_w\frac{\varepsilon_1-\varepsilon_c}{\varepsilon_1+2\varepsilon_c}+\theta_c\left(1+f_v\right)\alpha(t)\frac{\varepsilon_2-\varepsilon_c}{\varepsilon_2+2\varepsilon_c}+\theta_c\left[1-\alpha(t)\right]\frac{\varepsilon_3-\varepsilon_c}{\varepsilon_3+2\varepsilon_c}$$
$$+\theta_{Agg}\frac{\varepsilon_4-\varepsilon_c}{\varepsilon_4+2\varepsilon_c}+\left\{1-\theta_w-\left[1+f_v\alpha(t)\right]\theta_c-\theta_{agg}\right\}\frac{\varepsilon_5-\varepsilon_c}{\varepsilon_5+2\varepsilon_c}=0$$

The strength of the new approach is the calibration step which is conducted for each composite material based on the measured data. This activity can produce improved results without any assumptions for intrinsic properties such as constituent dielectric constants. The calibration of subsurface soil material in each LTPP SMP site is a key step to account for environmental differences between the sites, which are not

accounted for in the existing approaches. As well, the calibration of PCC can give the explanation on significant differences in ingredients (cement, aggregate, and water) of concrete mixture. The site or material specific calibration of the approach accounts for these differences as well as variation in geological composition of the composite materials. The new model also incorporates the dielectric constant of air within the multiphase system, which leads to a reduction in systematic error over the empirical methods.

The validations performed using soil and PCC indicated that the results obtained from the new approach had significantly less error than those from existing methods. For soil mixture, the evaluation was performed by comparing the moisture estimates to the measured data from Klemunes' laboratory test and LTPP forensic studies. The percent differences of new approach are less than 10 percent while those of existing methods currently used are much higher. Also, the new approach provides the capability of estimating dry density from TDR measurements although the previous procedures did not have a mechanism for estimating dry density. As well, the validation for PCC indicated that it was highly accurate at less than 11 percent with vast majority falling 10 percent for estimates of free water. The estimate of volumetric HCP content shows high accuracy with a maximum error of less than 4 percent.

The computer program was developed to facilitate the interpretation of TDR and the estimate of water content and dry density of soil material consisting of three components. While the SID method can solve several parameters in the self consistent model accurately, it needs to run a complicated loop system in the parameter adjustment algorithm. The program includes the capability to implement the algorithm rapidly with supporting a use-friendly interface for easy process and providing the QC tools. The post-processing QC review provided the understanding of seasonal variation of water content and dry density of each site.

RECOMMENDATIONS FOR FURTHER STUDY

It was shown in the study that the dielectric constant can be a key parameter to estimate volume fractions of composite materials. Also, the new approach based on the self consistent model and the site specific calibration was worked well with composite pavement materials. However, the validation to verify the new approach was based on the limited pavement materials of soil and PCC mixtures. The approach can be used to estimate volume fraction of HMA surface layer which is expected to consist of water, asphalt cement, aggregate, and air, in the field. For HMA surface, GPR will be a proper device to measure composite dielectric constant since HMA layers need deep measurement of dielectric constant from the surface and HMA material has relatively higher volumetric air content as compared to soil or cement concrete materials. Furthermore, another computational program may need to be developed to estimate volume fractions of multiphase materials consisting of more than three components. Although the program was developed in this study, it can be used only to interpret TDR trace and then estimate volumetric water content and dry density of soil consisting of 3-phase. Therefore, the development of the analysis package can facilitate to estimate the volume fraction of PCC or HMA, which may be helpful to understand the behavior or the materials.

REFERENCES

AASHTO. (2000). "Standard method of test for laboratory determination of moisture content of soils." Standard Specifications for Transportation Materials and Methods of Sampling and Testing, T265-93, Washington, D.C.

AASHTO. (2004a). "Specific gravity and absorption of fine aggregate." Standard Specifications for Transportation Materials and Methods of Sampling and Testing, T84-00, Washington, D.C.

AASHTO. (2004b). "Standard method of test for specific gravity and absorption of coarse aggregate." Standard Specifications for Transportation Materials and Methods of Sampling and Testing, C85-91, Washington, D.C.

Adek LLC. (2009). http://www.adek.ee/. Adek Percometer, Saku Harjumaa, Estonia.

Ajo-Franklin, J. B., Geller, J. T., and Harris, J. M. (2004). "The dielectric properties of granular media saturated with DNAPL/water mixtures." *Geophysical Research Letters*, 31, 17501-17609.

ASI Instruments, Inc. (2002). http://www.asiinstr.com/technical/Dielectric%20 Constants.htm. Dielectric constant reference guide, Houston, TX.

ASTM. (2008a). *Standard test method for in-place density and water content of soil and soil-aggregate by nuclear method*. ASTM Standards, D6938-08a, West Conshohocken, PA.

ASTM. (2008b). *Standard test methods for density, relative density (specific gravity), and absorption of coarse aggregate*. ASTM Standards, C127-07, West Conshohocken, PA.

ASTM. (2008c). *Standard test methods for density, relative density (specific gravity), and absorption of fine aggregate*. ASTM Standards, C128-07a, West Conshohocken, PA.

ASTM. (2008d). *Standard test methods for laboratory determination of water (moisture) content of soil and rock by mass*. ASTM Standards, D2216-05, West Conshohocken, PA.

Avelar Lezama, I. (2005). "Preliminary non-destructive assessment of moisture content, hydration and dielectric properties of Portland cement concrete." M.S. thesis, Texas A&M University, College Station, TX.

Baran, E. (1994). "Use of time domain reflectometry for monitoring moisture changes in crushed rock pavements." *Proceedings, Symposium and Workshop on Time Domain Reflectometry in Environmental, Infrastructure, and Mining Application*, Spec. Publ. SP 19-94, 349-356.

Barry, C. R., Schwartz, C., and Boudreau, R. (2006). *Geotechnical aspects of pavements*. Report No. FHWA NHI-05-037. National Highway Institute, Federal Highway Administration, Washington, DC.

Birchak, J. R., Gardner, C. G., Hipp, J. E., and Victor, J. M. (1974). "High dielectric constant microwave probes for sensing soil moisture." *Proceedings of the IEEE*, 62 (1), 93-98.

Boersma, A., and van Turnhout, J. (1999). "Average particle size in polymer blends obtained by dielectric spectroscopy." *Proceedings. 10th International Symposium, Electrets, ISE 10*, Athens, Greece, 789-792.

Bohl, H., and Roth, K. (1994). "Evaluation of dielectric mixing models to describe the θ(ε)-relation." *Symposium on Time Domain Reflectometry in Environmental, Infrastructure and Mining Applications*, US Bureau of Mines Special Publication, 19, 309-319.

Böttcher, C., and Bordewijk, P. (1978). *Theory of electric polarization*, Elsevier, Amsterdam, Netherlands.

Böttcher, C. J. F. (1938). "The dielectric constant of dipole liquids." *Physica*, 5(7), 635-639.

Breugel, K. (1991). "Simulation of hydration and formation of structure in hardening cement-based materials." Ph.D. dissertation, Tech. Univ. Delft, Netherlands.

Brown, W. F. (1956). *Theory of dielectrics*, Springer-Verlag, Berlin, Germany.

Camp, P. R., and Bilotta, S. (1989). "Dielectric properties of Portland cement paste as a function of time since mixing." *Journal of Applied Physics*, 66(12), 6007-6013.

Copeland, L. E., and Hayes, J. C. (1953). "Determination of non-evaporable water in hardened Portland cement paste." *ASTM Bulletin*, 194, 70-74.

Dalton, F. N., Herkelrath, W. N., Rawlins, D. S., and Rhoades, J. D. (1984). "Time-domain reflectometry: Simultaneous measurement of soil water content and electrical conductivity with a single probe." *Science*, 224(4652), 989-990.

Daniels, D. J. (1996). "Surface-penetrating radar." *Electronics & Communications Engineering Journal*, 8(4), 165-182.

Das, B. M. (2002). *Principles of geotechnical engineering*, Brooks Cole/Thompson Learning, Pacific Grove, CA.

Dasberg, S., and Hopmans, J. W. (1992). "Time domain reflectometry calibration for uniformly and nonuniformly wetted sandy and clayey loam soils." *Soil Science Society of America Journal*, 56(5), 1341-1345.

Davis, J., and Chudobiak, W. (1975). "In situ meter for measuring relative permittivity of soils." *Geological Survey of Canada*, 75(1A), 75-79.

Davis, J. L., and Annan, A. P. (1989). "Ground-penetrating radar for high-resolution mapping of soil and rock stratigraphy." *Geophysical Prospecting*, 37(5), 531-551.

De Loor, G. P. (1956). "Dielectric properties of heterogeneous mixtures." Ph.D. dissertation, Univ. of Leiden, Netherlands.

De Loor, G. P. (1968). "Dielectric properties of heterogeneous mixtures containing water." *Journal of Microwave Power*, 3(2), 67-73.

Debye, P., and Hückel, E. (1923). "The theory of electrolytes. I. Freezing point depression and related phenomena." *Physics*, 24, 185-206.

Diefenderfer, B., Al-Qadi, I., and Loulizi, A. (2000). "Laboratory calibration and in situ measurements of moisture by using time-domain reflectometry probes." *Transportation Research Record: Journal of the Transportation Research Board*, 1699, 142-150.

Diefenderfer, B. K. (2002). "Moisture content determination and temperature profile modeling of flexible pavement structures." Ph.D. dissertation, Virginia Polytechnic Institute and State University.

Dirksen, C., and Dasberg, S. (1993). "Improved calibration of time domain reflectometry soil water content measurements." *Soil Science Society of America Journal*, 57(3), 660-667.

Dobson, M. C., Ulaby, F. T., Hallikainen, M. T., and El-Rayes, M. A. (1985). "Microwave dielectric behavior of wet soil-Part II: Dielectric mixing models." *IEEE Transactions on Geoscience and Remote Sensing*, GE-23(No.1), 35-46.

Elkins, G., Schmalzer, P., Thompson, T., and Simpson, A. (2003). *Long-term pavement performance information management system pavement performance database user reference guide*. Report No. FHWA-RD-03-088, US Dept. of Transportation, Federal Highway Administration, Washington, D.C.

Feldman, R., and Sereda, P. (1970). "A new model for hydrated Portland cement and its practical implications." *Engineering Journal*, 53(8-9), 53-59.

Gallone, G., Carpi, F., De Rossi, D., Levita, G., and Marchetti, A. (2007). "Dielectric constant enhancement in a silicone elastomer filled with lead magnesium niobate–lead titanate." *Materials Science & Engineering*, C 27, 110-116.

Gu, P., and Beaudoin, J. (1996). "Dielectric behaviour of hardened cement paste systems." *Journal of Materials Science Letters*, 15(2), 182-184.

Hager III, N., and Domszy, R. (2004). "Monitoring of cement hydration by broadband time-domain-reflectometry dielectric spectroscopy." *Journal of Applied Physics*, 96, 5117-5128.

Hashin, Z. (1969b). "Theory of composite materials." *Mechanics of Composite Materials*, *Proceedings of the Fifth Symposium on Naval Structural Mechanics*, Philadelphia, 201-242.

Hashin, Z., and Shtrikman, S. (1962). "A variational approach to the theory of the effective magnetic permeability of multiphase materials." *Journal of Applied Physics*, 33, 3125-3131.

Herkelrath, W. N., Hamburg, S. P., and Murphy, F. (1991). "Automatic, real-time monitoring of soil moisture in a remote field area with time domain reflectometry." *Water Resources Research*, 27(5), 857-864.

Jackson, N., and Dhir, R. (1983). *Civil engineering materials*, Palgrave Macmillan, London.

Jacobsen, O. H., and Schjønning, P. (1993). "A laboratory calibration of time domain reflectometry for soil water measurement including effects of bulk density and texture." *Journal of Hydrology*, 151(2), 147-157.

Jacobsen, O. H., and Schjønning, P. (1995). "Comparison of TDR calibration functions for soil water determination." *Proceedings of the Symposium: Time-domain Reflectometry Applications in Soil Science*, Lyngby, Denmark, 25-33.

Jiang, Y. J., and Tayabji, S. D. (1999). *Analysis of time domain reflectometry data from ltpp seasonal monitoring program test sections-final report*. Report No. FHWA-RD-99-115, Federal Highway Administration, Washington, D.C.

Klemunes, J. A. (1995). "Determining volumetric moisture using the time domain reflectometry response." M.S. thesis, University of Maryland, College Park, MD.

Klemunes, J. A. (1998). *Determining soil volumetric moisture content using time domain reflectometry*. Report No. FHWA-RD-97-139, Federal Highway Administration, Washington, D.C.

Krugler, P. E., Tahmoressi, M., and Rand, D. A. (1992). "Improving the precision of test methods used in VMA determination." *Asphalt Paving Technology*, 61, 272-303.

Landauer, R. (1952). "The electrical resistance of binary metallic mixtures." *Journal of Applied Physics*, 23(7), 779-784.

Lane, J. A., and Saxton, J. A. (1952). "Dielectric dispersion in pure polar liquids at very high radio frequencies. III: The effect of electrolytes in solution." *Proceedings of the Royal Society of London. Series A, Mathematical and Physical Sciences*, A213, 531-545.

Ledieu, J., De Ridder, P., De Clerck, P., and Dautrebande, S. (1986). "A method of measuring soil moisture by time-domain reflectometry." *Journal of Hhydrology(Amsterdam)*, 88(3-4), 319-328.

Lee, S., Zollinger, D., and Lytton, R. (2008). "Determining moisture content of soil layers with time domain reflectometry and micromechanics." *Transportation Research Record: Journal of the Transportation Research Board*, 2053, 30-38.

Lee, S., Zollinger, D. G., and Lytton, R. L. (2006). "Determination of volumetric moisture content of pavement sublayers using time domain reflectometry based on micromechanics." *Proceedings of 2006 Time Domain Reflectometry*, Purdue University, West Lafayette, IN.

Lichtenecker, K., and Rother, K. (1931). "Die herleitung des logarithmischen mischungsgesetzes aus allgemeinen prinzipien der stationaeren stroemung." *Physikalische Zeitschr*, 32, 255–260.

Lin, C. (1999). "Time domain reflectometry for soil properties." Ph.D. dissertation, Purdue University, West Lafayette, IN.

Liu, W., and Scullion, T. (2009). "PAVECHECK: Integrating deflection and GPR for network condition surveys." Texas Transportation Institute, College Station, TX.

LTPP. (2009). http://www.ltpp-products.com. LTPP database, Federal Highway Administration.

Lytton, R. (1995). "System identification and analysis of subsurface radar signals (SIDAR), U.S. Patent No. 5,384,715." The Texas A&M University System, licensed to Lyric Technonoties, Inc., Houston, Texas.

Lytton, R. L. (2000). "Characterizing asphalt pavements for performance." *Transportation Research Record: Journal of the Transportation Research Board*, 1723, 5-16.

Malicki, M., Plagge, R., and Roth, C. (1996). "Improving the calibration of dielectric TDR soil moisture determination taking into account the solid soil." *European Journal of Soil Science*, 47(3), 357-366.

Mamlouk, M., and Zaniewski, J. (2005). *Materials for civil and construction engineers*, Prentice Hall, Upper Saddle River, NJ.

Mandel, M. (1961). "The dielectric constant and Maxwell-Wagner dispersion of suspensions of oriented prolate spheroids." *Physica*, 27(9), 827-840.

Martinez, A., and Byrnes, A. P. (2001). "Modeling dielectric-constant values of geologic materials: An aid to ground-penetrating radar data collection and interpretation." *Bulletin of the Kansas Geological Survey*, 247(Part 1), 1-16.

Maser, K. (2000). "Pavement characterization using ground penetrating radar: state of the art and current practice." *Nondestructive Testing of Pavements and Backcalculation of Moduli: Third Volume*, ASTM STP 1375. American Society for Testing and Materials, West Conshohocken, PA., 313.

Maxwell-Garnett, J. C. (1904). "Colours in metal glasses and in metal films." *Trans. Roy. Soc. London*, 203, 385–420.

Mazumdar, S. K. (2002). *Composites manufacturing: Materials, product, and process engineering*, CRC Press, Boca Raton, FL.

Mehta, P. K., and Monteiro, P. J. M. (2006). *Concrete: Microstructure, properties, and materials*, McGraw-Hill, New York.

Mindess, S., Young, J. F., and Darwin, D. (2003). *Concrete*, Prentice-Hall, Upper Saddle River, NJ.

Moran, M., and Shapiro, H. (1988). *Fundamentals of engineering thermodynamics*, John Wiley & Sons, New York.

Nadler, A., Dasberg, S., and Lapid, I. (1991). "Time domain reflectometry measurements of water content and electrical conductivity of layered soil columns." *Soil Science Society of America Journal*, 55(4), 938-943.

Natke, H. G. (1982). *Identification of vibrating structures*, Springer-Verlag, New York.

Neville, A. M. (1995). *Properties of concrete*, Pearson Education, London, England.

Nicholls, R. L. (1976). *Composite construction materials handbook*, Prentice-Hall, Englewood Cliffs, NJ.

Nielsen, L. (2005). *Composite materials: Properties as influenced by phase geometry*, Springer, New York.

Parrot, L., Geiker, M., and Gutteridge, W. (1990). "Monitoring Portland cement hydration--comparison of methods." *Cement and Concrete Research*, 20(6), 919-26.

Peirce, L. (1995). *LTPP seasonal monitoring program, site installation and initial data collection, section 404165*. FHWA, LTPP Division, McLean, VA.

Powers, T. (1947). "A discussion of cement hydration in relation to the curing of concrete." *Proceedings of the Highway Research Board, Bulletin 25*, 178-188.

Powers, T., and Brownyard, T. (1946). "Studies of the physical properties of hardened Portland cement paste." *Journal of American Concrete Institute*, 18, 101-132.

Rada, G., Elkins, G., Henderson, B., Sambeek, R., and Lopez, A. (1995). *LTPP seasonal monitoring program: Instrumentation installation and data collection guidelines*. Report No. FHWA-RD-94-110, Federal Highway Administration.

Rayleigh, L. (1892). "On the influence of obstacles arranged in rectangular order upon the properties of a medium." *Phil. Mag*, 34, 481-502.

Robbins, M. (2007). "Predicting the early age temperature response of concrete using isothermal calorimetry." M.S. thesis, University of Toronto, Toronto, Canada.

Roberts, F. L., Kandhal, P. S., Brown, E. R., Lee, D. Y., and Kennedy, T. W. (1996). *Hot mix asphalt materials, mixture design, and construction*, NAPA Education Foundation, Lanham, MD.

Roth, C. H., Malicki, M. A., and Plagge, R. (1992). "Empirical evaluation of the relationship between soil dielectric constant and volumetric water content as the basis for calibrating soil moisture measurements by TDR." *European Journal of Soil Science*, 43(1), 1-13.

Roth, K., Schulin, R., Fluhler, H., and Attinger, W. (1990). "Calibration of time domain reflectometry for water content measurement using a composite dielectric approach." *Water Resources Research*, 26(10), 2267-2273.

Schmidtgen. (2009). "Brochure: Percometer V.7 - Dielectric value and electrical conductivity meter brochure." Schmidtgen Engineering Service, Germany.

Shen, L. C., and Kong, J. A. (1995). *Applied electromagnetism*, PWS Engineering Foundation, Boston, MA.

Somayaji, S. (2001). *Civil engineering materials*, Prentice Hall, Upper Saddle River, NJ.

Taylor, H. (1997). *Cement chemistry*, Thomas Telford, London.

Tinga, W. R., Voss, W. A. G., and Blossey, D. F. (1973). "Generalized approach to multiphase dielectric mixture theory." *Journal of Applied Physics*, 44(9), 3897-3902.

Topp, G., Davis, J., and Annan, A. (1982a). "Electromagnetic determination of soil water content using TDR: I. Applications to wetting fronts and steep gradients." *Soil Science Society of America Journal*, 46(4), 672-678.

Topp, G., Davis, J., and Annan, A. (1982b). "Electromagnetic determination of soil water content using TDR: II. Evaluation of installation and configuration of parallel transmission lines." *Soil Science Society of America Journal*, 46(4), 678-684.

Topp, G. C., Davis, J. L., and Annan, A. P. (1980). "Electromagnetic determination of soil water content: Measurements in coaxial transmission lines." *Water Resources Research*, 16(3), 574-582.

TransTech System, Inc. (2003). *Effect of water and temperature on hot mix asphalt density measurement using electromagnetic sensing*. Schenectady, NY.

Troxler Electronic Laboratories, Inc. (2006). *Manual of operation and instruction: Model 3430 surface moisture-density guage*. Research Triangle Park, NC.

TxDOT. (2005). "Tex-201-F: Bulk specific gravity and water absorption of aggregate." Test Specification Manual, Texas Department of Transportation, Austin, TX.

van Beek, A., van Breugel, K., and Hilhorst, M. (1997). "In-situ moitoring system based on dielectric properties of hardening concrete." *Structural Faults+ Repair, Edinburg*, 2, 407-414.

van Beek, A., van Breugel, K., and Hilhorst, M. (1999). "Monitoring the hydration in LWA-concrete by dielectric measurements." *5th International Symposium on Utilization of High Strength/High Performance Concrete*, Sandefjord, Norway, 1007-1016.

van Beek, L. K. H. (1967). "Dielectric behaviour of heterogeneous systems." *Progress in Dielectrics*, 7, 69-114.

van Sambeek, R., and Urbach, R. (1996). *LTPP seasonal monitoring program site installation report for GPS section 274040*. FHWA, LTPP Division, McLean, VA.

Verbeck, G. (1956). *Hardened concrete-pore structure*. ASTM STP 169, Portland Cement Association. Research and Development Laboratories, Philadelphia, PA.

Wang, F., and Lytton, R. L. (1993). "System identification method for backcalculating pavement layer properties." *Transportation Research Record 1384, TRB, National Research Council, Washington, D.C.*, pp.1-7.

Wang, J. R., and Schmugge, T. J. (1980). "An empirical model for the complex dielectric permittivity of soils as a function of water content." *IEEE Transactions on Geoscience and Remote Sensing*, GE-18(No. 4), 288-295.

Weiler, K., Steenhuis, T., Boll, J., and Kung, K. (1998). "Comparison of ground penetrating radar and time-domain reflectometry as soil water sensors." *Soil Science Society of America Journal*, 62(5), 1237-1239.

Weitz, A., Grauel, W., Keller, M., and Veldkamp, E. (1997). "Calibration of time domain reflectometry technique using undisturbed soil samples from humid tropical soils of volcanic origin." *Water Resources Research*, 33(6), 1241-1249.

Whalley, W. R. (1993). "Considerations on the use of time-domain reflectometry (TDR) for measuring soil water content." *Journal of Soil Science*, 44, 1-9.

Wiener, O. (1912). "Abhandl. math.-phys." *Kl. Königl. Sachsischen Gesell*, 32, 509.

Zhang, X., Ding, X., Ong, C., Tan, B., and Yang, J. (1996). "Dielectric and electrical properties of ordinary Portland cement and slag cement in the early hydration period." *Journal of Materials Science*, 31(5), 1345-1352.

Zollinger, D. G., Lee, S., Puccinelli, J., and and Jackson, N. (2008). *LTPP computed parameter: Moisture content*. Report No. FHWA-HRT-08-035, Federal Highway Administration, Washington, D.C.

APPENDIX A

DERIVATION OF LOWER AND UPPER BOUNDS FOR COMPOSITE DIELECTRIC CONSTANT

There is a homogeneous and isotropic (uniform) sphere of radius (r_b) and permeability (μ) as seen in Figure A-1 (a). On the surface of the body, a potential (ψ) is prescribed which creates magnetic field intensity (H_0) (Hashin and Shtrikman 1962). The relationship between the permeability and the field strength can be expressed as (Shen and Kong 1995):

$$B_0 = \mu H_0 \tag{A-1}$$

where

B_0 = magnetic flux density (webers per square meter, Wb/m^2)

μ = permeability (Henry per meter, H/m)

H_0 = magnetic field strength (intensity) (amperes per meter, Am/m)

Let consider that the sphere material is replaced, without changing the surface potential, by a composite sphere material consisting of an inner part of radius (r_a) and permeability (μ_a) and a concentric shell with permeability (μ_b). If the field strength (H_0) outside of the shell (r_b) remains unchanged, there will be no change in the total energy stored in the uniform body due to the replacement (Hashin and Shtrikman 1962). Figure A-1 presents the changed sphere materials in a spherical coordinate system (r, θ, φ).

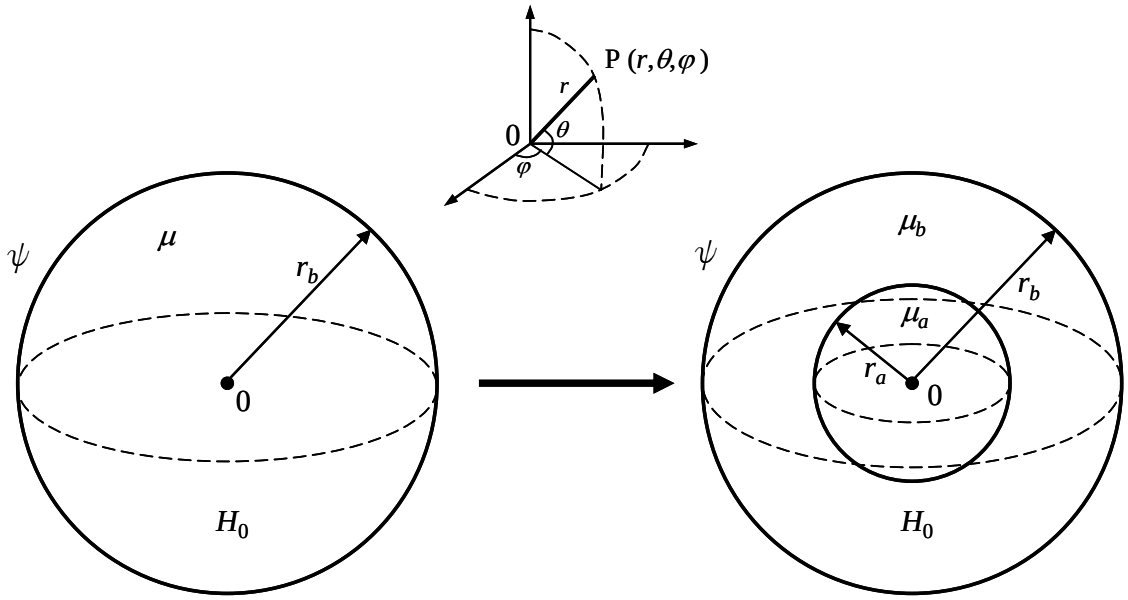

(a) Uniform sphere (b) Composite sphere

Figure A-1 Homogeneous and composite sphere materials

In the spherical coordinate system of which center coincides with the center of the sphere body, the potential of the uniform sphere before the change can be defined as (Hashin and Shtrikman 1962):

$$\psi = -H_0 r \cos\theta \tag{A-2}$$

where

ψ = surface potential

r = radius of sphere

On the other hand, the potential of the composite sphere is obtained from Laplace's equation as (Hashin and Shtrikman 1962):

$$\psi = \left(C_1 r + C_2 r^{-2}\right)\cos\theta \quad \text{for} \quad r_a \le r \le r_b \tag{A-3}$$

$$\psi = C_3 r \cos\theta \qquad \text{for} \quad r \le r_a \qquad \text{(A-4)}$$

where

C_1, C_2, C_3 = integration constants

Based on Equation (A-3) and (A-4), the boundary conditions at radiuses r_a and r_b of the sphere are obtained as follows:

$$-H_0 r_b \cos\theta = \left(C_1 r_b + C_2 r_b^{-2}\right)\cos\theta \qquad \text{for } \psi \text{ at } r = r_b \qquad \text{(A-5a)}$$

$$\mu H_0 \cos\theta = \mu_b \left(C_1 - 2C_2 r_b^{-3}\right)\cos\theta \qquad \text{for } \frac{\partial\psi}{\partial r}\mu \text{ at } r = r_b \qquad \text{(A-5b)}$$

$$\left(C_1 r_a + C_2 r_a^{-2}\right)\cos\theta = C_3 r_a \cos\theta \qquad \text{for } \psi \text{ at } r = r_a \qquad \text{(A-5c)}$$

$$\mu_b \left(C_1 - 2C_2 r_a^{-3}\right)\cos\theta = \mu_a C_3 \cos\theta \qquad \text{for } \frac{\partial\psi}{\partial r}\mu \text{ at } r = r_a \qquad \text{(A-5d)}$$

Each boundary condition derived above can be expressed as:

$$H_0 r_b + C_1 r_b + C_1 r_b^{-2} = 0 \qquad \text{(A-6a)}$$

$$H_0 \mu - C_1 \mu_b + 2C_2 r_b^{-3} \mu_b = 0 \qquad \text{(A-6b)}$$

$$C_1 r_a + C_2 r_a^{-2} - C_3 r_a = 0 \qquad \text{(A-6c)}$$

$$C_1 \mu_b - 2C_2 r_b^{-3} \mu_b - C_3 \mu_a = 0 \qquad \text{(A-6d)}$$

Matrix of the boundary conditions in Equation (A-6) is obtained as:

$$\begin{bmatrix} r_b & r_b & r_b^{-2} & 0 \\ \mu & -\mu_b & 2r_b^{-3}\mu_b & 0 \\ 0 & r_a & r_a^{-2} & -r_a \\ 0 & \mu_b & -2r_a^{-3}\mu_b & -\mu_a \end{bmatrix} \begin{bmatrix} H_0 \\ C_1 \\ C_2 \\ C_3 \end{bmatrix} = \begin{bmatrix} 0 \\ 0 \\ 0 \\ 0 \end{bmatrix} \qquad \text{(A-7)}$$

In order that the boundary conditions are self-consistent, the determinant of the matrix Equation (A-7) should be zero as:

$$r_b\begin{bmatrix} -\mu_b & 2r_b^{-3}\mu_b & 0 \\ r_a & r_a^{-2} & -r_a \\ \mu_b & -2r_a^{-3}\mu_b & -\mu_a \end{bmatrix} - \mu\begin{bmatrix} r_b & r_b^{-2} & 0 \\ r_a & r_a^{-2} & -r_a \\ \mu_b & -2r_a^{-3}\mu_b & -\mu_a \end{bmatrix} = 0 \qquad \text{(A-8)}$$

which can be expressed as:

$$r_b\left[\frac{\mu_a\mu_b}{r_a^2} - \frac{2r_a\mu_b^2}{r_b^3} + \frac{2r_a\mu_a\mu_b}{r_b^3} + \frac{2\mu_b^2}{r_a^2}\right] - \mu\left[-\frac{r_b\mu_a}{r_a^2} - \frac{r_a\mu_b}{r_b^2} - \frac{2r_b\mu_b}{r_a^2} + \frac{r_a\mu_a}{r_b^2}\right] = 0 \qquad \text{(A-9)}$$

Equation (A-9) can be simplified with respect to the permeability based on volume fraction as follows:

$$\mu = \mu_b + \frac{v_a}{\dfrac{1}{\mu_a - \mu_b} + \dfrac{v_b}{3\mu_b}} \qquad \text{(A-10)}$$

where

$$v_a = \left(r_a/r_b\right)^3$$

$$v_b = 1-\left(r_a/r_b\right)^3$$

$$v_a + v_b = 1$$

The permeability of uniform sphere can be determined by Equation (A-10) under a specific ratio of radiuses (r_a/r_b). Therefore, the bounds for the permeability of two

phase material can be defined with the variation of inner and outer materials. For $\mu_{1,2} = \mu_{a,b}$ and $v_{1,2} = v_{a,b}$,

$$\mu_+ = \mu_2 + \frac{v_1}{\frac{1}{\mu_1 - \mu_2} + \frac{v_2}{3\mu_2}} \tag{A-11}$$

For $\mu_{1,2} = \mu_{b,a}$ and $v_{1,2} = v_{b,a}$,

$$\mu_- = \mu_1 + \frac{v_2}{\frac{1}{\mu_2 - \mu_1} + \frac{v_1}{3\mu_1}} \tag{A-12}$$

where $\mu_2 > \mu_1$.

The bounds (A-11) and (A-12) are defined as lower bound and upper bound for composite permeability, respectively. The bound conditions can be used for not only the permeability but also the dielectric constant since their mathematical analyses are similar, as follows (Hashin and Shtrikman 1962):

$$\varepsilon_+ = \varepsilon_2 + \frac{v_1}{\frac{1}{\varepsilon_1 - \varepsilon_2} + \frac{v_2}{3\varepsilon_2}} \tag{A-13}$$

$$\varepsilon_- = \varepsilon_1 + \frac{v_2}{\frac{1}{\varepsilon_2 - \varepsilon_1} + \frac{v_1}{3\varepsilon_1}} \tag{A-14}$$

where $\varepsilon_2 > \varepsilon_1$.

APPENDIX B

DERIVATION OF THE COMPOSITE DIELECTRIC MODEL

Consider a composite sphere consisting of an inner part of radius (r_a) and permeability (μ_a) and a concentric shell of radius (r_b) and permeability (μ_b) as shown in Figure B-1 (a). Since the composite sphere is identical with that employed in Appendix A, Equation (A-10) can be used for the composite sphere as:

$$\mu = \mu_b + \frac{\left(r_a/r_b\right)^3}{\dfrac{1}{\mu_a-\mu_b}+\dfrac{1-\left(r_a/r_b\right)^3}{3\mu_b}} = \mu_b + \frac{v_a}{\dfrac{1}{\mu_a-\mu_b}+\dfrac{1-v_a}{3\mu_b}} \tag{B-1}$$

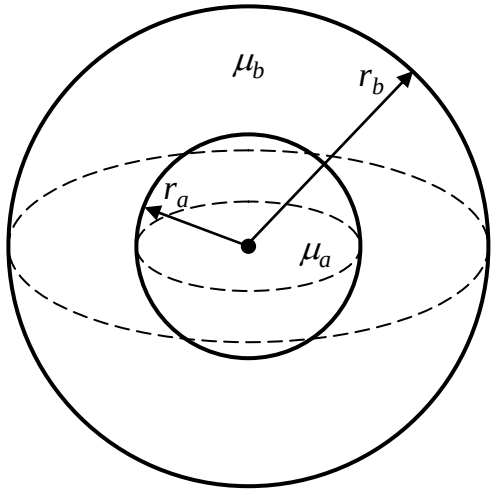

Figure B-1 Composite sphere with 2-phase

Equation (B-1) can be derived with respect to the permeability (μ_b) of outer material as:

$$\mu = \mu_b + \frac{v_a}{\frac{1}{3\mu_b}\left(\frac{\mu_a + 2\mu_b}{\mu_a - \mu_b} - v_a\right)} = \mu_b + \frac{3\mu_b}{\frac{1}{v_a}\left(\frac{\mu_a + 2\mu_b}{\mu_a - \mu_b}\right) - 1} \tag{B-2}$$

If the permeability (μ_b) of the shell is equal to effective permeability of the composite, Equation (B-2) can be expressed as:

$$\mu = \mu^* + \frac{3\mu^*}{\frac{1}{v_a}\left(\frac{\mu_a + 2\mu^*}{\mu_a - \mu^*}\right) - 1} \tag{B-3}$$

where

μ^* = effective permeability of composite sphere

When the 2-phase material is replaced by a *n*-phase material, μ_a and v_a are replaced by μ_i and v_i, respectively. So, the permeability of *n*-phase composite material can be defined as:

$$\mu = \mu^* + \frac{3\mu^*}{\sum_{i=1}^{n} \frac{1}{v_i}\left(\frac{\mu_i + 2\mu^*}{\mu_i - \mu^*}\right) - 1} \tag{B-4}$$

where

n = number of constituents

$\sum_{i=1}^{n} v_i$ = 1.0

In order to make the permeability (μ) of the uniform sphere equal to the effective permeability (μ^*) of *n*-phase composite sphere, the denominator of the right side of Equation (B-4) should be infinite as:

$$\sum_{i=1}^{n} \frac{1}{v_i} \left(\frac{\mu_i + 2\mu^*}{\mu_i - \mu^*} \right) = \infty \tag{B-5}$$

From the condition of Equation (B-5), the following function can be derived as:

$$\frac{1}{\sum_{i=1}^{n} \frac{1}{v_i} \left(\frac{\mu_i + 2\mu^*}{\mu_i - \mu^*} \right)} = \sum_{i=1}^{n} v_i \left(\frac{\mu_i - \mu^*}{\mu_i + 2\mu^*} \right) = 0 \tag{B-6}$$

As mentioned in Appendix A, Equation (B-6) can be used for not only the permeability but also the dielectric constant since their mathematical analyses are similar, as follows:

$$\sum_{i=1}^{n} v_i \left(\frac{\varepsilon_i - \varepsilon^*}{\varepsilon_i + 2\varepsilon^*} \right) = 0 \tag{B-7}$$

where

ε^* = effective dielectric constant of *n*-phase material

APPENDIX C

CHARACTERIZATION OF ERROR IN THE SYSTEM IDENTIFICATION

Relative to the least squares error associated with linear regression, suppose that $y_i = ax_i + b$, then the error (r_i) and the variance (r_i^2) at a point can be expressed respectively, as:

$$r_i = y_i - ax_i - b \tag{C-1}$$

and

$$r_i^2 = y_i^2 + a^2x_i^2 + b^2 - 2ax_iy_i - 2by_i + 2abx_i \tag{C-2}$$

where

r = errors
i = number of data (= 1, 2 …, n)
y = actual observed value
x = independent value
a, b = regression coefficients

The total variance (the sum of the squares of the errors) over all points (n) is defined as:

$$\sum_{i=1}^{n} r_i^2 = \sum_{i=1}^{n} \left(y_i^2 + a^2x_i^2 + b^2 - 2ax_iy_i - 2by_i + 2abx_i \right) \tag{C-3}$$

The estimate of coefficients *a* and *b* should result in a line that is a best fit to the data. Setting the derivatives of the variance with respect to the coefficients *a* and *b* to zero gives as follows:

$$\frac{\partial \sum_{i=1}^{n} r_i^2}{\partial a} = \sum_{i=1}^{n} \left(2ax_i^2 - 2x_i y_i + 2bx_i \right) = 0 \qquad \text{(C-4)}$$

and

$$\frac{\partial \sum_{i=1}^{n} r_i^2}{\partial b} = \sum_{i=1}^{n} \left(2b - 2y_i + 2ax_i \right) = 0 \qquad \text{(C-5)}$$

The least squares estimators of *a* and *b* must satisfy Equation (C-4) and (C-5). These equations can be expressed as a matrix for the two unknown coefficients *a* and *b* as:

$$\begin{bmatrix} 2\sum_{i=1}^{n} x_i^2 & 2\sum_{i=1}^{n} x_i \\ 2\sum_{i=1}^{n} x_i & 2\sum_{i=1}^{n} 1 \end{bmatrix} \begin{bmatrix} a \\ b \end{bmatrix} = \begin{bmatrix} 2\sum_{i=1}^{n} x_i y_i \\ 2\sum_{i=1}^{n} y_i \end{bmatrix} \qquad \text{(C-6)}$$

Equation (C-6) expresses the definition of linear regression. In the matrix form where there are independent variables associated with observations (dependent variables), a matrix of independent variables ($x_{i,j}$) can be expressed as:

$$\underline{y} = X\,\underline{a} + \underline{r} \qquad \text{(C-7)}$$

where

$\underline{y}$ = vector of observations

X = matrix of independent variables ($x_{i,j}$)

j = number of independent variables

$\underline{a}$ = vector of unknown coefficients

$\underline{r}$ = vector of regression errors

Equation (C-7) can be solved for $\underline{a}$ as:

$$X^T X \underline{a} = X^T \underline{y} - X^T \underline{r} \tag{C-8}$$

and then

$$\underline{a} = \left[X^T X \right]^{-1} X^T \underline{y} - \left[X^T X \right]^{-1} X^T \underline{r} \tag{C-9}$$

The second part of above expression represents the residual regression error. The residual error part is formulated on the basis of partial derivatives as:

$$\underline{r} = \underline{y} - X \underline{a} \tag{C-10}$$

and

$$\sum_{i=1}^{n} r_i^2 = \underline{r}^T \underline{r} = \left[\underline{y} - X \underline{a} \right]^T \left[\underline{y} - X \underline{a} \right] \tag{C-11}$$

They can be differentiated with respect to the vector of unknown coefficients ($\underline{a}$) and set to zero as follows:

$$\frac{\partial \sum_{i=1}^{n} r_i^2}{\partial \underline{a}} = \frac{\partial \left[\underline{r}^T \underline{r} \right]}{\partial \underline{a}} = \frac{\partial \left\{ \left[\underline{y} - X \underline{a} \right]^T \left[\underline{y} - X \underline{a} \right] \right\}}{\partial \underline{a}}$$
$$= \frac{\partial \left\{ \left[\underline{y} \right]^T \left[\underline{y} - X \underline{a} \right] - \underline{a}^T X^T \underline{y} + \underline{a}^T X^T X \underline{a} \right\}}{\partial \underline{a}} \qquad \text{(C-12)}$$
$$= \frac{\partial \left\{ \left[\underline{y} \right]^T \underline{r} \right\}}{\partial \underline{a}} - X^T \underline{y} + X^T X \underline{a} \; = \; \underline{0}$$

By being rearranged and solved for $\underline{a}$, Equation (C-12) can be expressed:

$$X^T X \underline{a} = X^T \underline{y} - \frac{\partial \left[\underline{y}^T \underline{r} \right]}{\partial \underline{a}} \qquad \text{(C-13)}$$

and then

$$\underline{a} = \left[X^T X \right]^{-1} X^T \underline{y} - \left[X^T X \right]^{-1} \frac{\partial \left[\underline{y}^T \underline{r} \right]}{\partial \underline{a}} \qquad \text{(C-14)}$$

Again, the second part of the above expression represents the residual regression error. Drawing the analogy to the system identification method (SID):

$$\underline{y} = \underline{y}_m \left(\underline{a} \right) - \frac{\partial \underline{y}_m \left(\underline{a} \right)}{\partial \underline{a}} \partial \underline{a} \qquad \text{(C-15)}$$

where

$\underline{y}_m \left(\underline{a} \right)$ = matrix of model predictions.

Equation (B-15) can be rearranged as:

$$\frac{\partial \underline{y}_m \left(\underline{a} \right)}{\partial \underline{a}} \partial \underline{a} \; = \; \underline{y} - \underline{y}_m \left(\underline{a} \right) \; = \; \underline{r} \qquad \text{(C-16)}$$

and expressed as:

$$[F][\beta]=[r] \tag{C-17}$$

where

$[F]$ = $\left[\frac{\partial y_m}{\partial \underline{a}}\right]$ which is a rectangular sensitivity matrix ($n \times k$)

k = number of coefficients in $\underline{a}$

$[\beta]$ = $\partial \underline{a}$ which is the matrix of change in the model coefficient ($k \times 1$)

$[r]$ = the matrix of change in model prediction or the residual error ($n \times 1$)

In order to solve $[\partial \underline{a}]$, Equation (C-17) can be presented as:

$$\left[\frac{\partial \underline{y}_m(\underline{a})}{\partial \underline{a}}\right]^T\left[\frac{\partial \underline{y}_m(\underline{a})}{\partial \underline{a}}\right][\partial \underline{a}]=\left[\frac{\partial \underline{y}_m(\underline{a})}{\partial \underline{a}}\right]^T[\underline{r}] \tag{C-18}$$

and then

$$[\partial \underline{a}]=\left\{\left[\frac{\partial \underline{y}_m(\underline{a})}{\partial \underline{a}}\right]^T\left[\frac{\partial \underline{y}_m(\underline{a})}{\partial \underline{a}}\right]\right\}^{-1}\left[\frac{\partial \underline{y}_m(\underline{a})}{\partial \underline{a}}\right]^T[r] \tag{C-19}$$

or

$$[\beta]=\left[F^T F\right]^{-1}[F]^T[r] \tag{C-20}$$

This yields a solution for the changes in the model coefficients based on the residual error in the model prediction.

APPENDIX D

TRANSMISSION LINE EQUATION

The new approach for calculating soil dielectric constant based on TDR trace involves the transmission line equation. The following describes the basic theories and concepts of electromagnetics and the transmission line equation.

MAXWELL'S EQUATIONS

In the study of electromagnetics, the four vector quantities called electromagnetic fields which are function of space and time, are involved:

E = electric field strength (volts per meter, V/m)
D = electric flux density (coulombs per square meter, C/m^2)
H = magnetic field strengths (amperes per meter, Am/m)
B = magnetic flux density (webers per square meter, Wb/m^2)

The fundamental theory of electromagnetic fields is based on Maxewell's equations governing the fields E, D, H, and B:

$$\nabla \times E = -\frac{\partial B}{\partial t} \tag{D-1}$$

$$\nabla \times H = J + \frac{\partial D}{\partial t} \tag{D-2}$$

$$\nabla \cdot B = 0 \tag{D-3}$$

$$\nabla \cdot D = \rho_V \tag{D-4}$$

where

J = electric current density (Am/m^2)

ρ_v = electric charge density (C/m^3)

J and ρ_v are the sources generating the electromagnetic field. The equations express the physical laws governing the *E*, *D*, *H*, and *B* fields and the sources *J* and ρ_v at every point in space and at all times. In order to understand concepts of Maxwell's equations, some definitions and vector identities are described. The symbol ∇ in Maxwell's equations represents a vector partial-differentiation operator as following,

$$\nabla = \hat{x}\frac{\partial}{\partial x} + \hat{y}\frac{\partial}{\partial y} + \hat{z}\frac{\partial}{\partial z} \text{ } (\nabla \text{ operator}) \tag{D-5}$$

where

$\hat{x}$, $\hat{y}$, and $\hat{z}$ = unit vectors along the x, y, and z axes

If *A* and *B* are vectors, the operation $\nabla \times A$ is called the curl of *A*, and the operation $\nabla \cdot B$ is called the divergence of *B*. The former is a vector and the latter is a scalar. In addition, if $\phi(x, y, z)$ is a scalar function of the coordinates, the operation $\nabla\phi$ is called the gradient of ϕ. The operator as a vector is only permissible in rectangular coordinates. Some useful vector identities are as follows:

$$\nabla \times (\nabla \times A) \equiv \nabla(\nabla \cdot A) - \nabla^2 A, \tag{D-6}$$

$$\nabla \cdot (\nabla \times A) \equiv 0, \tag{D-7}$$

$$\nabla \times \nabla\phi \equiv 0, \text{ and} \tag{D-8}$$

$$\nabla \cdot (A \times B) \equiv B \cdot (\nabla \times A) - A \cdot (\nabla \times B) \tag{D-9}$$

where

$$\nabla^2 = \frac{\partial^2}{\partial x^2} + \frac{\partial^2}{\partial y^2} + \frac{\partial^2}{\partial z^2} \text{ (Laplacian operator)}$$

Conservation Law of Electric Charge

The Maxwell equation (D-2) can be presented using the vector identity (Equation D-7) and multiplying both sides by ∇ as follows:

$$\nabla \cdot J + \frac{\partial}{\partial t} \nabla \cdot D = \nabla \cdot (\nabla \times H) = 0 \qquad \text{(D-10)}$$

By being replaced with Equation (D-4), the conservation law for current and charge densities is defined as following:

$$\nabla \cdot J + \frac{\partial \rho_V}{\partial t} = 0 \qquad \text{(D-11)}$$

The conservation law means that the rate of transfer of electric charge out of any differential volume is equal to the rate of decrease of total electric charge in that volume. This law is also known as the continuity law of electric charge. In fact, to solve electromagnetic-field problems, it is essential to assume that the sources J and ρ_v are given and satisfy the continuity equation.

Constitutive Relations

The constitutive relations can provide physical information for the environment in which electromagnetic fields occur, such as free space, water, or composite media. Also, it can characterize a simple medium mathematically with permittivity and permeability as follows:

$$D = \varepsilon E \qquad \text{(D-12)}$$

$$B = \mu H \qquad \text{(D-13)}$$

where

ε = permittivity (Farad/meter, F/m)

μ = permeability (Henry/meter, H/m)

Maxwell's Equations for Time-Harmonic Fields

Time-harmonic data is the large class of physical quantities that vary periodically with time. While physical quantities are usually described mathematically by real variables of space and time, and by vector quantities, the time-harmonic real quantities are represented by complex variables. A time-harmonic real physical quantity that varies sinusoidally with time can be expressed as follows:

$$V(t) = V_0 \cos(\omega t + \phi) \qquad \text{(D-14)}$$

where

$V(t)$ = time-harmonic real physical quantity
V_0 = amplitude of $V(t)$
ω = angular frequency (= $2\pi f$)
f = frequency of $V(t)$
t = time
ϕ = phase angle of $V(t)$

Figure D-1 illustrates $V(t)$ as a function of time t.

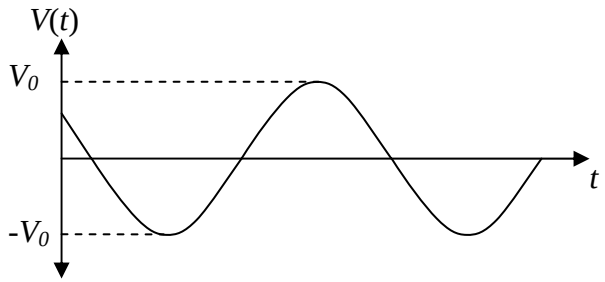

Figure D-1 Time-harmonic function $V(t)$

The $V(t)$ can be expressed by using the symbol of Re{ }, which means taking the real part of the quantity in the brace as follows:

$$V(t) = \mathrm{Re}\left\{Ve^{j\omega t}\right\} = \mathrm{Re}\left\{V_0 e^{j\phi} e^{j\omega t}\right\} \tag{D-15}$$

Hence, the derivation with respect to time can be expressed as

$$\frac{\partial}{\partial t}V(t) = -\omega V_0 \sin(\omega t + \phi) = \mathrm{Re}\{j\omega V_0 e^{j\phi} e^{j\omega t}\} \tag{D-16}$$

and so,

$$\frac{\partial}{\partial t}V(t) \leftrightarrow j\omega V \tag{D-17}$$

As shown in Equation (D-17), the time derivative ∂/∂t can be replaced by $j\omega$ in the complex representation of time-harmonic quantities. In short, it means the conversion of time derivation to phasor notation. Maxwell's equations can be expressed with respect to the complex representations for the time-harmonic quantities as follows:

$$\nabla \times E = -\frac{\partial B}{\partial t} = -j\omega B \tag{D-18}$$

$$\nabla \times H = J + \frac{\partial D}{\partial t} = J + j\omega D \tag{D-19}$$

$$\nabla \cdot B = 0 \tag{D-20}$$

$$\nabla \cdot D = \rho_V \tag{D-21}$$

UNIFORM PLANE WAVES IN FREE SPACE

Given electromagnetic fields are generated in free space by source J and ρ_v in a localized region, then, for electromagnetic fields outside the region, J and ρ_v are equal to zero and

Maxwell's equation can be expressed with free space constitutive relations of Equations (D-12) and (D-13) as the following:

$$\nabla \times E = -j\omega B = -j\omega\mu_0 H \tag{D-22}$$

$$\nabla \times H = j\omega D = j\omega\varepsilon_0 E \tag{D-23}$$

$$\nabla \cdot B = \nabla \cdot H = 0 \tag{D-24}$$

$$\nabla \cdot D = \nabla \cdot E = 0 \tag{D-25}$$

where

μ_0 = permittivity in free space (= $4\pi\times10^{-7}$ H/m)

ε_0 = permeability in free space (= 8.85×10^{-12} F/m)

By taking the curl of Equation (D-22) and substituting Equation (D-23), the followings can be obtained:

$$\nabla \times (\nabla \times E) = \omega^2 \mu_0 \varepsilon_0 E \tag{D-26}$$

The wave equation for *E* can be obtained with regard to vector identity (C-7) and Equation (D-25) as follows:

$$\nabla^2 E + \omega^2 \mu_0 \varepsilon_0 E = 0 \tag{D-27}$$

The wave equation (D-27) is a vector second-order differential equation. By the simple solution where the *E* field is parallel to the *x*-axis and is a function of *z*-coordinate only, the wave equation is expressed as follows;

$$\frac{\partial^2 E_x}{\partial z^2} + \omega^2 \mu_0 \varepsilon_0 E_x = 0 \tag{D-28}$$

Therefore, the above differential equation can be solved as:

$$E = \hat{x}E_0 e^{-jkz} \tag{D-29}$$

where

E_0 = amplitude of E ($\neq 0$)

k = wavenumber

Equation (D-29) presents the electric field of a uniform wave. From Equation (D-27) and (C-29), the following is obtained;

$$k^2 = \omega^2 \mu_0 \varepsilon_0 \tag{D-30}$$

The magnetic field H of the wave can be determined from Equation (D-22) or (D-23):

$$H = \hat{y}\sqrt{\frac{\varepsilon_0}{\mu_0}} E_0 e^{-jkz} \tag{D-31}$$

In Equation (D-31), the factor $\sqrt{\varepsilon_0/\mu_0}$ is known as the intrinsic impedance of free space,

$$\eta = \sqrt{\frac{\mu_0}{\varepsilon_0}} \tag{D-32}$$

where

η = intrinsic impedance of a medium of free space

The wave has the electric field E in the $\hat{x}$-direction and the magnetic field H in the $\hat{y}$-direction, and propagates in the $\hat{z}$-direction. Figure D-2 shows the velocity of propagation with time in a sinusoidal wave.

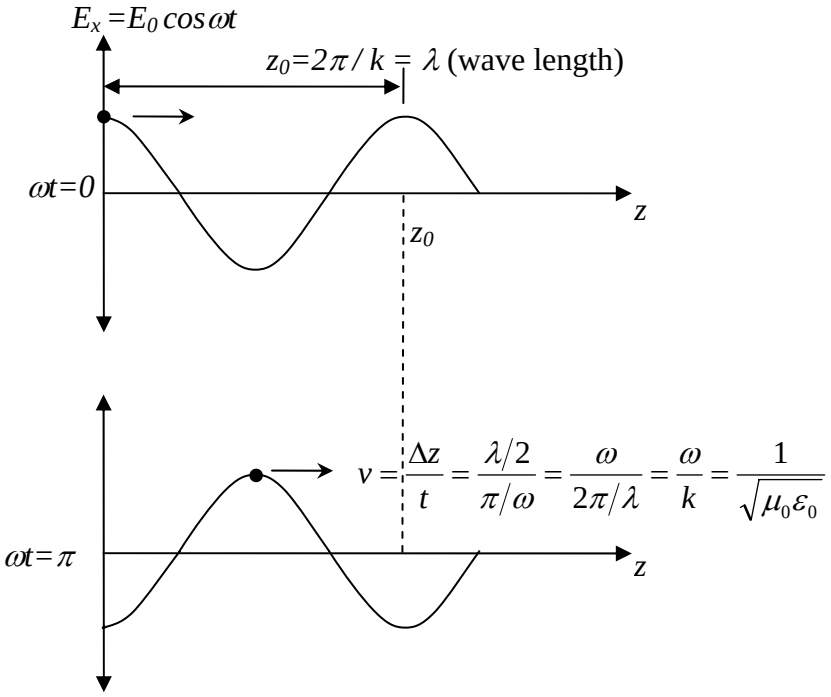

Figure D-2 Electric field as a function of z direction at different times

Therefore, the velocity of light in free space becomes:

$$v = \frac{\omega}{k} = \frac{1}{\sqrt{\mu_0 \varepsilon_0}} \tag{D-33}$$

TRANSMISSION LINE EQUATION OF COAXIAL TRANSMISSION LINE

In the case that electromagnetic waves propagate in free space, the path of the wave is straight, and the intensity is uniform on the transverse plane. However, if the wave is guided along a curved and limited path, the wave is not uniform on the transverse plane

and the intensity is limited to a finite cross section. The finite structure transmitting electromagnetic waves is called a waveguide or transmission line. The wave can be transmitted along different types of waveguides: parallel-plate waveguides, rectangular waveguides, and coaxial lines. This study considers the coaxial lines, which is involved in TDR probe.

Coaxial Lines

The most commonly used transmission line to guide the electromagnetic wave is the coaxial line. The coaxial line consists of inner and outer conductors and an inner dielectric insulator. As shown in Figure D-3, a coaxial line has an inner conductor of radius (a) and an outer conductor of inner radius (b) insulated by a dielectric layer of permittivity (ε). Figure D-4 presents the cylindrical coordinate system for the solution inside coaxial lines.

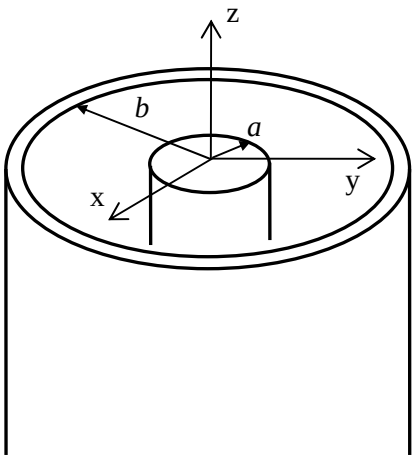

Figure D-3 Coaxial line

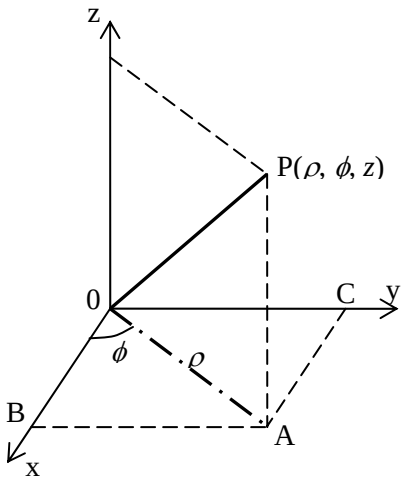

Figure D-4 Cylindrical coordinate system

In the cylindrical coordinate, coordinate ρ is the distance from the z-axis or length OA, ϕ is the angle between OA and the x-axis, and z represents the distance form

the *x*-*y* plane. The three coordinates, ρ, ϕ, and *z* represent the point *P* and are expressed in terms of unit vectors, $\hat{\rho}$, $\hat{\phi}$ and $\hat{z}$.

Transverse Electric and Magnetic (TEM) Mode in a Coaxial Line

In order to explain the fundamental mode on the coaxial line, it is necessary to consider the case where the inner radius (*a*) is close to the outer radius (*b*). When the coaxial line in Figure D-3 is cut along the *x*-*y* plane and unfolded into a parallel strip, the line can be illustrated as Figure D-5:

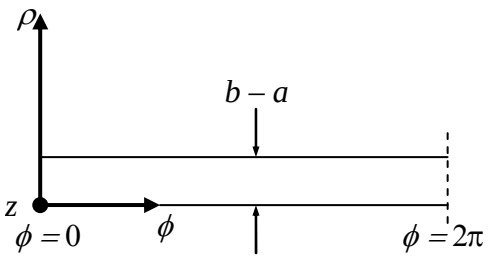

Figure D-5 Coaxial line developed into a parallel-plate waveguide

From Figure D-5, it can be realized that the wave has the electric field *E* in the $\hat{\rho}$-direction and the magnetic field *H* in the $\hat{\phi}$-direction, and propagates in the $\hat{z}$-direction. Therefore, the *E* and *H* are as follows:

$$E = \hat{\rho}\frac{V_0}{\rho}e^{-jkz} \tag{D-34}$$

$$H = \hat{\phi}\frac{V_0}{\eta\rho}e^{-jkz} \tag{D-35}$$

where

$k = \omega\sqrt{\mu\varepsilon}$ (propagation constant)

$\eta = \sqrt{\frac{\mu}{\varepsilon}}$ (proportionality constant)

Since the *E* and *H* are transverse to the direction of wave propagation, the set of Equations (D-34) and (D-35) is called the transverse electromagnetic (TEM) mode of the coaxial line.

Transformation Rules for Transmission Lines

The following rules are for transforming the field quantities into network parameters.

Rule 1. Voltage $V(z) = \alpha_1 \int_{C_t} E \cdot ds$ (D-36)

where

α_1 = proportional constant

C_t = integration path transverse to z

Rule 2. Current $I(z) = \alpha_2 \oint_{C_0} H \cdot ds$ (D-37)

where

α_2 = proportional constant

C_0 = closed contour of integration

The power relationship must hold:

Rule 3. $1/2\,\mathrm{Re}[V(z)I(z)] = \int_A da\,\hat{z} \cdot 1/2\,\mathrm{Re}[E \times H]$ (D-38)

where

A = cross-sectional area of the transmission line or waveguide

Transmission Line Equation

The electric and magnetic fields *E* and *H* for a coaxial line in the TEM mode can be expressed as:

$$E_\rho = \frac{V_0}{\rho} e^{-jkz} \tag{D-39}$$

$$H_\phi = \frac{V_0}{\eta\rho} e^{-jkz} \tag{D-40}$$

By applying the field equations to the transformation rule, the following equations can be defined as:

$$V(z) = \alpha_1 \int_a^b d\rho E_\rho = \alpha_1 V_0 \ln\frac{b}{a} e^{-jkz} \tag{D-41}$$

$$I(z) = \alpha_2 \oint_{C_0} \rho\, d\phi\, H_\phi = \alpha_2 \frac{2\pi V_0}{\eta} e^{-jkz} \tag{D-42}$$

where α_1, α_2 = calibration constants

V_0 = applied voltage

Since the calibration constants are one ($\alpha_1 = \alpha_2 = 1$) to satisfy the transformation rule 3, Equation (D-41) and (D-42) become:

$$E_\rho = \frac{V(z)}{\ln(b/a)} \frac{1}{\rho} \tag{D-43}$$

$$H_\phi = \frac{I(z)}{2\pi} \frac{1}{\rho} \tag{D-44}$$

Maxwell's equations for electric and magnetic fields can be cast in the standard form of transmission line equations in terms of voltage (V) and current (I) by using

cylindrical coordinate. Maxwell's two curl equations are defined as the following transmission line equations:

$$\frac{dV}{dz} = -j\omega\mu\frac{I}{2\pi}\ln(b/a) \tag{D-45}$$

$$\frac{dI}{dz} = -j\omega\varepsilon\frac{V}{\ln(b/a)}2\pi \tag{D-46}$$

By eliminating *I* from Equation (D-45) and (D-46), a wave equation for the voltage (*V*) can be obtained as follows:

$$\frac{d^2V}{dz^2} = -\omega^2\mu\varepsilon V \tag{D-47}$$

Voltage (*V*) has two solutions of $e^{-j\omega\sqrt{\mu\varepsilon}z}$ and $e^{+j\omega\sqrt{\mu\varepsilon}z}$. Each solution has an integration constant as a multiplier. Voltage (*V*) can be expressed by introducing the directions of amplitude of voltage (*V*) as:

$$V(z) = V_+e^{-jkz} + V_-e^{+jkz} \tag{D-48}$$

where

$V(z)$ = voltage on a transmission line

V_+ = amplitude in positive *z*-direction (incident wave)

V_- = amplitude in negative *z*-direction (reflected wave)

The amplitude of V_+ represents a wave traveling in the positive *z*-direction and the amplitude of V_- represents a wave traveling in the negative *z*-direction.

APPENDIX E

PROGRAM MANUAL

INTRODUCTION

This manual is organized to facilitate navigation through many features of the program. It helps to run the executable file and defines all the objects present on various forms. In an effort to minimize repetition, topics that are identical in different parts of the program are usually only covered once in detail; when topics are repeated, the reader is referred to previous explanations. The program manual is divided into three main sections:

- Introduction to program
- Getting started in program
- Program features

Each section serves as a comprehensive guide to a specific part of the program.

Getting Started

In Getting Started, user will learn the minimum system requirements for running the program on your computer, how to install the program on your computer, and how to start using the program.

Program Features

This section provides descriptions of the different functions and capabilities of the program. The functions of the different menus, tool bars, and screen buttons within the program are described in this section.

About Program

The objective of the program is to view and interpret Time Domain Reflectometry (TDR) traces collected by TDR probes installed in granular materials (unbound base and sub grade). The program was developed using Microsoft® Visual Basic®. The program has database (Microsoft® Access®) connectivity to read the input data corresponding to the traces used to determine the inflection points and hence the dielectric constant via time analysis technique. Use of the program requires the user to be familiar with TDR based data collection and the concepts underlying the interpretation of TDR traces.

Overview of Program

In 1992, the Seasonal Monitoring Program (SMP) was initiated within the Long Term Pavement Performance (LTPP) study in order to understand the environmental factors and the relationship with pavement performance. 64 LTPP test sections were selected for the SMP according to pavement type, thickness, environment, and subgrade type. Several instruments were installed at each section to acquire data on moisture content and temperature of sublayers, change in frost depth, and depth to ground water. As part of this program, TDR technology was selected to measure in-situ moisture content of pavement sublayers. TDR data was collected with 8-inch TDR probes developed by the Federal Highway Administration (FHWA). 10 TDR probes are placed at specified depths in different sublayer types and thicknesses below the outer wheel path.

The volumetric moisture content is estimated based on soil dielectric constant measured and analyzed through TDR trace. The dielectric constant was computed using the apparent length method from the TDR trace and the volumetric moisture content was empirically calculated using regression to relate the dielectric constant to the moisture content. However, these two methods can result in significant systematic errors because they are not able to fully consider the composite nature of the soil material.

In order to improve the accuracy of the interpretation of TDR data for calculating the volumetric moisture content, a new approach was developed using transmission line equation and self consistent scheme. Also, based on the new approach, this computer program was developed to view and process TDR traces. The program takes the TDR trace data from a table containing TDR trace point data in a Microsoft® Access® database and shows the smoothed trace on the screen. The trace shown on the screen is processed automatically using the algorithm implemented by the program, and then the identified inflection points will show up on the same screen to be reviewed.

The soil dielectric constant is determined using the data between inflection points and then is used to calculate the volumetric moisture content based on the self consistence scheme. The program can process the TDR traces in the following ways:

- Program automatically processes all the TDR traces collectively and shows the identified inflection points on the screen for review.
- For quality check of TDR trace, user is allowed to make changes in the inflection point locations in case of any discrepancy. Changed inflection points automatically get recorded as new points on the trace and are hence used for the calculation.

The location of the first and second inflection points and the corresponding trace pattern or error code are stored in the SMP_TDR_MOISTURE table for review. In addition, the tool buttons are available for easy navigation within the TDR trace table, namely "**Next Trace**", "**Previous Trace**", and "**Go To**". In short, this program provides a user-friendly interface for viewing and interpreting TDR traces. It is also a very efficient tool for quality control of the TDR computed parameters.

GETTING STARTED

Getting started with the new program is easy, especially if user has already installed Windows XP operating system and is familiar with its operating environment. The following describes the procedures for installing and operating the program on your computer.

System Requirements

To run the program on your computer, the following minimum hardware and software requirements must be met:

- IBM-compatible Pentium processor
- 512 MB of RAM (1 GB recommended)
- 1 MB of available hard disk space, depending on the size of the TDR trace table
- Super video graphics adapter with at least 800×600 resolution and 256 colors
- Microsoft mouse or compatible pointing device
- Microsoft Windows XP operating system.

Installing and Running Program

It is an executable file which doesn't need to be installed. To run, we just need to click on the icon.

PROGRAM FEATURES

The program was developed to allow users to analyze TDR trace and estimate moisture content easily. However, a first-user may not understand the features and procedure of the program. This section covers the features of program and the procedure for analyzing TDR traces.

Raw TDR Trace Data

In order to estimate the moisture content, the raw TDR traces data should be obtained from Information Management System (IMS) into Microsoft® Access® database. The database is the table SMP_TDR_AUTO that contains a flat representation of the TDR

waveform sampled 245 intervals and stored in the WAVEP_1 through WAVP_245 field. This table can be renamed SMP_TDR_AUTO_*, if necessary.

TDR Depth Records

The TDR depth records, SMP_TDR_DPETH_LENGTHS, should be also imported into Microsoft® Access® database from IMS LTPP. This table contains the physical information of the TDR probes such as the depths at which the probes are installed, their installation date, and the length of TDR probe. This table is used to link to SMP_TDR_AUTO to determine the depth corresponding to a TDR trace, using the STATE_CODE, SHRP_ID, TDR_NO, and CONSTRUCTION_NO.

TDR Calibration Records

To estimate the soil parameters, the new program needs the values calibrated from the ground truth data obtained during equipment installation. The database is SMP_TDR_CALIBRATE table which contains the calibrated dielectric constants of soil components and specific gravity. The calibrated values are supported to calculate moisture content by linking SMP_TDR_CALIBRATE by STATE_CODE, SHRP_ID, and TDR_NO fields.

Starting Program

When the program is started, the main TDR data processing window appears. The user must first open a Microsoft® Access® database containing a TDR trace table as described in Raw TDR Trace Data section.

TDR Program Menus

Menus in the program are context-sensitive; both the available menus and their context change based on what part of the program is active. Menu features are briefly discussed in this section. The toolbar buttons provide shortcuts to all the menu items. The menu items and corresponding toolbar buttons are both described below.

Menu bar:

- **OPEN**: opens dialog box to select the database for processing.
- **EXIT**: ends the program, closing all the connections and the database.

Toolbar: Contains icons in order as mentioned below

- **OPEN**: open dialog box to select the database for processing.
- **CLOSE**: exit the program.
- **Previous Trace**: move to previous trace.
- **Go To**: go to specific trace number.
- **Next Trace**: move to next trace.
- **Show Trace**: Show trace in case that the window is not showing any trace which happens when it is open for long time.
- **Change Inflection Points**: change inflection point in case that user needs to change the inflection points manually.
- **Write Dielectric Output**: compute dielectric constant of TDR trace
- **Write Moisture Output**: compute moisture content

The screen contains a combo box showing trace numbers having errors. It has a title of "**Dubious Records**". TDR traces with no negative slope or wrong inflection points fall into this category. Screen also show text boxes depicting SHRP_ID, STATE CODE, CONSTRUCION NUMBER, SMP DATE, TDR TIME, TDR NUMBER, DIST_WAV and RECORD NUMBER on the left side.

Output Table after Running Program

After running the program with input database table, SMP_TDR_AUTO, the program generates two output tables, SMP_TDR_AUTO_DIELECTRIC and SMP_TDR_ MOISTURE, in the database. SMP_TDR_AUTO_DIELECTRIC table contains the calculated parameters (dielectric constant, conductivity, and reflectivity) corresponding to TDR automatic trace. This table is generated by running the tool menu of "**Write**

Dielectric Output". SMP_TDR_ MOISTURE table contains the dry density and the volumetric and gravimetric moisture content computed from TDR traces and is generated by running the tool menu of "**Write Moisture Output**".

APPENDIX F

VARIATION OF VOLUMETRIC WATER CONTENT AND DRY DENSITY OF LTPP TEST SECTIONS

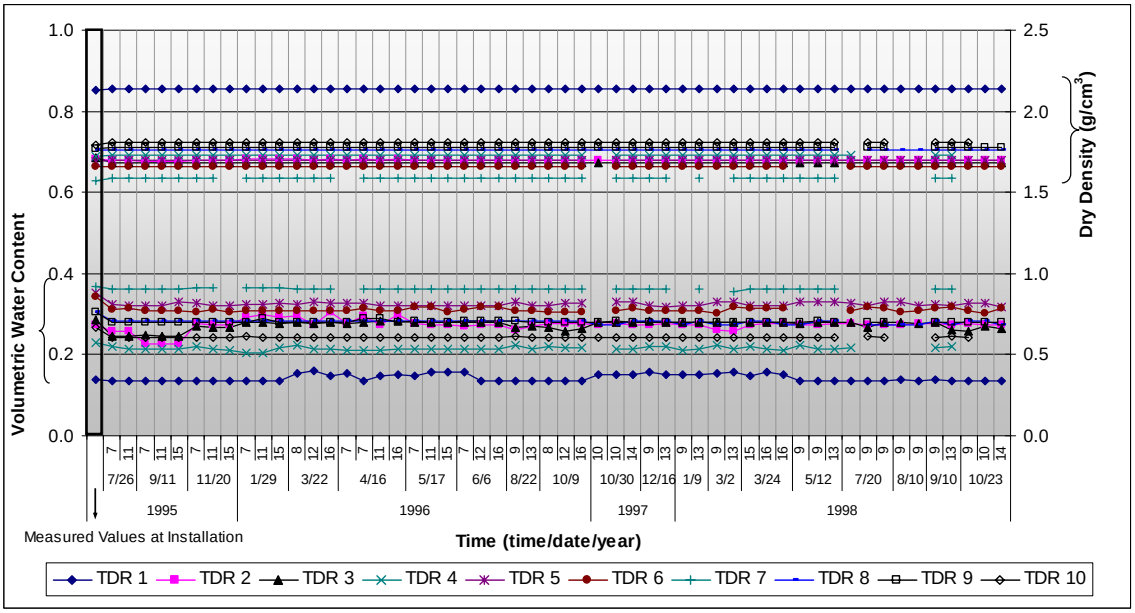

Figure F-1 Variation of water content and density for LTPP section 010101 (Opelika, Alabama)

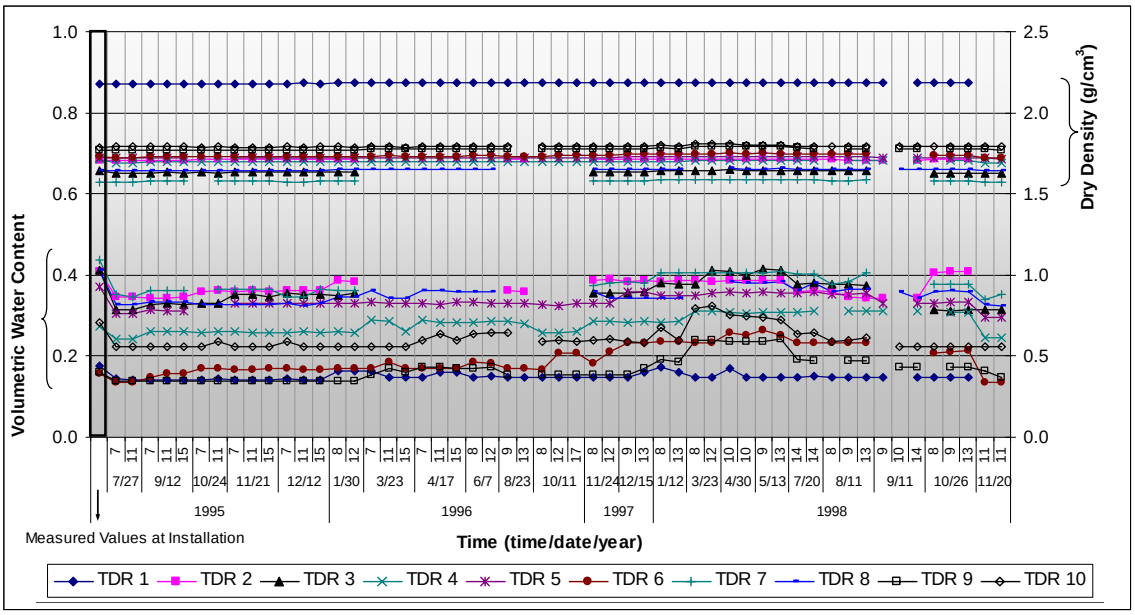

Figure F-2 Variation of water content and density for LTPP section 010102 (Opelika, Alabama)

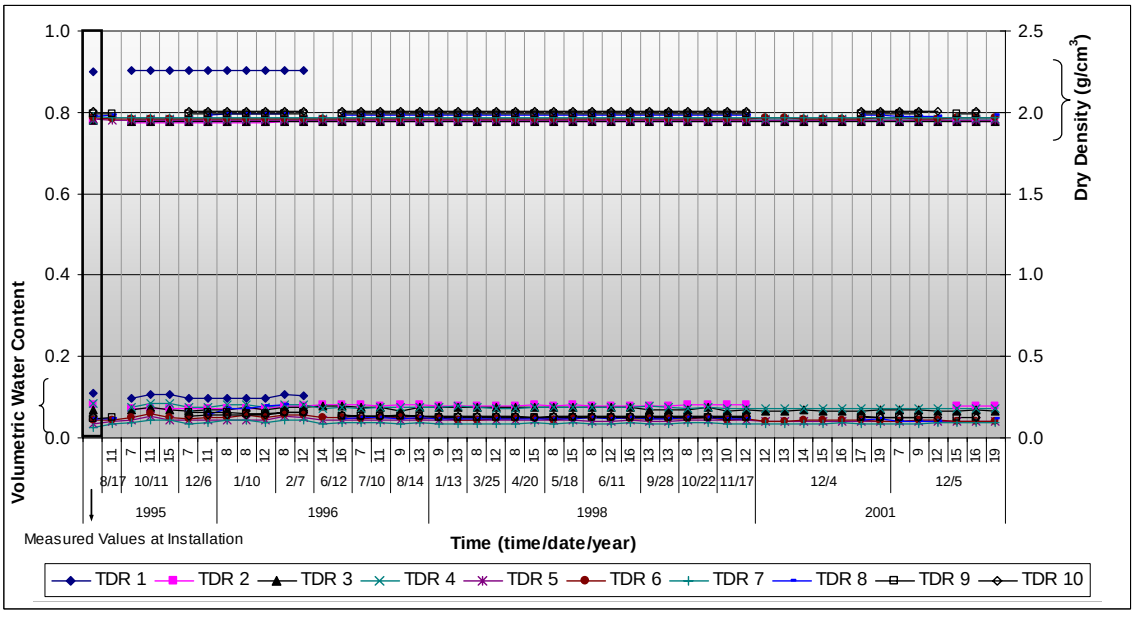

Figure F-3 Variation of water content and density for LTPP section 040113 (Kingman, Arizona)

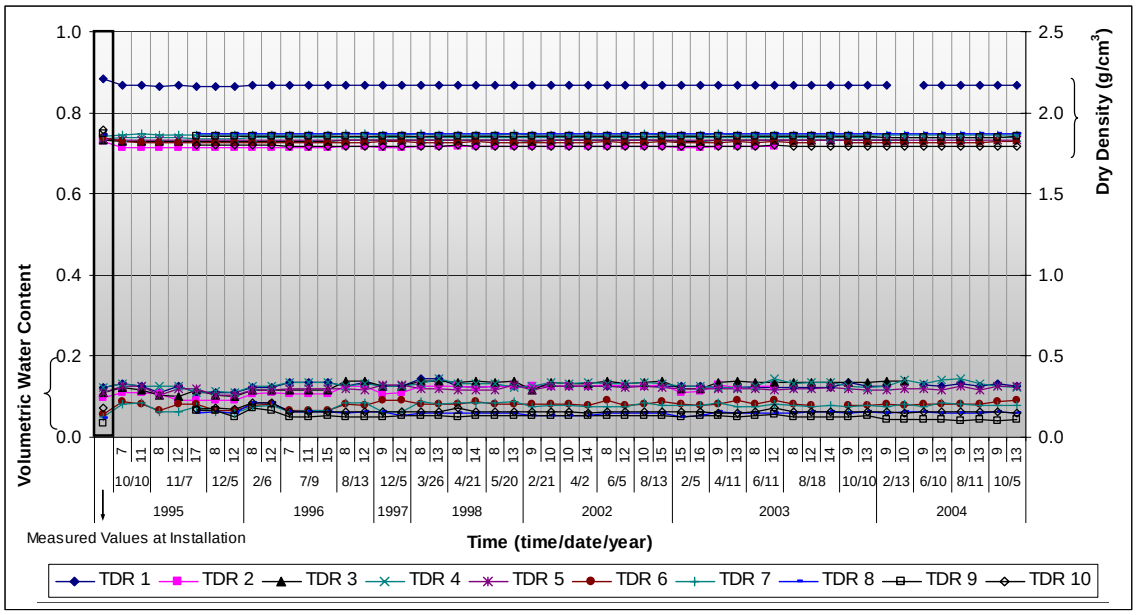

Figure F-4 Variation of water content and density for LTPP section 040114 (Kingman, Arizona)

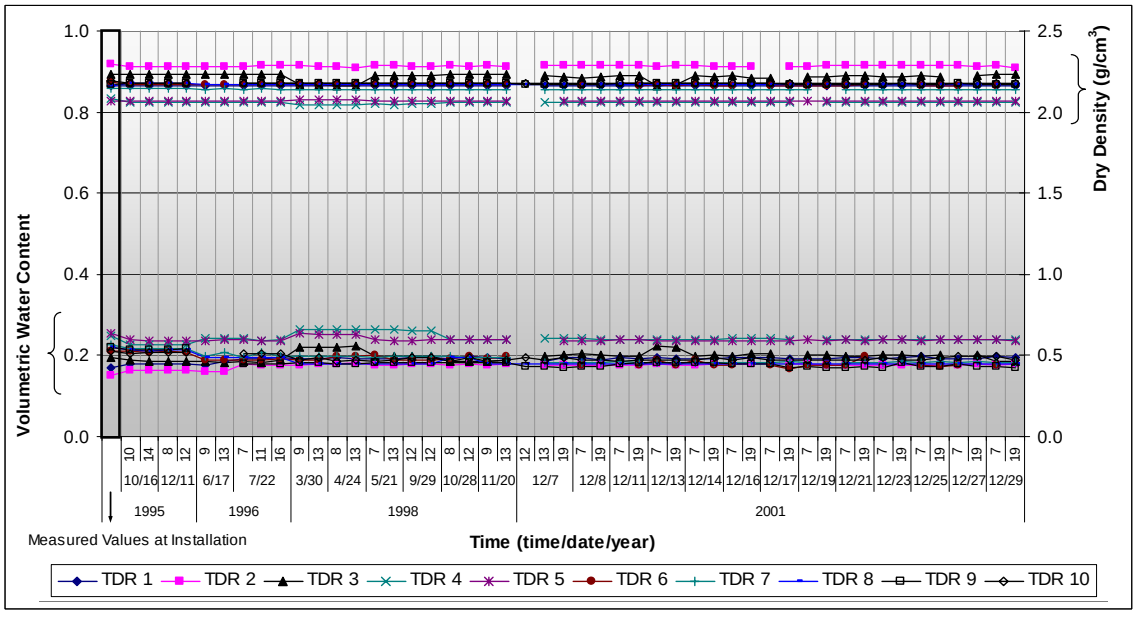

Figure F-5 Variation of water content and density for LTPP section 040215 (Phoenix, Arizona)

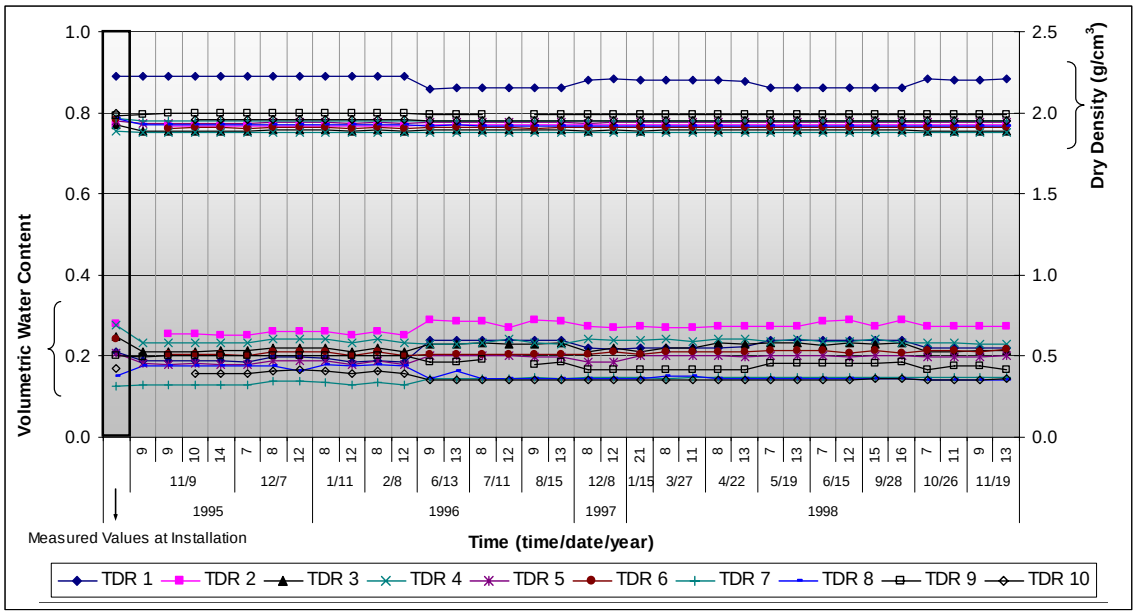

Figure F-6 Variation of water content and density for LTPP section 041024 (Flagstaff, Arizona)

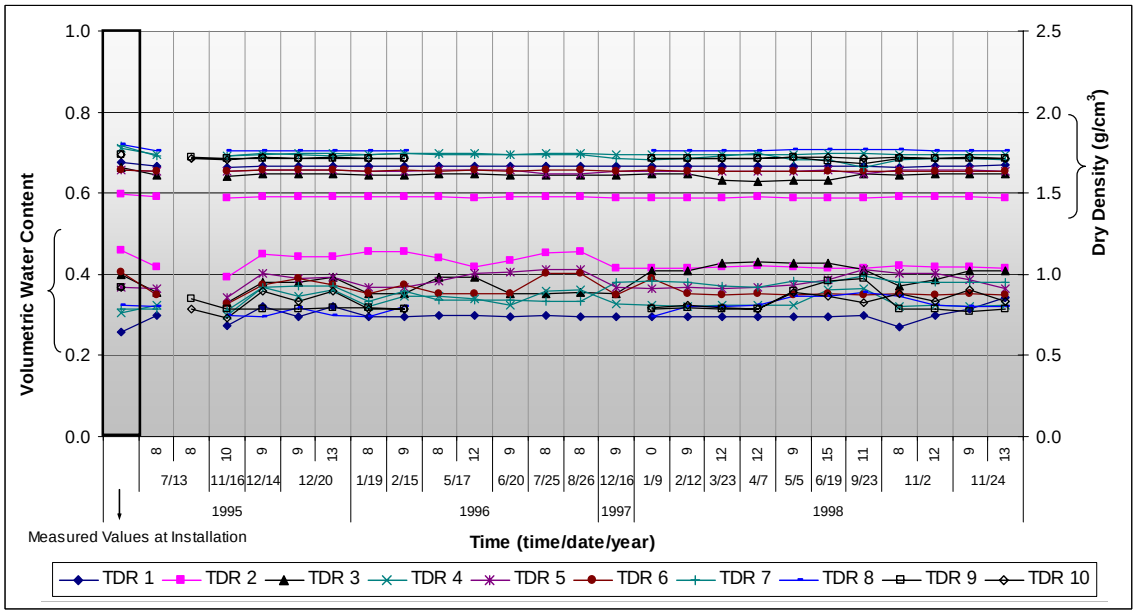

Figure F-7 Variation of water content and density for LTPP section 063042 (Lodi, California)

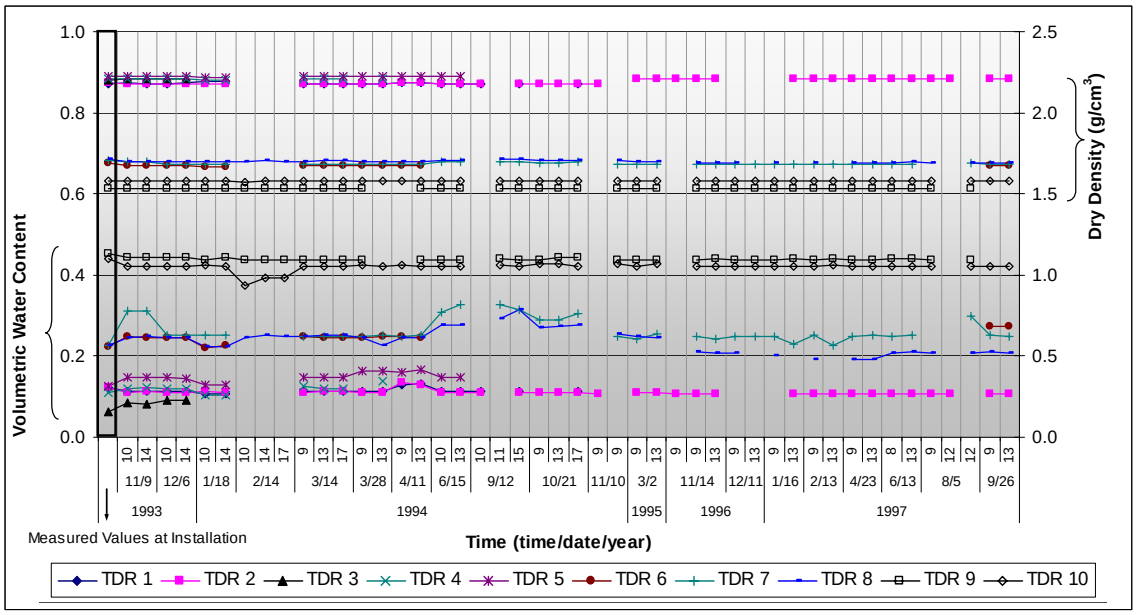

Figure F-8 Variation of water content and density for LTPP section 081053 (Delta, Colorado)

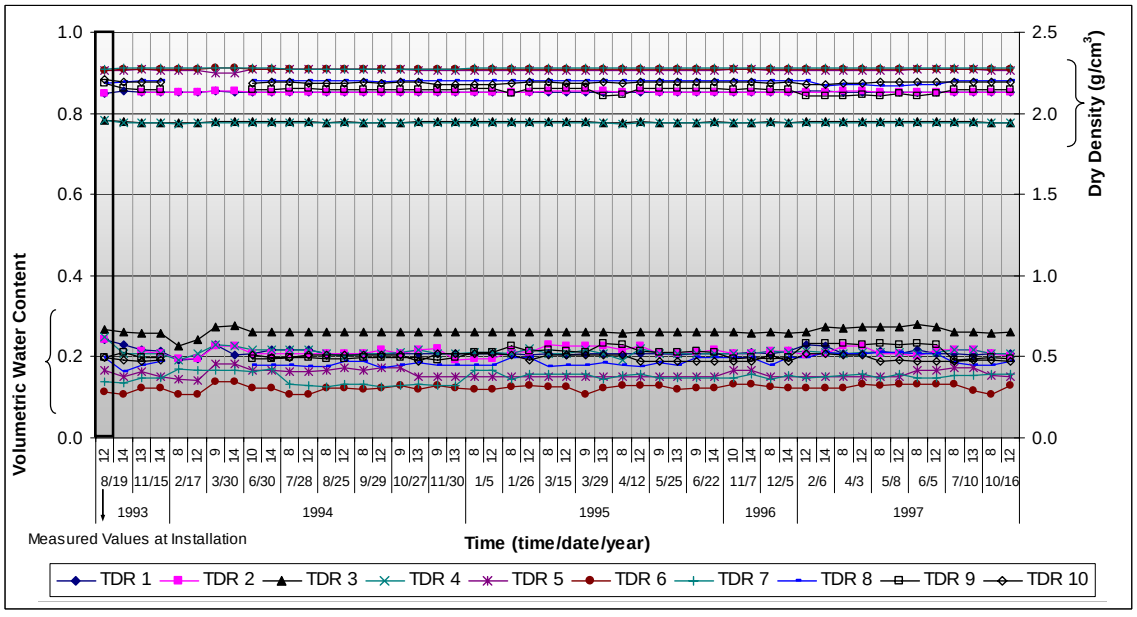

Figure F-9 Variation of water content and density for LTPP section 091803 (Groton, Connecticut)

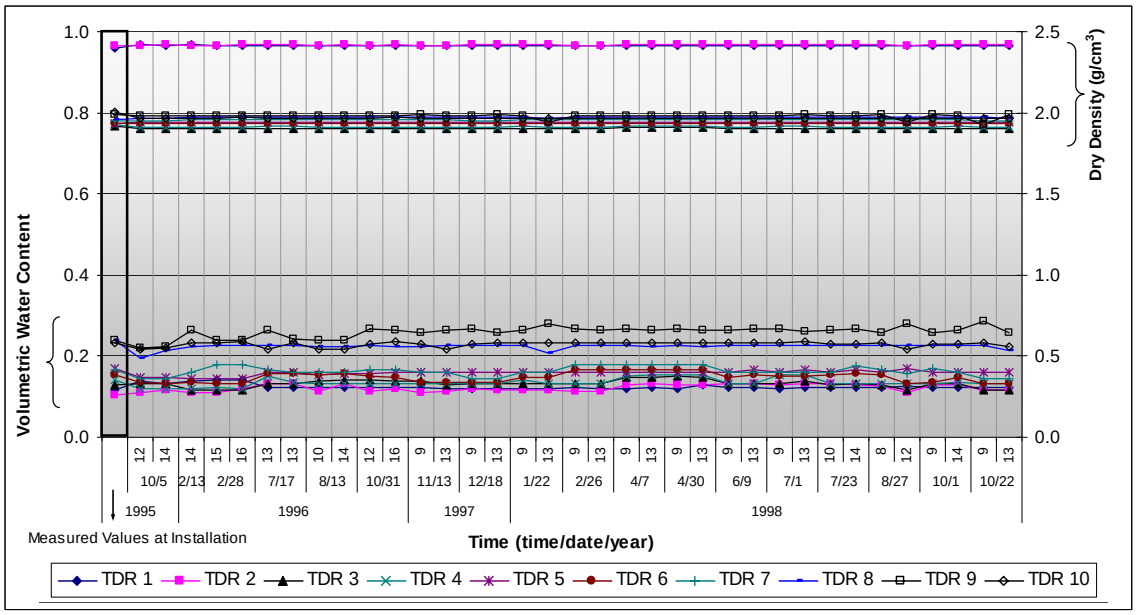

Figure F-10 Variation of water content and density for LTPP section 100102 (Ellendale, Delaware)

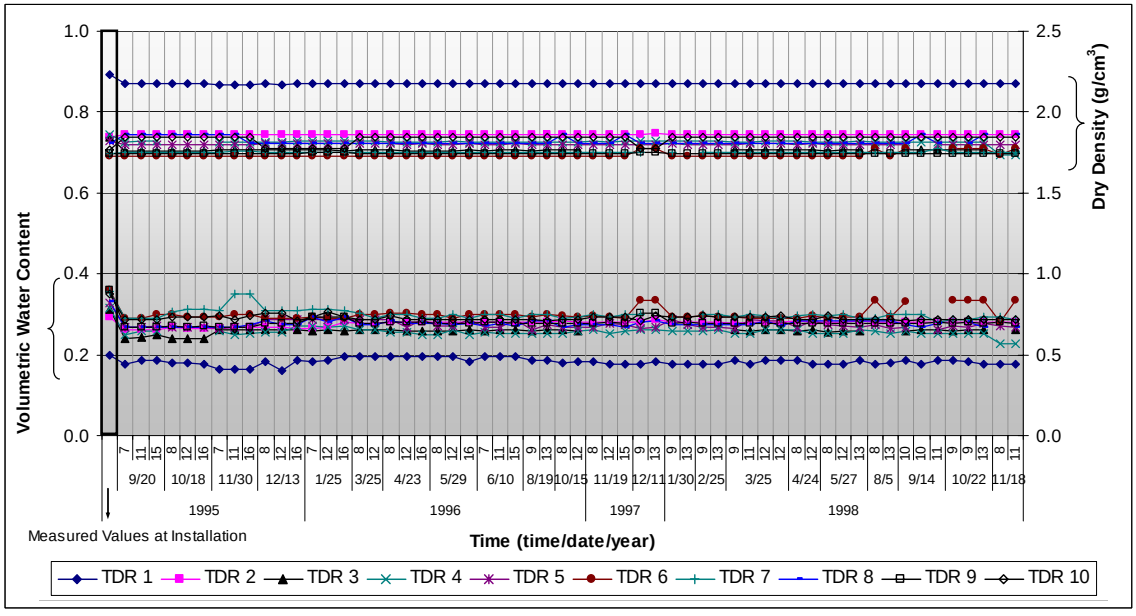

Figure F-11 Variation of water content and density for LTPP section 131005 (Warner Robins, Georgia)

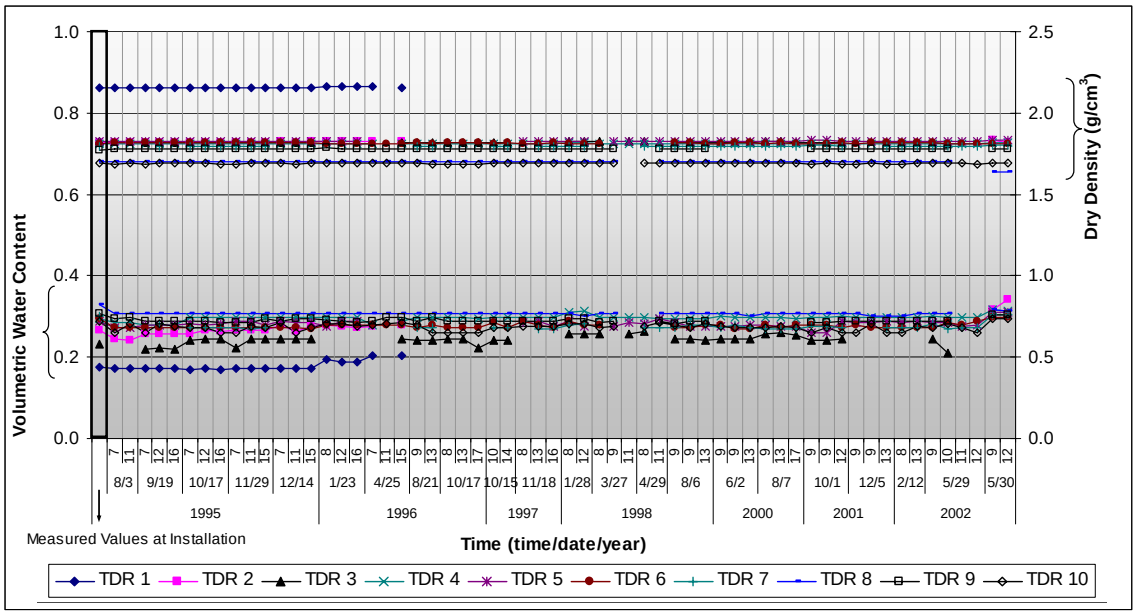

Figure F-12 Variation of water content and density for LTPP section 131031 (Dawsonville, Georgia)

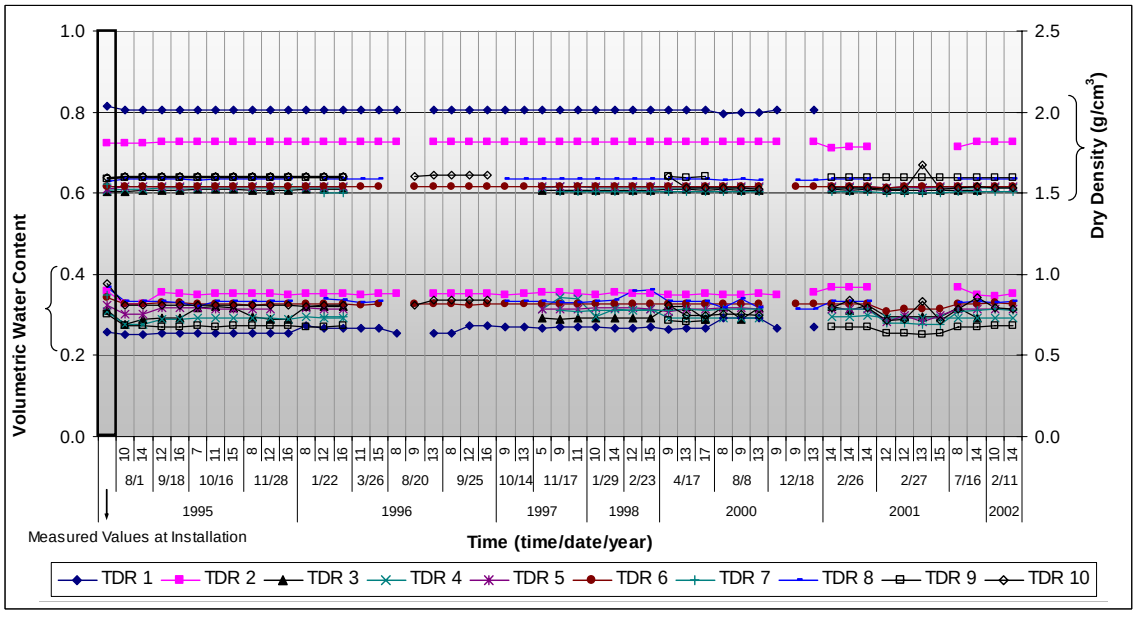

Figure F-13 Variation of water content and density for LTPP section 133019 (Gainesville, Georgia)

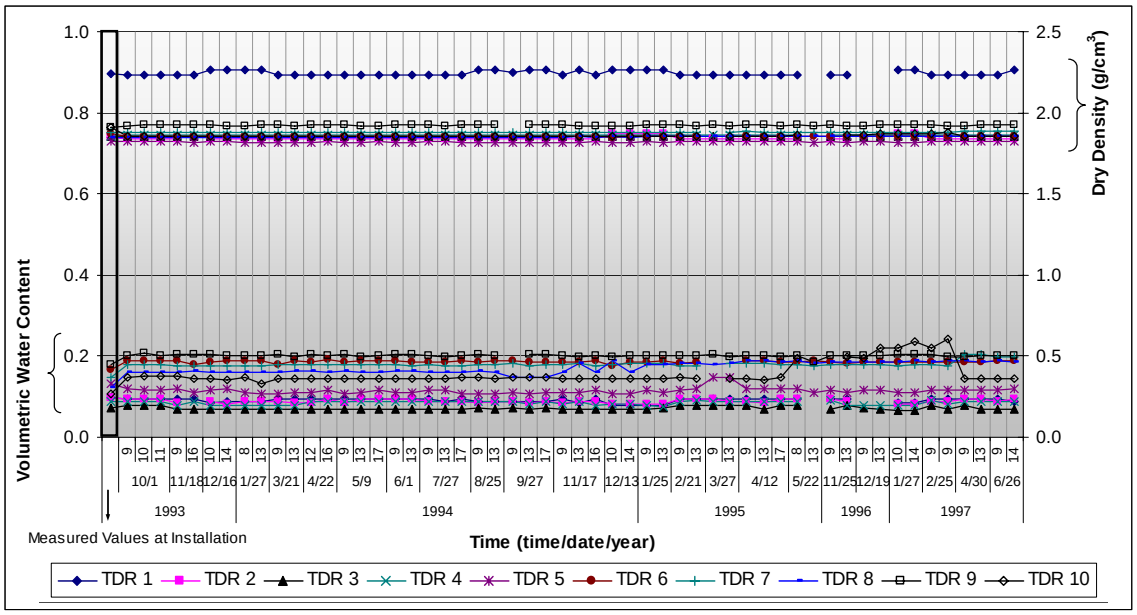

Figure F-14 Variation of water content and density for LTPP section 161010 (Idaho Falls, Idaho)

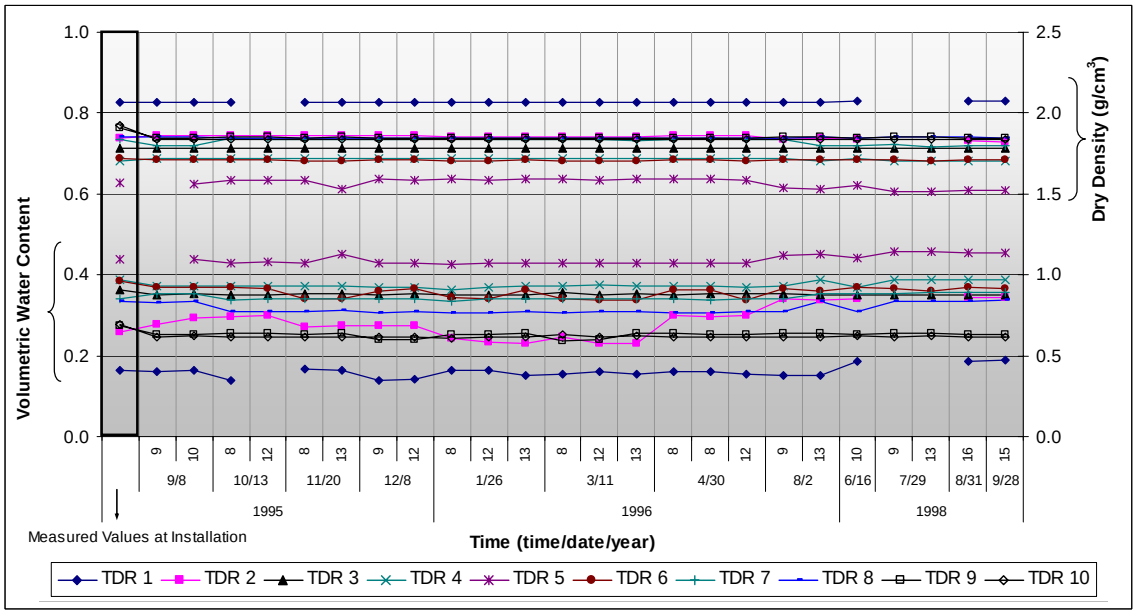

Figure F-15 Variation of water content and density for LTPP section 183002 (Lafayette, Indiana)

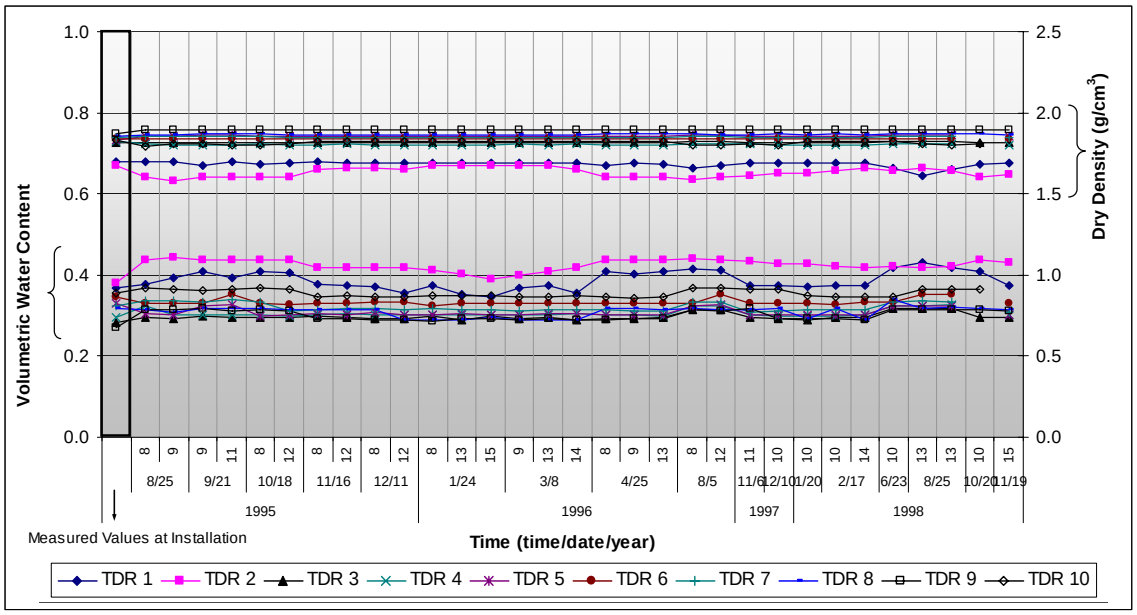

Figure F-16 Variation of water content and density for LTPP section 204054 (Enterprise, Kansas)

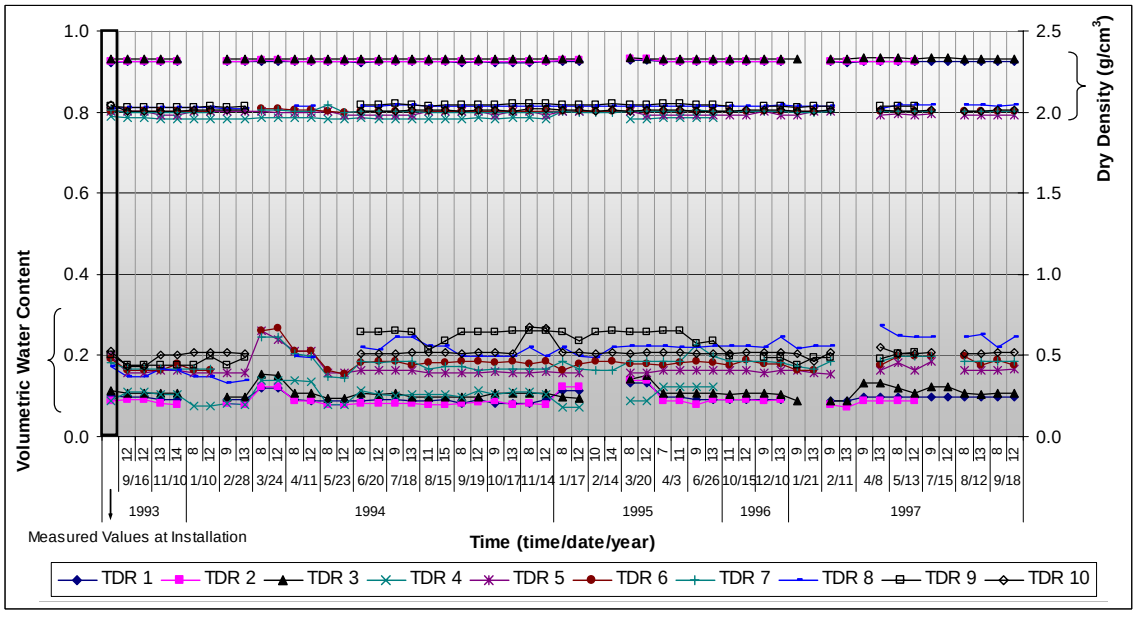

Figure F-17 Variation of water content and density for LTPP section 231026 (East Dixfield, Maine)

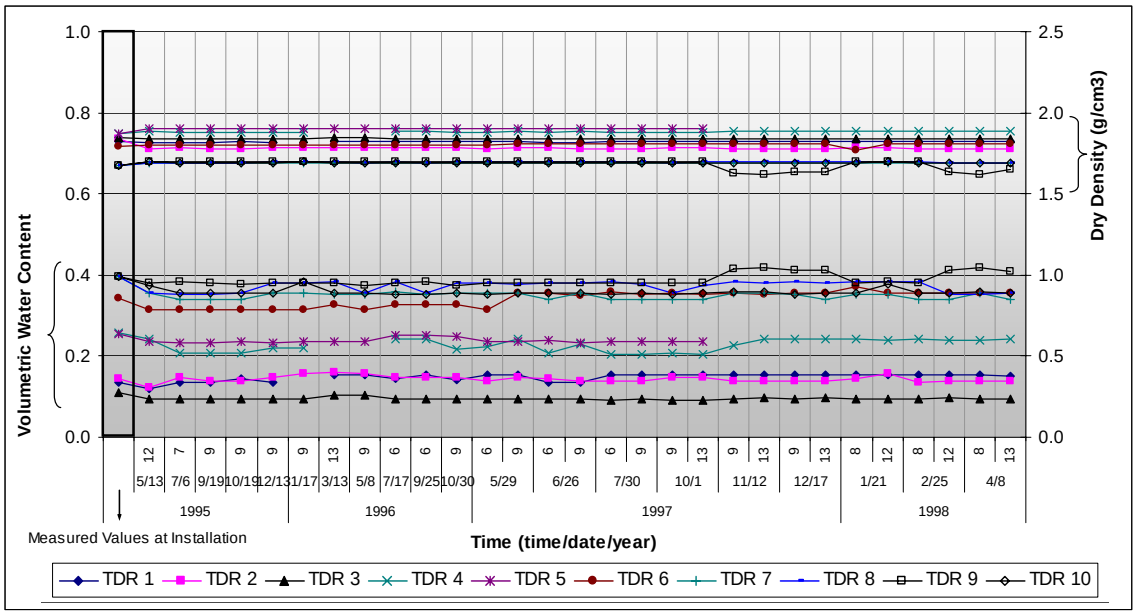

Figure F-18 Variation of water content and density for LTPP section 241634 (Ocean City, Maryland)

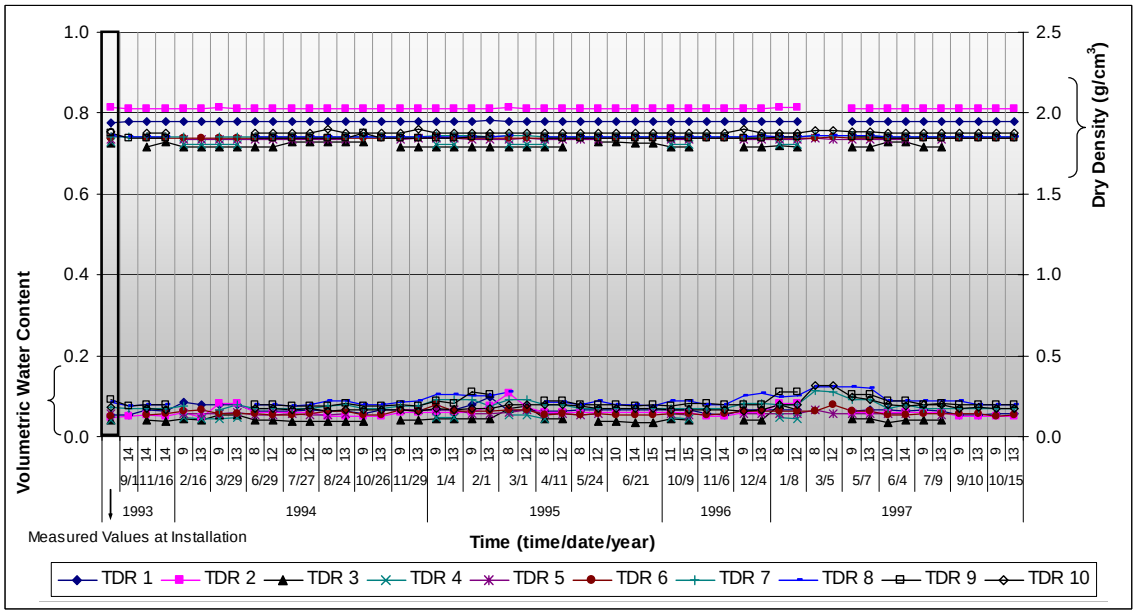

Figure F-19 Variation of water content and density for LTPP section 251002 (Chicopee, Massachusetts)

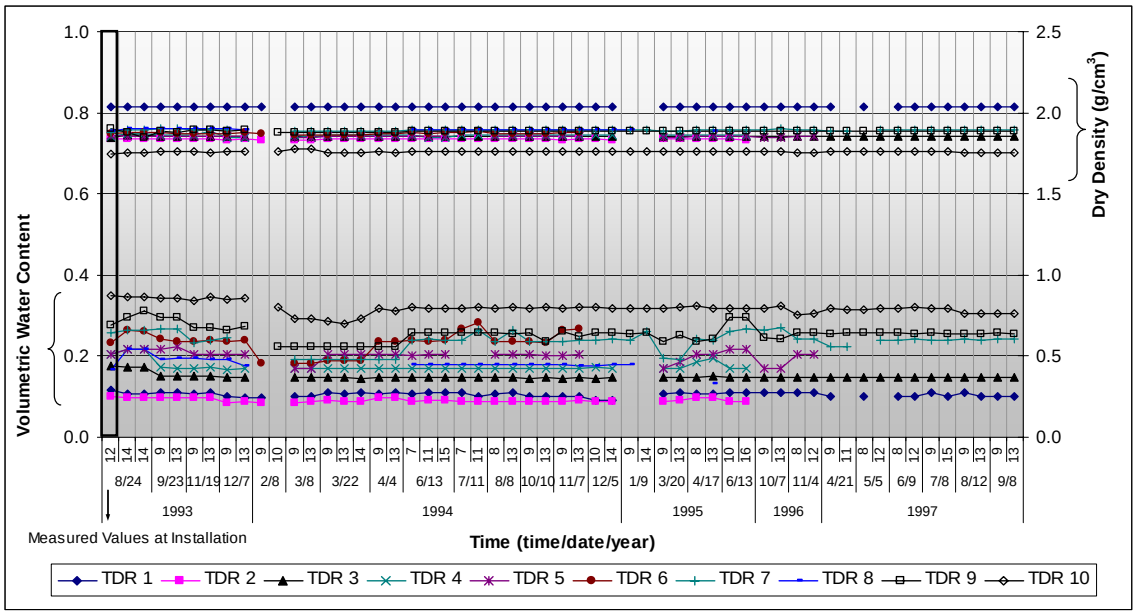

Figure F-20 Variation of water content and density for LTPP section 271018 (Little Falls, Minnesota)

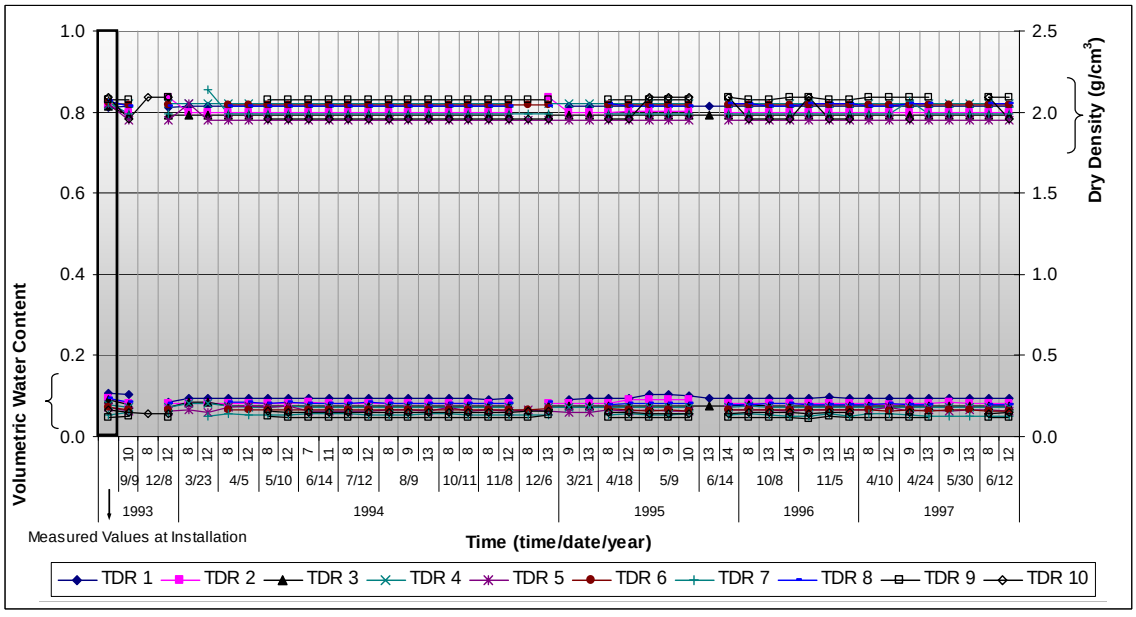

Figure F-21 Variation of water content and density for LTPP section 271028 (Detroit Lakes, Minnesota)

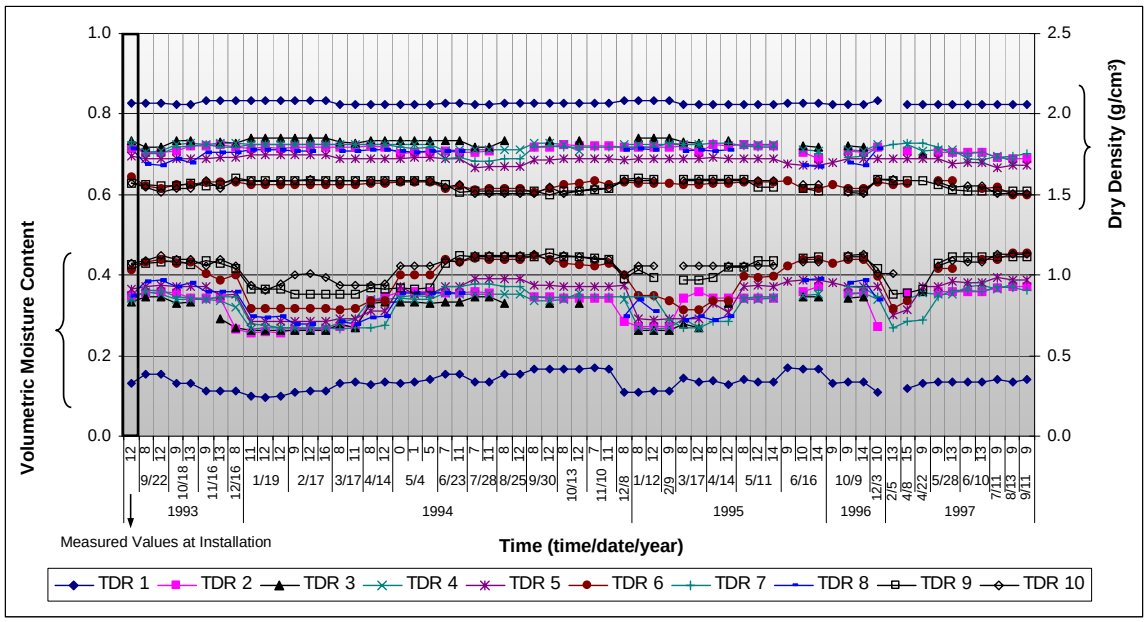

Figure F-22 Variation of water content and density for LTPP section 274040 (Grand Rapids, Minnesota)

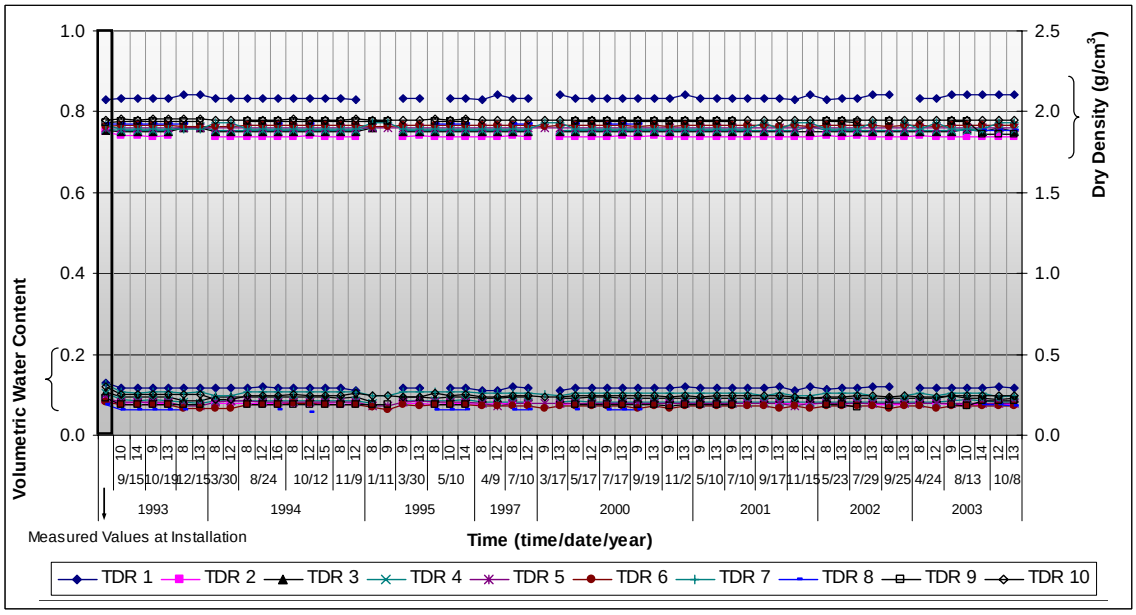

Figure F-23 Variation of water content and density for LTPP section 276251 (Bemidji, Minnesota)

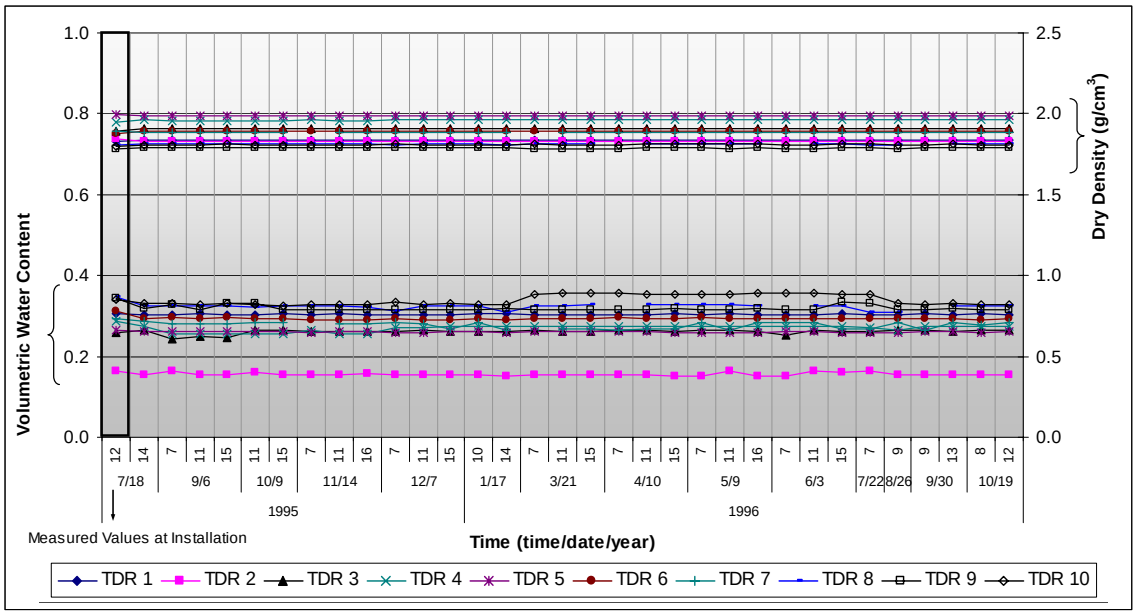

Figure F-24 Variation of water content and density for LTPP section 281016 (Kosciusko, Mississippi)

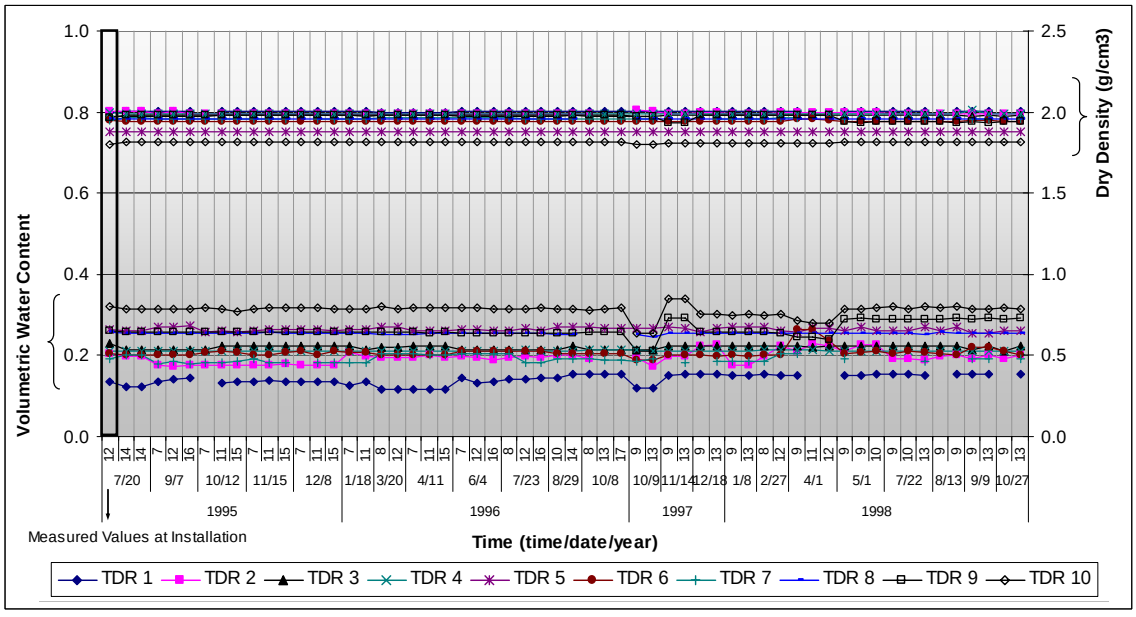

Figure F-25 Variation of water content and density for LTPP section 281802 (Laurel, Mississippi)

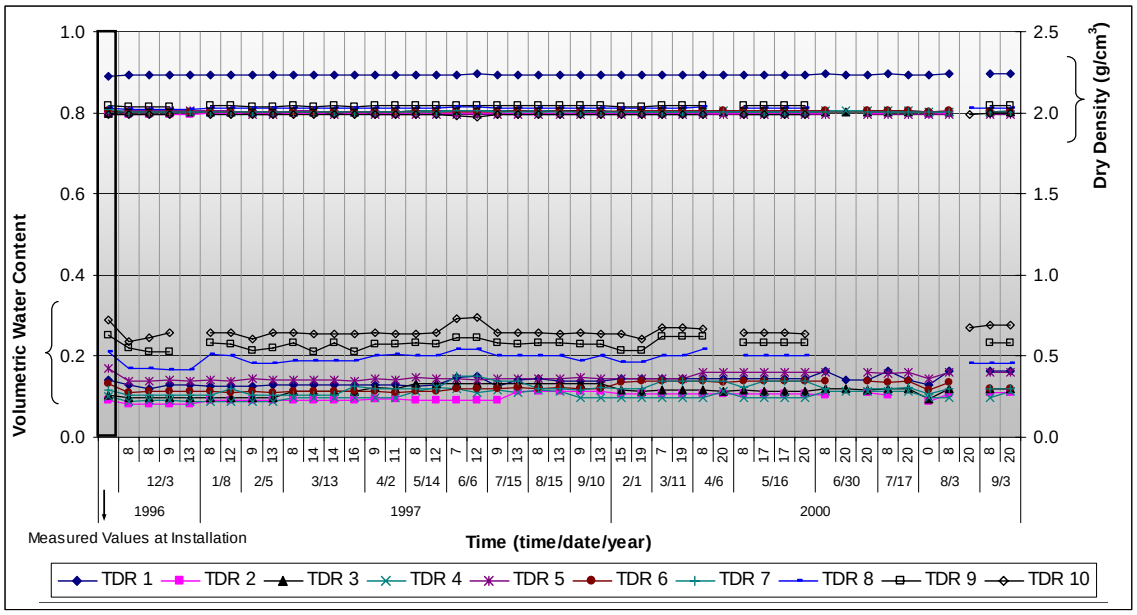

Figure F-26 Variation of water content and density for LTPP section 300114 (Great Falls, Montana)

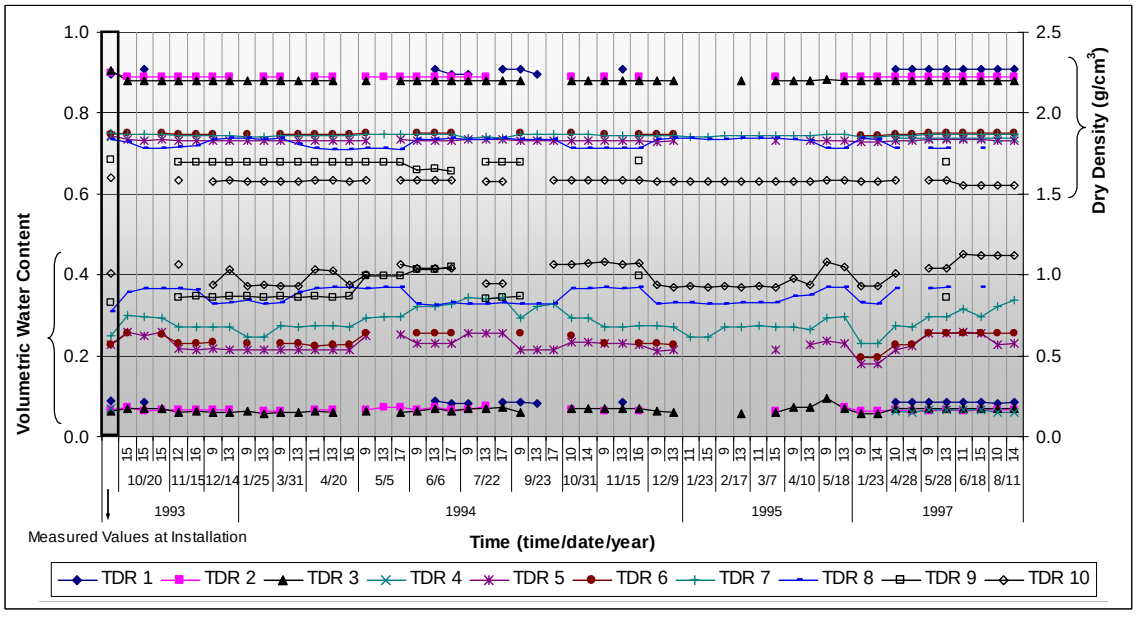

Figure F-27 Variation of water content and density for LTPP section 308129 (Ryegate, Montana)

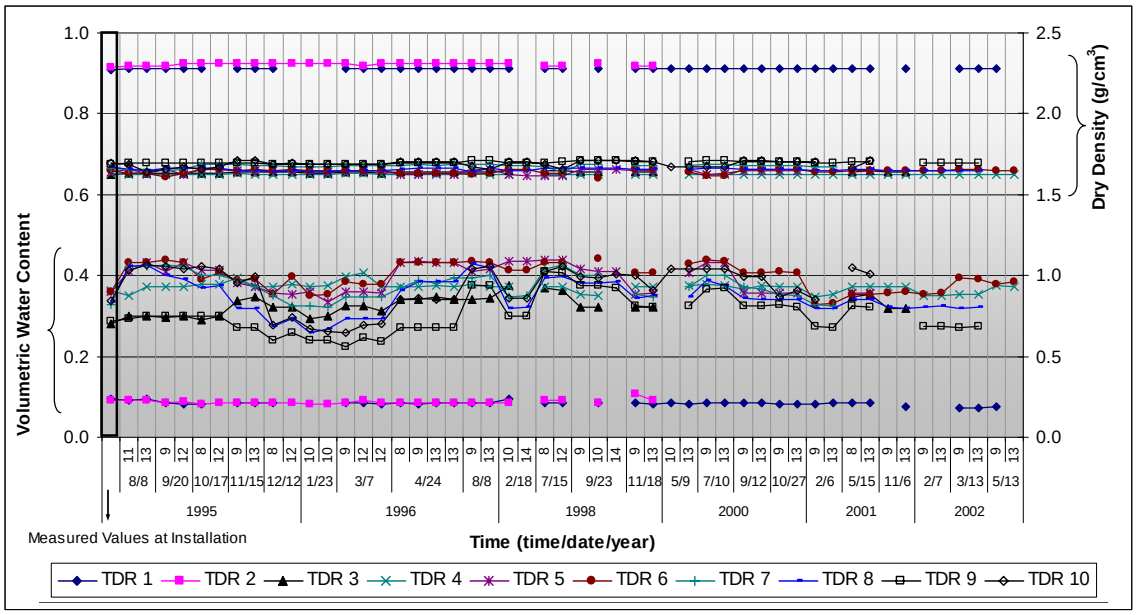

Figure F-28 Variation of water content and density for LTPP section 310114 (Hebron, Nebraska)

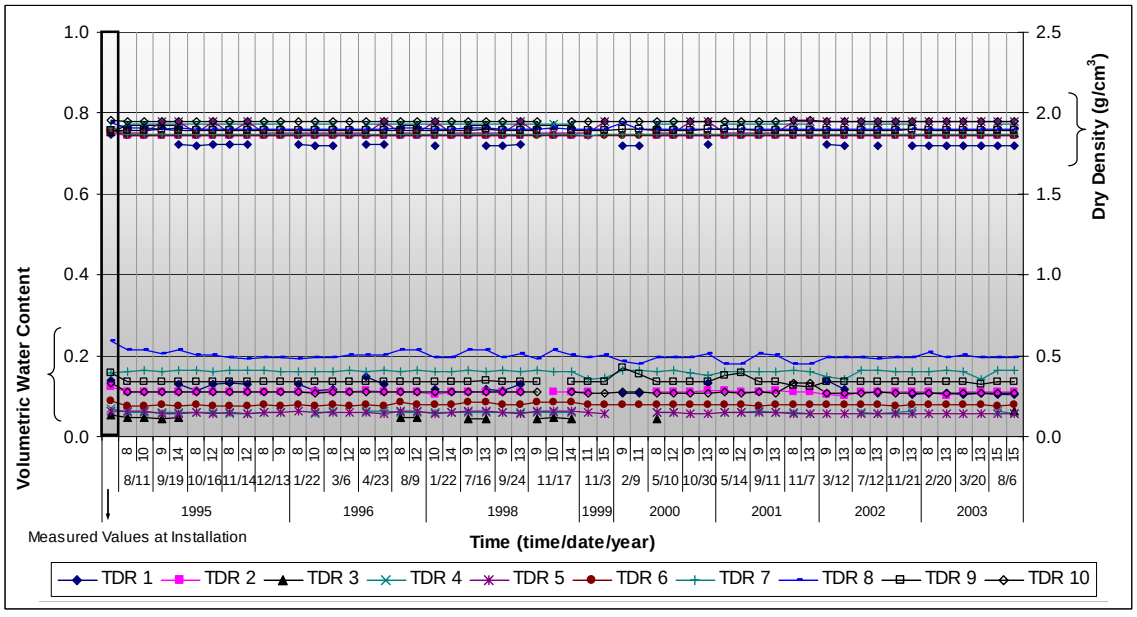

Figure F-29 Variation of water content and density for LTPP section 313018 (Kearney, Nebraska)

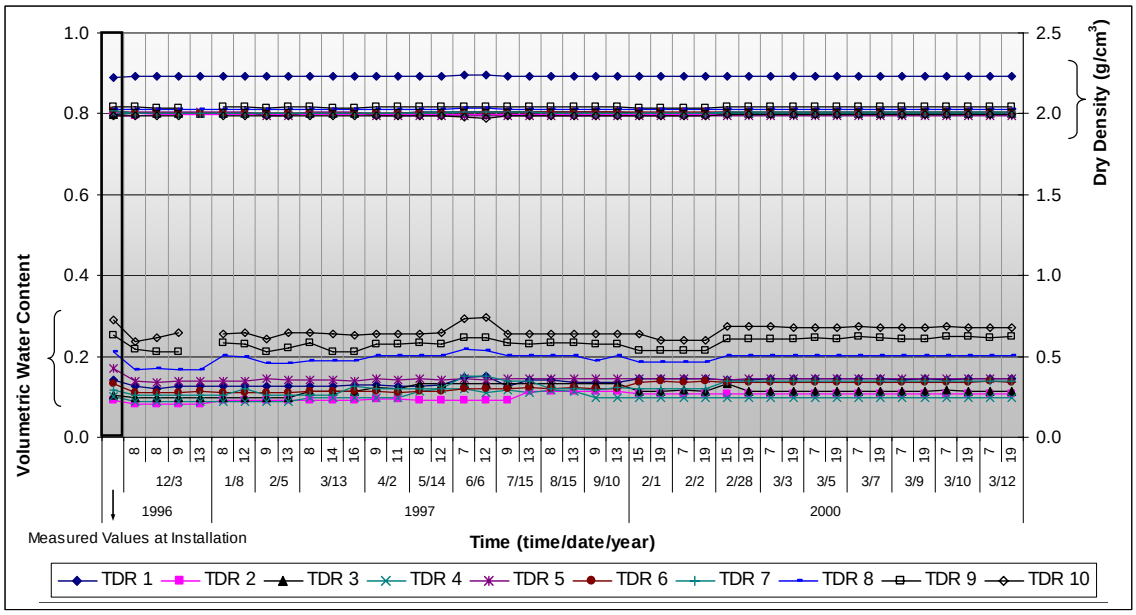

Figure F-30 Variation of water content and density for LTPP section 320101 (Battle Mountain, Nevada)

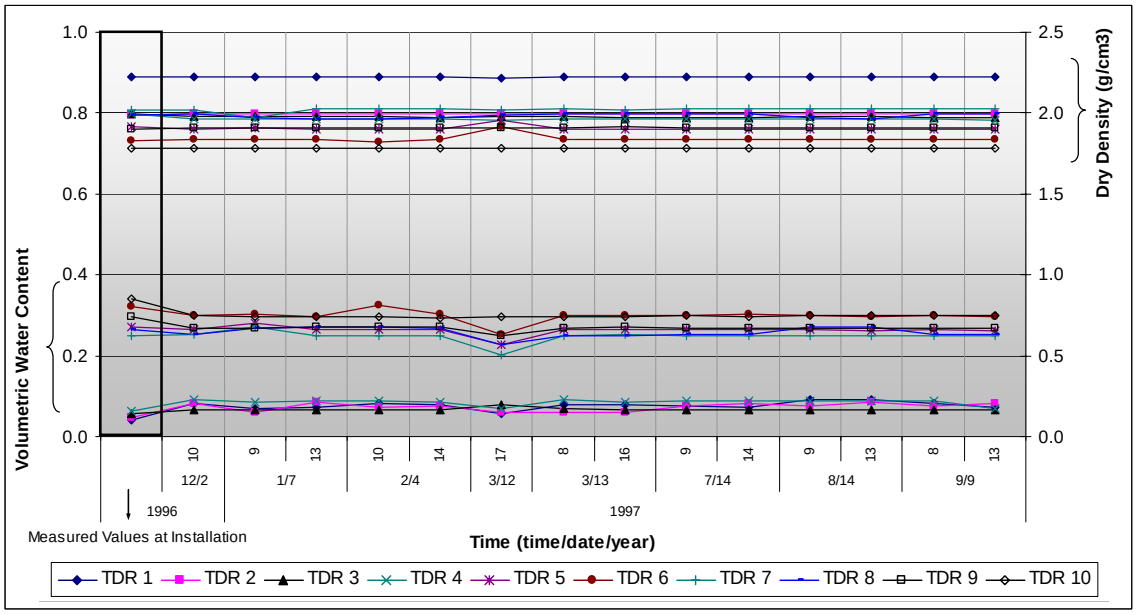

Figure F-31 Variation of water content and density for LTPP section 320204 (Battle Mountain, Nevada)

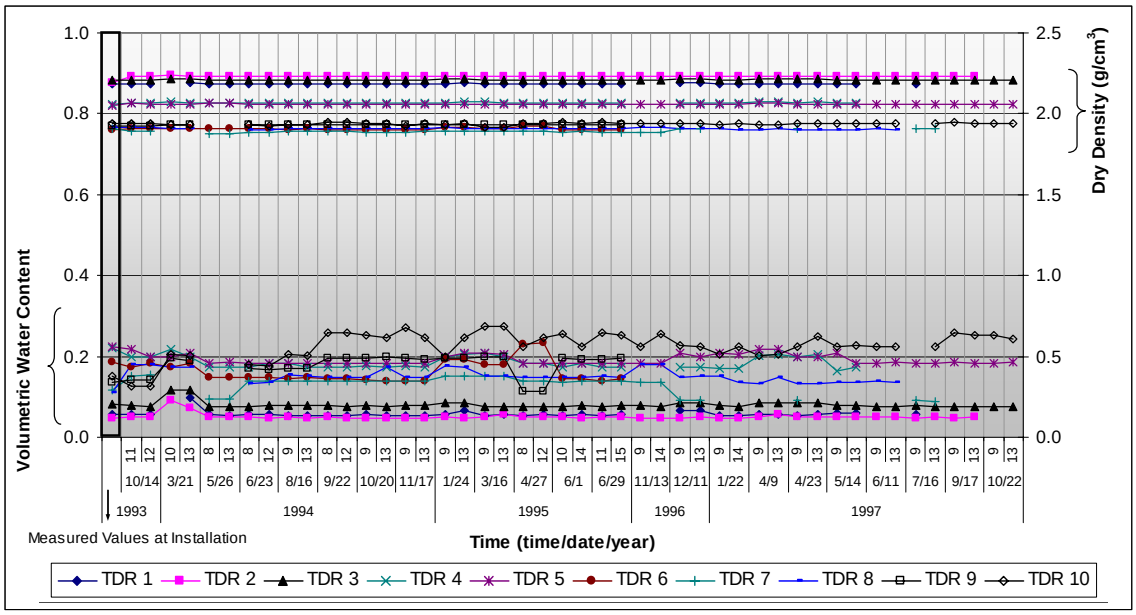

Figure F-32 Variation of water content and density for LTPP section 331001 (Concord, New Hampshire)

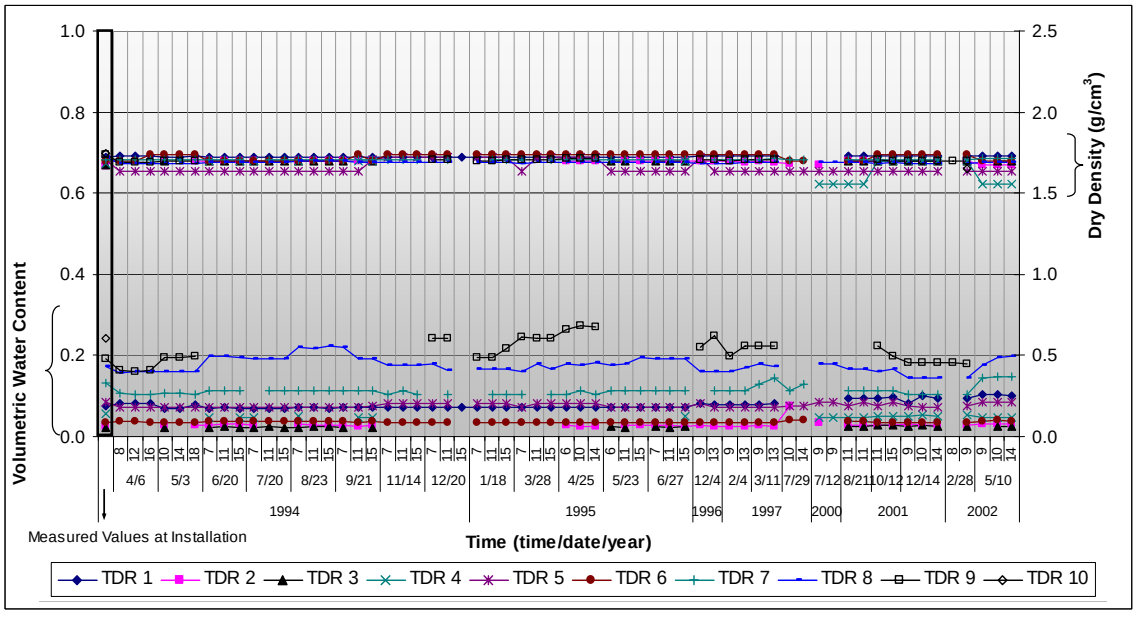

Figure F-33 Variation of water content and density for LTPP section 351112 (Hobbs, New Mexico)

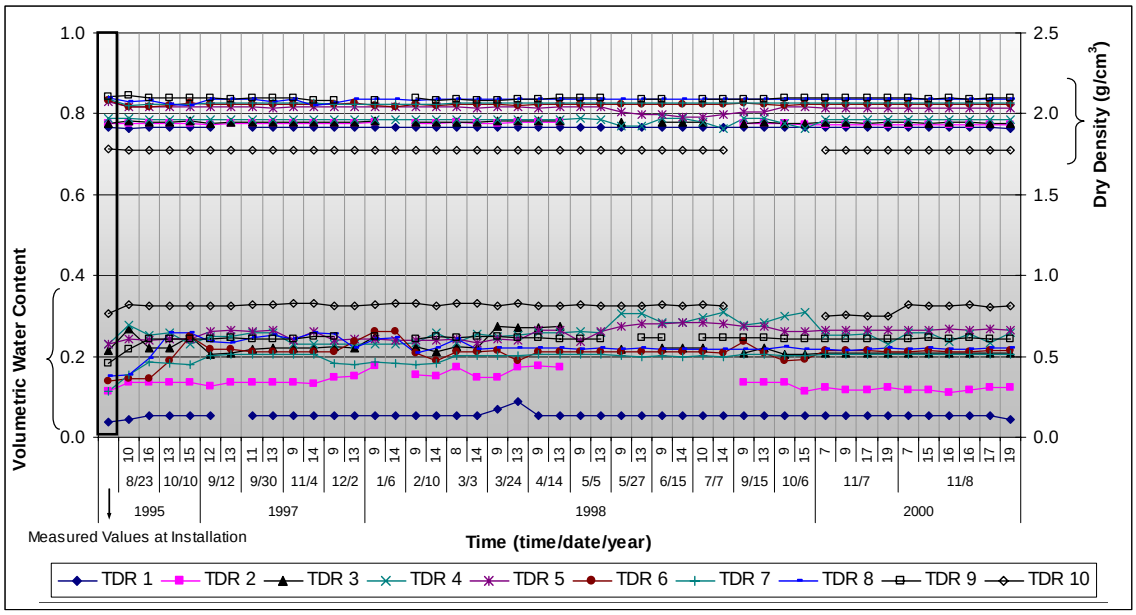

Figure F-34 Variation of water content and density for LTPP section 360801 (Hamlin, New York)

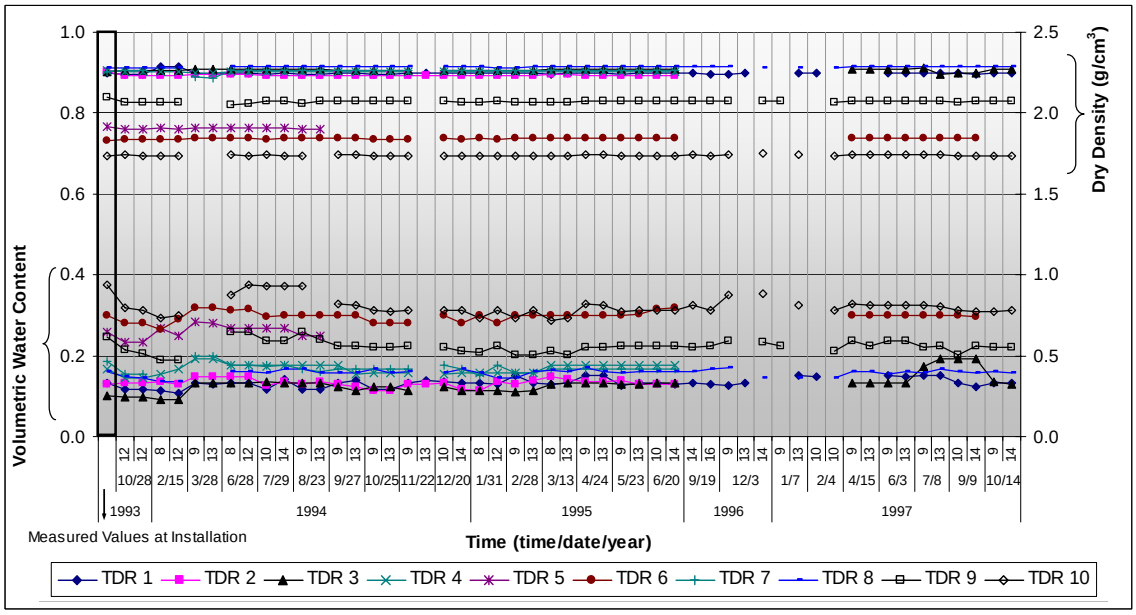

Figure F-35 Variation of water content and density for LTPP section 364018 (Oneonta, New York)

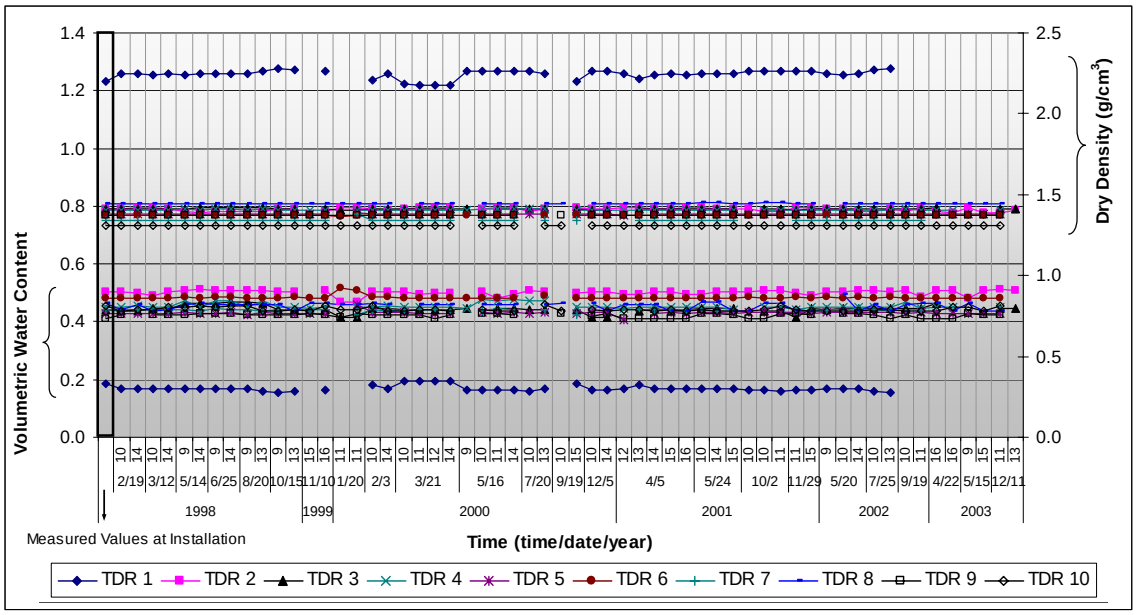

Figure F-36 Variation of water content and density for LTPP section 370201 (Lexington, North Carolina)

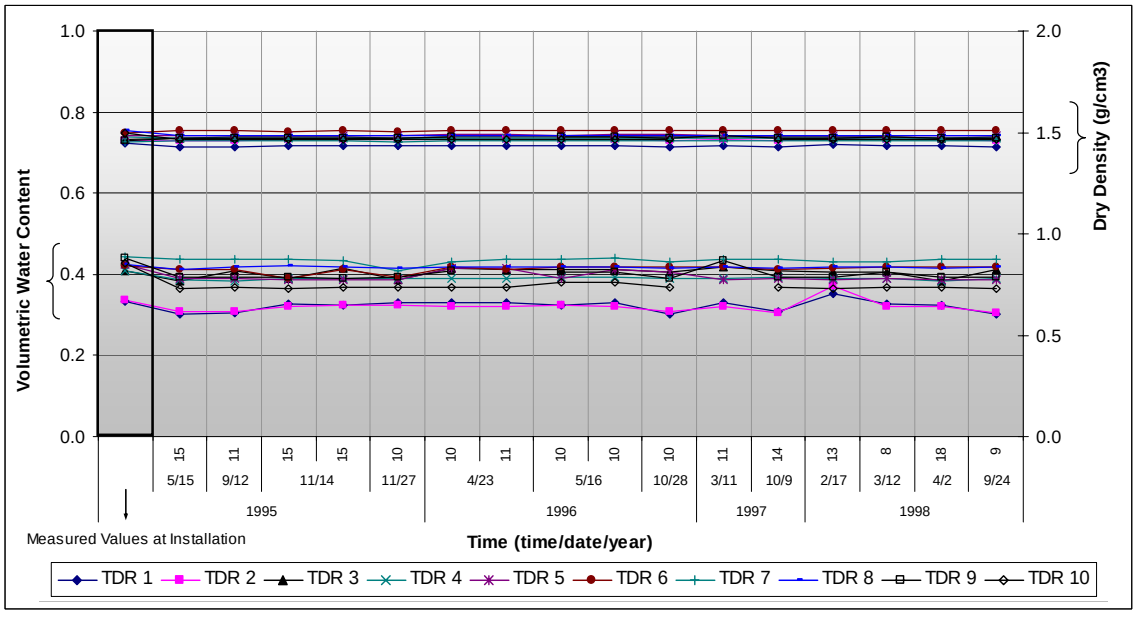

Figure F-37 Variation of water content and density for LTPP section 370205 (Lexington, North Carolina)

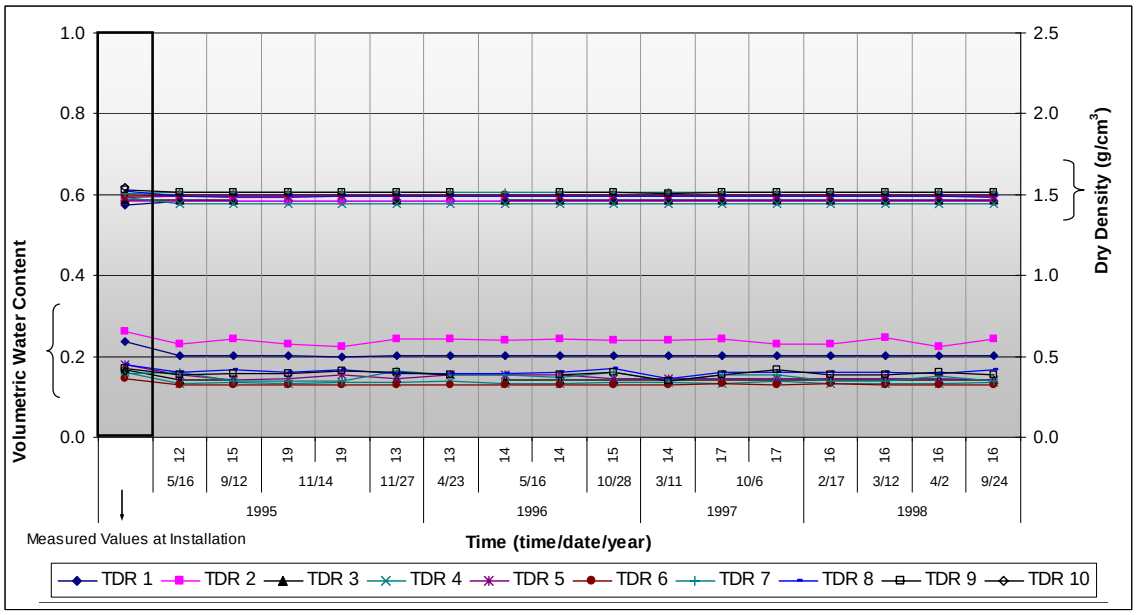

Figure F-38 Variation of water content and density for LTPP section 370208 (Lexington, North Carolina)

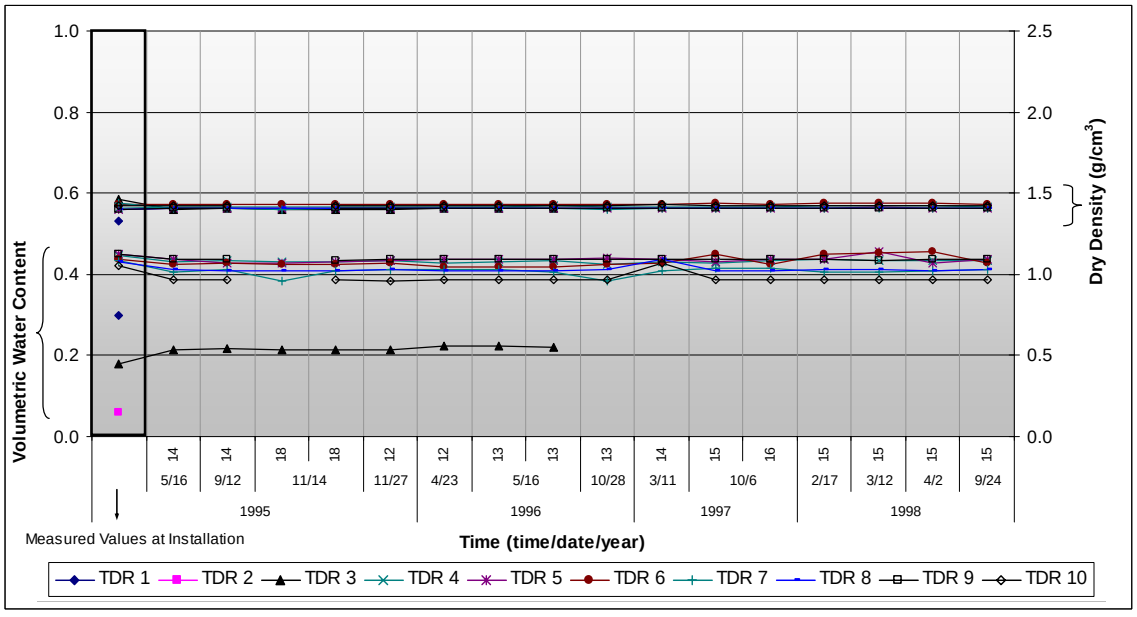

Figure F-39 Variation of water content and density for LTPP section 370212 (Lexington, North Carolina)

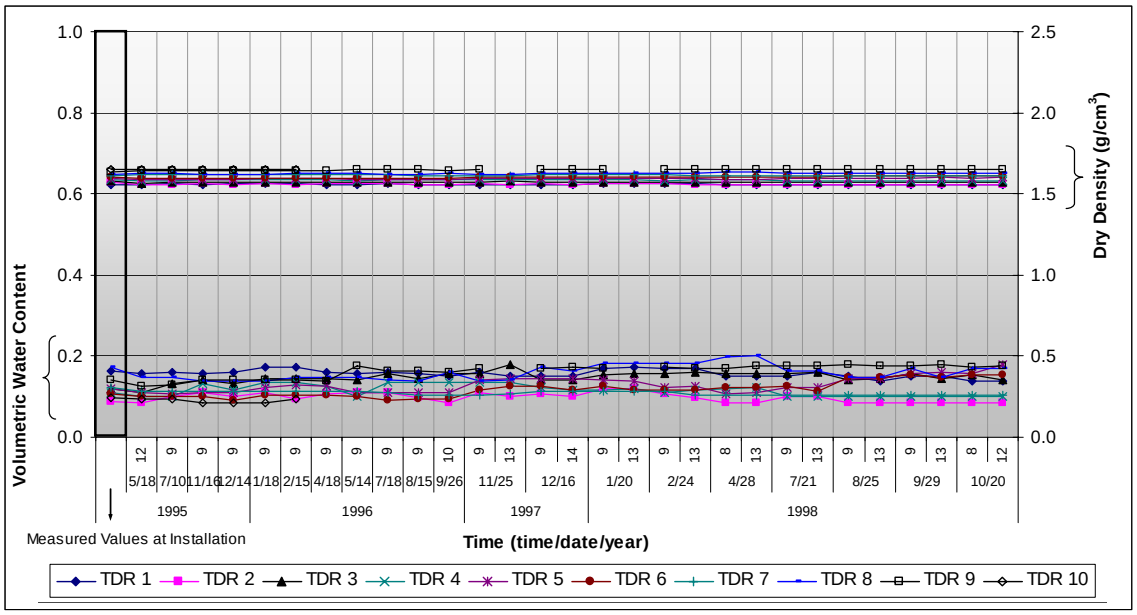

Figure F-40 Variation of water content and density for LTPP section 371028 (Elizabeth City, North Carolina)

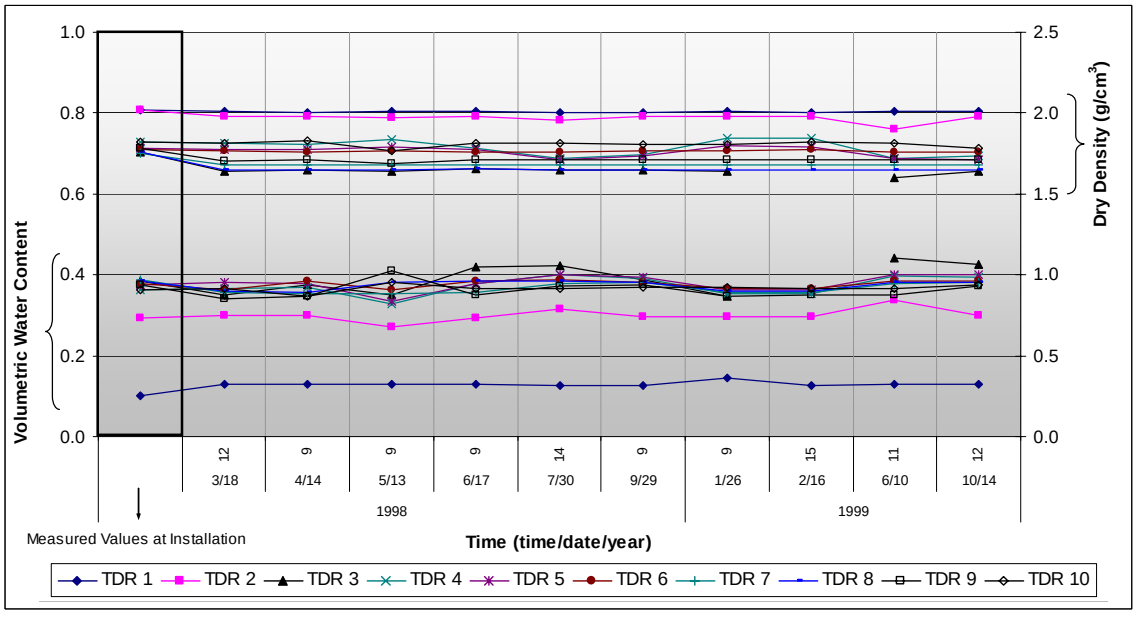

Figure F-41 Variation of water content and density for LTPP section 390204 (Delaware, Ohio)

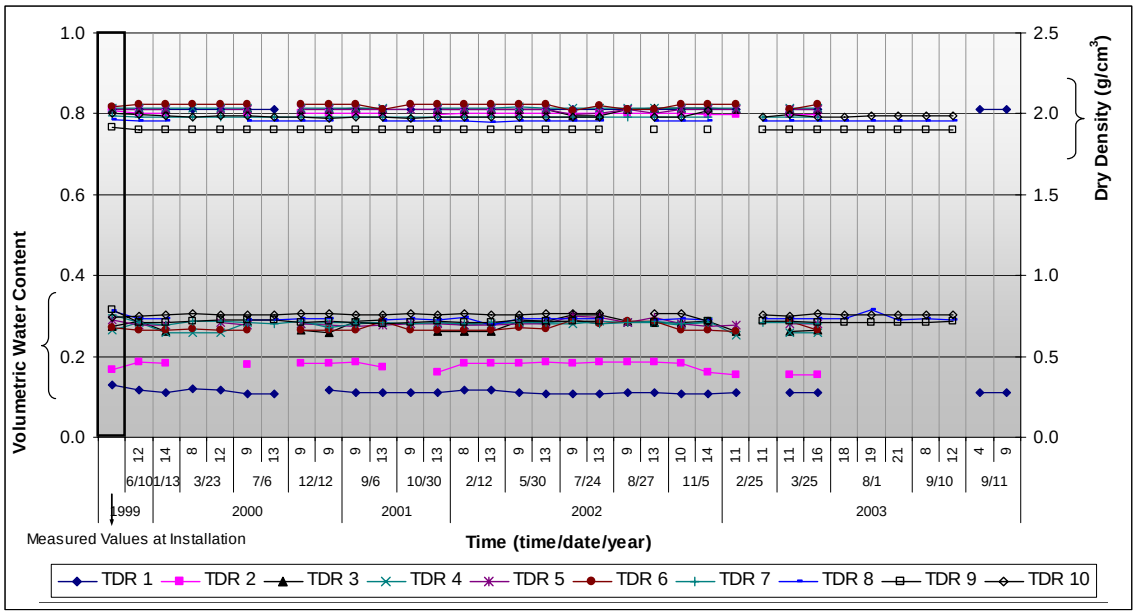

Figure F-42 Variation of water content and density for LTPP section 390901 (Delaware, Ohio)

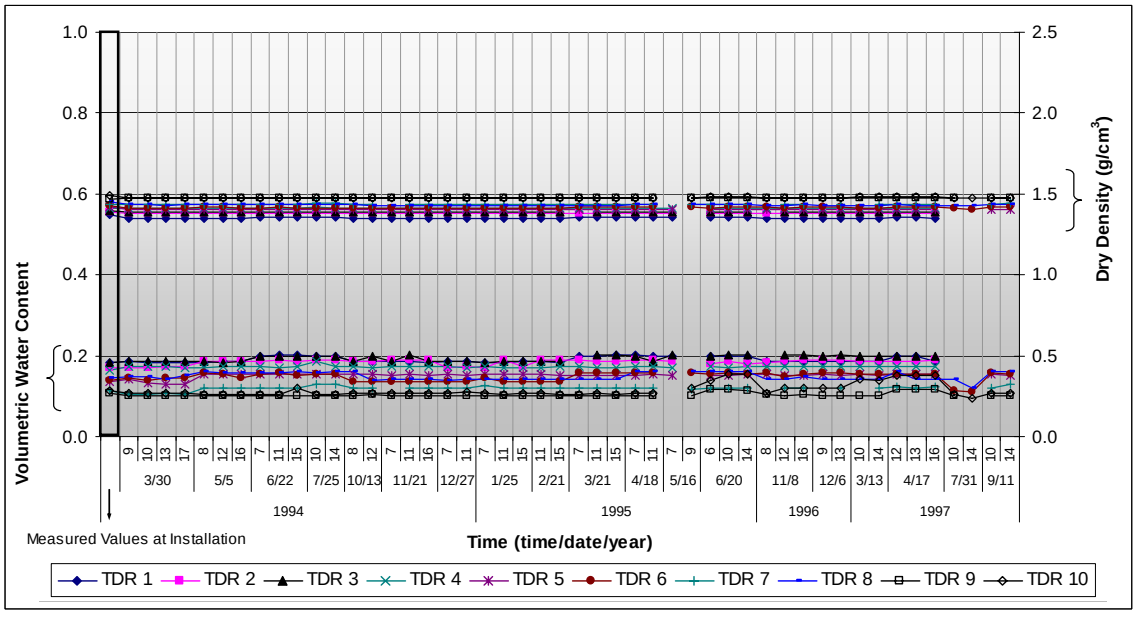

Figure F-43 Variation of water content and density for LTPP section 404165 (Cleo Springs, Oklahoma)

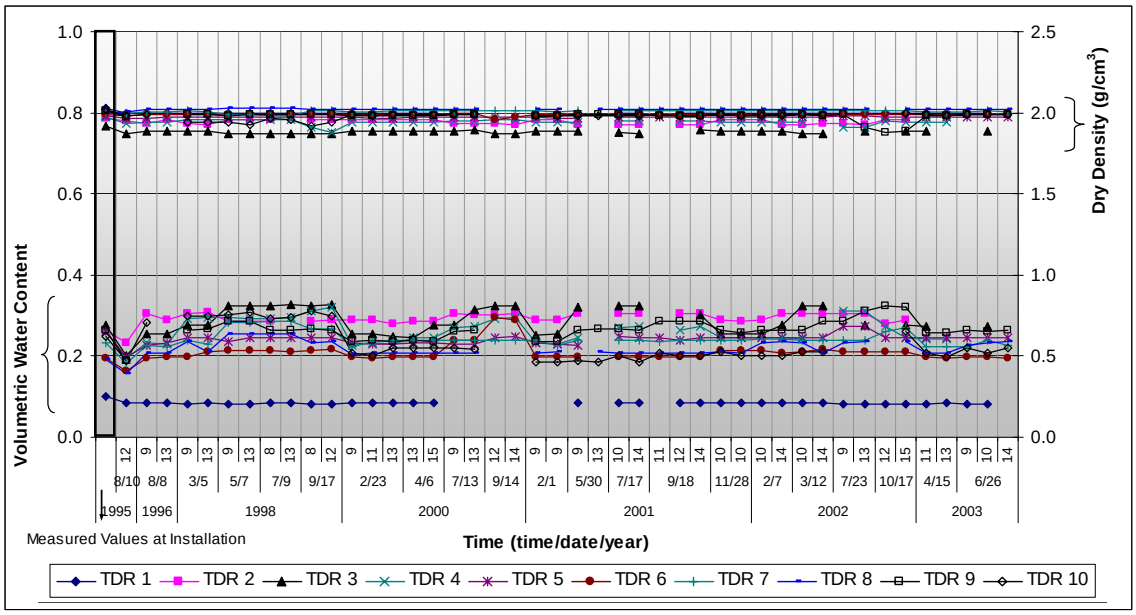

Figure F-44 Variation of water content and density for LTPP section 421606 (Altoona, Pennsylvania)

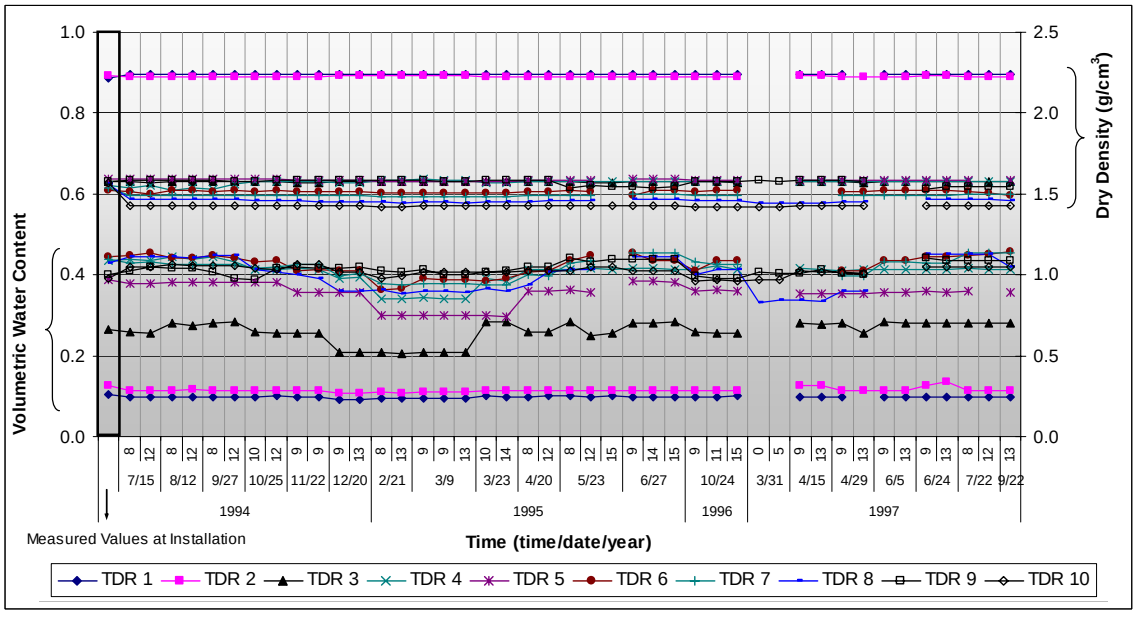

Figure F-45 Variation of water content and density for LTPP section 460804 (Pollock, South Dakota)

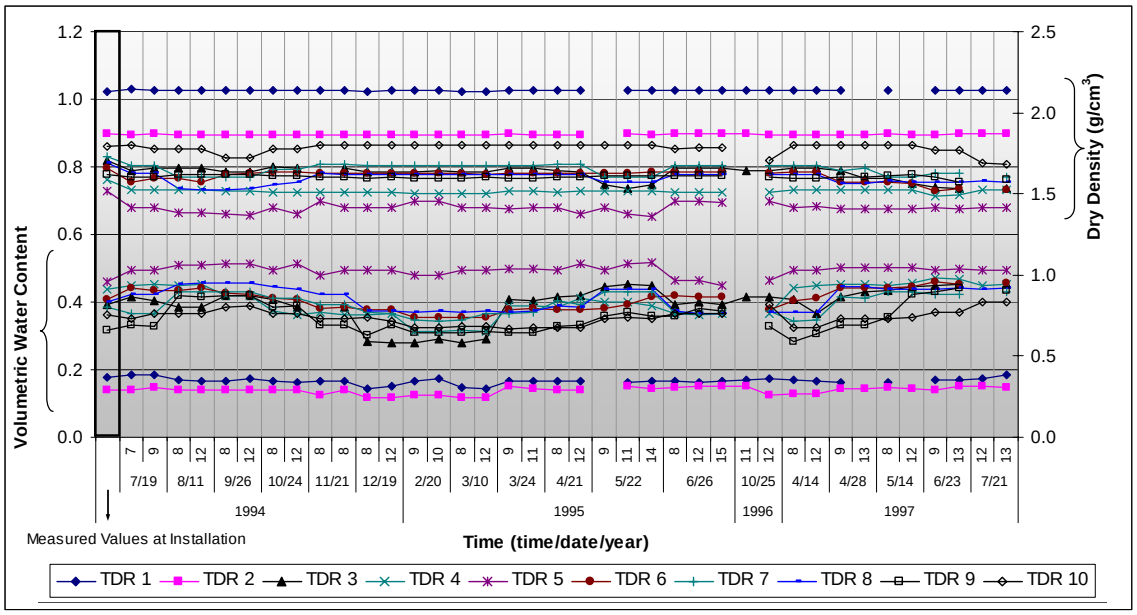

Figure F-46 Variation of water content and density for LTPP section 469187 (Faith, South Dakota)

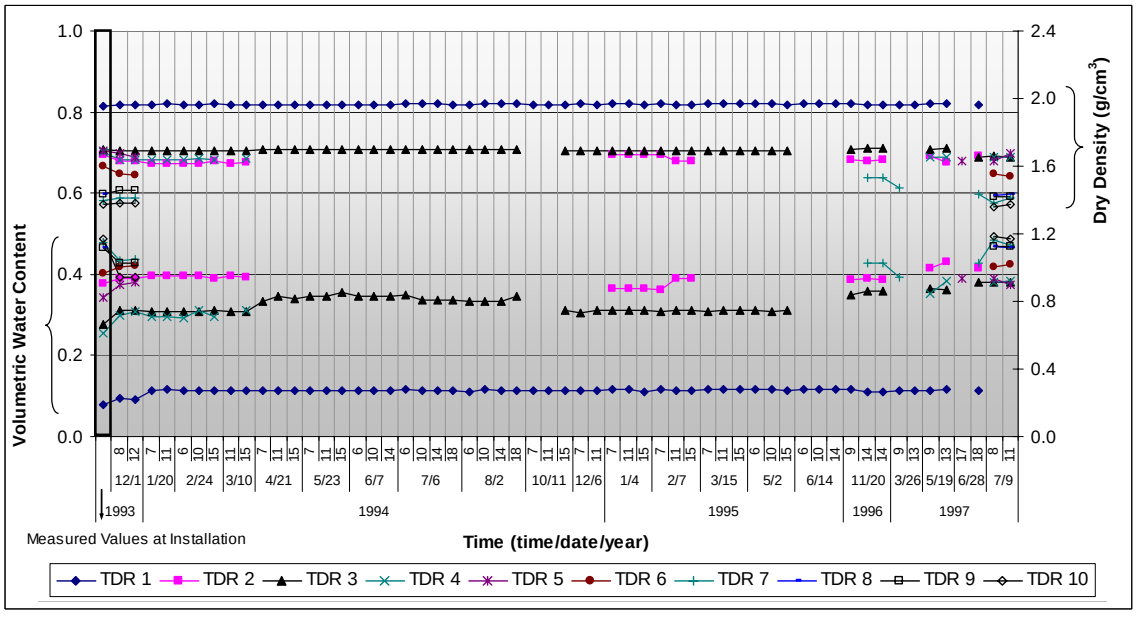

Figure F-47 Variation of water content and density for LTPP section 481060 (Victoria, Texas)

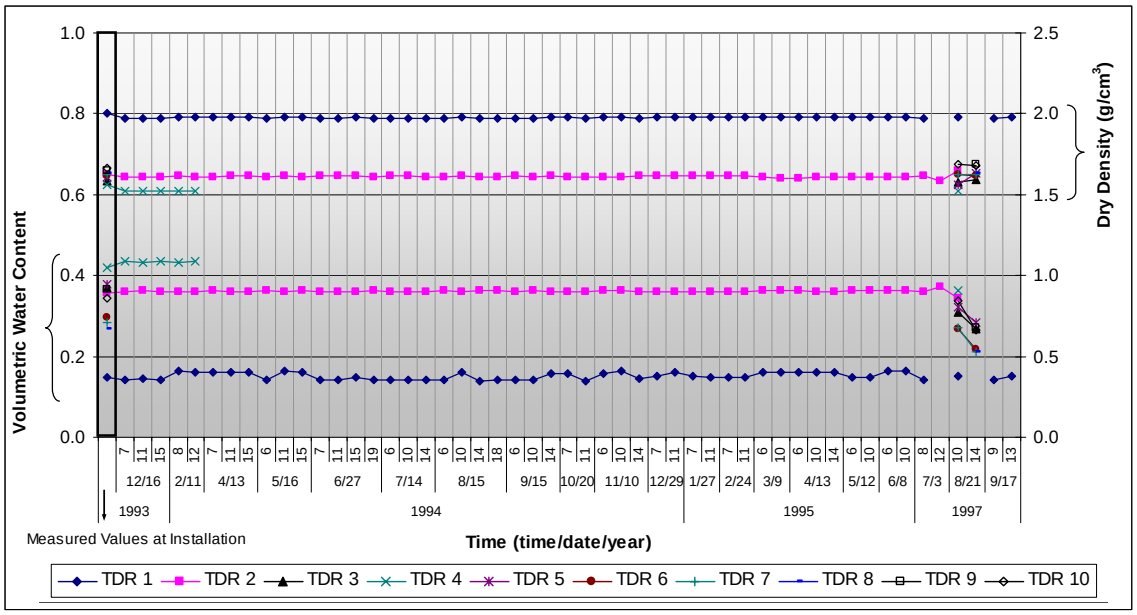

Figure F-48 Variation of water content and density for LTPP section 481068 (Paris, Texas)

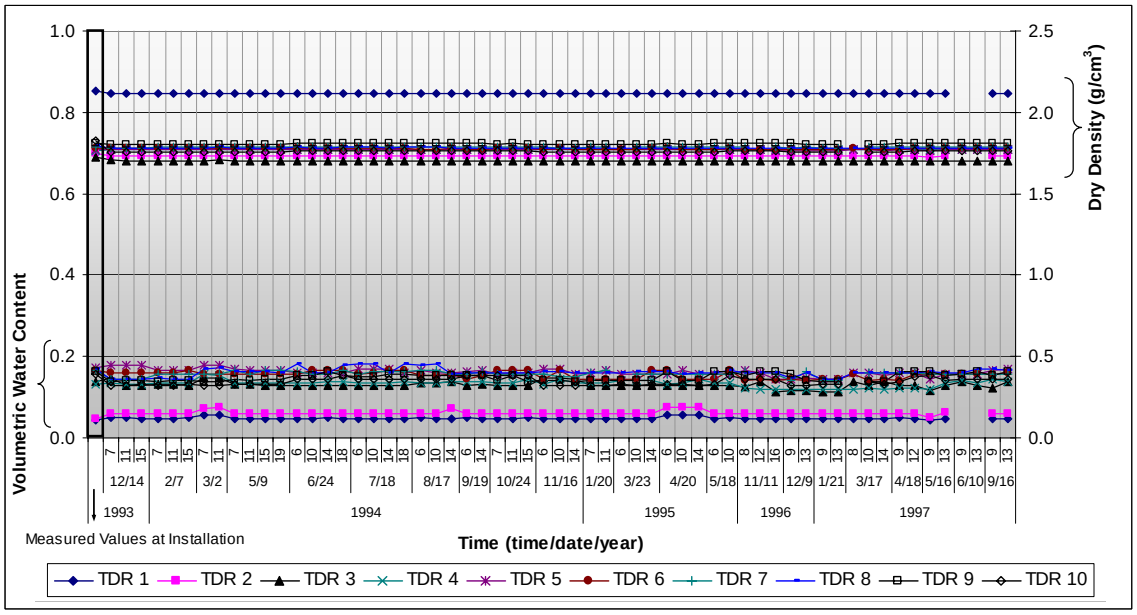

Figure F-49 Variation of water content and density for LTPP section 481077 (Estelline, Texas)

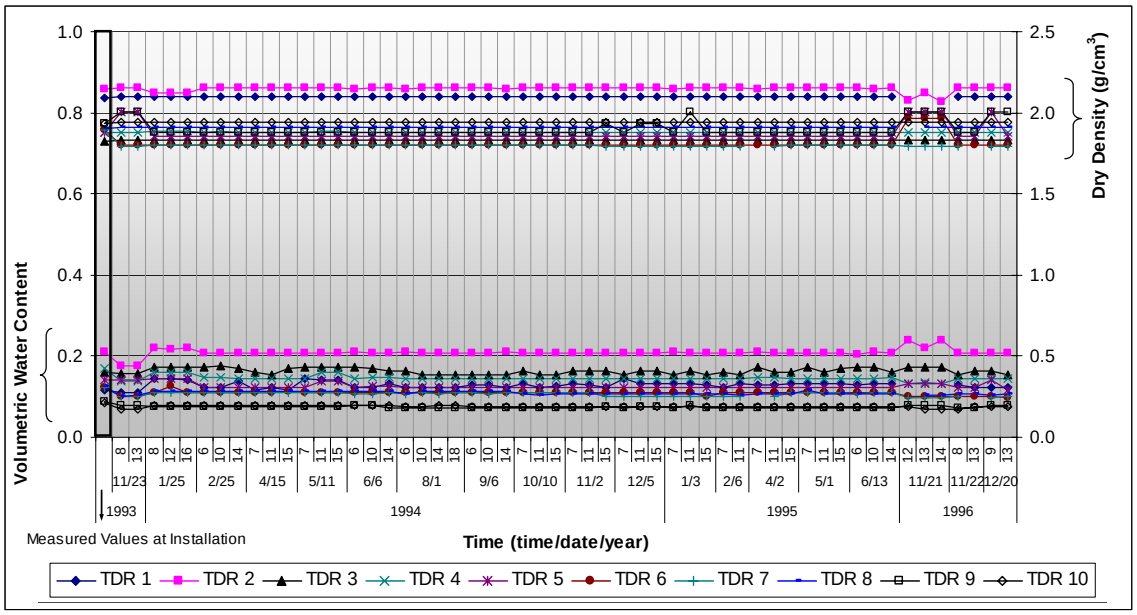

Figure F-50 Variation of water content and density for LTPP section 481122 (Floresville, Texas)

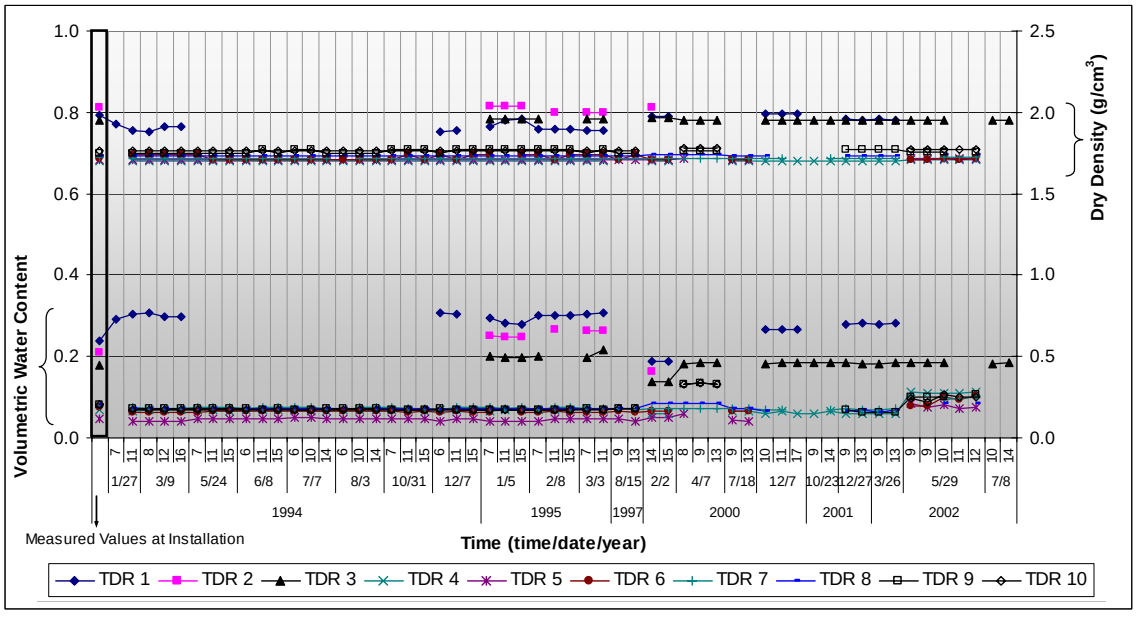

Figure F-51 Variation of water content and density for LTPP section 483739 (Kingsville, Texas)

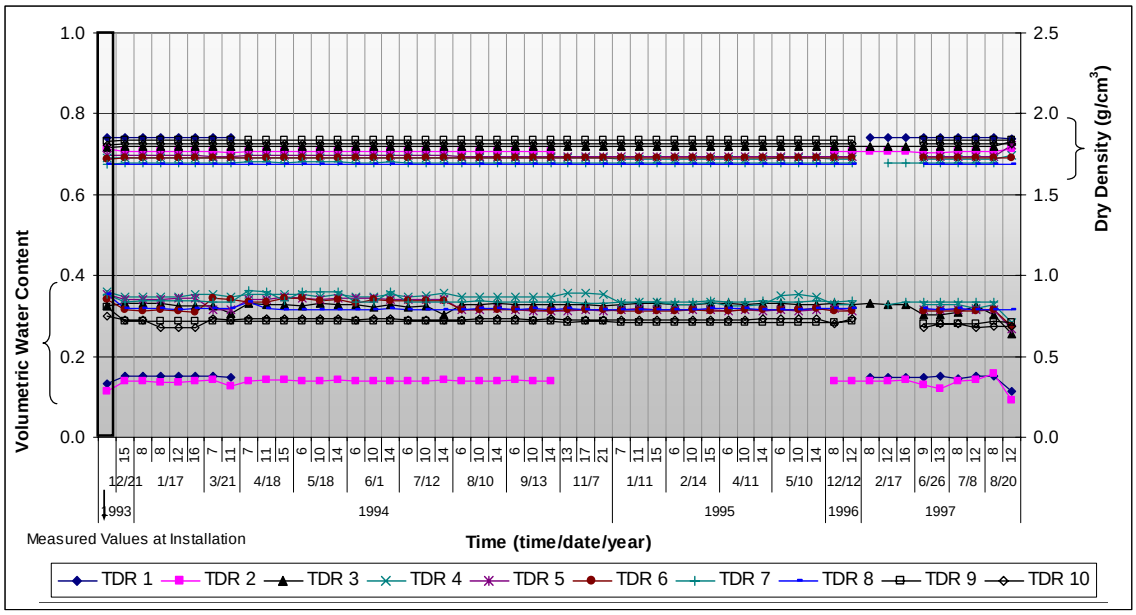

Figure F-52 Variation of water content and density for LTPP section 484142 (Jasper, Texas)

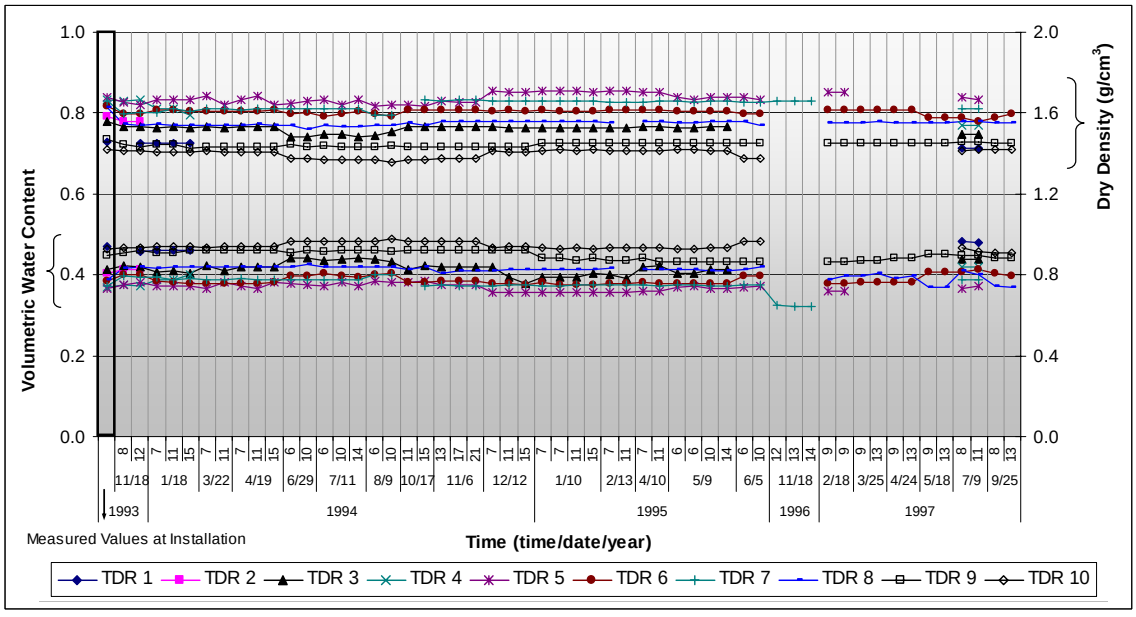

Figure F-53 Variation of water content and density for LTPP section 484143 (Beaumont, Texas)

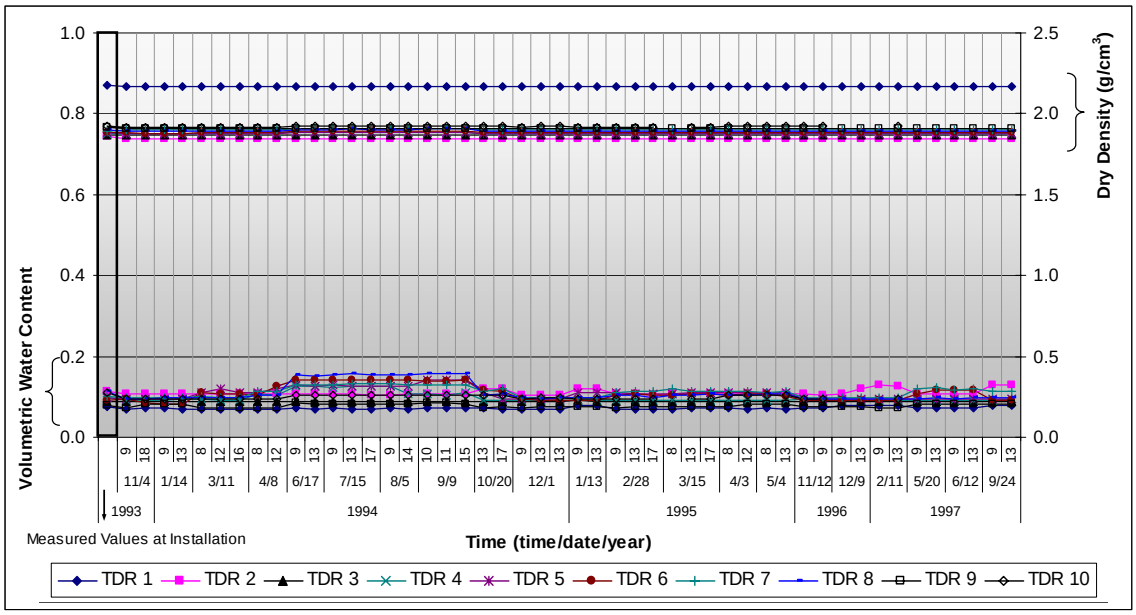

Figure F-54 Variation of water content and density for LTPP section 491001 (Bluff, Utah)

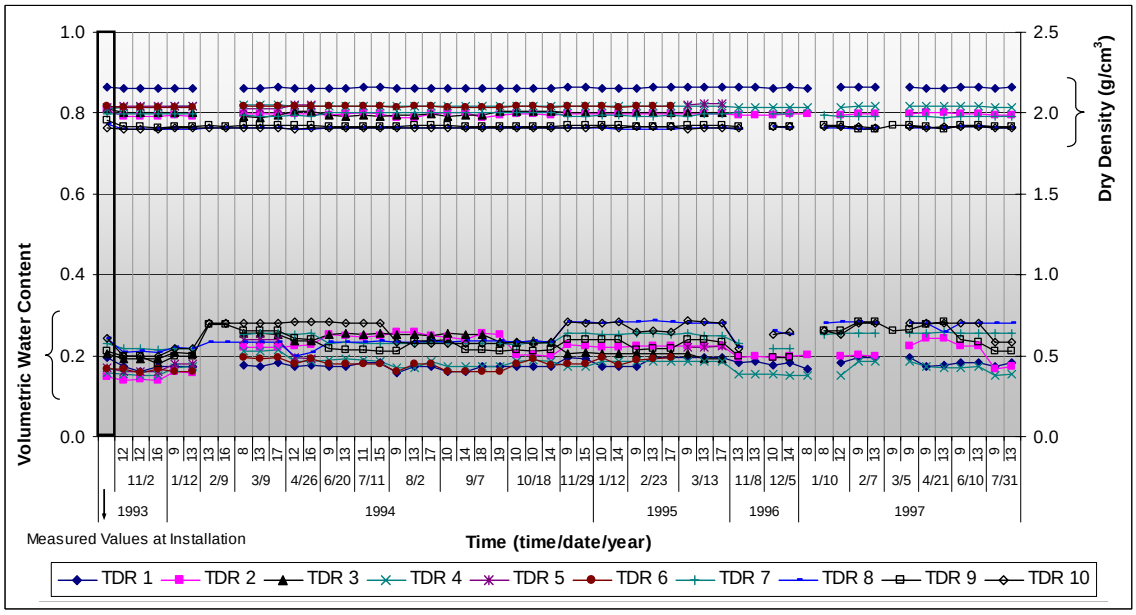

Figure F-55 Variation of water content and density for LTPP section 493011 (Nephi, Utah)

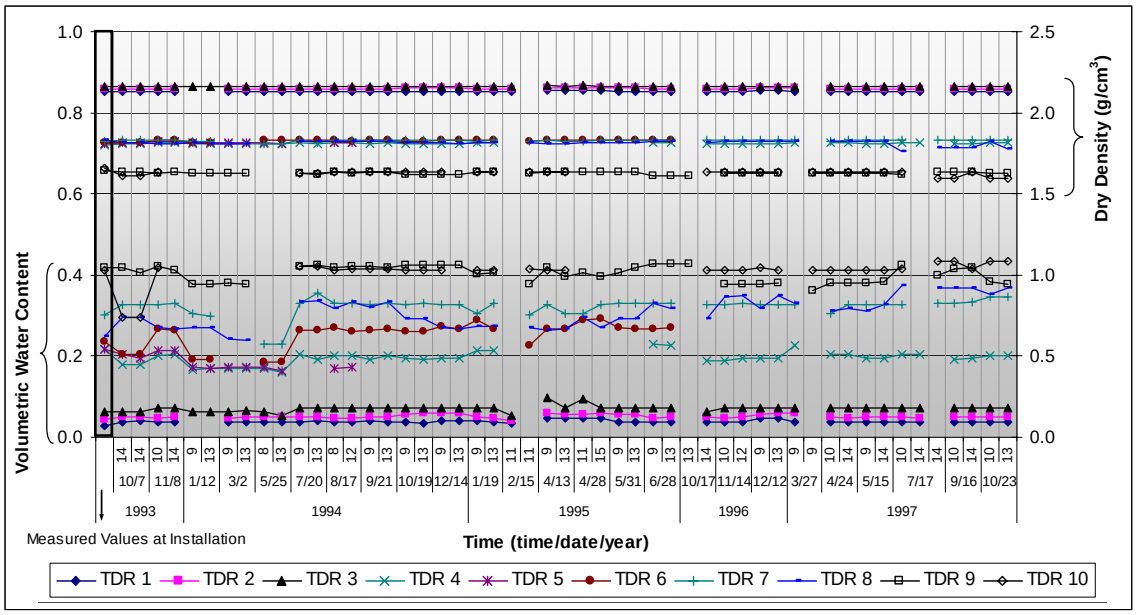

Figure F-56 Variation of water content and density for LTPP section 501002 (New Haven, Vermont)

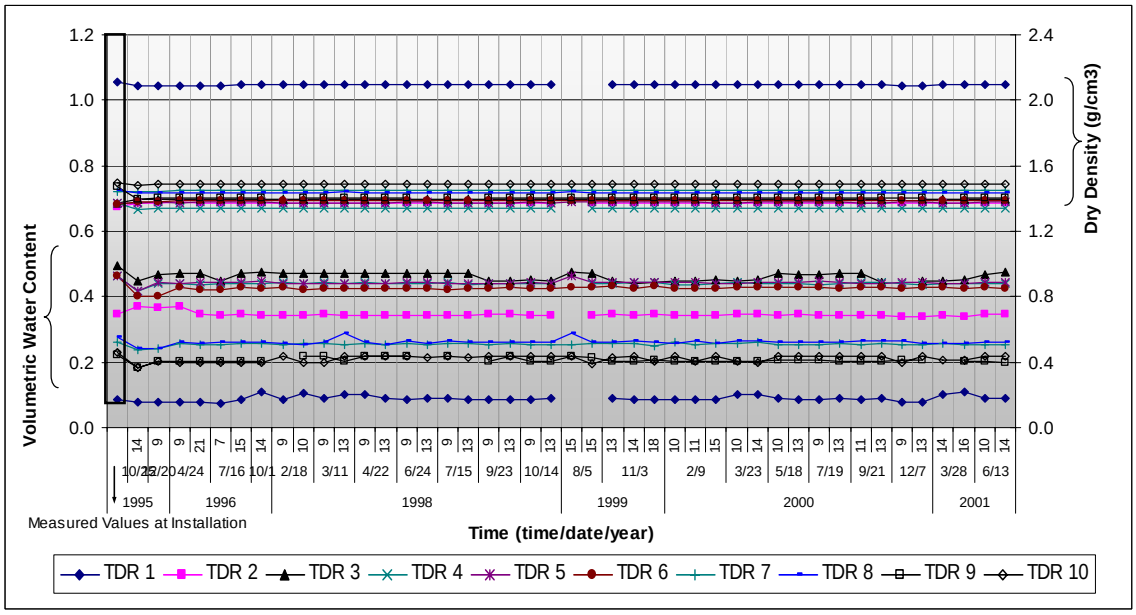

Figure F-57 Variation of water content and density for LTPP section 510113 (Danville, Virginia)

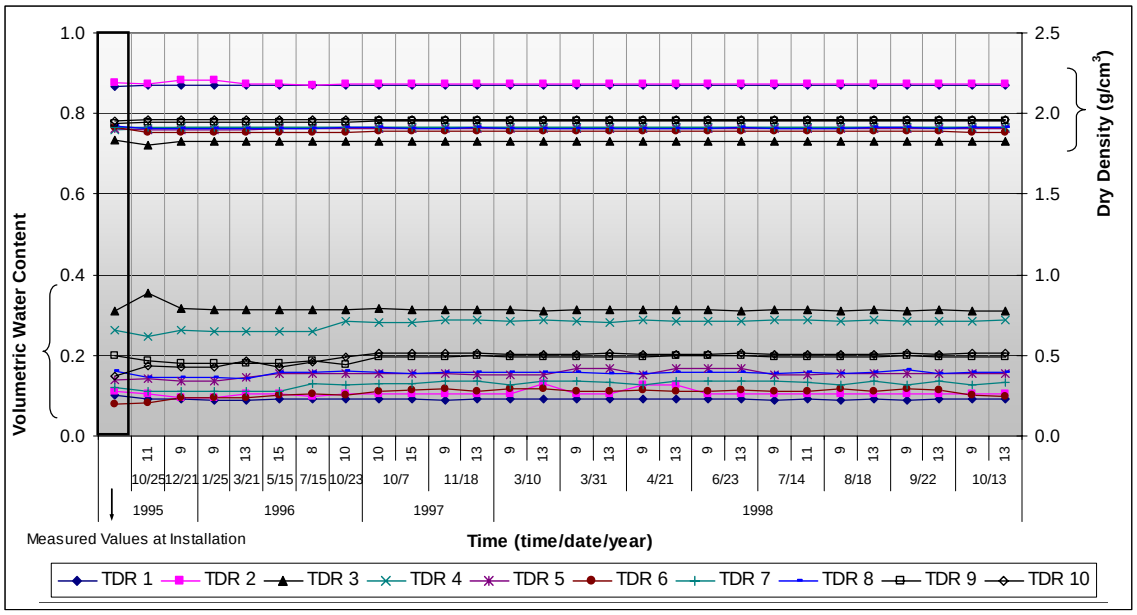

Figure F-58 Variation of water content and density for LTPP section 510114 (Danville, Virginia)

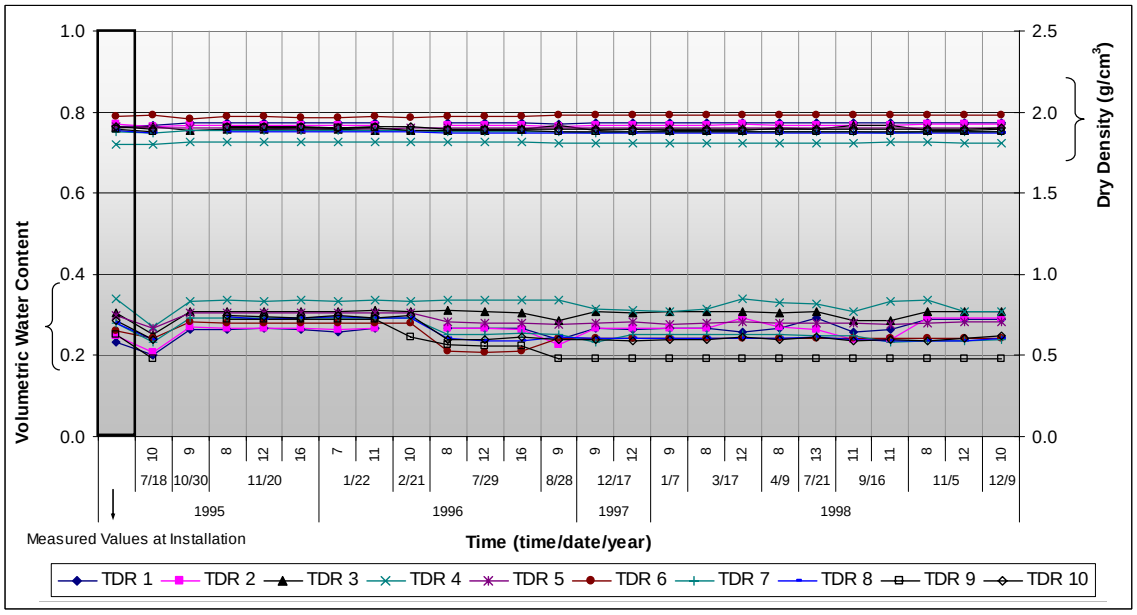

Figure F-59 Variation of water content and density for LTPP section 533813 (Camas, Washington)

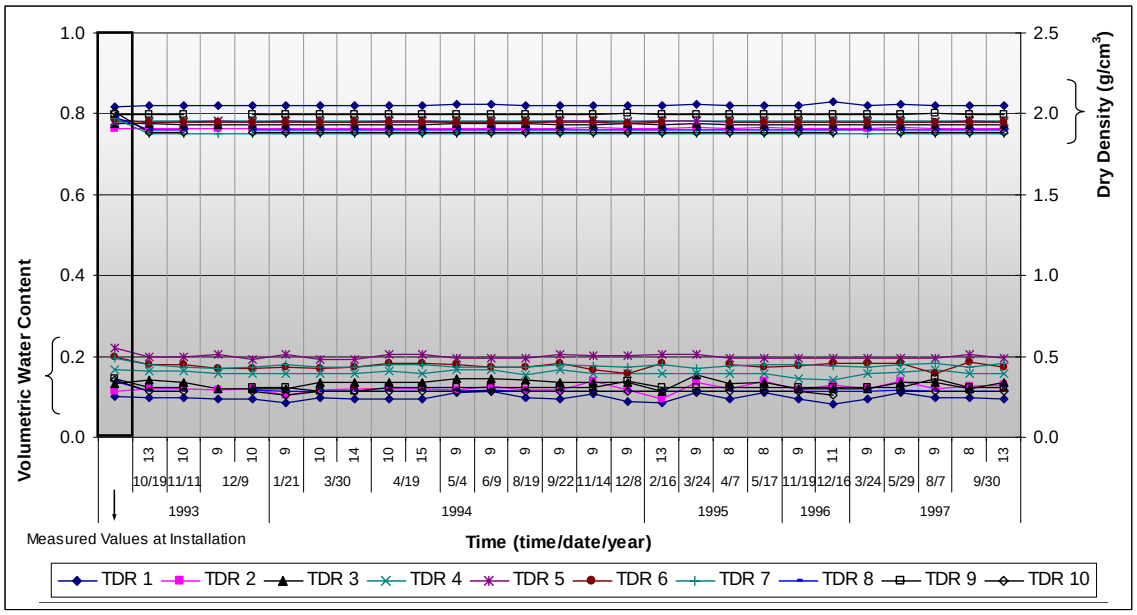

Figure F-60 Variation of water content and density for LTPP section 561007 (Cody, Wyoming)

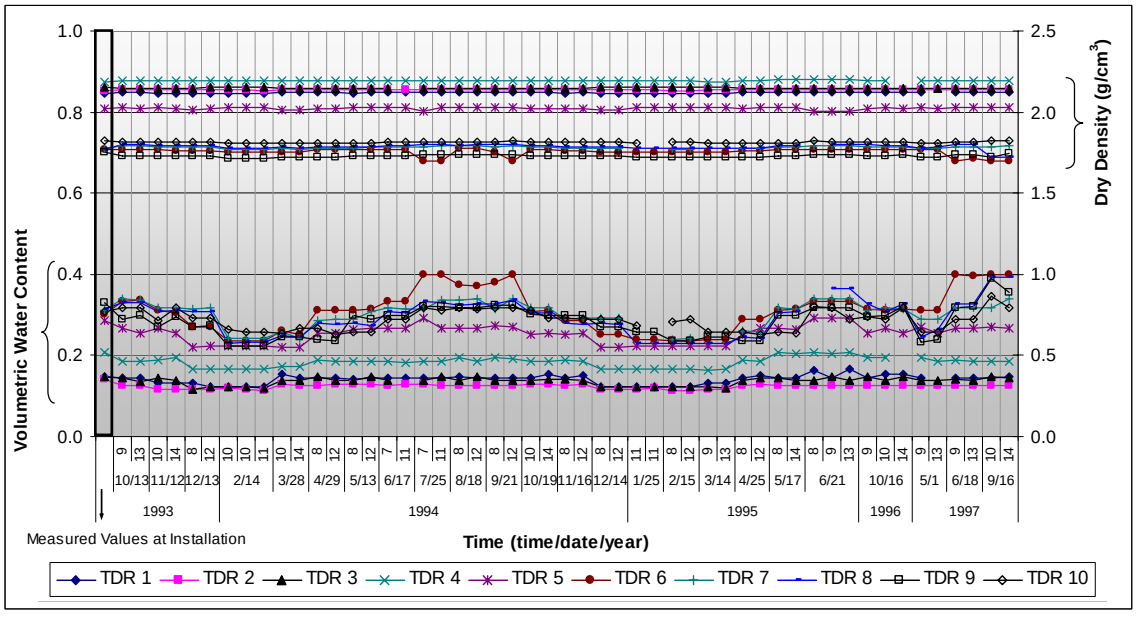

Figure F-61 Variation of water content and density for LTPP section 831801 (Oak Lake, Manitoba)

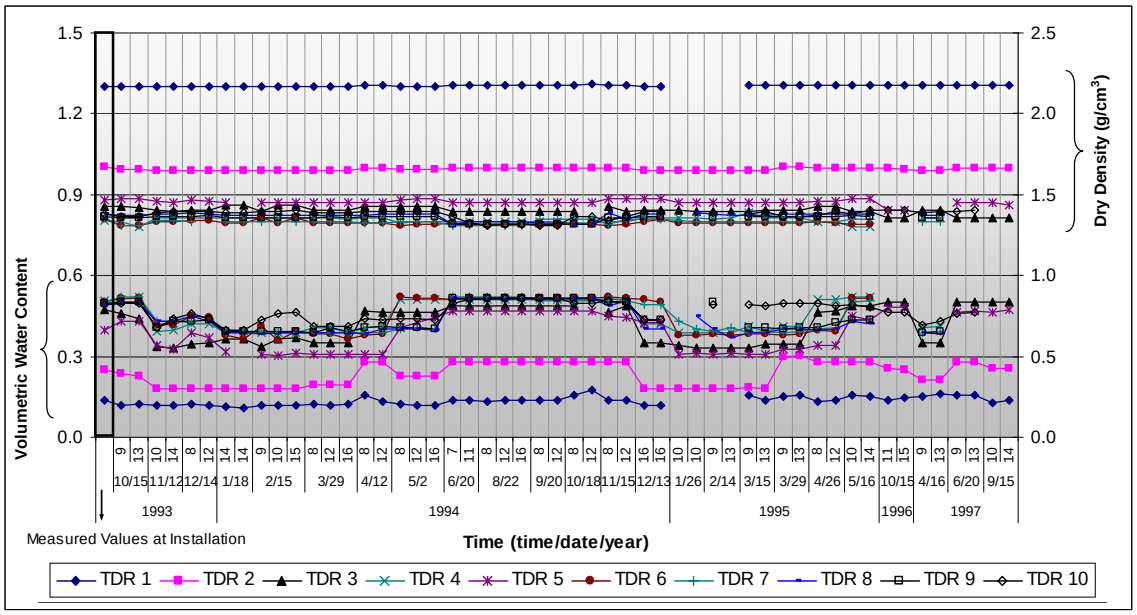

Figure F-62 Variation of water content and density for LTPP section 833802 (Glenlea, Manitoba)

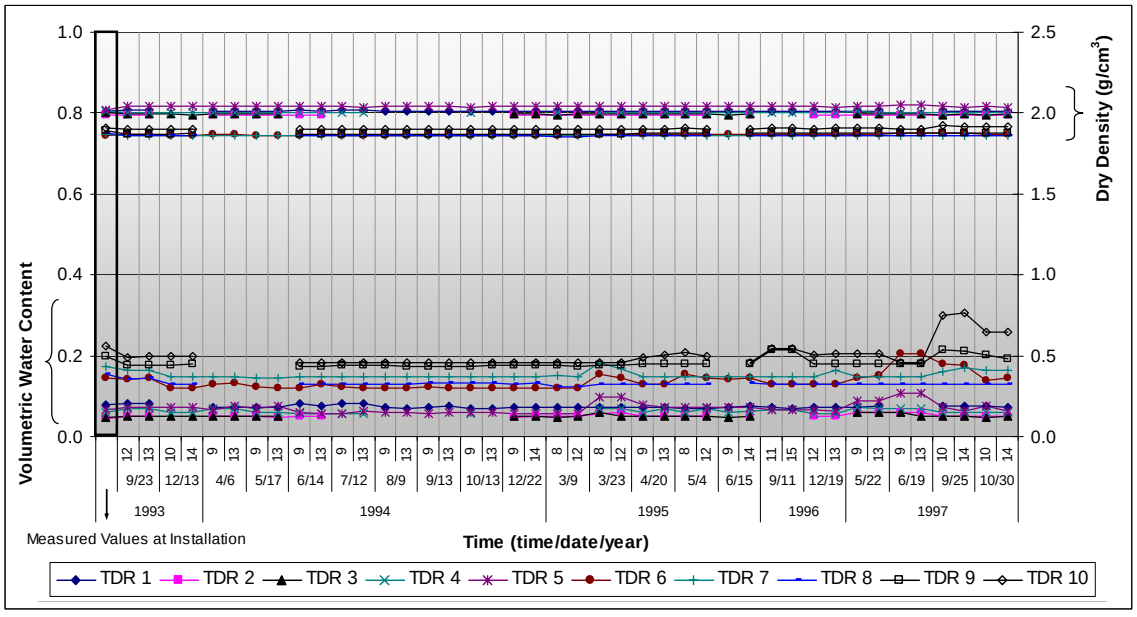

Figure F-63 Variation of water content and density for LTPP section 871622 (Bracebridge, Ontario)

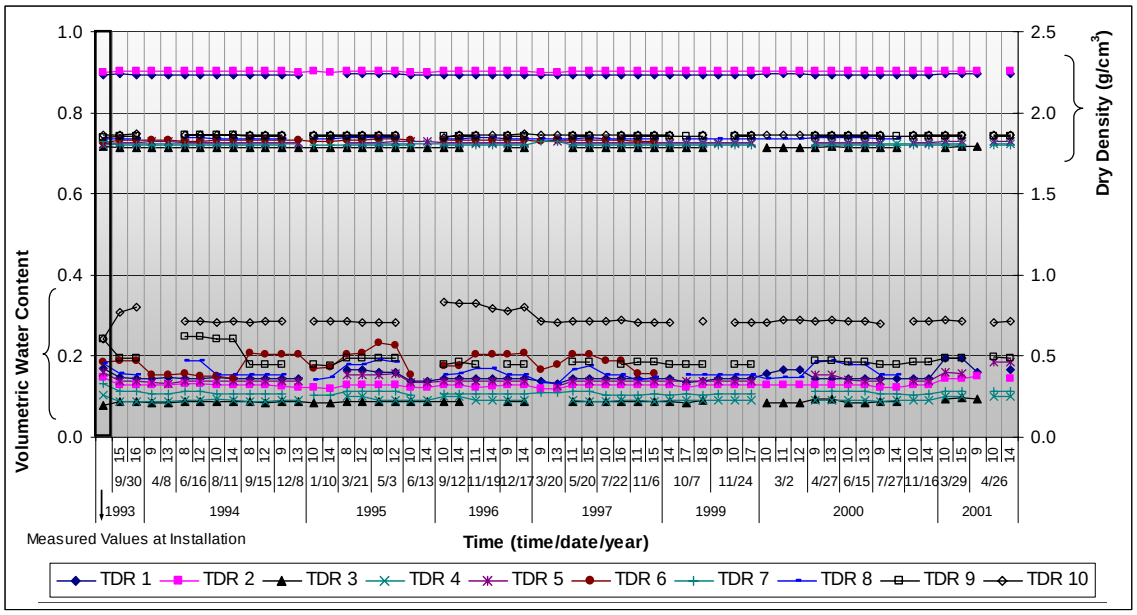

Figure F-64 Variation of water content and density for LTPP section 893015 (Trois-Rivieres, Quebec)

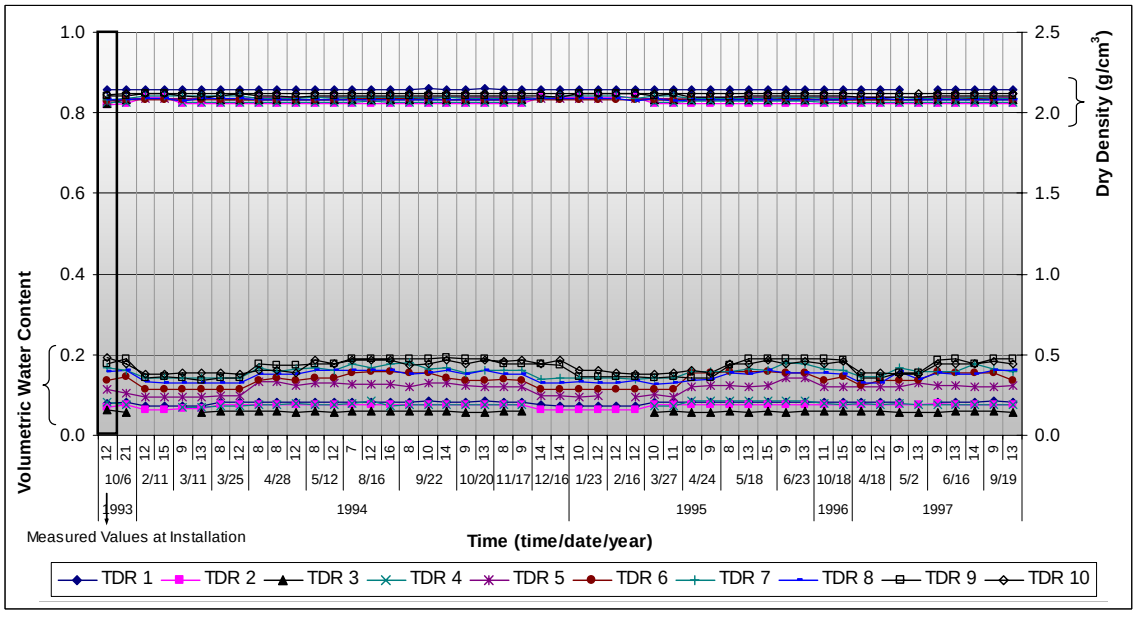

Figure F-65 Variation of water content and density for LTPP section 906405 (Plunkett, Saskatchwen)

VITA

Name:	Sang Ick Lee
Address:	Zachry Department of Civil Engineering Texas A&M University College Station, TX 77843-3136
Email Address:	sangicklee@tamu.edu

Education:	Ph.D., Civil Engineering, Texas A&M University, 2010 M.S., Civil Engineering, Chung-Ang University, Korea, 1999 B.S., Civil Engineering, Chung-Ang University, Korea, 1997
Research Interest:	Micromechanics of Pavement Materials Pavement Design, Analysis, and Management Non-destructive Testing Analysis and Evaluation on Long-Term Pavement Performance